5-14-2010

Representative Environments for Reduced Estimation Time of Wide Area Acoustic Performance

Josette Fabre
University of New Orleans

Representative Environments for Reduced Estimation Time of Wide Area Acoustic Performance

A Dissertation

Submitted to the Graduate Faculty of the
University of New Orleans
in partial fulfillment of the
requirements for the degree of

Doctor of Philosophy
in
Engineering and Applied Science
Physics

by

Josette Paquin Fabre

B.S. Millsaps College, 1988
M.S. University of New Orleans, 1996

May 2010

Dedication

This dissertation is dedicated to the memory of my father, Dr. James E. Paquin. His positive attitude, appreciation for all the good in the world, his extreme wisdom and his sense of humor have influenced and guided me throughout my life.

Acknowledgements

The author acknowledges and appreciates the sponsorship of the Office of Naval Research (ONR) and SPAWAR PEO-C4I PMW-120.

The author would like to thank the following people for their help and many helpful technical discussions: Dr. Stanley Chin-Bing, Dr. Michael Porter, Dr. Robert Zingarelli, Dr. David King, Dr. Frank Bub, Richard Keiffer, David Fabre, Tracy Hall, Steven Dennis, Dr. James Fulford, Dr. Joe Murphy, Dr. Juliette Ioup, Dr. Maria Kalcic, and Dr. George Ioup.

Finally, the author truly appreciates all the support and encouragement from David, Russel, Peter, Marilyn, and Stan without whom it would not have been completed.

Table of Contents

Table of Figures

Acronym List

AIX	Advanced Interactive eXecutive
AOI	Area of interest
ASTRAL	ASEPS TRAnsmission Loss
ASEPS	Automated Signal Excess Prediction System
BEM	Bounded Elliptical Modes
C4I	Command, Control, Communications, Computers, Intelligence
CASS	Computer Aided Sonar System
CM	Conformal Mapping
dB	decibel
DBDB-V	Digital Bathymetry Database - Variable resolution
DI	Directivity Index
DT	Detection Threshold
DTG	Date/Time Group
DTIC	Defense Technical Information Center
EAGLE	Efficient Adaptive Gridder for Littoral Environments
ETOPO2	Earth TOPOgraphy digital dataset version 2
FEPE	Finite Element Parabolic Equation
FOM	Figure of Merit
GRAB	Gaussian Ray Bundle
rms	root mean square
HDF	Hierarchical Data Format
IAC	Integrated Acoustic Coverage
IAMPS	Integrated Acoustic Multi-environmental Processing System
IEEE	Institute of Electric and Electronic Engineers
ISE	Integrated Signal Excess
LVA	Loss versus Angle
MTS	Marine Technical Society
NAVO	Naval Oceanographic Office
NCOM	Navy Coastal Ocean Model
NDIA	National Defense Industrial Association

NetCDF	Network Common Data Form
NGDC	National Geophysical Data Center
NL	Noise Level
NOAA	National Oceanic and Atmospheric Agency
NRL	Naval Research Laboratory
OGRES	Objective Grid/Radials using Environmentally-sensitive Selection
ONR	Office of Naval Research
OT	Okinawa Trough
PAC	Percentage Area Covered
PC	Personal Computer
PE	Parabolic Equation
PEO	Program Executive Office
PMW	Program Management, Warfare
RAM	Range Dependent Acoustic Model
SBIR	Small Business Innovative Research
SE	Signal Excess
SL	Source Level
SLD	Sonic Layer Depth
SMGC	Surface Marine Gridded Climatology
SOCAL	Southern California
SPAWAR	Space and Naval Warfare
SS	Sound Speed
TDA	Tactical Decision Aid
TL	Transmission Loss
UBAND	Uncertainty Band
WMO	World Meteorological Organization

Abstract

Advances in ocean modeling (Barron *et al.*, 2006) have improved such that ocean forecasts and even ensembles (*e.g.*, Coelho *et al.*, 2009) representing ocean uncertainty are becoming more widely available. This facilitates nowcasts (current time ocean fields / analyses) and forecasts (predicted ocean fields) of acoustic propagation conditions in the ocean which can greatly improve the planning of acoustic experiments. Modeling of acoustic transmission loss (TL) provides information about how the environment impacts acoustic performance for various systems and system configurations of interest. It is, however, very time consuming to compute acoustic propagation to and from many potential source and receiver locations for multiple locations on an area-wide grid for multiple analysis / forecast times, ensembles and scenarios of interest. Currently, to make such wide area predictions, an area is gridded and acoustic predictions for multiple directions (or radials) at each grid point for a single time period or ensemble, are computed to estimate performance on the grid. This grid generally does not consider the environment and can neglect important environmental acoustic features or can over-compute in areas of environmental acoustic isotropy.

This effort develops two methods to pre-examine the area and time frame in terms of the environmental acoustics in order to prescribe an environmentally optimized computational grid that takes advantage of environmental-acoustic similarities and differences to characterize an area, time frame and ensemble with fewer acoustic model predictions and thus less computation time. Such improvement allows for a more thorough characterization of the time frame and area of interest. The first method is based on critical factors in the environment that typically indicate acoustic response, and the second method is based on a more robust full waveguide mode-based description of the environment. Results are shown for the critical factors method and show that this proves to be a viable solution for most cases studied. Limitations are at areas of high loss, which may not be of concern for exercise planning. The mode-based method is developed for range independent environments and shows significant promise for future development.

Keywords: Underwater acoustics, acoustic provincing, environmental data, acoustic modeling, uncertainty

Chapter 1. Introduction

Transmission of Sound through the Ocean

Light does not travel far underwater due to scattering. Therefore, in the ocean, acoustic sensing is frequently used to detect objects in the water, objects on the sea floor, or the sea floor itself. In order to estimate the path and intensity of sound travelling through the ocean, the acoustic wave equation is derived from conservation of mass, Euler's equation for a fluid (or Newton's second law), and the pressure density relationship (*e.g.*, Pierce, 1991). The following derivation is given in Pierce (1991). The conservation of mass states that the change with time of a mass in a volume must be equal to the mass entering the volume per unit time less the mass leaving the volume per unit time. After applying Gauss's theorem which relates a volume integral to a surface integral, the differential equation for the conservation of mass becomes

$$\frac{\partial \rho}{\partial t} + \nabla \cdot \rho \vec{v} = 0 \quad ,$$

where ρ is the density in the medium, t is time and v is the particle velocity.

Euler's equation for a fluid (or Newton's second law in terms of pressure) states that the mass times the acceleration of the center of mass of the fluid is equal to the net force on the mass from the environment and external forces (*e.g.* pressure). Again applying Gauss's theorem, Euler's equation for a fluid becomes

$$\rho \frac{D\vec{v}}{Dt} + \nabla P = 0 \quad ,$$

where P is acoustic pressure due to the sound wave and

$$\frac{D\vec{v}}{Dt} = \frac{\partial \vec{v}}{\partial t} + (\vec{v} \cdot \nabla)\vec{v} \quad .$$

The pressure density relation is obtained by assuming conservation of energy with specific entropy remaining constant. Using thermodynamics, the pressure is therefore a function of density and entropy (s):

$$P = P(\rho, s)$$

Now, assume that the acoustic field can be broken into an ambient state plus small perturbations in pressure, density, and velocity:

$$P = P_0 + P'$$
$$\rho = \rho_0 + \rho'$$
$$v = v_0 + v'.$$

A homogenous, quiescent media is assumed so that the pressure is equal to the ambient pressure everywhere and the ambient velocity is zero everywhere. Substituting the above acoustic field equations into the conservation of mass equation, ignoring second order terms of the perturbed fields and applying the homogenous, quiescent assumption, Euler's equation and the equation of state, respectively, obtains

$$\frac{\partial \rho}{\partial t} + \nabla \cdot \rho \vec{v} = 0$$
$$\frac{\partial (\rho_0 + \rho')}{\partial t} + \nabla \cdot (\rho_0 + \rho')(\vec{v}_0 + \vec{v}') = 0$$
$$\frac{\partial \rho'}{\partial t} + \rho_0 \nabla \cdot \vec{v}' = 0.$$

Euler's equation becomes

$$\rho \frac{D\vec{v}}{Dt} + \nabla P = 0$$
$$(\rho_0 + \rho')\left[\frac{\partial (\vec{v}_0 + \vec{v}')}{\partial t} + (\vec{v}_0 + \vec{v}') \cdot \nabla (\vec{v}_0 + \vec{v}')\right] + \nabla (P_0 + P') = 0$$
$$\rho_0 \frac{\partial \vec{v}'}{dt} + \nabla P' = 0,$$

and the pressure density relation, or equation of state, becomes

$$P = P(\rho, s)$$
$$P_0 + P' = P(\rho_0 + \rho', s_0 + s').$$

Expanding P using a Taylor series, neglecting higher order terms and using the ambient plus perturbation relations gives:

$$P(\rho, s) = P(\rho_0, s_0) + \left.\frac{\partial P}{\partial \rho}\right|_{\rho_0 s_0} (\rho - \rho_0) + \ldots$$
$$P' = P_0 + c^2 \rho'.$$

Thermodynamic considerations require the constant c^2 to be positive, and wave interpretation of the solutions to this equation imply that c is the speed of the wave. Now substitute the equation of state into the conservation of mass equation and take the derivative with respect to time:

$$\frac{1}{c^2}\frac{\partial P'}{\partial t} + \rho_0 \nabla \cdot \vec{v}' = 0$$
$$\frac{1}{c^2}\frac{\partial^2 P'}{\partial t^2} + \rho_0 \nabla \cdot \frac{\partial \vec{v}}{\partial t}' = 0.$$

Next substitute this equation into Euler's equation and assume that we are only discussing the perturbations, so we can drop the primed notation. The wave equation for acoustic pressure (*P*) due to a sound source is

$$\nabla^2 P - \frac{1}{c^2}\frac{\partial^2 P}{\partial t^2} = 0.$$

Numerical modeling of the acoustic energy traveling in a waveguide can be done by solving the wave equation in the time domain, but is often calculated in the frequency domain. Solutions to the wave equation can be described as harmonic plane wave disturbances through the media:

$$P(r,t) = P(r)e^{-i\omega t},$$

where *i* is the square root of -1 and ω is the angular frequency ($2\pi f$). Substituting this solution into the conservation of mass equation gives

$$-i\omega P + c^2 \rho_0 \nabla \cdot \vec{v} = 0.$$

Euler's equation becomes

$$-i\omega\rho_0 \frac{\partial \vec{v}}{\partial t} + \nabla P = 0,$$

and the wave equation becomes the Helmholtz equation:

$$\nabla^2 P + k^2 P = 0,$$

where *k* is the wave number:

$$k = \frac{\omega}{c} = \frac{2\pi f}{c},$$

with *c* the speed of sound in the medium through which the acoustic energy is traveling. If one allows r to be a function of position, then the resulting Helmholtz equation is

$$\rho \nabla \cdot \left(\frac{1}{\rho} \nabla P \right) + k^2 P = 0.$$

The wavelength of the sound is important and therefore acoustic systems are designed with various acoustic wavelengths, or frequencies. Frequency (*f*) and wavelength (λ) are inversely related: $f = c / \lambda$.

The acoustic models solve the acoustic wave (Helmholtz) equation, with various boundary conditions and simplifying assumptions (*e.g.* the plane-wave assumption, Pierce 1991), to predict the acoustic pressure due to the sound source at ranges and depths of interest. The average intensity of a plane wave is related to pressure, density and sound speed. The average intensity is then converted to a loss of energy or transmission loss (TL). TL is expressed in decibels (dB) referenced to a plane wave some distance from the source:

$$TL(r,z)[dB\ re\ 1\mu Pa] = 10log_{10}\frac{I(r,z)}{I_{ref}},$$

where *I(r,z)* is the acoustic pressure at range *r* from the source and depth *z* from the surface, and I_{ref} is the intensity at a reference range from the source, usually 1 m. The 0 dB level is set for a plane wave of root mean square (*rms*) pressure $1\mu Pa$ (*e.g.* Jensen *et al.*, 2000) to give a measure for the "loss" of intensity of the sound source as it travels through the waveguide.

Acoustic Modeling

There are multiple ways of solving the Helmholtz equation including the methods of normal modes, Airy functions, rays and parabolic equations, and therefore, there are many acoustic models. This effort uses a parabolic equation model (Collins, 1989) to compute the TL for the performance calculations and most other analyses. The Kraken normal mode model (Porter, 2001) is used to compute the modes versus depth for each grid point for the ξ parameter (described later) mode computation only, and the Bellhop ray model (Rodriguez, 2008) is used to do a mode angle analysis.

Overall Acoustic Provincing Concept

In order to calculate the acoustic performance over a large area, many source and receiver combinations must be computed. The most direct way to do this is to identify an equally spaced grid and place a source at each grid point, compute the TL in multiple radial directions from that grid point, then compute a performance metric due to the various sound sources at each receiver.

The acoustic model is two dimensional (2D) and running it for multiple radials is described as an Nx2D approach. It is used, for example, by Gough *et al*. (2009) in generating acoustic performance maps. Another common approach to this problem, as in Porter (1993) and Kuperman *et al.* (1991) for example, is to compute the normal modes for each grid point on a triangular grid over a geographic area, then specify source locations and compute the field (with range and depth) for the radials of interest using adiabatic mode sums. This approach is limited by the adiabatic assumption, which is not valid for many realistic environments (*e.g.*, Dennis and Fabre, 2007).

Another approach to reducing the run time requirements is iteratively modifying the grid based on the environment (*e.g.*, Pflug and Delbalzo, 2006; Rike and Delbalzo, 2002, 2003 and 2005). These methods are known as the Objective Grid/Radials using Environmentally-sensitive Selection (OGRES) which grids adaptively based on variations of neighboring TL estimates; and the Efficient Adaptive Gridder for Littoral Environments (EAGLE), which uses interpolation schemes to fill in intermediate TL predictions. Monach (2008), in his Adaptive Gridding method uses previously run TL (for example using historical environments) to determine which radials to run at each grid point, rather than running fixed radials. This method uses Bayesian neural networks to compare TL and identify the appropriate radials to run.

These approaches rely on TL having been modeled prior to analysis. As discussed, TL is obtained for a given source depth and frequency, which suggests a limitation on the computationally intensive TL results. Here, the goal is to avoid this limitation and examine the environment quickly prior to computing TL. The approach described in this work examines the environment in terms of the features that most impact the acoustics, and use that information to determine optimal locations and bearings of acoustic runs given the parameters of interest. If the parameters change, for example when a new ocean prediction becomes available, the analysis can be quickly redone.

Chapter 2 describes the provincing and environmental cost function development in detail, as well as the sources of environmental information and the tools that are used and have been developed for these tasks. Chapter 3 presents results for multiple cases using the critical factors approach and results using a preliminary development of the mode-based environmental parameter. Chapter 4 gives a brief overview of some of the applications of this method. Finally, Chapter 5 gives conclusions and recommendations for further development.

Chapter 2. Method

Acoustic provincing represents a new way to setup, run and process acoustic TL predictions. An overview of the provincing method is presented here, followed by a description of the inputs to the provincing routine. A brief discussion of the models and an introduction to the acoustic performance estimate calculation is then followed by a discussion of the uncertainty algorithm used. The description of a tool that combines all the data extractions, modeling and prediction estimates is provided. Finally, the development of the environmental descriptions or cost functions is given, followed by a discussion of the mathematical provincing routine and its application to this effort. A cost function is simply a mathematical characterization of a process or state. In this case the cost functions are based on the environment and described as a function of range for the critical factors application and a function of range and depth for the mode-based application.

Environmental Acoustic Provincing Overview

The overall objective of this effort is to develop fast, efficient and scientifically valid methodologies for generating acoustically equivalent representatives of complex ocean-acoustic environments. A representative environment takes into account only those features of the real environment that significantly change the acoustic performance measure. The representative environment is a function of the acoustic frequency and neglects environmental features that have a secondary effect on the acoustics at a particular frequency. Eliminating environmental features that have little to no effect on the acoustic propagation at a particular frequency will allow for a significant increase in computational speed associated with accurate wide area predictions of performance metrics, thus allowing estimation of more performance prediction scenarios within the computational and application times. Additionally, these representative environments would provide insight into the sensitivities of the acoustic performance to more basic environmental parameters. Representative environments, by design, are simplified everywhere possible without degrading the performance prediction beyond 80% of the brute force prediction.

In order to characterize acoustic performance over an area, a brute-force approach is to choose equally spaced grid points in an area of interest (AOI) and place a source at each grid point and receivers in various radial directions from that source. Figure 1 shows an example of a

3 x 2 area, with 8 radials at each grid point, resulting in 48 acoustic TL predictions. Next a performance metric is computed from the TL at each location and a map of the performance is generated. In this case the map would have 6 pixels, each representing the integrated (over the radials) performance at that grid point. Directional maps can also be generated to show performance as it varies across the radials, but that can be difficult to interpret.

The concept of provincing presented here characterizes the environment for each radial in a way that indicates the acoustics but doesn't compute the acoustic performance or TL. Then each range dependent environmental description is fed to the mathematical provincing (or clustering) routine and an acoustic run is computed only for a representative of each province. Using the 3 x 2 grid point example, 48 environmental descriptions or cost functions are fed to the provincing routine, requesting 9 provinces. The provincing routine computes vector differences between each environmental cost function and groups them into 9 provinces, where the differences within the provinces have been minimized. The centroid of the province is chosen to be the representative, and the acoustic model is run only for the centroid, which is now known as the representative of the province. This representative is the actual environment for the radial that is the centroid of the province; no environmental averaging or estimating is done when computing the acoustic prediction. It is emphasized that each radial represents an acoustic run from a source to a receiver, and is characterized by a mathematical cost function computed from the environment and then provinced according to the distances between each cost function. There is no geographic information regarding the location of the radial, so the provinces represent similar environments, not necessarily adjacent to each other. Because of the dependence of propagation on slope, provinces frequently follow bathymetry features, but two similar environments can be at opposite ends of the AOI. Figure 2 illustrates the overall provincing concept discussed here. The 48 points have been provinced into 9 provinces. Nine representative acoustic runs (demonstrated in the lower portion of the figure) are computed. The single representative acoustic prediction is then inserted into the grid at the appropriate locations to build the performance map. In this example, all the red (#1) radials shown in the top half of Figure 2 would use the acoustic prediction from the single acoustic run of the centroid of the red province. These radials are the members of province 1 and the representative that was run is the centroid of the province.

Each province has a spread characterized by the members of the province. This spread is in terms of the environmental cost function. By examining how the cost function spread relates to the TL spread, the uncertainty of the performance of each province is characterized. This is done using the uncertainty band algorithm (UBAND) developed by Zingarelli (2008). UBAND takes the *rms* difference of various acoustic model inputs and translates that to upper and lower bands on the TL curve. UBAND will be discussed in more detail later.

The approach to estimating the environmental cost function upon which to province is two-fold: First, a critical factors approach will be taken: the environmental features such as water depth in terms of propagating acoustic modes and sonic layer depth for near surface trapped energy will be examined to mathematically cluster the area and determine the sensitivity of the acoustic performance to the features. Because critical factors analysis can not capture all features in the environment that may be pertinent, a second, more robust approach is developed: an environmental acoustic parameter arrived at during the derivation of the Airy function solution to the wave equation will be presented and used with grouped acoustic normal mode eigenvalues computed for the area(s) of interest, and other approximation techniques. The modes are grouped based on their propagation angle properties and the area is provinced using these properties.

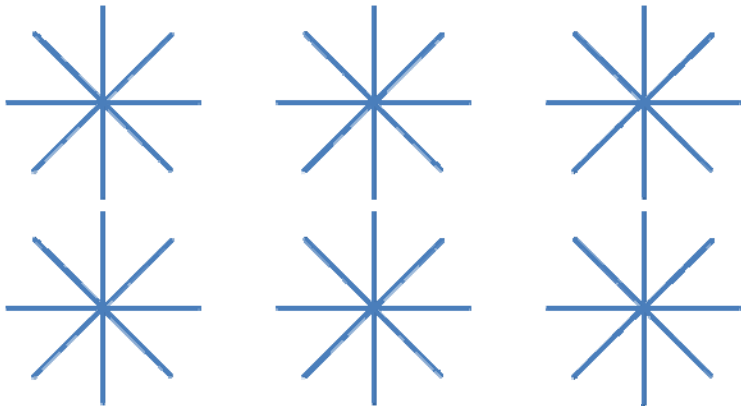

Figure 1. Six grid points (3x2), with 8 radials each, for the brute-force option results in 48 acoustic runs.

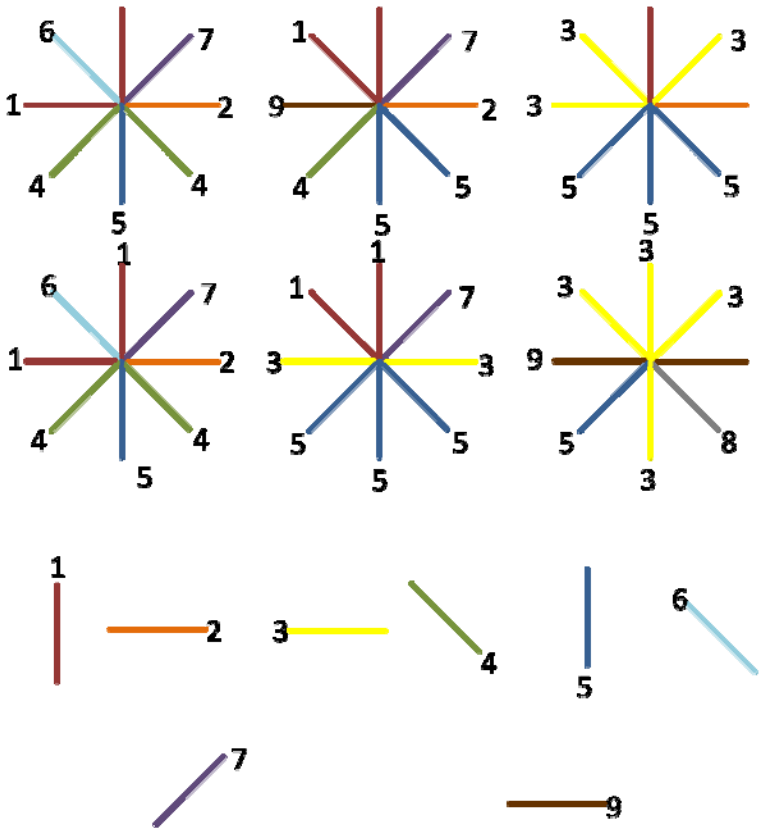

Figure 2. Illustration of the provincing concept for the 3x2 example. Nine acoustic provinces are computed, so 9 acoustic computations will be done using the centroid environment, that is the environment closest to the center of the province.

Environmental Characterization

The acoustic models rely on a description of the wave guide that includes the surface of the ocean, the water column, water depth and a sediment description. These are input as wind speed, sound speed versus depth, water depth and geoacoustic parameters (sound speed, density and attenuation) versus depth in the sediment, respectively. The sources of each of these environmental components are discussed below.

Gradients of sound speed in the oceanic waveguide determine how the sound will travel in the wave guide. Recently, significant advances have been made in modeling and predicting the ocean and it's variability. Such advances have culminated in the Naval Research Laboratory's (NRL's) Navy Coastal Ocean Model (NCOM) (*e.g.* Barron *et al.*, 2009) which is a primitive equation ocean circulation model that uses ocean dynamics and measured data to predict nowcasts and forecasts of the oceanography including temperature, salinity, currents and wind

stress. The sound speed is computed using the temperature and salinity from NCOM and the Chen-Millero-Li (Chen and Millero, 1977 and Millero and Li, 1994) algorithm. Wind speed or wave height determine the surface boundary condition for the acoustic model. NCOM also uses winds as the surface boundary condition and outputs horizontal and vertical components of wind stress. The wind speed is computed using wind stress from NCOM as described by Powell *et al*., 2003 and implemented by Rowley (2009).

The Digital Bathymetry Data Base - Variable resolution (DBDBV) (NAVO, 2007) is used for the water depth. DBDBV contains nominal depth, which is the depth assuming a constant sound speed through the water column (*e.g.* Fabre and Fabre, 2007). True depth is the depth accounting for the vertical sound speed in the water column. For the acoustic modeling in this effort, the nominal depth data is extracted and converted to true depth using the Carter (1980) tables.

The geology is either obtained from a data base or from a geologic analysis. Fulford (1993) provided geoacoustic descriptions for the AOIs used in this effort. A database of this geoacoustic information has been developed, in netCDF (Rew, 2010) format for this and related efforts.

The next section discusses the acoustic modeling approach. For testing purposes, for the test cases presented here, the brute force approach is taken, then the province representatives are chosen from that brute data set. In practice, only the province representatives would be computed.

Acoustic Modeling

This effort uses a parabolic equation model (Collins, 1989), the Range Dependent Acoustic Model (RAM), to compute the transmission loss (TL) for the performance parameter calculations and most other analyses. The Kraken normal mode model (Porter, 2001) is used to compute the modes versus depth for each grid point for the ξ parameter mode computation only. The Bellhop ray model (Rodriguez, 2008) is used for the preliminary angle analysis related to the mode-based environmental cost function.

RAM is a finite element parabolic equation (PE) model that "is based on a user-selected multiple-term Padé approximation of the PE operator. Because this solution allows range steps much greater than the acoustic wavelength and does not require fine vertical gridding, RAM is a

very fast research model. (Collins *et al*., 1996) Additionally, RAM's grid can be tuned to smoothly trade accuracy and speed as the operational situation requires". (Zingarelli and King, 2003).

Acoustic Performance Estimates

Once the acoustic model is run the TL is converted to a performance estimate using the sonar equation. For passive acoustics, the sonar equations, as given by Urick (1983) is

$$SL - TL = NL - DI + DT$$

$$SE = SL - TL - NL + DI - DT$$

$$SE = FOM - TL$$

where SL is source level, TL is transmission loss, NL is noise level, DI is directivity index, DT is detection threshold, SE is signal excess, (that is, the amount of signal remaining once noise and other factors are estimated) and FOM is the figure of merit which includes all the terms other than TL as one number.

Acoustic coverage area (Dennis and Hemsteter, 2007) is the area covered by a sensor centered at the grid point. Acoustic coverage, described in Fabre and Dennis (2007), is simply the area for which acoustic TL is below a threshold, or the area over which there is positive or some threshold (FOM) of signal excess. For the purposes of this study, this threshold is set to a constant around 85 dB. Figure 3, from Fabre (2007), illustrates the concept of acoustic coverage. The blue lines in the left portion of the plot are the TL subtracted from the threshold with a black line at 0, to show the threshold. Any values above the threshold are considered "covered" by the sensor and are shaded. The coverage area or coverage is then the area covered by that sector as illustrated in the right side of Figure 3. A coverage map can be a display of single coverage values at each grid point that indicates the sum of the coverage over all the radial sectors at that point or a percentage of the area covered (PAC) for each depth of interest. Coverage or PAC are nice metrics because the units are square area or percent and can be mathematically manipulated without, for example, concern for logarithmic units (used for TL or SE).

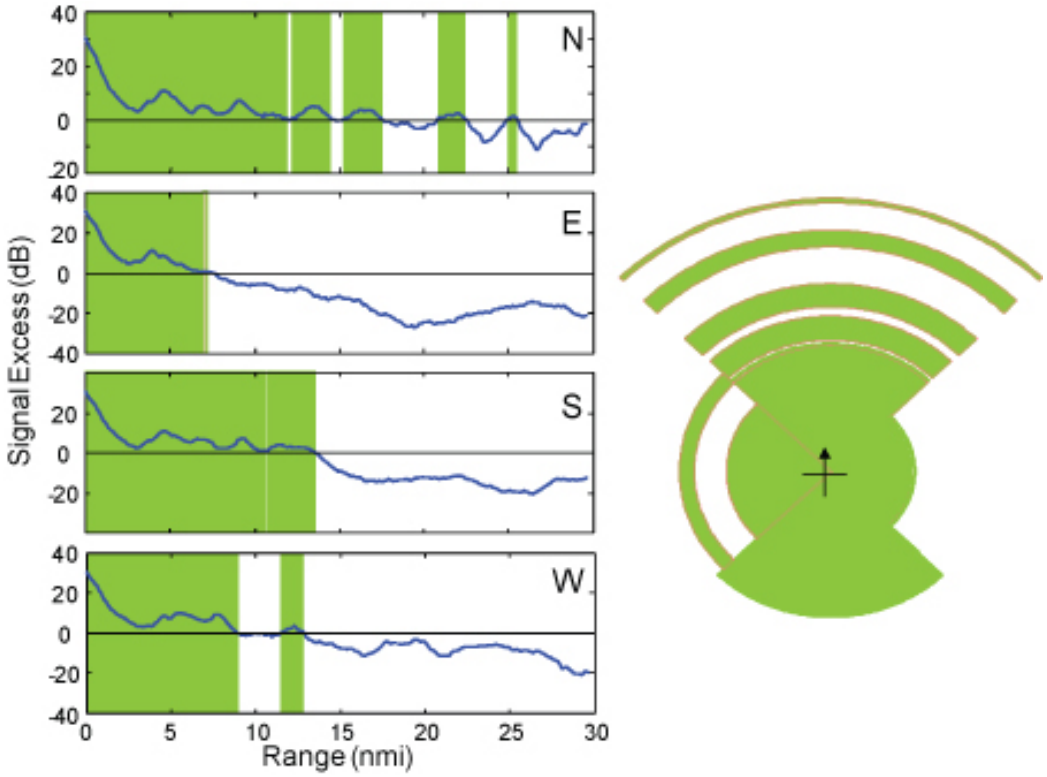

Figure 3. Acoustic coverage concept, after Fabre, 2007.

Characterizing Uncertainty

Uncertainty is an unavoidable part of any measurement or modeling process. Uncertainties in environmental quantities such as bathymetry, water sound speed profiles, and acoustic system parameters are fairly straight-forward to quantify. A method for mapping these values into overall uncertainty in sound TL levels has been developed by Zingarelli (2008) and is known as the uncertainty band, or UBAND algorithm. UBAND is used here to translate uncertainty in the ocean waveguide, as described by the spread of the environmental cost functions, into TL and system performance uncertainty.

The UBAND algorithm (Zingarelli, 2008) is based on Harrison and Harrison (1995), who noted that a range average of TL is very similar to a frequency average over the system band width, due to the mathematical similarity of the two techniques using sums over normal modes. Zingarelli (2008) extended that range averaging technique to calculate upper and lower boundaries on a TL prediction by estimating an uncertainty in the number of modes used in the mode sum, based on the uncertainty in the environmental inputs. This technique has been shown (*e.g.* Zingarelli and Fabre, 2009) to be quite accurate for various applications and should be

accurate enough for the provincing developed here. Figure 4 shows an example of an upslope TL at two frequencies. The black lines are the typical range averaged TL predictions and the blue lines are the upper and lower uncertainty boundaries as predicted by UBAND, given uncertainty in the environment and in the bandwidth.

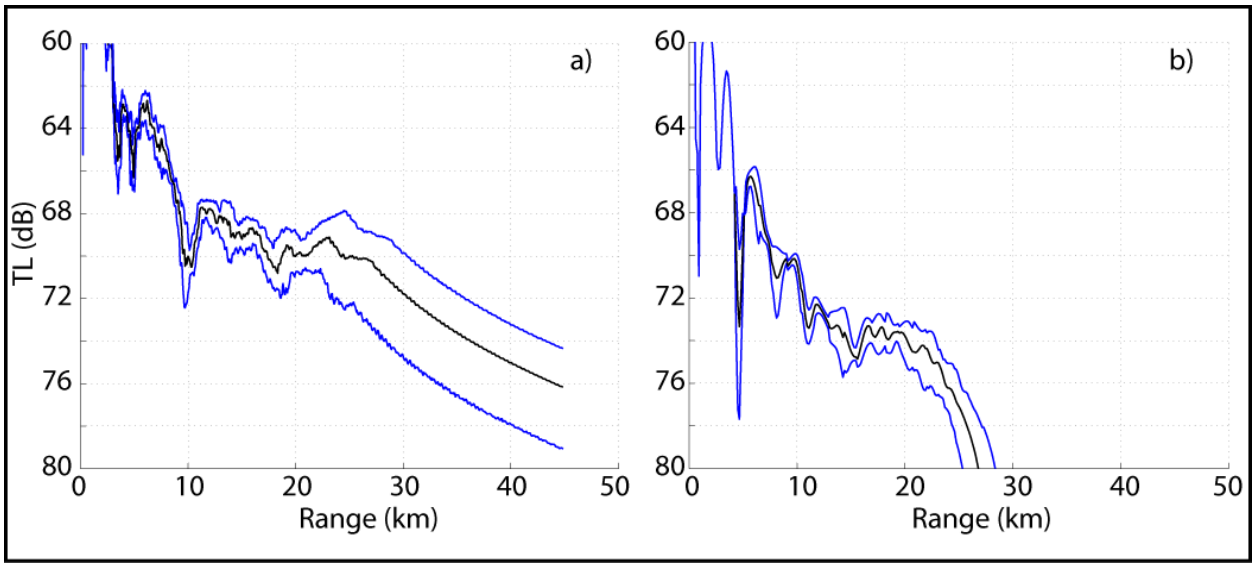

Figure 4. Examples of the UBAND algorithm from Zingarelli and Fabre (2009) for an up-slope case at two frequencies. For the higher frequency case (left) the uncertainties increase as the sound travels up the slope. At the lower frequency (right), the energy falls off before the uncertainty gets too high.

The inputs to the UBAND algorithm are root mean square (*rms*) errors in various acoustic model input parameters such as bathymetry, sound speed, frequency band, source depth and receiver depth. For the provinces, the environmental parameter *rms* differences are computed over the members of the province and input to UBAND, along with standard estimates of frequency, source and receiver depth uncertainty to estimate the TL uncertainty for that province.

Integrated Acoustic Multi-environmental Processing System (IAMPS)

Integrating all the environmental extractions, setting up the models to run and processing the output can be complicated. In order to automate this process, software has been developed over a number of years and projects to set up and execute user described acoustic predictions for time series or ensemble oceanographic environments on single or multi-processor computers. This Integrated Acoustic Multi-environmental Processing System (IAMPS) reads NCOM ocean analysis, predictions and /or ensembles, a bathymetry database, a sediment database and user inputs. It then sets up the source / receiver locations given the user's sensor parameters and geographic area of interest; converts NCOM fields to sound speed and wind speed as described

above; converts nominal water depth to true depth; computes and saves various acoustic parameters, to be described later; writes acoustic model input files and batch scripts to run the acoustic model of choice based on the computer resources available and the user's inputs. Once the acoustic runs are completed, it reads the transmission loss (TL) and computes a performance estimate, such as acoustic coverage (*e.g.* Dennis and Fabre, 2007) or PAC.

IAMPS provides an automated way to set up and execute many acoustic runs to characterize the acoustic system performance over an area of interest. This capability exists for an equally spaced grid or for user defined tracks and has been modified to accept a list of locations and bearings (or radials) to support the provincing application. IAMPS has also been modified to compute UBAND uncertainty estimates. A more detailed description of IAMPS follows.

IAMPS is written in C and calls a small number of Fortran subroutines. It is linked to NetCDF (*e.g.* Rew, 1990) and HDF5 (*e.g.* HDF Group, 2009) libraries for compatibility with oceanographic and bathymetric data file formats. IAMPS was written to be run on a Linux or AIX multiple processer computer, but it also can be compiled and run on Windows PCs or Macintosh computers. The inputs to IAMPS include the path of the working directory, the acoustic model to run, flags to indicate the source of the oceanographic, sediment, wind and bathymetry data, the AOI, the number of sources and receivers and their depths, the number of frequencies and the frequencies of interest, and the maximum range to which to run the acoustic model. If equally spaced gridding is to be run, the number of radial bearings to run at each grid point is entered and the number of grid points to compute, otherwise a file from which to read the positions and bearings to be run is given (for the purposes of provincing or analysis). The final sets of inputs are the wind filenames if the user chose to read the wind from a file, and the NCOM filenames with the forecast date time group (DTG) to be extracted from the file. If the UBAND algorithm is to be run, a separate input file is provided containing inputs specific to UBAND.

The models that can be executed via IAMPS include RAM (Collins, 1989), Computer Aided Sonar System (CASS)/GRAB (*e.g.* Keenan, 2000) in 3 configurations, the Kraken normal mode model (Porter, 2001), and the ASEPS (Automated Signal Excess Prediction System) Transmission Loss (ASTRAL) model (Spofford, 1979). Additionally, IAMPS can be run to

obtain the environmental parameters only, that is, no acoustic model will be run, only the environmental acoustic analysis will be computed and saved.

First IAMPS reads the input file and sets up for the appropriate run type (model, etc.). The bathymetry is then extracted from DBDB-V (NAVO, 2007). Next, for each NCOM file, which can represent a time series or an ensemble, the temperature and salinity at the appropriate DTG and area of interest are extracted and converted to sound speed (SS); the wind is extracted or computed as appropriate; and the sediment description is extracted. The environmental acoustic parameters, deep sound channel axis, depth excess, critical depth, sound speed at critical depth, sonic layer depth (SLD), cutoff frequency, below layer gradient, in layer gradient, sound speed at sonic layer depth, vertical and horizontal sound speed gradients are all computed and saved to a NetCDF file along with bathymetry. The SS gradients in the entire waveguide, the sound speed ratio at the interface and the minimum and maximum SS are then computed and saved to another NetCDF file for use in computing the acoustic mode parameters. Within this loop over the NCOM files, if the acoustic model flag is set, IAMPS constructs the grid, the radials at each grid point and generates the appropriate acoustic model input files in a directory for that time epoch or ensemble member. Finally, if the option to run the acoustic models on the gridded area was chosen, the batch scripts are set up for the selected computer system of interest.

If the provincing analysis is done and the file listing the representatives as well as the file mapping representatives into other radial locations is read by IAMPS and the appropriate batch scripts are set up for the computer system of interest, the rest of the process is the same.

The batch scripts are then executed and the performance module is executed. The acoustic performance module reads the appropriate acoustic model output, reads either a single figure of merit (FOM) to be used for the whole area or a file containing FOMs versus grid location, applies the FOM and computes the following acoustic performance metrics: acoustic coverage area, probability of detection and maximum detection range.

A suite of plotting routines have been developed in Matlab^{TM} for IAMPS and related output and are used for the analysis presented here. Additionally, there are a number of post-processors that re-format the IAMPS output for other tactical decision aids (TDAs).

Environmental Acoustic Factors Provincing

A number of environmental acoustic parameters are frequently used for various acoustic analyses and are known as critical factors. These parameters are used in this effort to characterize the environment for the critical factors provincing applications. The assumption is that various aspects of the environment dominate the acoustic problem and can therefore be used to analyze the environment in terms of acoustics. This frequently isn't the case, and because the transmitted acoustic energy interacts with the full environment (water column, surface, bottom), this sort of analysis can be incomplete, but for the first stage of this effort, the assumption is made that particular aspects of the environment can be used to infer the acoustic response. With the knowledge that there are limitations to this approach, it is used for the first phase of this effort.

The bathymetry, bathymetry slope and sediment properties are important critical factors for acoustic propagation. Acoustic propagation can be described by the acoustic normal modes that are excited by the source. These modes characterize the full depth extent of the waveguide. Computation of the modes can be done in a number of ways. A normal mode model, for example Kraken (Porter, 2001) can be used. For this work, a faster, bounded elliptical modes (BEM) (Smith, 2007) approximation was used to predict the number of modes and the eigenvalues for each environment in the grid. This technique assumes the elliptical dependence of wave number on the mode number to estimate the modal wave numbers given the sound speed and sediment geo-acoustics. This method was compared to eigenvalue predictions by Dennis and Fabre (2007) using the Kraken normal mode acoustic model (Porter, 2001) and was shown to be sufficient for this application. The cost function for this environmental critical factor is the number of modes as a function of range from the source to the receiver. This cost function describes an overall description of how the sound will travel with range. Another critical factor significant particularly at mid-frequencies is the sonic layer depth.

A surface duct or sonic layer is the depth from the ocean surface to a maximum in sound speed. A sonic layer, when present, can significantly impact the propagation of sound near the ocean surface. Because of this, the sonic layer depth (SLD) is sometimes used as a proxy for acoustic performance. The strength of a surface duct depends on the sound speed in addition to the surface waves, the acoustic frequency and the gradients in and near the duct. Because of this dependence, using SLD alone as a proxy for acoustic performance can be misleading. Wind produces mixing that can lead to a duct, but "wind also creates a rough surface and breaking

waves inject air bubbles into the ocean" which can "introduce scattering and frequency dependent refraction effects" (Fabre *et al*., 2009). These high angle effects cause energy to escape the duct (often known as duct leakage) and therefore increase the energy below the duct and decrease the energy in the duct. The SLD is also a frequency-dependent concept, below a certain frequency (known as the cutoff frequency) the sound will not stay trapped in the duct. The duct is also a range dependent phenomenon, if the duct is not persistent in range, energy will dump out of the duct at certain ranges. Therefore, when considering the SLD in terms of the acoustics, the frequency and the source depth as well as the wind and the strength and persistence of the duct must be considered.

This SLD concept is demonstrated below for a case for which the cutoff frequency is approximately 400Hz. Figure 5, adapted from Fabre *et al*. (2009) shows the transmission loss at 800 Hz (well above cutoff frequency), with a source in the duct computed with no wind speed (no surface loss), a surface loss versus angle (LVA) estimated based on wind speed (*e.g.* Moore-Head, 1989) and a more realistic, conformal mapped (CM) surface description (*e.g.* Norton and Novarini, 1996) with bubbles, all for an 8 m/s wind speed. This shows the impact of the surface loss on the TL in the duct, which is almost 10 dB at a typical range of 50 km. For this case the wind speed used in the modeling was extracted from the Surface Marine Gridded Climatology (SMGC) database (NAVO, 1996), however the wind speed reported in the NCOM output was 17 m/s. This analysis was done because frequently, the full NCOM field is not available to the acoustic model so the historical or flat surfaces are used, and the impact of this substitution on the modeling can be significant and must be understood, particularly when analyzing critical factors. Figure 5 and Figure 6 emphasize the importance of using appropriate wind speeds in the acoustic modeling, particularly when the source or receiver are near the surface, where there are ducts or in shallow water.

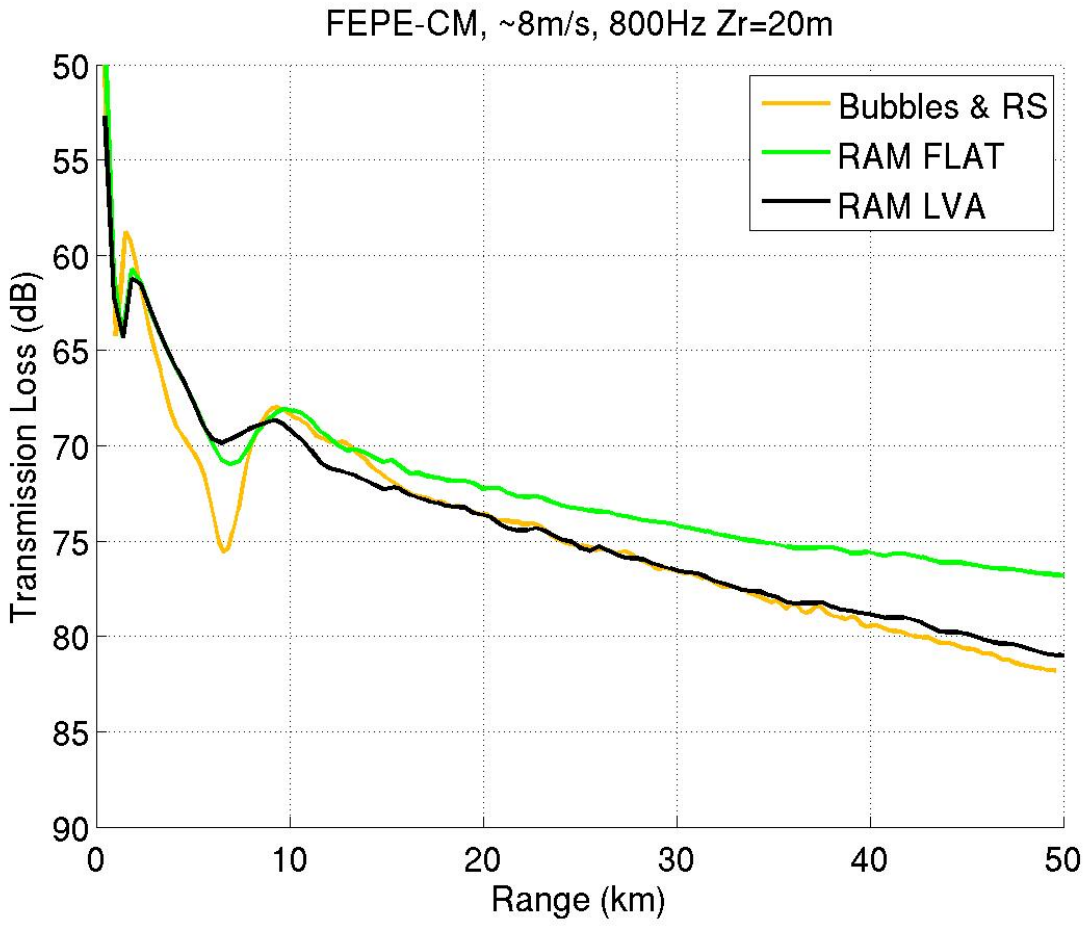

Figure 5. Modeled transmission loss for a source in a sonic layer. The green curve represents the loss for a flat surface, the black curve represents the loss for which the more realistic rough surface was included in the modeling. The yellow curve was generated using a research surface loss model (Norton and Novarini, 1996).

In order to include all appropriate mechanisms (surface scattering, source and receiver depth, range, etc.) in a sonic layer critical factor, the leakage coefficient, which accounts for sound escaping or leaking out of a duct (Baker, 1975) is used. Baker empirically derived estimates of a leakage coefficient from experimental measurements

$$B = \frac{25.5\,f}{[(1452 + 3.5T)H]^{0.5}}(1.4)^n\, dB/kyd,$$

where f is the frequency (kHz), T is the temperature (°C) from NCOM, H is the duct depth (ft) computed by IAMPS, and n is the sea state, which is estimated using the World Meteorological Organization (WMO) sea state code (*e.g.* Wikipedia, 2009). The loss in the duct at long ranges can then be computed after Baker (1975) as

$$TL_{SLD} = 10 \log R + 5 \log H + 50.9 + (A + B)R,$$

where R is range in kyds, and A is the absorption coefficient

$$A = \frac{.28 f^2}{T} dB / kyd.$$

Because the radials are consistently computed, the 10log$R$ term and the constant 50.9 term in the TL equation are ignored for the provincing application. The loss was computed as in Baker (1975) and compared to the modeled prediction in the case described above. The Baker estimate differs from the predicted values for a number of potential reasons. Primarily, this estimate is empirical and while very good, the modeling that it is being compared to may not include all the physical processes going on in the real world (see discussion in Fabre *et al*, 2009). For example, this loss includes absorption in the water column and the models do not. Because this Baker parameter is consistently computed for the different environments, accurately accounts for all the mechanisms involved, and is only being used to compare environments, it is valid and has been shown to be accurate for this application.

This metric can be modified to more closely match the model by disregarding absorption, however because absorption is a valid physical phenomenon, and for simplicity, it is left in for the purposes of provincing.

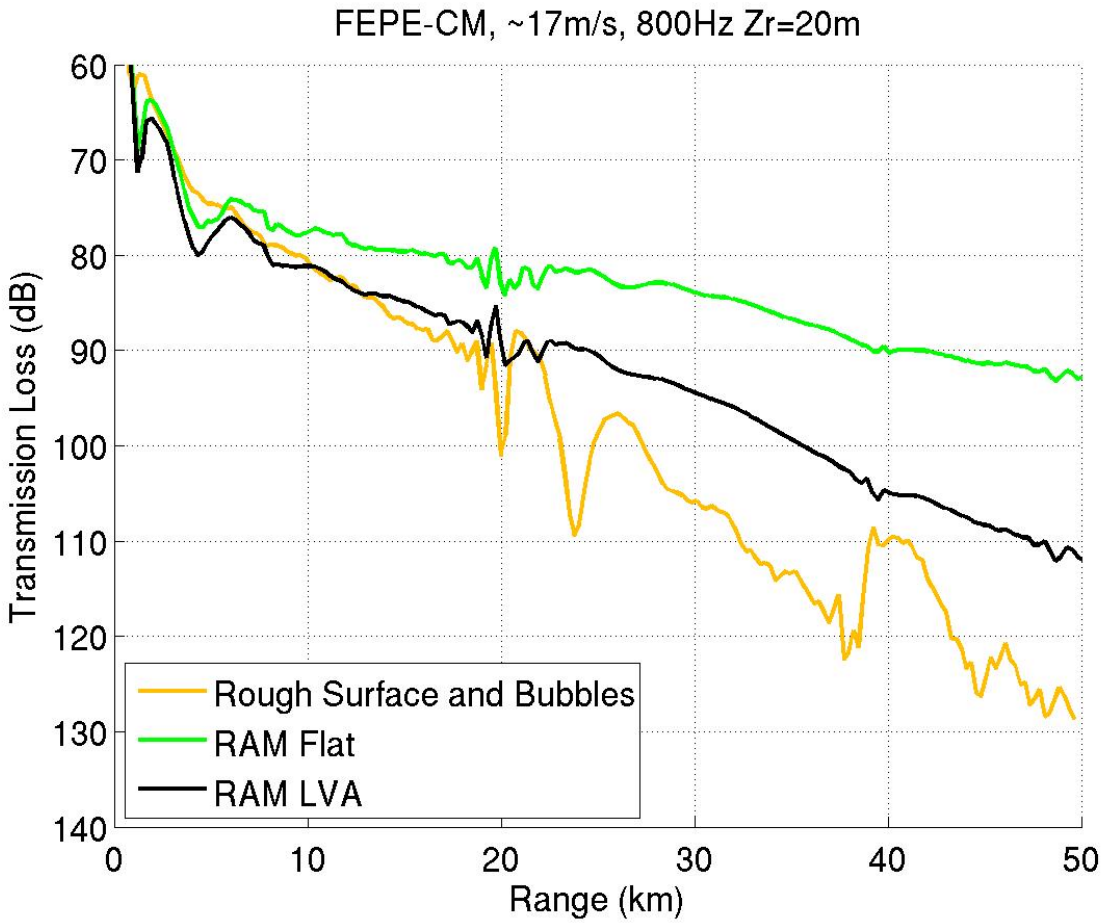

Figure 6. Modeled TL for case shown in Figure 5, but with the more realistic 17m/s wind speed. The green curve represents the loss for a flat surface, the black curve represents the loss for which the more realistic rough surface was included in the modeling. The yellow curve was generated using a research surface loss model (Norton and Novarini, 1996).

Mathematical Clustering

The critical factors provincing takes a stepped approach. First, the number of modes as a function of range is used as the cost function in the k-means clustering algorithm (Mathworks, 2009). Other mathematical clustering routines can be used, though k-means was chosen due to its availability in Matlab™ and its ease of use. The k-means algorithm takes the data and the user defined number of clusters and returns the cluster (or province) number for each data value, the centroid of the cluster and the cluster distances. The k-means centers were randomly initialized by the algorithm and the search was replicated 10 times to better converge. A faster k-means (Chen, 2009) was also implemented but proved to give provinces with spreads that were too

large. An example of the modes-versus-range cost function for a single province with 62 members is presented in Figure 7. The ordinate is the number of propagating modes computed as described above. This figure illustrates the way the k-means algorithm separates the provinces: areas of similar slope are grouped together. Initial efforts provinced on just the bathymetry, but it was found that the use of modes, and therefore the addition of sound speed and sediment properties, added significantly to the accuracy of this cost function. Figure 8 shows the TL versus range at a receiver depth of 15 m, corresponding to each member of this province. While the general shape of the mode functions for these provinces compare very well, the spread on the TL is fairly high. This will be overcome with the next step.

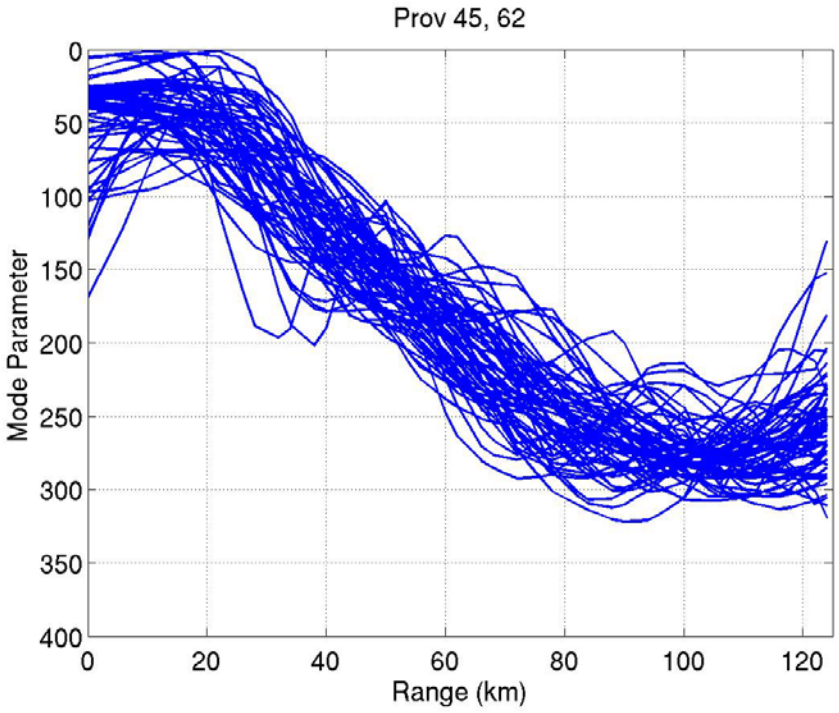

Figure 7. Example of acoustic modes versus range for a single acoustic mode province.

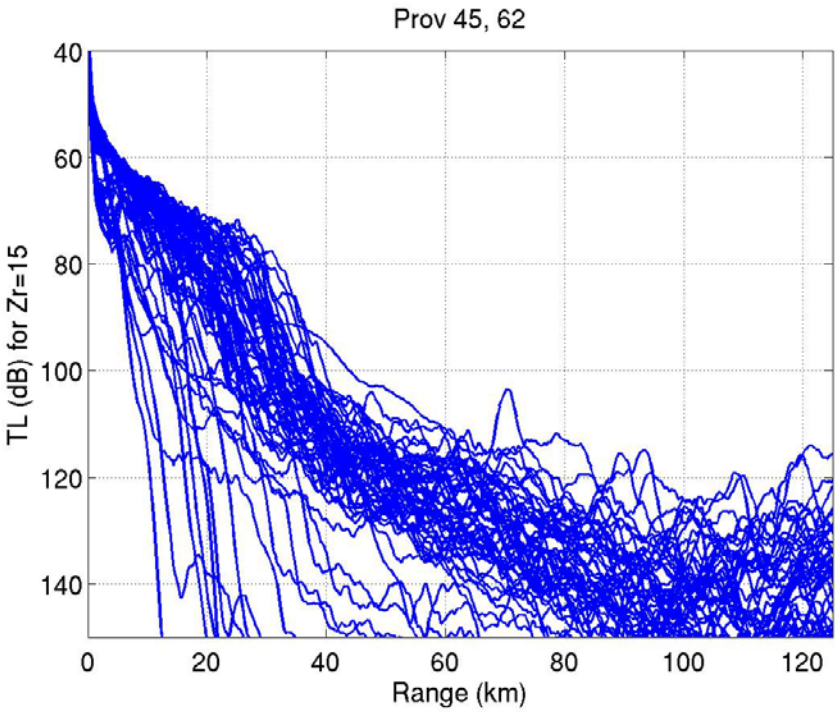

Figure 8. TL for the mode province shown in Figure 7.

The previous example is one of approximately 700 mode provinces. In order to incorporate more of the oceanographic features (or critical factors), and narrow the spread over the province, the second step in the critical factors provincing is to sub-province each of the mode provinces using the sonic layer depth cost function (described above) in the k-means clustering routine. Figure 9 shows all the SLD loss function versus range for the 62 members of the province show in Figure 7, which have not yet been sub-provinced.

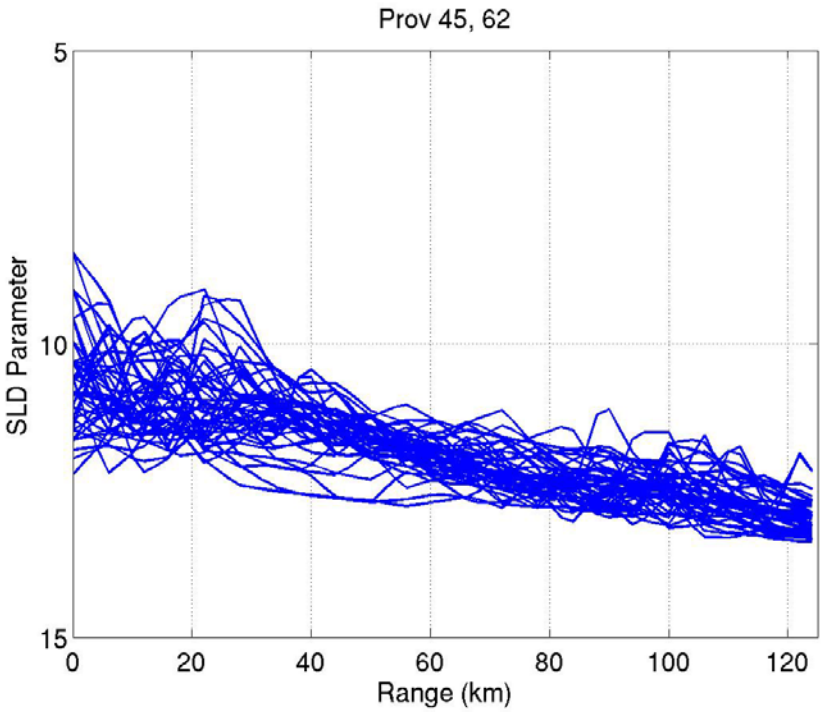

Figure 9. The SLD parameter (Baker, 1975) versus range for the mode province shown in Figure 7.

The number of sub-provinces is a constant fraction of the size of the province, usually 30-35%, therefore if a mode province has 1000 members, that province will be sub-provinced into 350 sonic layer provinces. This percentage can be reduced based on the complexity of the environment. Additionally, there are frequently provinces with no assigned value, so the number of sub-provinces is usually much smaller than this percentage, which is just used as a starting point. Figure 10 shows the SLD metric versus range for a single sub-province of the mode province shown in Figure 7, Figure 8 and Figure 9. The blue lines are the 9 members and the black line is the centroid. Figure 11 shows the corresponding mode provinces for the sub-provinced SLDs in Figure 10. The centroid is used as the representative environment, and it is one of the real environments in the province, not an average or subset. Figure 12 shows the TL for the sub-province discussed. While it looks as though the spread is large, it is largest at the high loss values, which are of not as much interest.

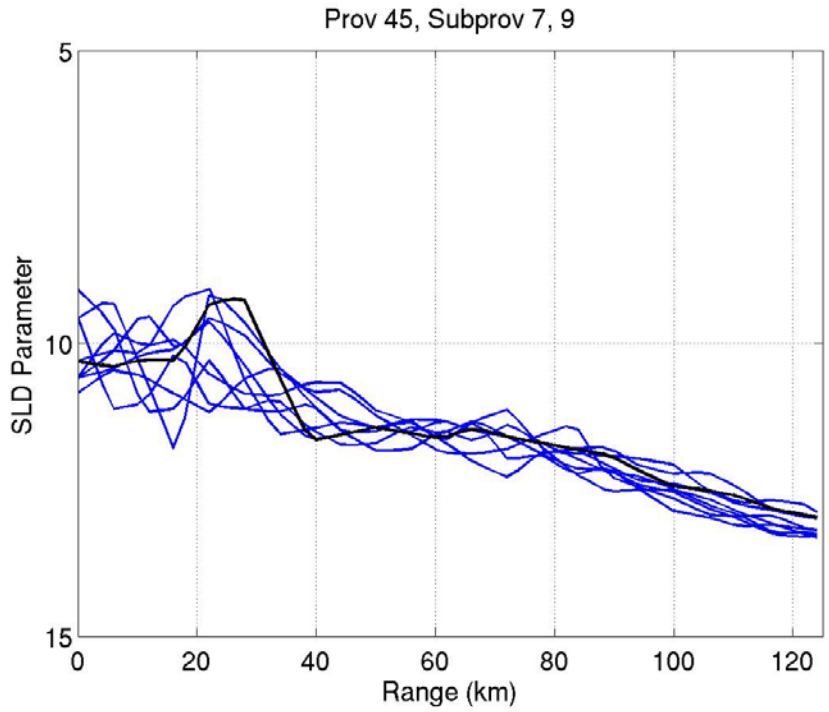

Figure 10. Example of sonic layer sub-province for a single acoustic mode province.

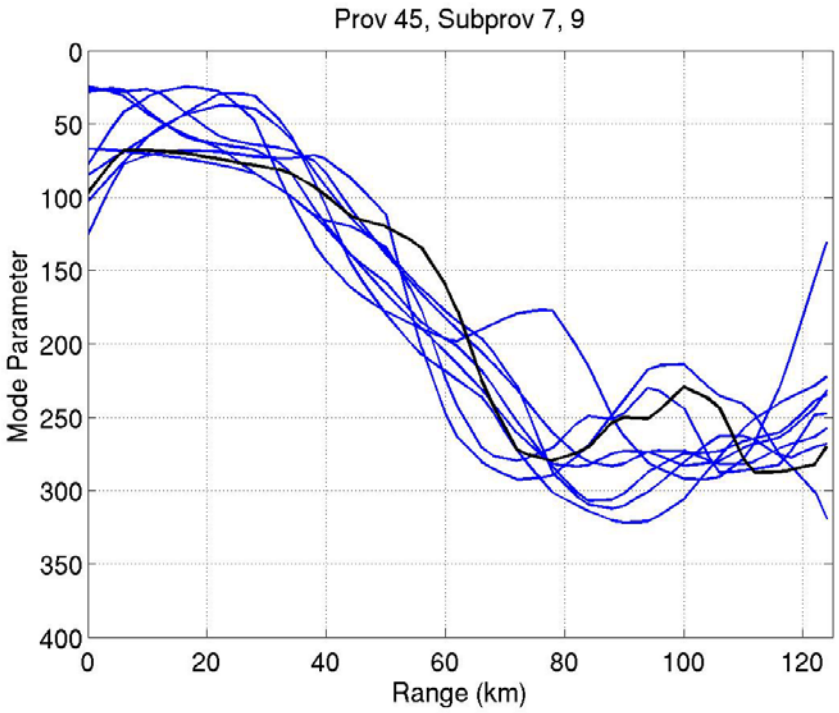

Figure 11. Subprovince of province 45 based on SLD.

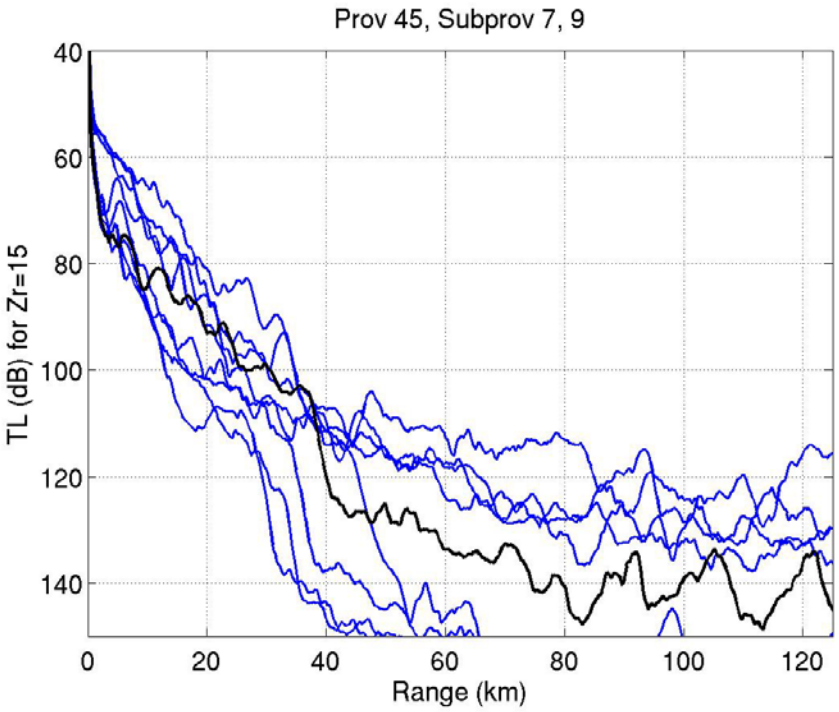

Figure 12. TL for the sub-province shown in Figure 10.

An example for another mode province is shown below. Figure 13 shows the mode function versus range for a different province with 105 members in the same area. Again these functions cluster nicely. One of the sub-provinces of this area is shown in Figure 14. The corresponding TL at a receiver depth of 15 m (in the sonic layer) for this sub-province is shown in Figure 15, which shows a very tight clustering indicating that the SLD has a strong effect in this case. This duct dependence is further evident in Figure 16 which shows the TL predictions at 150 m, below the duct. The spread is not as tight, but again varies the most at the high loss values. Single features in these range dependent curves, such as the dips in the representative curve (black line) at 25 and 50 km in Figure 16 do not generate big variations in the overall performance estimates because of the application of the FOM threshold and the area weighting a and integration over range and bearing, as discussed above.

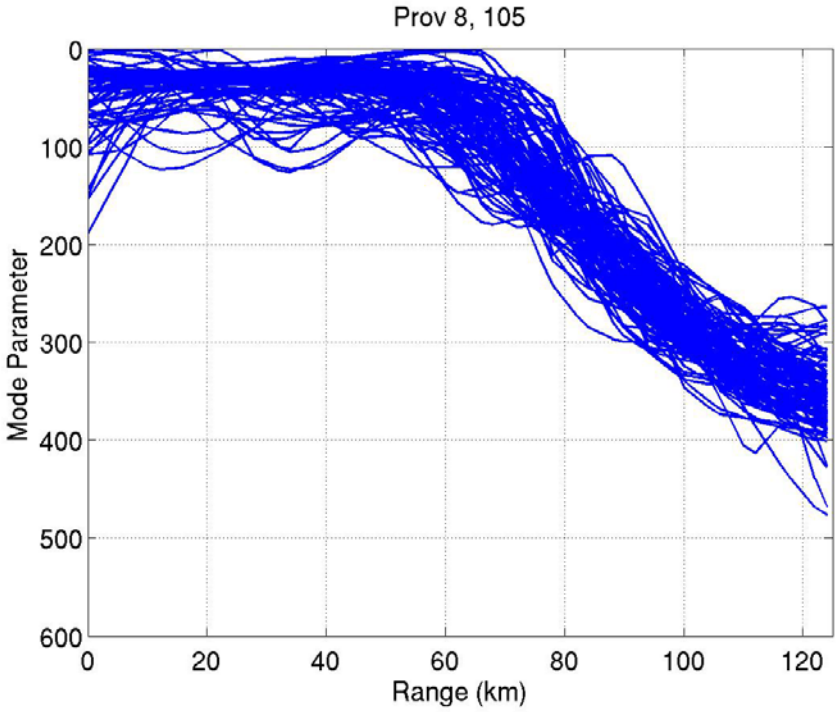

Figure 13. Mode cost function for a province with 105 members.

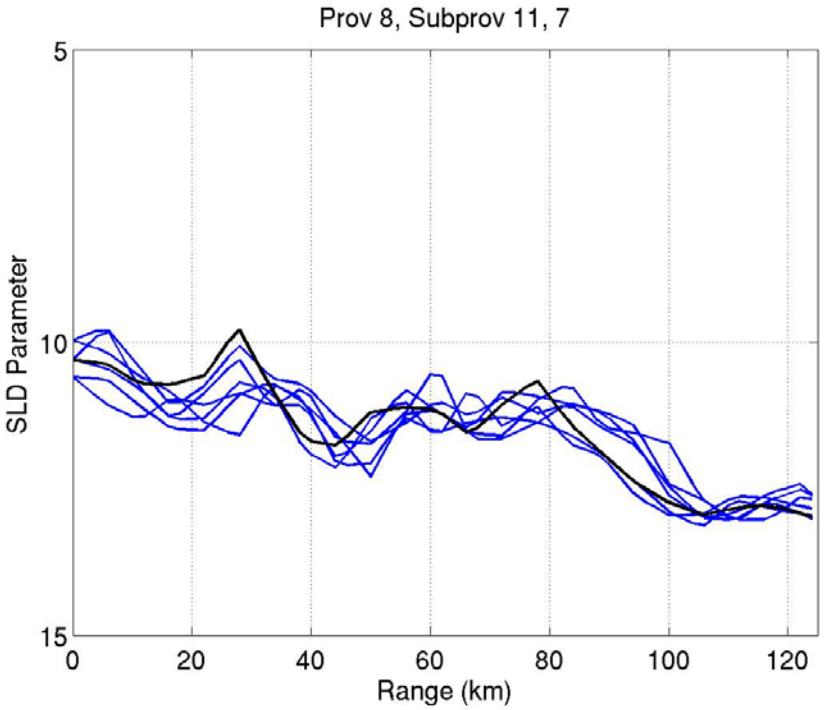

Figure 14. SLD metric versus range for a subprovince of the mode province shown in Figure 13. The black line is the representative.

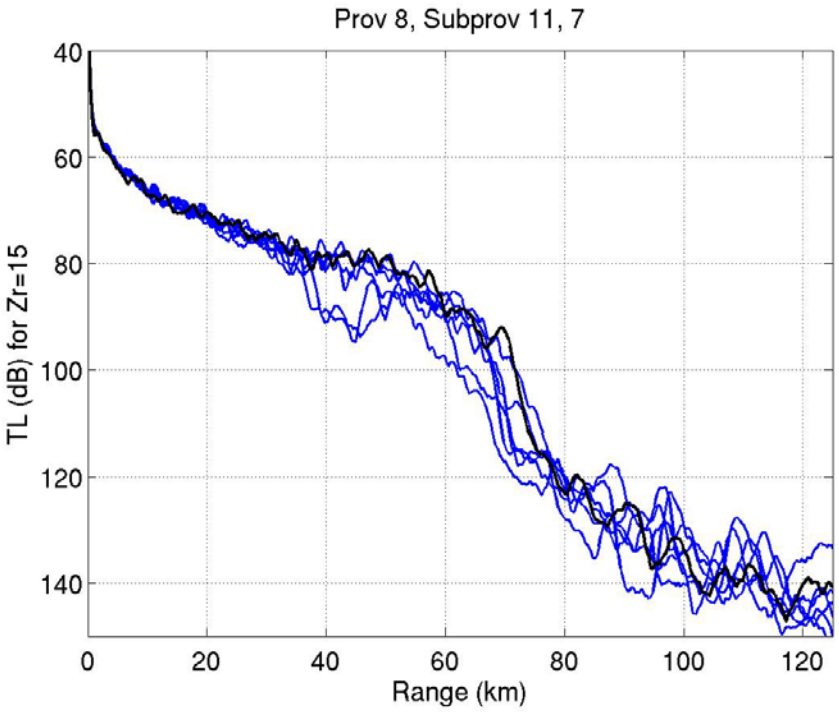

Figure 15. TL predictions at 15 m for each member of the sub-province shown in Figure 14. The black line is the representative that is used to estimate the PAC in the provinced performance prediction.

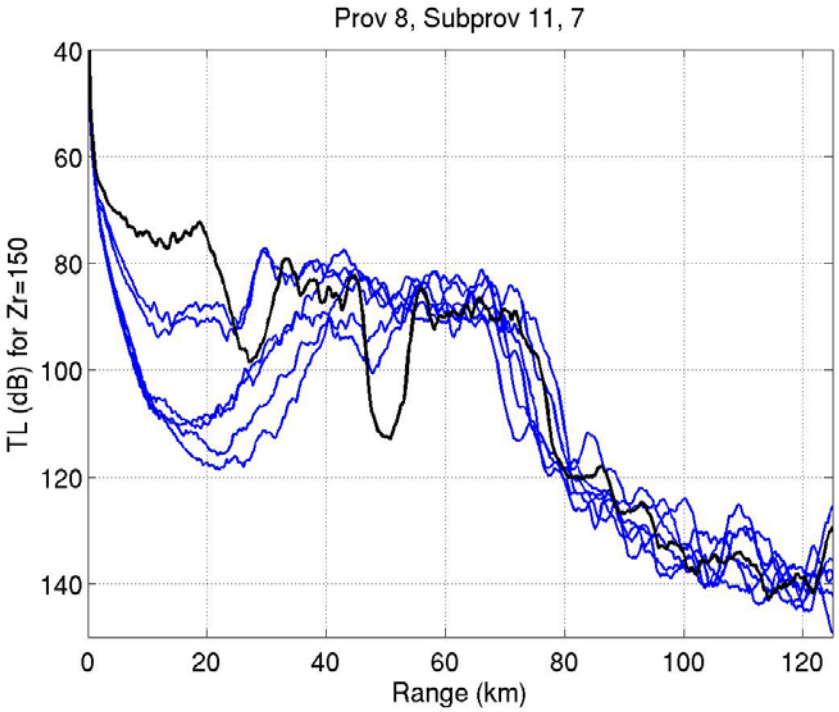

Figure 16. TL predictions at 150 m for each member of the sub-province shown in Figure 14. The black line is the representative that is used to estimate the PAC in the provinced performance prediction.

In most cases, but particularly in shallow water, there exists a province with many members that has no SLD loss, due to the lack of a duct, the source not in the duct, the frequency of interest not trapping or loss of the duct near the source range. This "no duct" province is sub-provinced using the mode cost functions.

Note that because the bathymetry-based analysis includes acoustic modes, all the provincing must be recomputed if frequency is modified. However, if the source depth changes, only the SLD-based provincing must be re-computed.

To generate PAC maps based on the critical factors provinced environments, as discussed above, the TL from the centroid of each province is substituted into all the radial locations and the acoustic PAC is computed. Results will be shown in the next chapter for multiple areas, frequencies, sources and receivers. The next section discusses an alternate environmental cost function that has been developed for future provincing applications

Environmental Parameter (Xi or ξ) Provincing

Because of the complexity of the environment and the difficulties that can arise in doing provincing and then sub-provincing, a more robust method of provincing has been devised that captures all the wave guide parameters in one environmental parameter or cost function, that can be used as the environmental cost function for provincing. An environmental parameter known as ξ is introduced during the derivation of the Airy function solution to the depth dependent portion of the wave equation (Pierce, 1991). Chin-Bing noted (2008) that this parameter contains information about the entire waveguide and could thus be compared to determine like environments and thus representative environments.

Derivation of ξ

Pierce (1991) and Chin-Bing (2008) demonstrate the Airy Function derivation of the wave equation. Starting with the wave equation

$$\nabla^2 \Phi - \frac{1}{c^2} \frac{\partial^2 \Phi}{\partial t^2} = 0,$$

where c is the speed of sound in the medium, t is time and Φ is related to acoustic pressure. The solution can be obtained using separation of variables in cylindrical coordinates, assuming azimuthal symmetry, so that

$$\Phi = R(r)Z(z)T(t),$$

where *R(r)* is the range dependent portion of the solution, *Z(z)* is the depth (*z*) dependent portion and *T(t)* is the time dependent portion. The wave equation is now

$$\frac{\partial^2\Phi}{\partial r^2}+\frac{1}{r}\frac{\partial\Phi}{\partial r}+\frac{\partial^2\Phi}{\partial z^2}-\frac{1}{c^2}\frac{\partial^2\Phi}{\partial t^2}=0.$$

Using the notation $R'=\frac{\partial}{\partial r}$ and $R''=\frac{\partial^2}{\partial r^2}$, multiplying through by $\frac{c^2}{RZT}$, and applying the separation constant -ω^2, the equation becomes

$$c^2\frac{R''}{R}+\frac{c^2}{r}\frac{R'}{R}+c^2\frac{Z''}{Z}-\frac{T''}{T}=-\omega^2.$$

The time dependent portion of the equation is

$$T+\omega^2 T=0,$$

and has two harmonic solutions with angular frequency ω. Applying a new separation constant, k_r^2 to the other half of the equation gives

$$\frac{1}{R}\left[R''+\frac{R'}{r}\right]+\frac{Z''}{Z}=\frac{-\omega^2}{c^2}=k_r^2.$$

The range dependent portion of the equation is now

$$R''+\frac{1}{r}R'+k_r^2R=0,$$

and can be solved by a fractional order Bessel function. The depth dependent portion is

$$Z''+\left[\frac{\omega^2}{c^2}-k_r^2\right]Z=0.$$

The k_r^2 term is the horizontal wave number, related to the total wave number, *k* and the mode angle, θ_0 as follows

$$k_r^2=k_0^2\sin^2\theta_0,$$

The wave number is related to the angular frequency ω and sound speed *c* by $k^2=\frac{\omega^2}{c^2}$. The depth dependent portion of the equation can then be written as

$$Z''+\left[k^2-k_0^2\sin^2\theta_0\right]Z=0.$$

Introducing the index of refraction, *n*, relating the sound speed in the layer to that in the layer above

$$n^2(z) = \frac{c_0^2}{c^2(z)},$$

the wave number can then be written as

$$k^2 = \frac{\omega^2}{c^2(z)} = \frac{\omega^2}{c_0^2}\frac{c_0^2}{c^2(z)} = k_0^2 n^2(z).$$

The depth dependent wave equation is now

$$Z'' + k_0^2\left[n^2(z) - \sin^2\theta_0\right]Z = 0$$

Assume that *c* is linear in each layer so that *c(z)* can be expressed in terms of *c*, the gradient *g* and *z* in the neighboring layer

$$g_1 = \frac{\Delta c}{\Delta z}$$
$$c(z) = c_1 + g_1 z.$$

The index of refraction is now

$$n^2(z) = \frac{c_0^2}{c^2(z)} = \frac{c_0^2}{(c_1 + g_1 z)^2} = \frac{n_0^2}{(1 + z g_1 / c_1)^2}.$$

The denominator of the previous expression can be expanded using Taylor series and higher order terms are ignored giving

$$\left(1 + \frac{g_1}{c_1} z\right)^{-2} = 1 + (-2)\left(1 + \frac{g_1}{c_1} z\right)^{-3}\Bigg|_{z=0} (z - 0)$$
$$\left(1 + \frac{g_1}{c_1} z\right)^{-2} = 1 - 2\frac{g_1}{c_1} z,$$

so the depth dependent wave equation becomes

$$Z'' + k_0^2\left[n_0^2\left(1 - 2\frac{g_1}{c_1} z\right) - \sin^2\theta_0\right]Z = 0.$$

A new variable is defined as

$$\xi = -ak_0^2(n_0^2 + gz - \sin^2\theta_0)$$
$$g = \frac{-2n_0^2 g_1}{c_1}$$

and the derivatives with *z* are recast in terms of ξ

$$\frac{\partial}{\partial z} = \frac{\partial \xi}{\partial z}\frac{\partial z}{\partial \xi} = -ak_0^2 g\frac{\partial}{\partial \xi}$$
$$\frac{\partial^2}{\partial z^2} = \frac{\partial}{\partial z}\frac{\partial \xi}{\partial z}\frac{\partial z}{\partial \xi} = a^2 k_0^4 g^2 \frac{\partial^2}{\partial \xi^2}.$$

Next the depth dependent wave equation is rewritten in terms of ξ vice *z*

$$a^3 k_0^4 g^2 \frac{\partial^2 Z}{\partial \xi^2} - \xi Z = 0.$$

define *a* as

$$a^3 = \frac{1}{k_0^4 g^2}$$
$$a = k_0^{-4/3} g^{-2/3},$$

so now ξ is

$$\xi = -k_0^{2/3} g^{-2/3}(n_0^2 + gz - \sin^2\theta_0),$$

and the depth dependent wave equation is

$$\frac{\partial^2 Z}{\partial \xi^2} - \xi Z = 0,$$

which is an Airy equation and can be solved using Airy functions. The importance to acoustic provincing is the argument ξ. It is a parameter that casts the environment in a way that indicates the acoustic response. It is a function of all the pertinent environmental and acoustic system parameters and provides a formal link between the environment and the acoustic pressure. A variation of this term will be used to province the environment.

Because ξ is dependent on normal mode angles θ_0 and eigenvalues *k*, and therefore individual modes, the modal dimensionality can be large and must be reduced. The angles will be "bundled" based on their interactions; that is, surface interacting angles, volume or non-

boundary-interacting angles and bottom interacting angles are "bundled" together as indicated in Figure 17, so that ξ will have a reduced dimensionality in θ_0 and k_0.

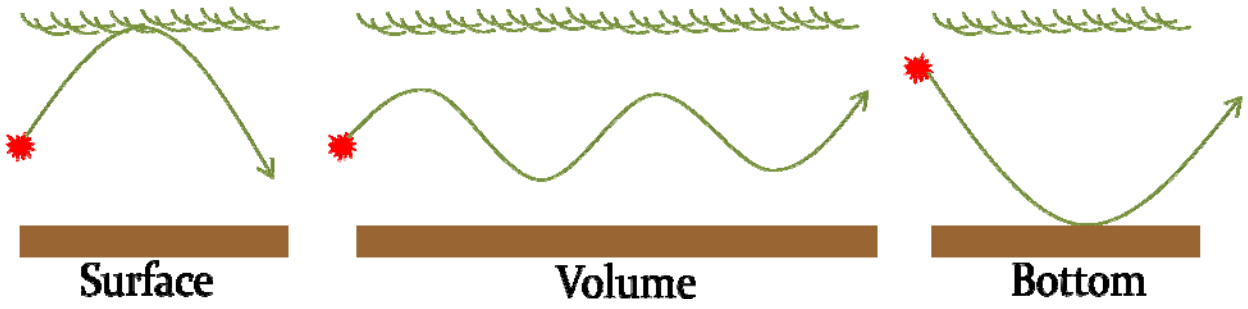

Figure 17. Mode bundling illustration.

The vertical gradients are then examined and layers with similar gradients are merged in order to reduce the depth dimensionality. Now, for each energy bundle *m*, on the reduced depth grid, the environmental parameter is

$$\xi = -\left[\frac{k_m}{g}\right]^{2/3}(n_0^2 + gz - \sin^2\theta_m).$$

This parameter is used in place of the critical factors cost function described above. Changes in pressure (or TL) can be analytically mapped in terms of ξ,

$$\Delta P = P^{(2)} - P^{(1)} = \sum_m \left(\xi_m^{(2)} - \xi_m^{(1)}\right)\frac{\partial P}{\partial \xi_m}\bigg|_{\xi_m = \xi_m^{(1)}},$$

and a metric or tolerance (ϑ) for the environmental acoustic parameter will determine the limiting acceptable variation in the transmission loss or pressure

$$-\vartheta < \sum_m \left(\xi_m^{(2)} - \xi_m^{(1)}\right)\frac{\partial P}{\partial \xi_m}\bigg|_{\xi_m = \xi_m^{(1)}} < \vartheta.$$

Preliminary Acoustic Mode Bundling

Another method of solving the wave equation is by tracing rays of sound and using the index of refraction (or sound speed gradients) to determine how the rays, launched at various angles from the source, travel through the media. Ray tracing is generally valid at higher

frequencies (*e.g.* GRAB, Keenan, 2000), but is used in various applications to determine arrival angles, ducts, etc. As noted above, ξ is dependent on mode and therefore angle. The number of modes can be significant in deep water or at mid to high frequencies, so to make the problem more tractable, the modes are grouped into bundles based on their interactions. This methodology is loosely based on the ASTRAL model (Spofford, 1979). ASTRAL begins with a range dependent, finite ocean with boundary conditions and a sound speed that is linear in the squared refractive index ($n^2 = c^2(z_2)/ c^2(z_1)$). The normal mode solution to the wave equation (*e.g.* Pierce, 1991) expresses the pressure, or intensity as a sum over modes of the normal mode depth functions. ASTRAL groups these modes and averages them into smoothed modes or smodes based on their ray angles measured relative to the axis of minimum sound speed. Because the ASTRAL mode grouping is complicated, to prove the concept here before applying this complex methodology, a ray model, Bellhop written by Mike Porter (Rodriguez, 2008) is run to obtain the rays that hit the surface and the bottom and the rays that do not interact with the boundaries (volume rays). Figure 18 shows an example Bellhop decimated ray trace for a 500 m source at 100Hz for a simple environment. The rays are color coded to identify the interactions, blue rays hit the bottom only, cyan (light blue) rays hit the surface only and red are the volume rays.

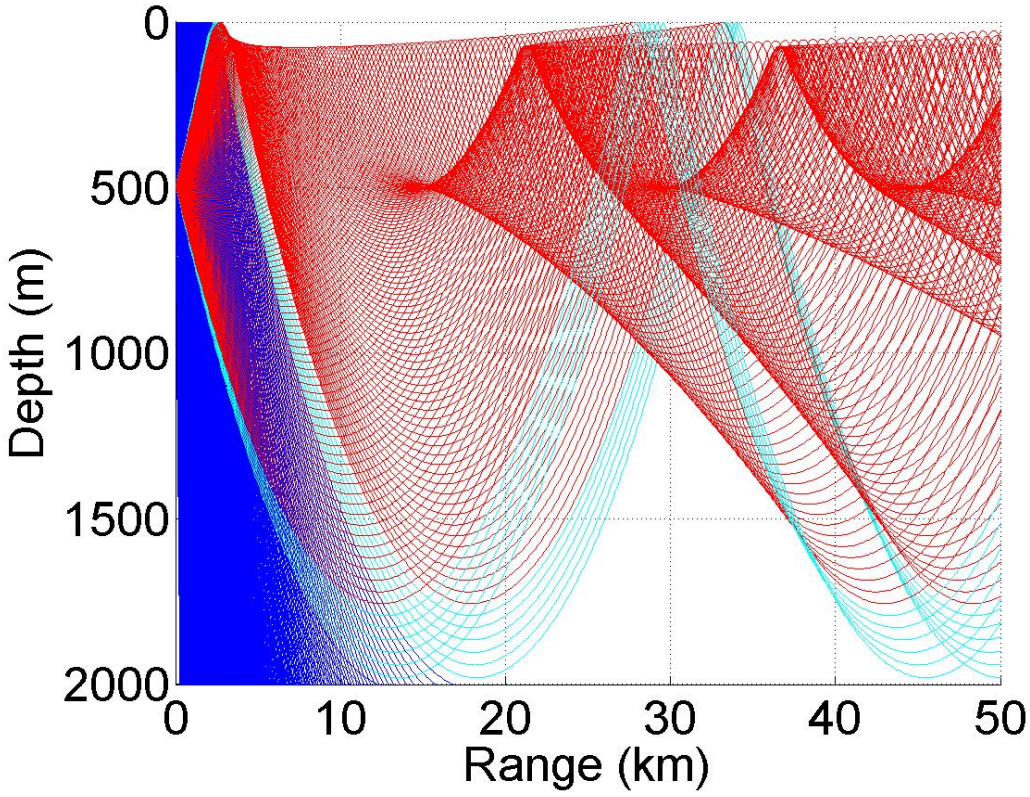

Figure 18. Example Bellhop decimated raytrace for a deep water test case, with a source at 15 m. Blue rays hit the bottom only, cyan rays hit the surface only and red are the volume rays.

Because ξ is based on modes, not rays, the Kraken model was also run (again to prove the concept) for each case to produce only the horizontal wavenumbers and the mode amplitude functions. The turning values of the rays from Bellhop are then converted to wavenumbers. The relationship between angle and wavenumber is

$$k_r = \frac{2\pi f}{c_{z_s}} \cos\theta_0,$$

where θ_0 is the launch angle measured from the horizontal and c_{zs} is the sound speed at the source. There are 948 modes in this case.

The ξ parameter is computed for every mode and depth in the problem. Figure 19 shows the magnitude of ξ as a function of wavenumber, k and depth, down to the bottom, approximately 2000 m for this example. The ξ is then reduced to three dimensions in the modal dimension. These values are still a function of a large number of depths.

In order to reduce the depth dimensionality, the gradient turning points are sought with a simple derivative test, and the values of ξ are linearized with depth between those points. This reduced ξ, which in this example is now an array of 4x23 (from the original 948x401, which gets larger with frequency and depth).

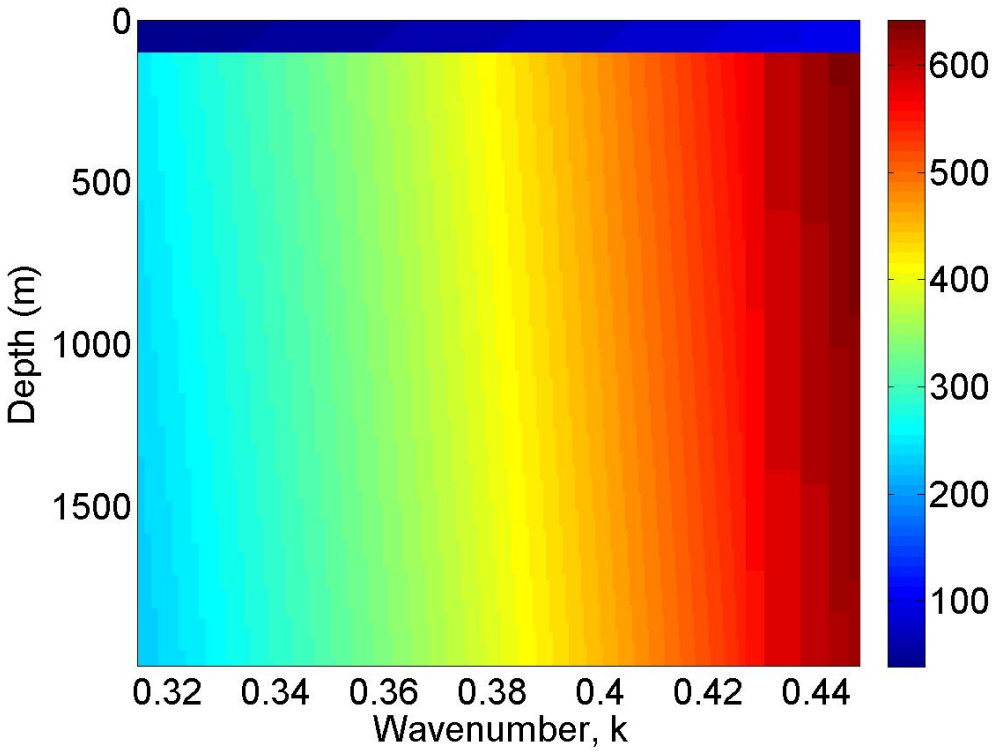

Figure 19. ξ as a function of wavenumber (*k*) and depth (m).

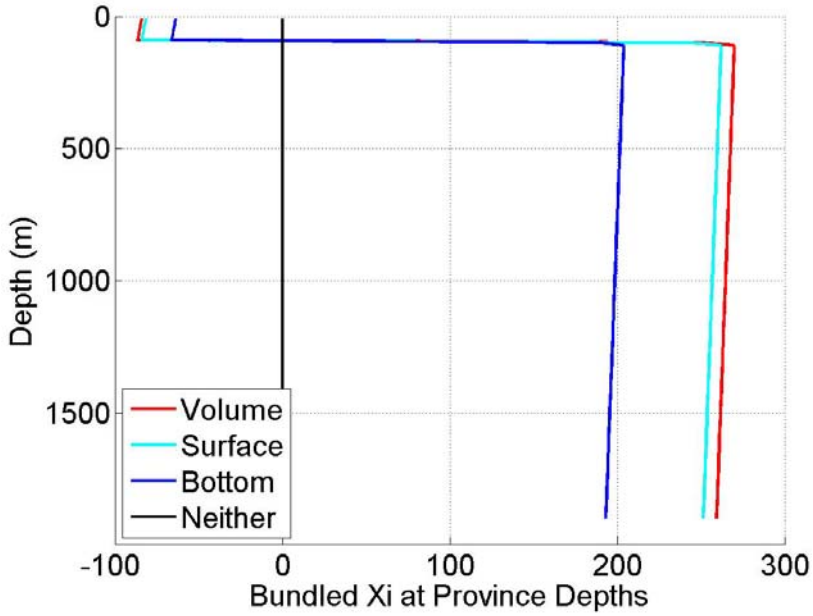

Figure 20. ξ after being grouped into volume, surface and bottom interacting "bundles", and reduced to the fixed depths.

The mathematical clustering routine requires as input (cost function) equal length vectors. That is, the cost function vectors must all have the same number of values. For the critical factors provincing, this was a minor issue because the environmental parameters were estimated as a function of range, and the maximum range could be, and was fixed. As evident in the discussion above, the ξ function has 4 fixed dimensions in the mode dimension, but the depth dimension will vary in length with water depth. Therefore the next challenge is to formulate the cost function in a format sufficient for the clustering routine. For this application the mode dimensions is fixed at 4 and the number of depth dimensions is set to 57. If an environment has fewer depth regimes, the values below the deepest depth are set to 0, and if an environment has more depth regimes, the deeper regimes with similar gradients in ξ are combined. The depths are spaced at 10 m from 0 to 200 m, at 50 m from 250 to 1000 m, at 100 m to 2000 m and at 1000 m to 11000 m. The bundled ξ at the standard province depths is shown in Figure 20, and color coded as the rays are above. Once this 4x57 array is constructed, it is unfolded to be a 1x228 length vector, where the first 4 values are the first value of each mode bundle. The array is unwrapped in that way and becomes the cost function for the clustering routines. Results for a simple case and a small canonical data set are given in the next chapter.

Range Dependent ξ

Because of the importance of using a range dependent description of the environment (*e.g.* Dennis and Fabre, 2007) the range independent development of ξ must be expanded to become range dependent. In future work, standard coupling techniques can be modified to compute coupling matrices for the energy bundles and the coupling intervals can be extended until there is a significant change. In this development, each range step from the source contains information about the ensonification and relation to the previous range set of normal mode bundles. The result is a coupled environmental range dependent parameter that will be input to the clustering algorithm as the cost function.

Chapter 3. Results

The critical factors provincing is applied here to several areas at several frequencies and source depths. Preliminary results using the range independent ξ cost function are presented and the concept is proven.

Critical Factors Provincing

Acoustic coverage (PAC) maps are generated for several areas, then critical factors provincing is computed and coverage maps are generated using the province representatives as discussed previously. The brute force and provinced PAC maps are compared for a number of areas and are presented here. Three frequency regimes, low frequency (250 Hz), mid-frequency (1000 Hz) and high frequency (3000 Hz) were computed and are presented.

TL was computed for all radials so that the brute force coverage could be computed for comparison purposes. As discussed previously, once the representatives were computed, a representative TL from each province is used in place of each member of the province to compute the area-wide coverage. For practical applications, the TL only needs to be run for the representatives.

Okinawa Trough

NCOM oceanographic analysis from an area in the Western Pacific Ocean near the Okinawa Trough (Barron *et al*., 2009) from October, 2007 was used to generate provinces and acoustic coverage. Bathymetry from DBDB-V (NAVO, 2007) for this area is shown in Figure 21 and the SLD and cutoff frequency computed using the NCOM analysis for this time snapshot are shown in Figure 22. This area contains multiple bathymetry regimes, shallow water in the northwest corner, and a fairly deep trench running from the southwest corner to the northeast corner. The sonic layer is spotty and is as deep as 100 m in some areas. The cutoff frequency is fairly low throughout the area, indicating that most frequencies will be trapped when a duct is present.

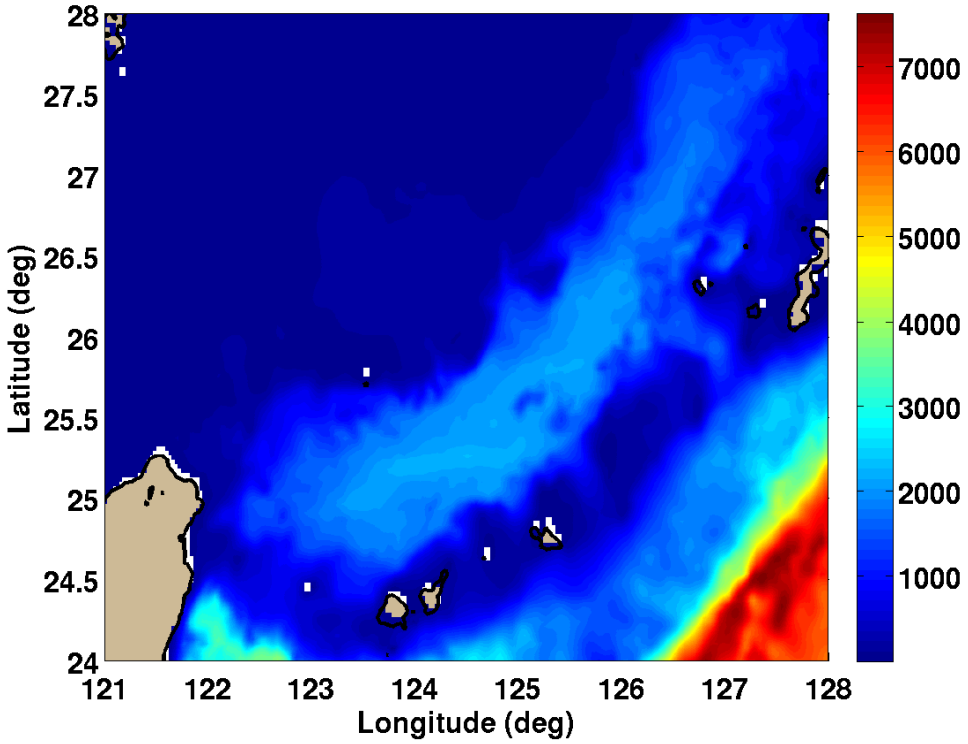

Figure 21. DBDB-V bathymetry in m for the Okinawa Trough area of interest.

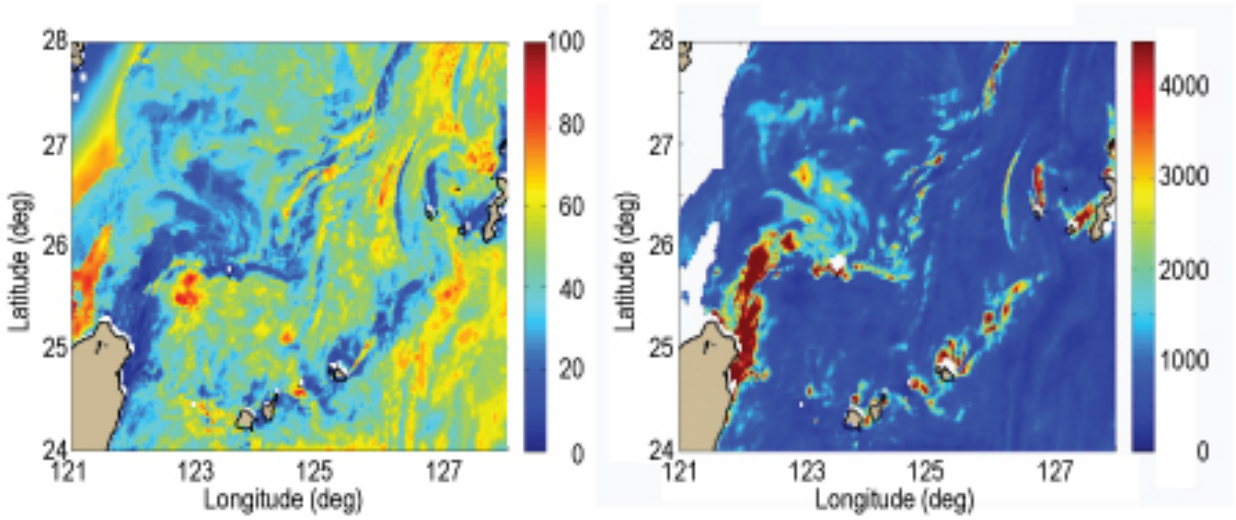

Figure 22. Sonic layer depth in m (left) and cutoff frequency in Hz (right) for Okinawa Trough area of interest.

Low Frequency

For the low frequency (250 Hz) acoustic predictions, three source depths were computed: 15 m so that if there is a layer, the source will be in it, 60 m, which will be in the layer some of the time; and 150 m, primarily below the layer. The total number of acoustic radials (TL predictions) used to compute coverage for this case (8 radials per grid point) is 14,720. The provincing identified 4,860 representative radials resulting in a computational savings of approximately 3-fold. Figure 23 shows the provinced results for this low frequency case. The coastline, plotted in black, for this and all subsequent figures is from ETOPO2 (NGDC, 2006). Each province is plotted as a different color. There are not enough colors in the pallet to show all the unique provinces, however, this gives a good view of the provinced results and indicates that the provinces fall along the areas of similar slope, that is they follow isobaths, as expected.

The left plots in Figure 24, Figure 26, Figure 28, Figure 30 and Figure 32 show the PAC computed using the brute force (14,720 TL predictions) method for the shallow source and receivers at 10, 15, 20, 150 m and 250 m, respectively. Other receivers were computed, but are not shown due to their similarity to the figures presented. The right plots in Figure 24, Figure 26, Figure 28, Figure 30 and Figure 32 show the corresponding PAC estimates using only representatives (4,860 TL predictions) from each province. In order to quantify the difference between the two surfaces, the difference between brute force coverage and PAC at each point is computed, and a boxcar average of the difference at each point and its eight neighbors is done. This somewhat captures the possibility of features being geographically displaced. Figure 25, Figure 27, Figure 29, Figure 31 and Figure 33 show this difference for the 15 m source and the 10, 15, 20, 150 m and 250 m receivers, respectively. These all represent differences of less than 10% and in most cases, less than 5%. That is, the PAC predictions made using the representative environments yield results within 90%-95% of the brute force answer. So for much less computation time, a very good estimate of the performance over the area is obtained.

The PAC computed using a deeper source (60 m) that is less frequently in the sonic layer, for similar receiver depths are shown in Figure 34, Figure 36, Figure 38 and Figure 40. The left side of these figures again show the brute force prediction and the right side shows the PAC generated using representatives. Figure 35, Figure 37, Figure 39 and Figure 41 show the boxcar averaged differences for this 60 m source depth for the 10 m, 15 m, 20 m and 150 m receivers, respectively. Results for the deepest source (150 m) well below the sonic layer is shown in

Figure 42 and Figure 43. These results are typical of a source at this depth, which is dominated by the waveguide mode parameter rather than the SLD loss parameter due to the proximity of the duct. Again, all results show less than 10% difference. Table 1 summarizes the maximum and mean differences for the OT AOI at 250Hz, shown in the boxcar averaged difference plots. The overall coverage features compare very well for both source depths. The provincing algorithm captures the broad shape of the coverage features, but does miss some of the finer scale details. The overall differences do not exceed 7% of the area in this case and are acceptable. The way this sort of display is used is to identify areas of relatively better acoustic performance for planning purposes. Once these broad areas of performance are identified, finer scale analysis in smaller areas, can be done with the full modeling capability. Therefore using the representatives to generate the performance estimates indicates a significant advance in the capability, as it allows more time and therefore more predictions to be available for the detailed analysis.

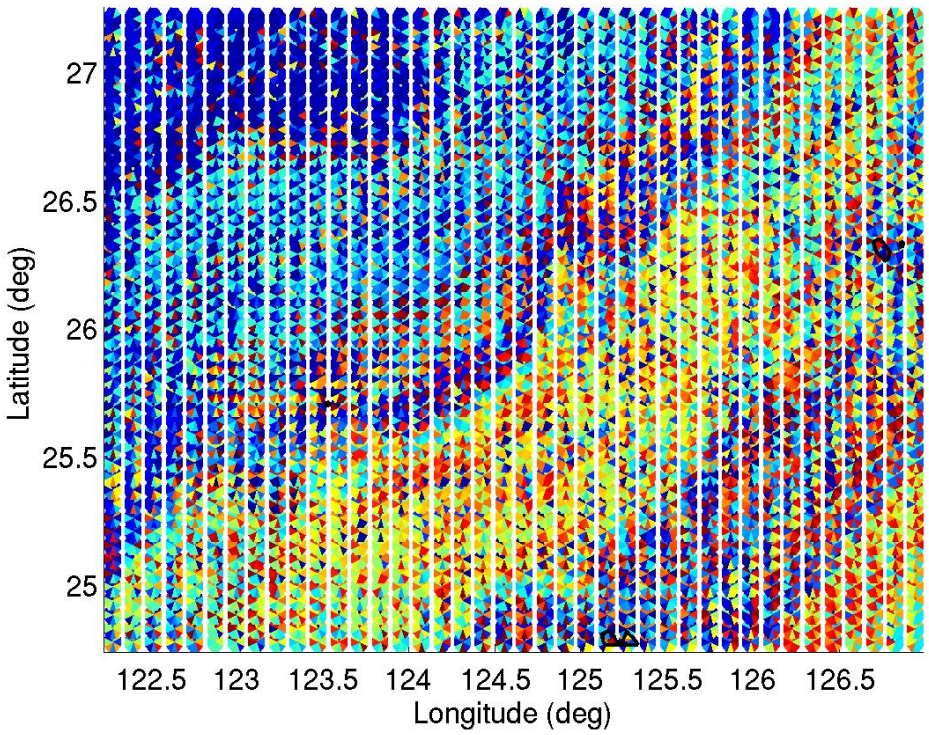

Figure 23. Low frequency mode provinces for the Okinawa Trough area.

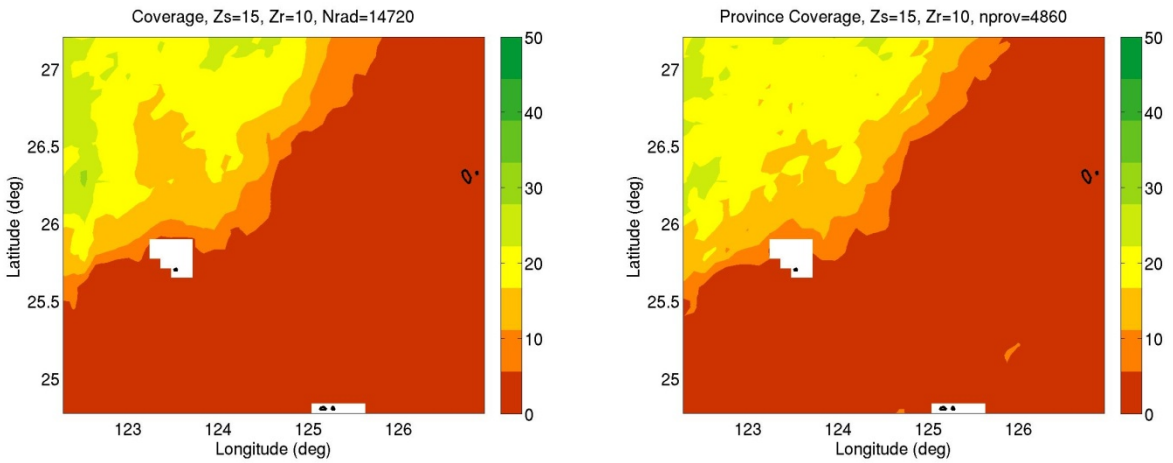

Figure 24. Brute force (left) and critical factors representative environment (right) PAC for 250 Hz, source at 15 m, receiver at 10 m.

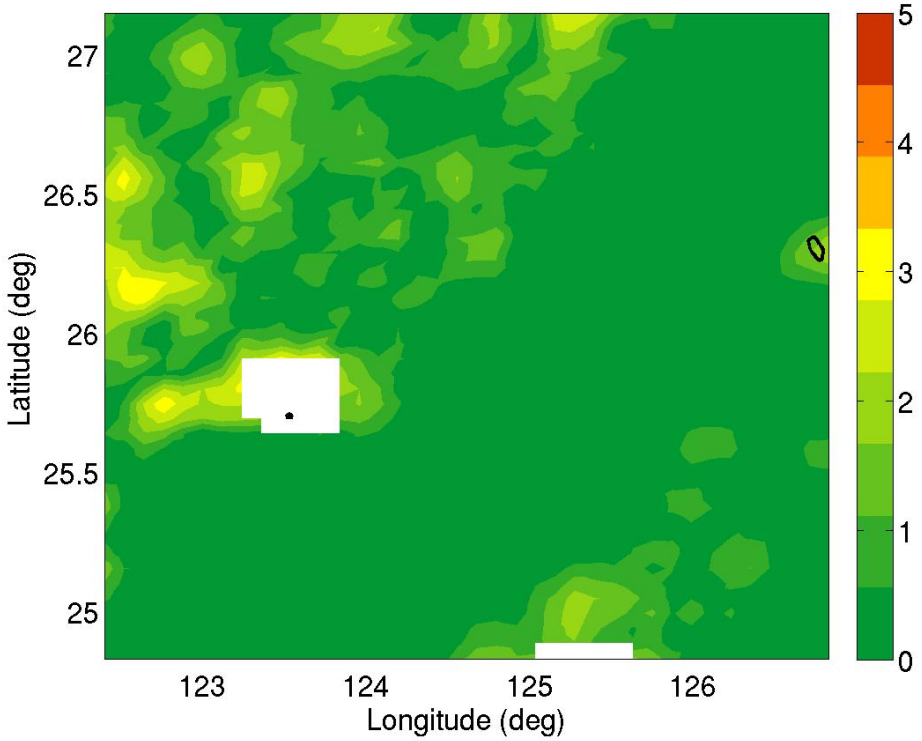

Figure 25. Averaged difference in percent between brute force and critical factors representative environment PAC for 250 Hz, source at 15 m, receiver at 10 m.

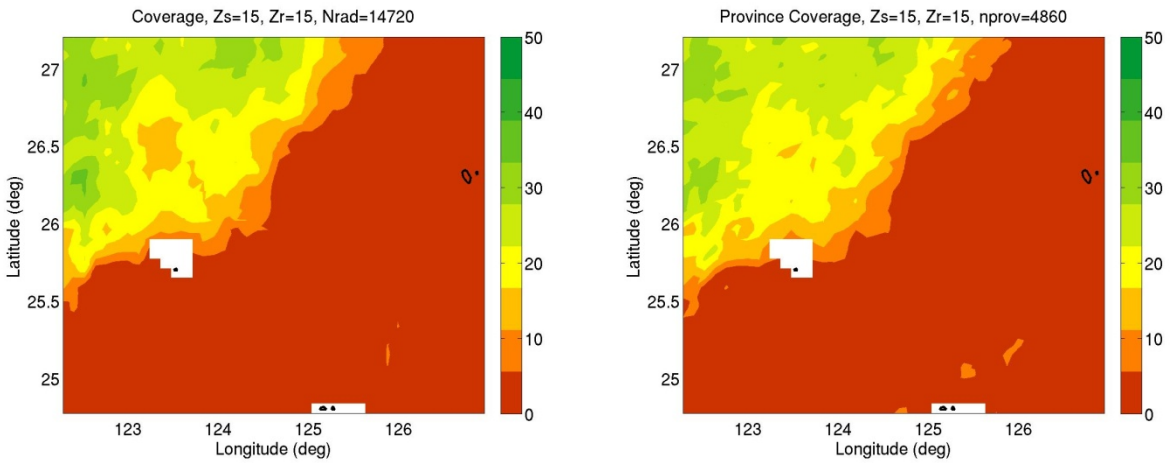

Figure 26. Brute force (left) and critical factors representative environment (right) PAC for 250 Hz, source at 15 m, receiver at 15 m.

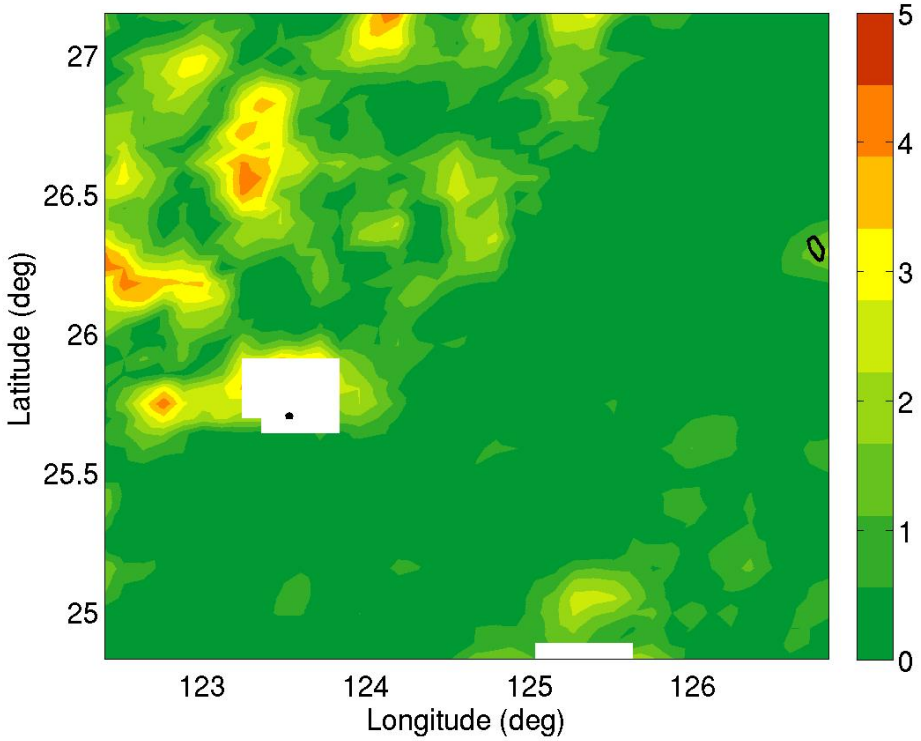

Figure 27. Averaged difference in percent between brute force and critical factors representative environment PAC for 250 Hz, source at 15 m, receiver at 15 m.

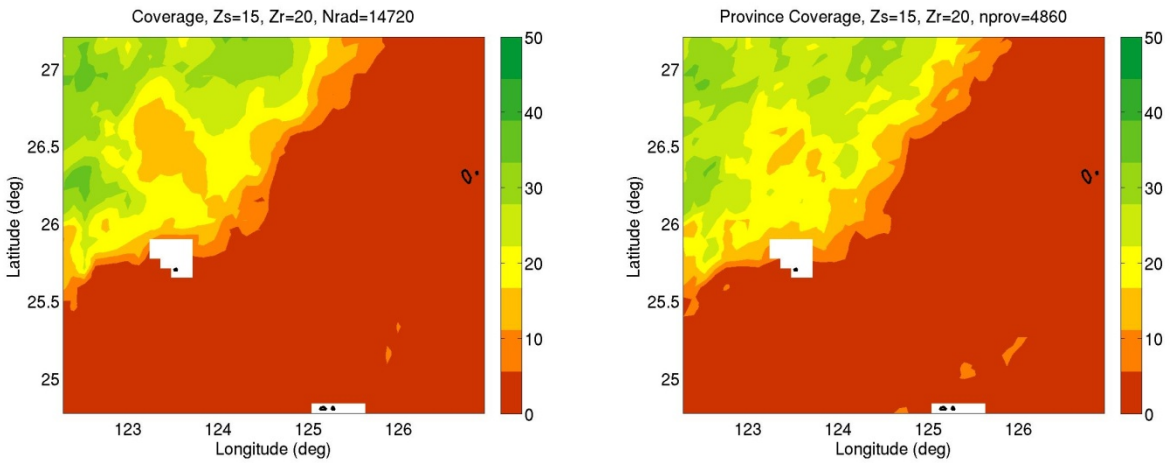

Figure 28. Brute force (left) and critical factors representative environment (right) PAC for 250 Hz, source at 15 m, receiver at 20 m.

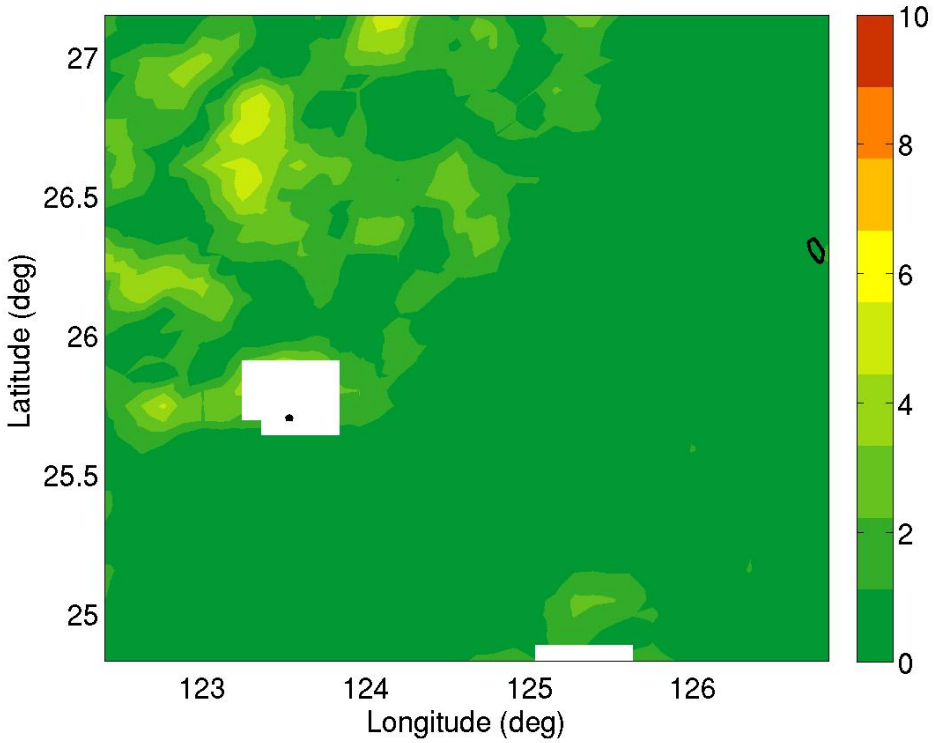

Figure 29. Averaged difference in percent between brute force and critical factors representative environment PAC for 250 Hz, source at 15 m, receiver at 20 m.

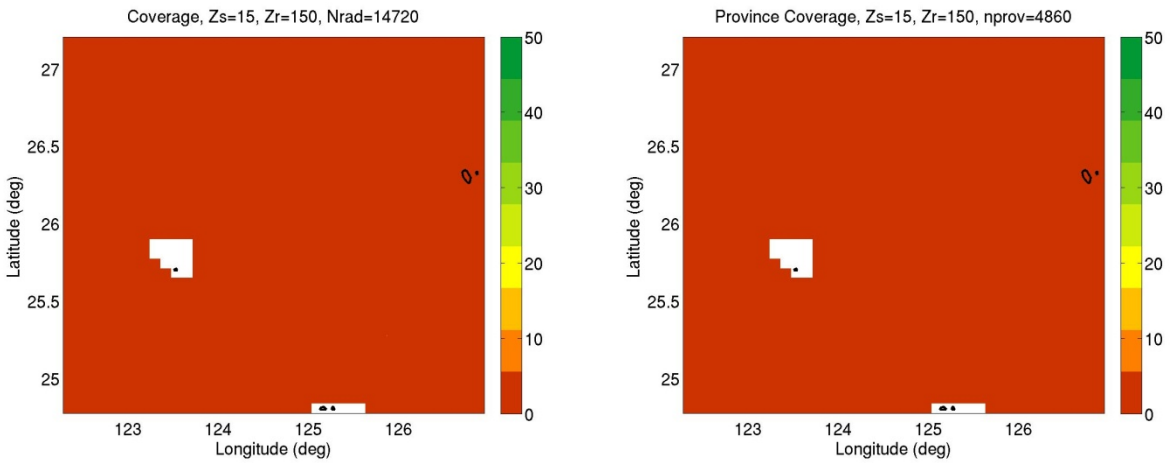

Figure 30. Brute force (left) and critical factors representative environment (right) PAC for 250 Hz, source at 15 m, receiver at 150 m.

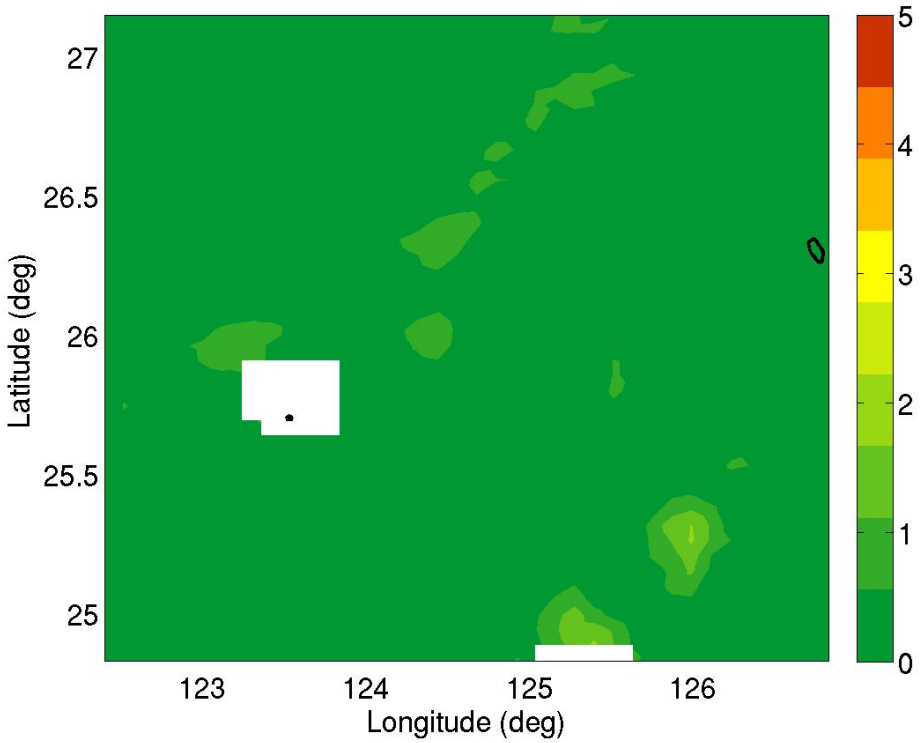

Figure 31. Averaged difference in percent between brute force and critical factors representative environment PAC for 250 Hz, source at 15 m, receiver at 150 m.

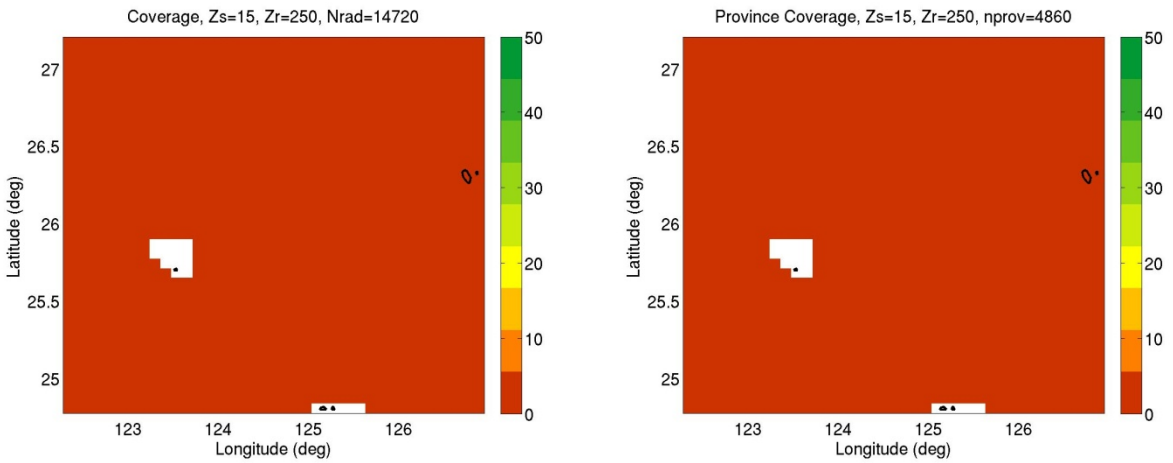

Figure 32. Brute force (left) and critical factors representative environment (right) PAC for 250 Hz, source at 15 m, receiver at 250 m.

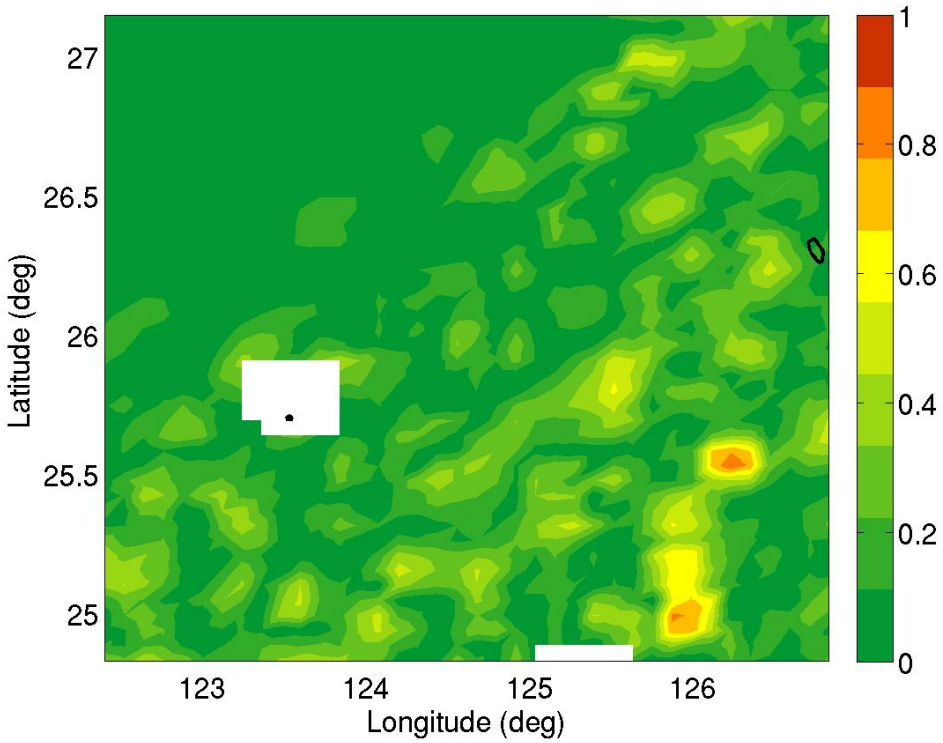

Figure 33. Averaged difference in percent between brute force and critical factors representative environment PAC for 250 Hz, source at 15 m, receiver at 250 m.

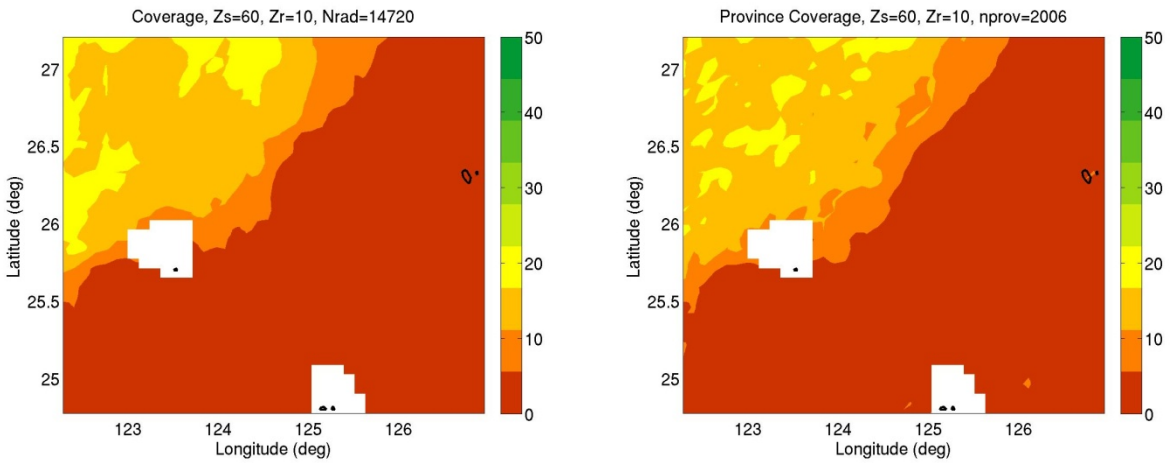

Figure 34. Brute force (left) and critical factors representative environment (right) PAC for 250 Hz, source at 60 m, receiver at 10 m.

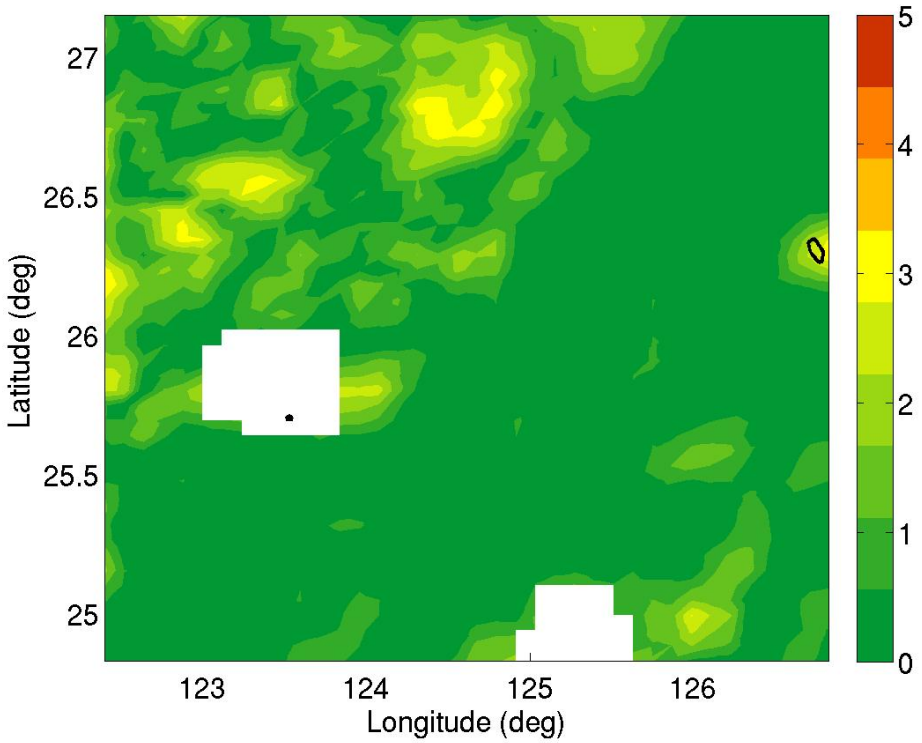

Figure 35. Averaged difference in percent between brute force and critical factors representative environment PAC for 250 Hz, source at 60 m, receiver at 10 m.

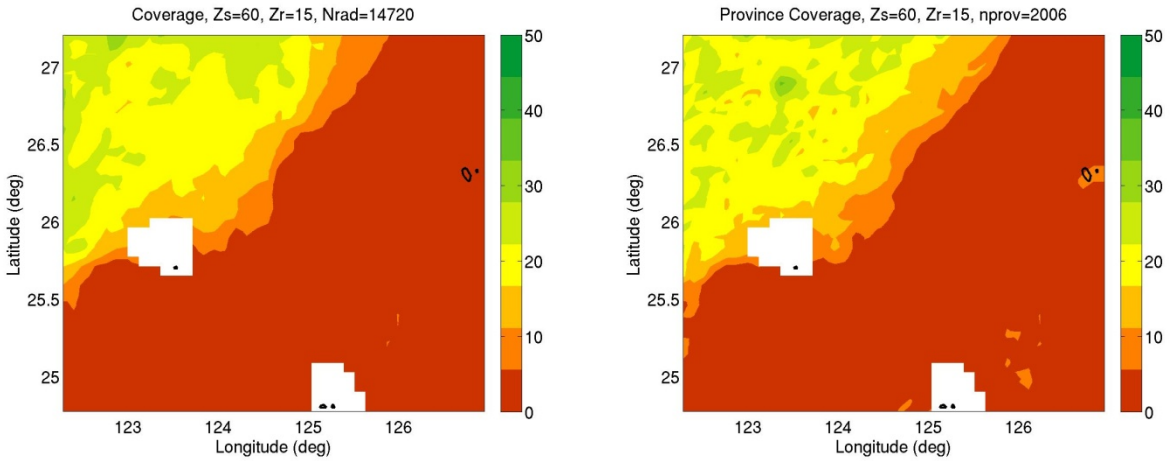

Figure 36. Brute force (left) and critical factors representative environment (right) PAC for 250 Hz, source at 60 m, receiver at 15 m.

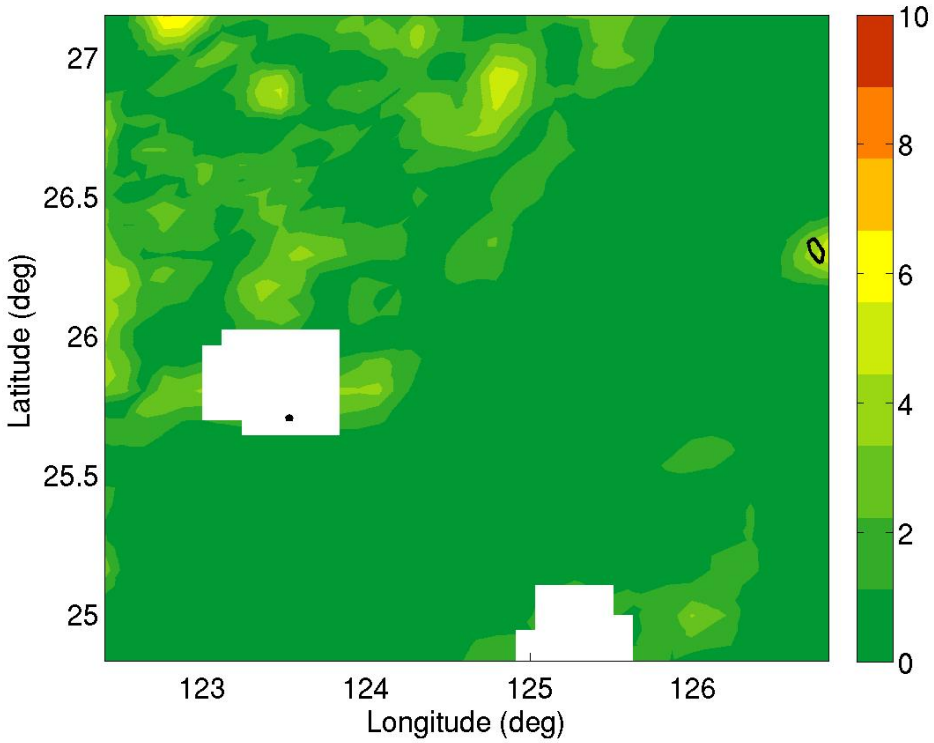

Figure 37. Averaged difference in percent between brute force and critical factors representative environment PAC for 250 Hz, source at 60 m, receiver at 15 m.

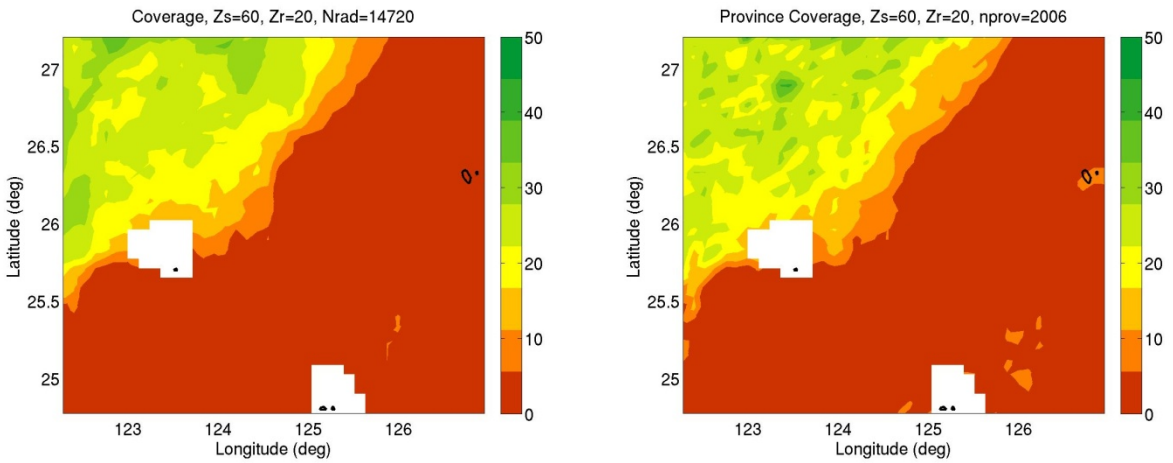

Figure 38. Brute force (left) and critical factors representative environment (right) PAC for 250 Hz, source at 60 m, receiver at 20 m.

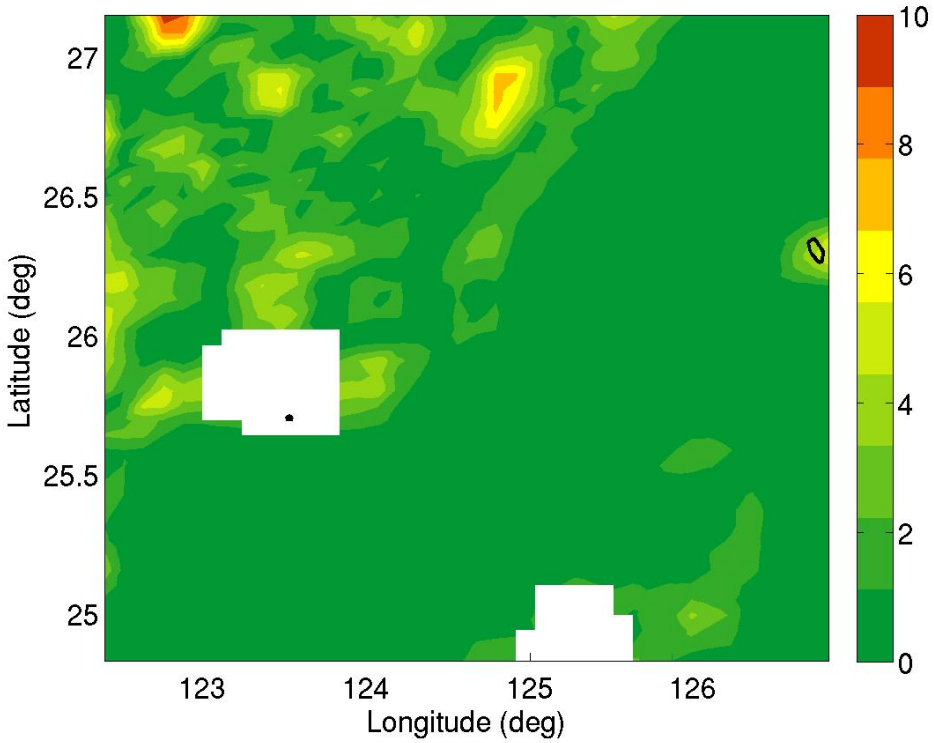

Figure 39. Averaged difference in percent between brute force and critical factors representative environment PAC for 250 Hz, source at 60 m, receiver at 20 m.

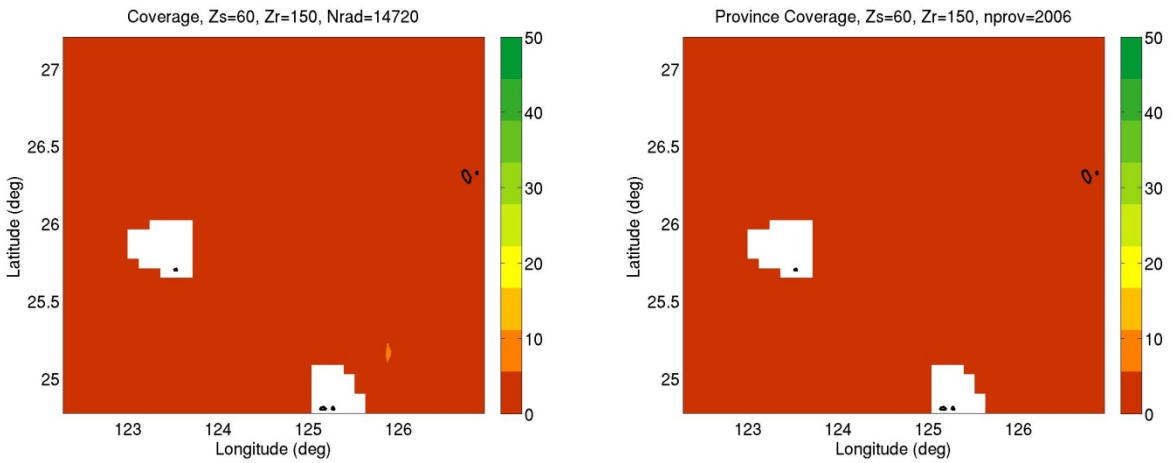

Figure 40. Brute force (left) and critical factors representative environment (right) PAC for 250 Hz, source at 60 m, receiver at 150 m.

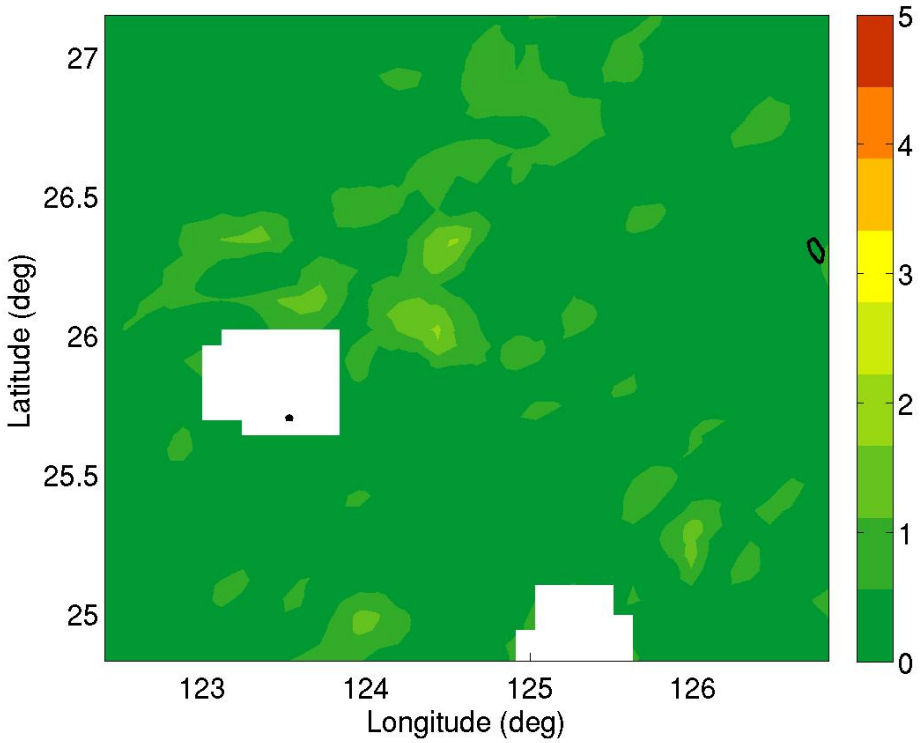

Figure 41. Averaged difference in percent between brute force and critical factors representative environment PAC for 250 Hz, source at 60 m, receiver at 150 m.

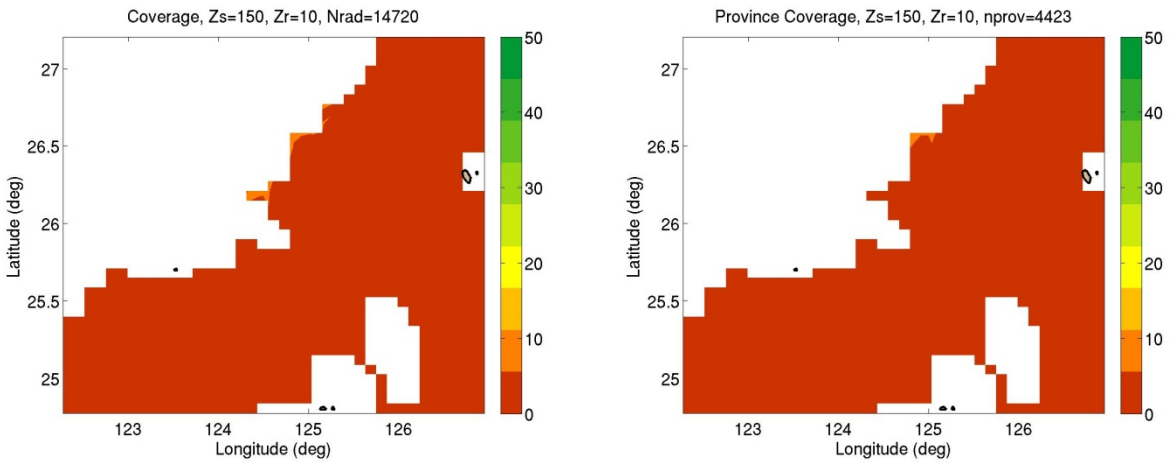

Figure 42. Brute force (left) and critical factors representative environment (right) PAC for 250 Hz, source at 150 m, receiver at 10 m.

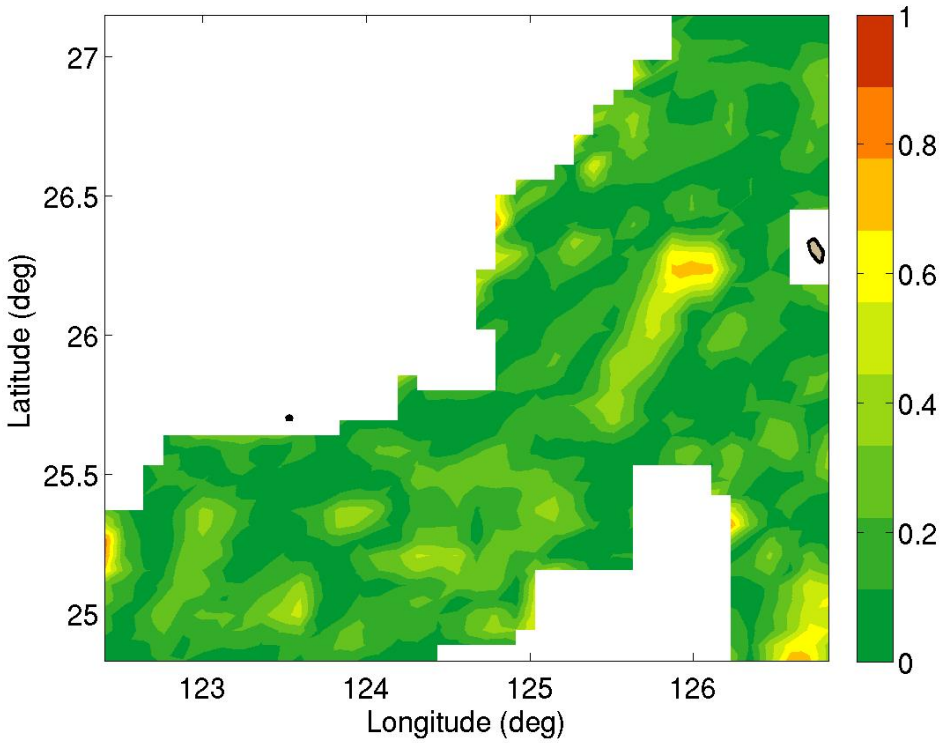

Figure 43. Averaged difference in percent between brute force and critical factors representative environment PAC for 250 Hz, source at 150 m, receiver at 10 m.

Table 1. Summary of maximum and mean PAC differences for OT AOI at 250 Hz.

Source Depth (m)	Receiver Depth (m)	Maximum % difference	Mean % difference
15	10	3.29	0.50
	15	4.37	0.67
	20	5.61	0.76
	150	1.77	0.20
	200	1.28	0.14
	250	0.88	0.14
	300	0.90	0.13
	500	0.71	0.12
	10	3.33	0.60
	15	6.84	0.82
60	20	9.60	0.98
	150	1.80	0.31
	200	1.48	0.22
	250	1.14	0.19
	300	1.33	0.19
	500	1.15	0.17
	10	0.96	0.17
	15	1.01	0.21
	20	1.64	0.22
	150	0.99	0.21
150	200	1.23	0.22
	250	1.19	0.24
	300	0.89	0.22
	500	0.84	0.22
	10	3.29	0.50
	15	4.37	0.67
	20	5.61	0.76
	150	1.77	0.20

It is useful to examine some of the point-wise differences in more detail. A tool was developed that displays the brute force and the provinced PAC and the difference. The user selects a point to analyze on the difference map, shown in the lower right of Figure 44, which contains the PAC and difference plots for the 15 m source and the 10 m receiver at 250 Hz. The selected point is plotted as a large black dot on all three plots. The representative that was used for that location in the province map is plotted as a red dot with a line representing the radial of the representative, shown here just south of the selected point. The small black dots with lines indicate the other members of the province that use that representative for the coverage. The plots along the left are the mode cost function, the SLD cost function and the TL for each member (in black) and for the representative (in red) versus range. This province has only two points and has a much larger spread, particularly in the mode cost function, but is fairly tight in the SLD function. This tool is very useful in analyzing the output of this provincing method. Currently, the TL for each member is available due to the developmental stage of the work. In the future, the TL can be computed on the fly, or just the representative TL with its UBAND can be displayed.

Another point on this same surface with a low difference is shown in Figure 45 in the central portion of the area. It is again shown as a large black dot, the representative is in red and happens to be the selected point. Again, the members of this province are shown in black. The TL does vary significantly but at high loss values, the spread of performance is low because the differences are reliant on the FOM. Future analysis could include the sensitivity of the performance metrics to the FOM, but for this effort, a single typical FOM around 85 dB is applied.

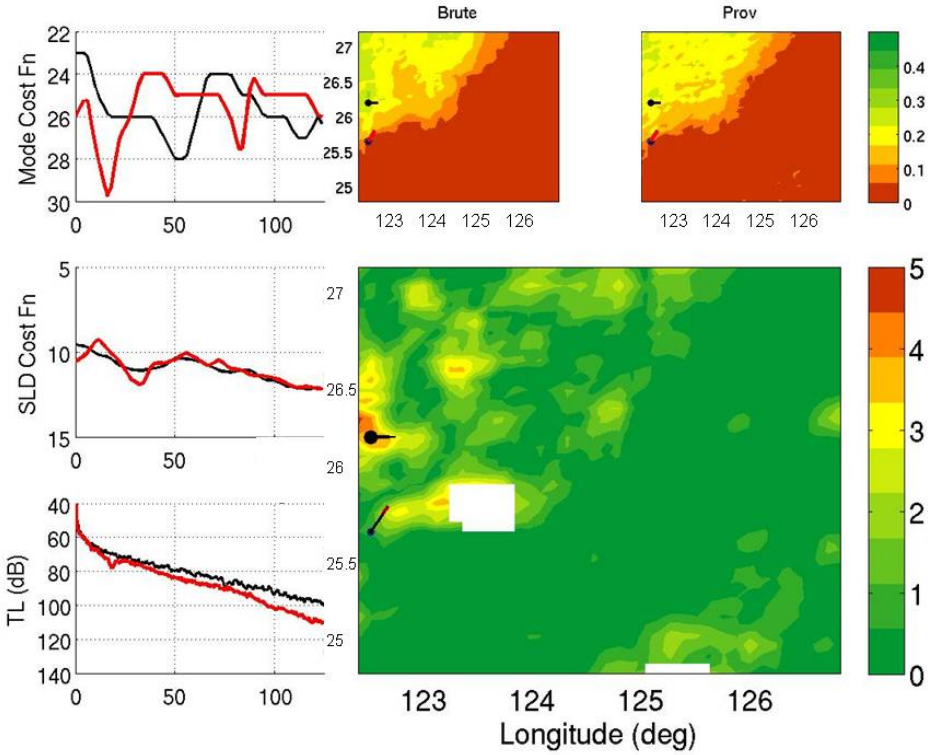

Figure 44. Single point (01) representative analysis for 250Hz, source at 15 m, receiver at 10 m.

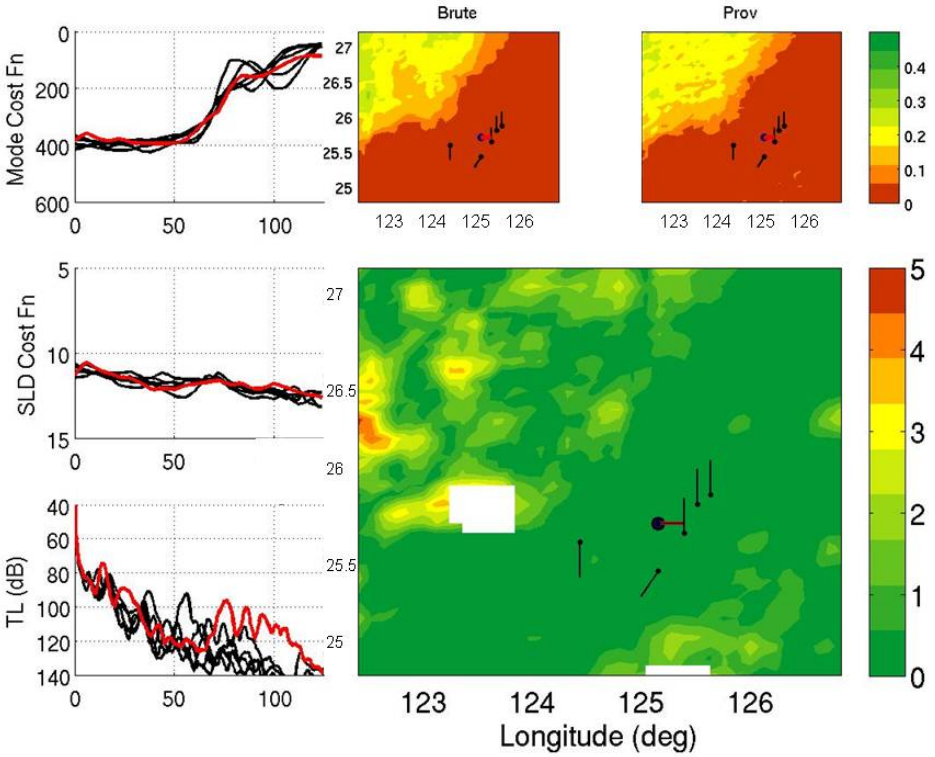

Figure 45. Single point (01b) representative analysis for 250Hz, source at 15 m, receiver at 15 m.

Figure 46 shows an example in an area of ~8% difference in PAC. The mode spread is as large, yielding a high spread in TL at the higher loss values. This is a case for which the SLD does not impact the acoustic problem.

Another high difference area for the deeper source (60 m) at the 20 m receiver depth is given in Figure 47. The chosen point is near 123E, 27N in the highest (~10%) difference regime. The representative is near 124E, 27N, 135° bearing. The 18 members are plotted in black. This is another case for which the SLD does not impact the problem. The differences in performance are due to a large spread in the mode cost function near the source.

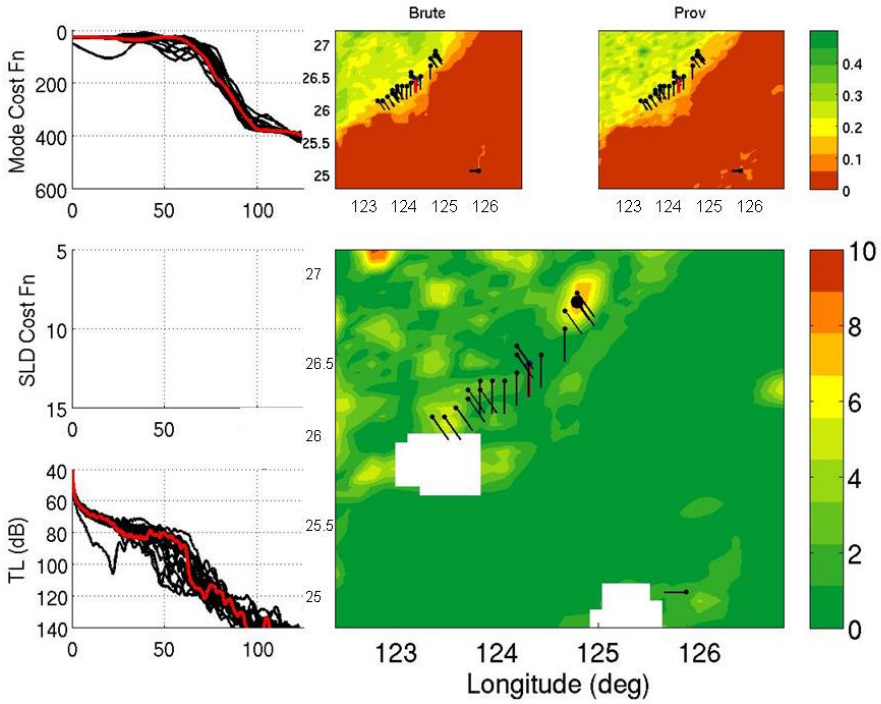

Figure 46. Single point (04b) representative analysis for 250 Hz, source at 60 m, receiver at 20 m, after re-provincing of large provinces was added.

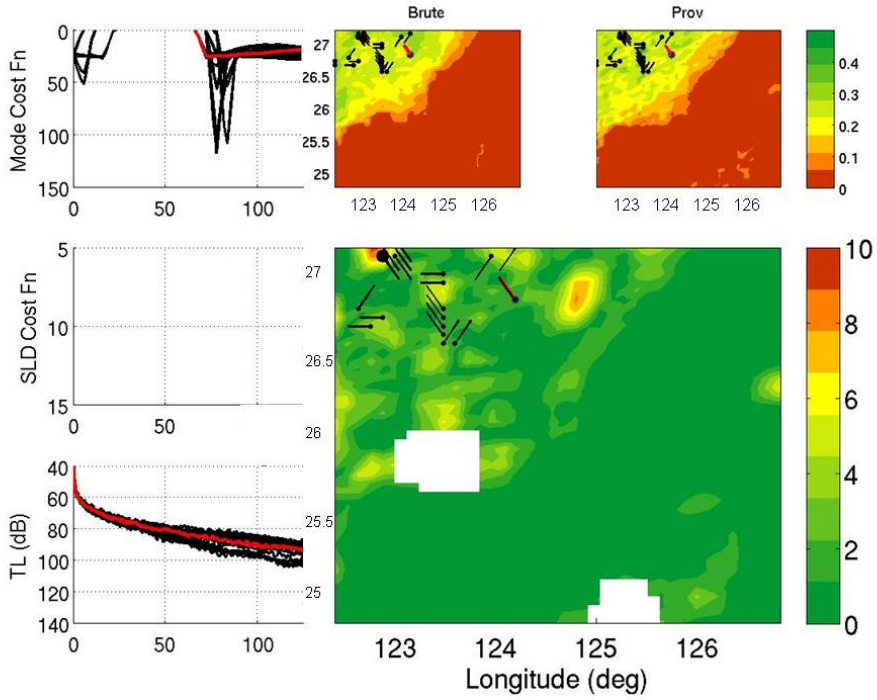

Figure 47. Single point (05) representative analysis for 250 Hz, source at 60 m, receiver at 20 m after re-provincing of large provinces was added.

Mid Frequency

Mid frequency (1000 Hz) acoustic predictions were examined next for the Okinawa trough area. Two source depths were computed: 20 m so that if there is a layer, the source will be in it and 80 m, which will be in the layer some of the time. As for the low frequency cases, the number of radials (TL predictions) used to compute coverage for this case (8 radials per grid point) is 14,720. The number of TL representatives identified to generate the provinced coverage is 4,933 resulting in a computational savings of approximately 5-fold.

The left plots in Figure 48, Figure 50, Figure 52, Figure 54 and Figure 56 show the PAC computed using the brute force (14,720 TL predictions) method for the shallow source and four receivers, 10, 15, 20, 150 m and 200 m, respectively. Other receivers were computed, but are not shown due to their similarity to the figures presented. The right plots in Figure 48, Figure 50, Figure 52, Figure 54 and Figure 56 show the corresponding PAC estimates using only representatives (4,933 TL predictions) from each province. The averaged differences between the brute force and the provinced PAC are shown in Figure 49, Figure 51, Figure 53, Figure 55

and Figure 57. The brute force (left) and provinced (right) PAC computed using a deeper source (80 m) for the same receiver depths are shown in Figure 58, Figure 60, Figure 62, Figure 64 and Figure 66. The areas of larger difference, as for example in Figure 55 near 125E, 25.5N are due to provinces with wide mode function spread.

The results using the shallow source show differences no greater than 15% and less than 10% at the deepest receiver, indicating that the representatives are indicating the appropriate acoustic features of interest. This remains a very good result for all other locations in the area.

Table 2 summarizes the maximum and mean differences for the OT AOI at 1,000Hz, shown in the boxcar averaged difference plots. The overall coverage features compare very well for both source depths. The provincing algorithm again captures the broad shape of the coverage features. The overall differences do not exceed ~19% of the area in this case for the shallower, in duct depths, and no more than 10% for the deeper depths, but are primarily smaller.

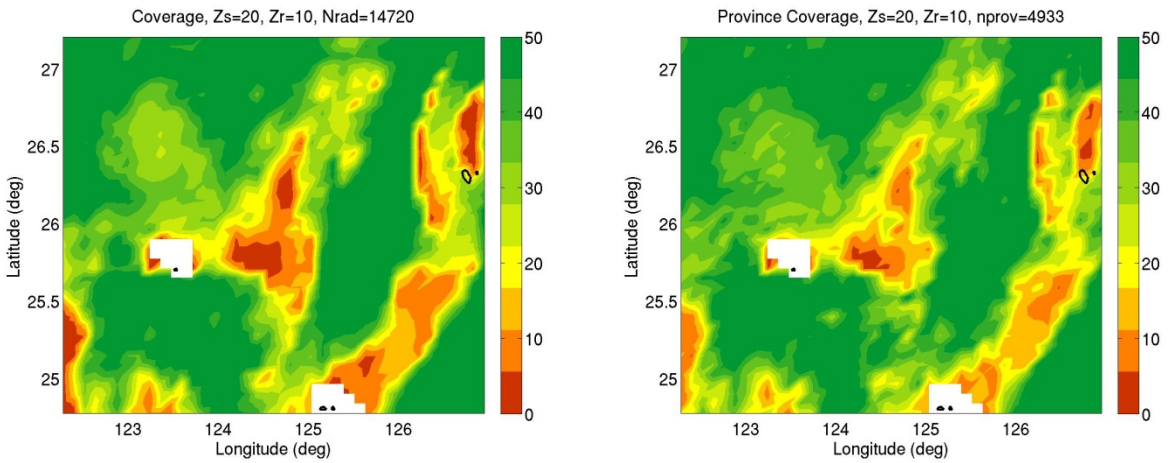

Figure 48. Brute force (left) and critical factors representative environment (right) PAC for 1000 Hz, source at 20 m, receiver at 10 m.

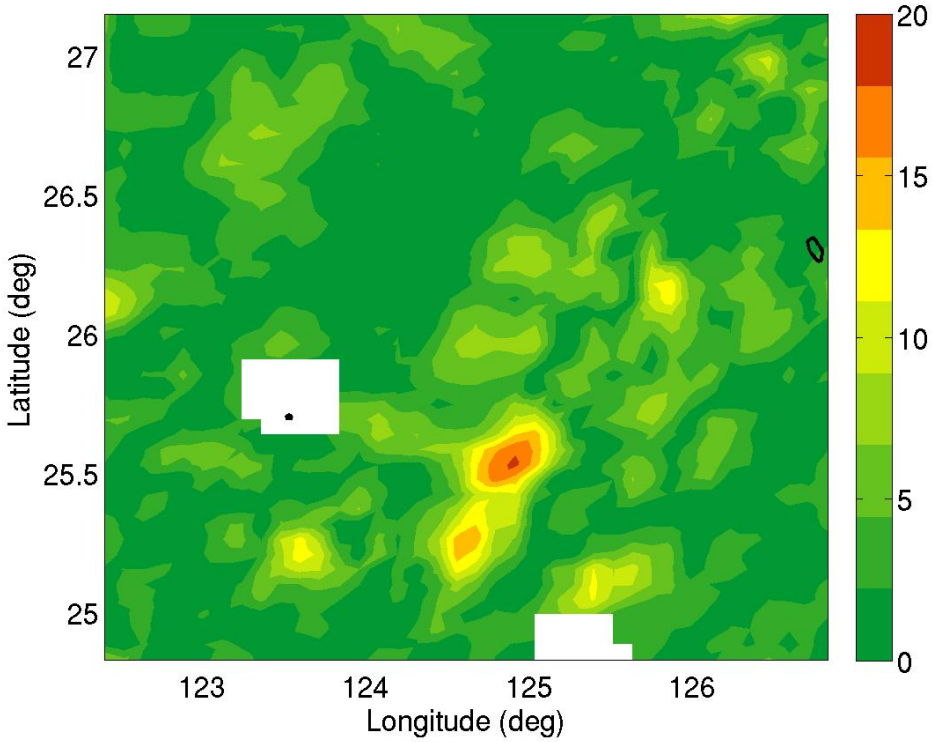

Figure 49. Averaged difference in percent between brute force and critical factors representative environment PAC for 1000 Hz, source at 20 m, receiver at 10 m.

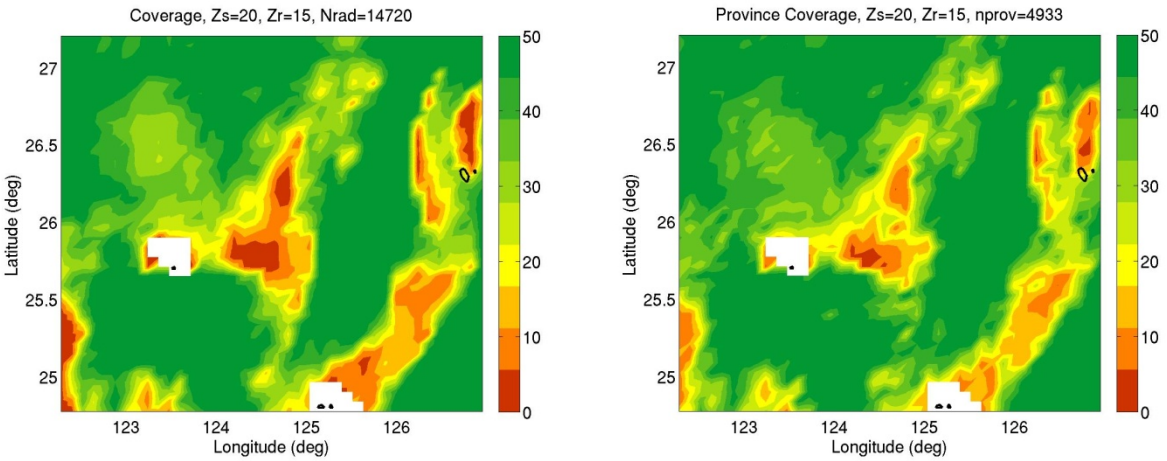

Figure 50. Brute force (left) and critical factors representative environment (right) PAC for 1000 Hz, source at 20 m, receiver at 15 m.

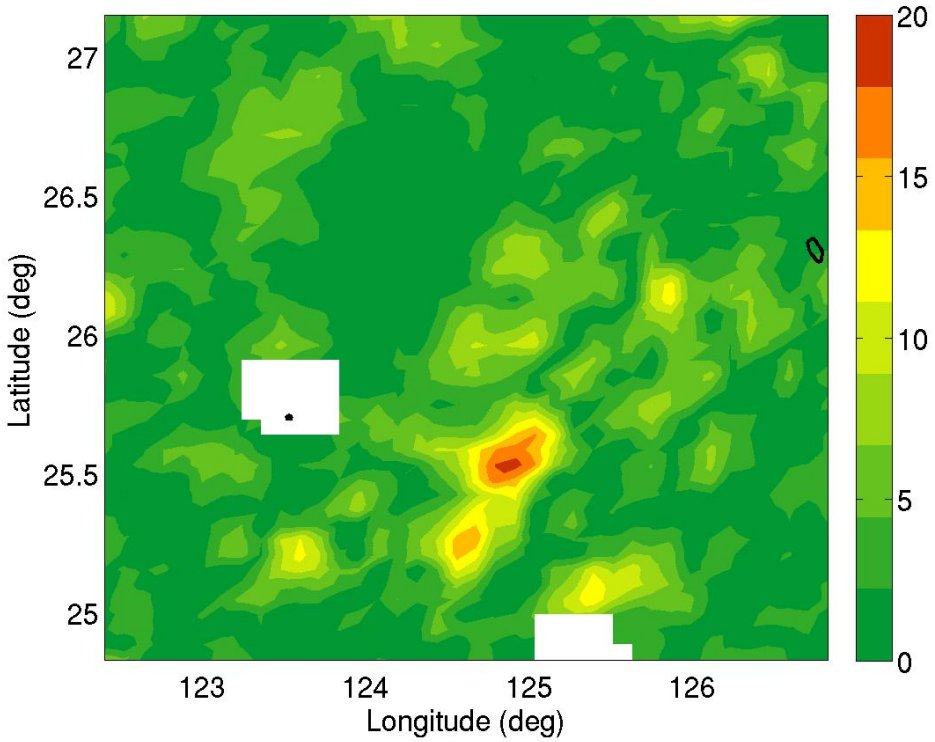

Figure 51. Averaged difference in percent between brute force and critical factors representative environment PAC for 1000 Hz, source at 20 m, receiver at 15 m.

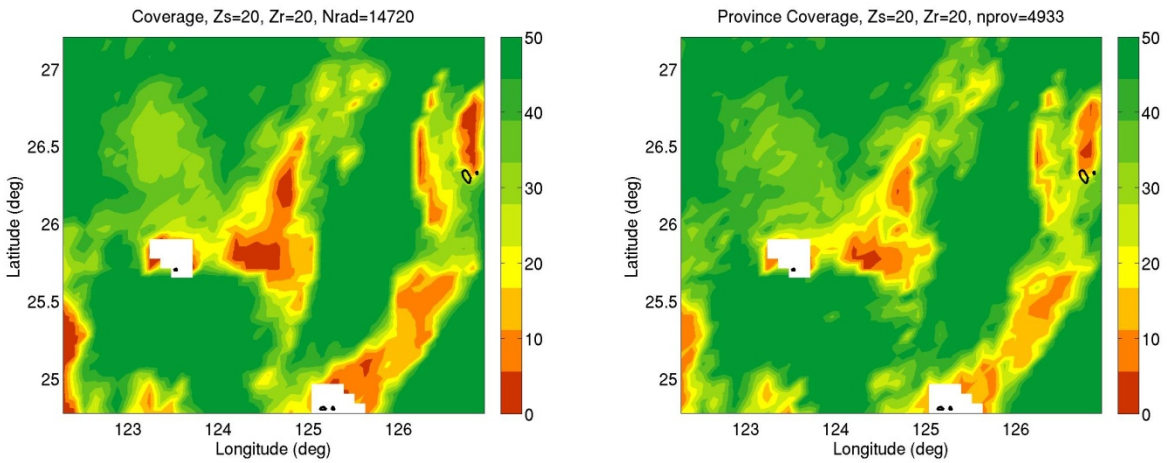

Figure 52. Brute force (left) and critical factors representative environment (right) PAC for 1000 Hz, source at 20 m, receiver at 20 m.

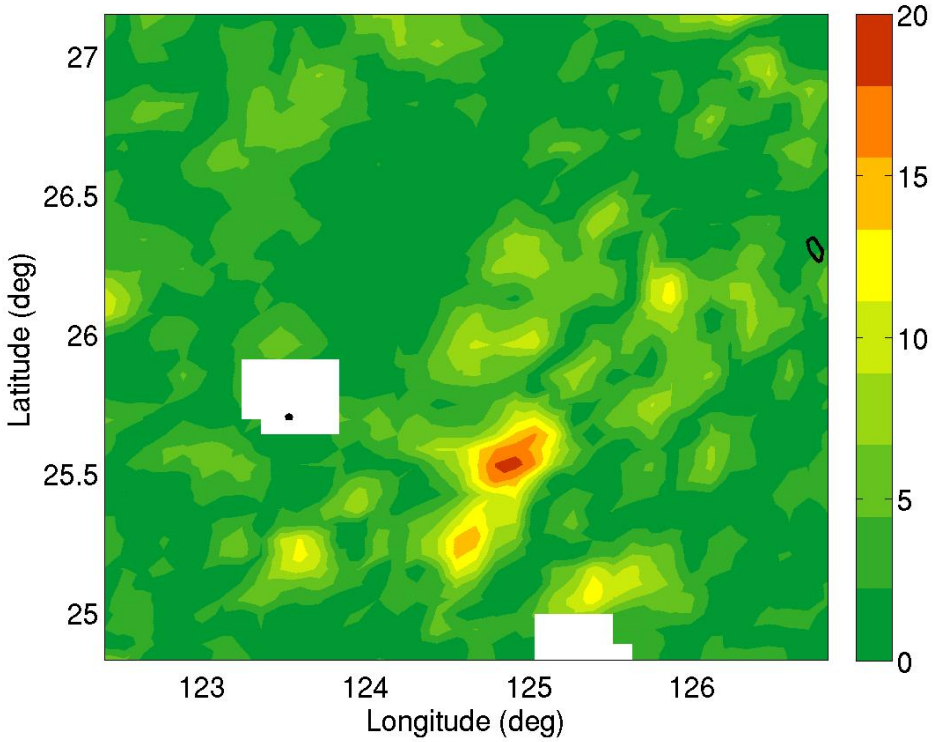

Figure 53. Averaged difference in percent between brute force and critical factors representative environment PAC for 1000 Hz, source at 20 m, receiver at 20 m.

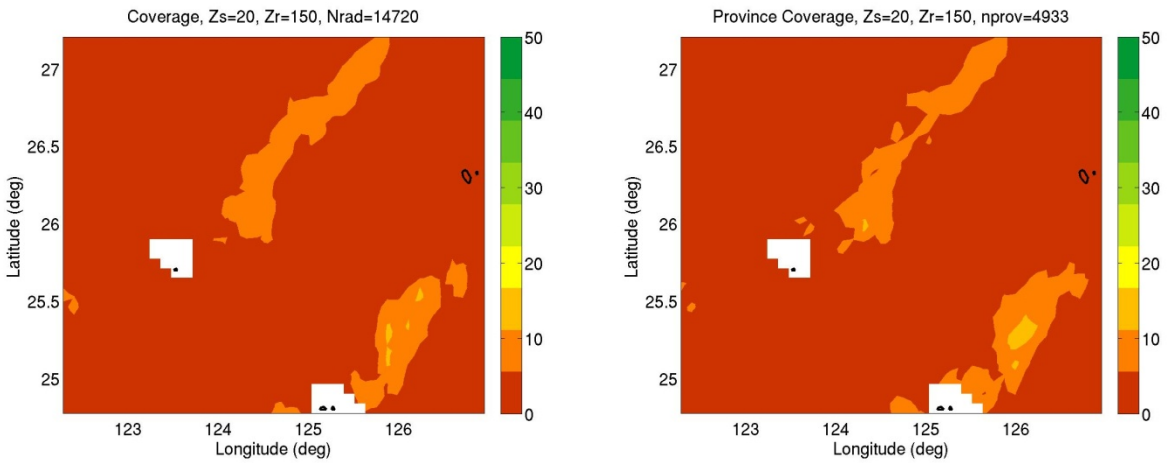

Figure 54. Brute force (left) and critical factors representative environment (right) PAC for 1000 Hz, source at 20 m, receiver at 150 m.

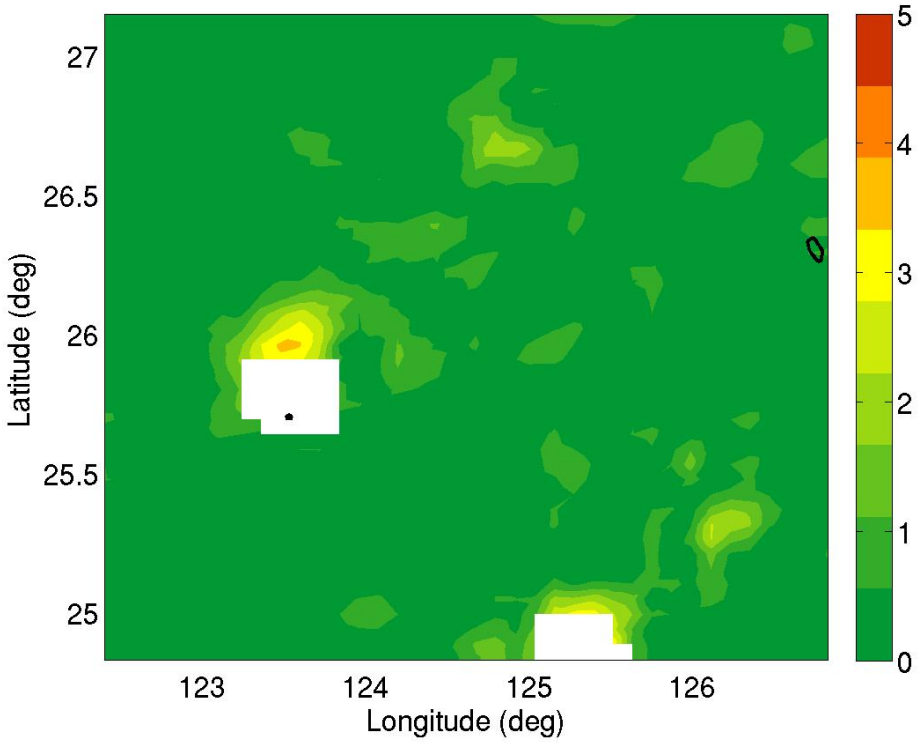

Figure 55. Averaged difference in percent between brute force and critical factors representative environment PAC for 1000 Hz, source at 20 m, receiver at 150 m.

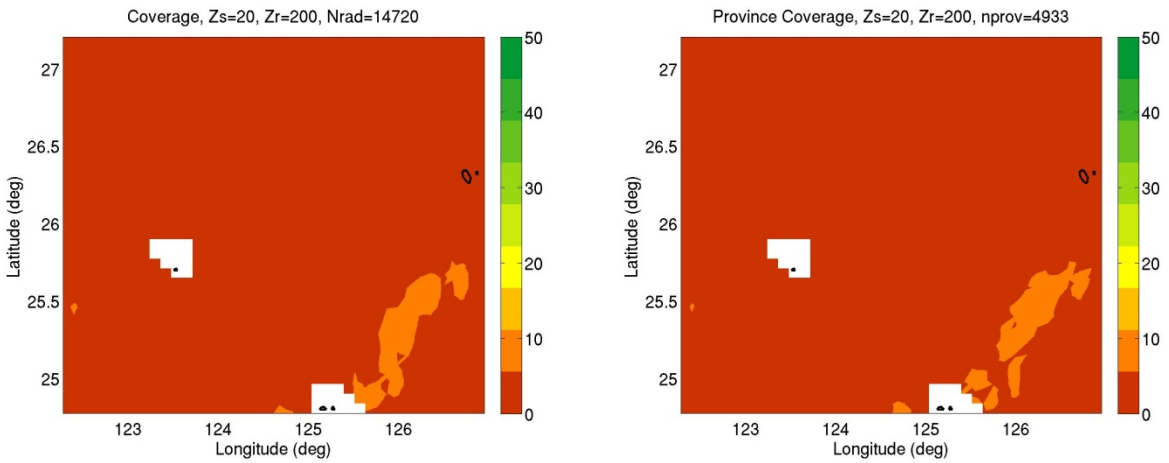

Figure 56. Brute force (left) and critical factors representative environment (right) PAC for 1000 Hz, source at 20 m, receiver at 200 m.

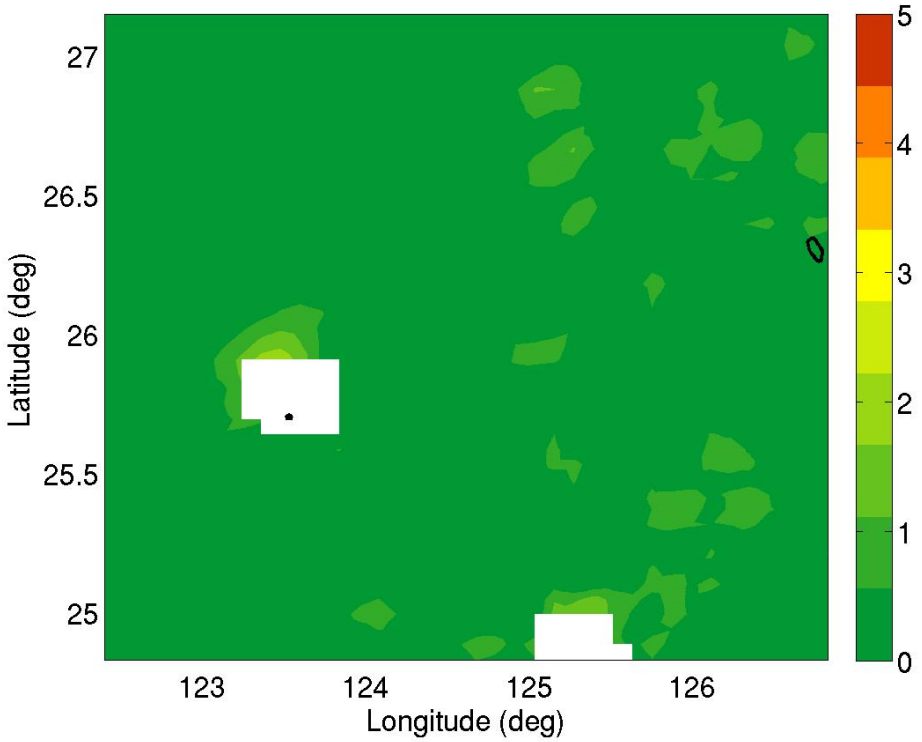

Figure 57. Averaged difference in percent between brute force and critical factors representative environment PAC for 1000 Hz, source at 20 m, receiver at 200 m.

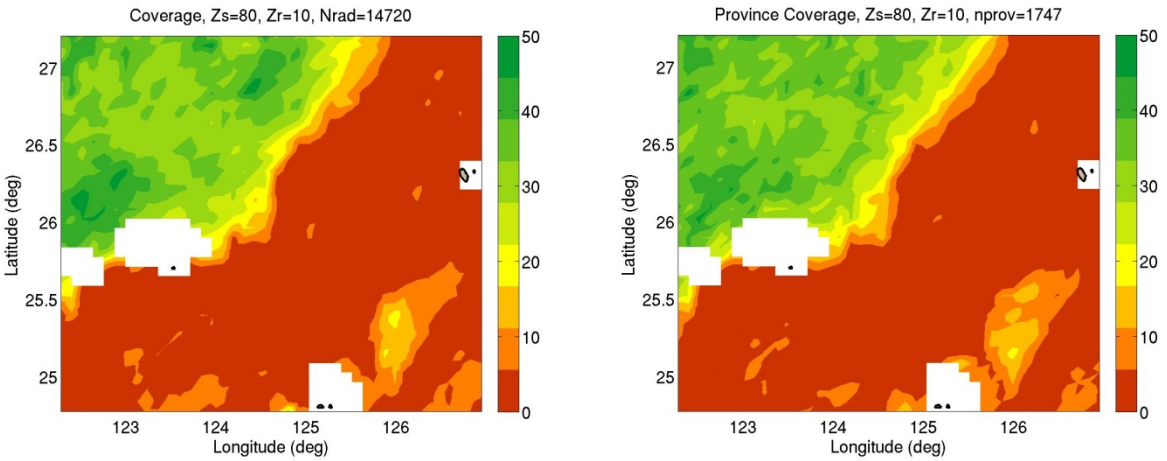

Figure 58. Brute force (left) and critical factors representative environment (right) PAC for 1000 Hz, source at 80 m, receiver at 10 m.

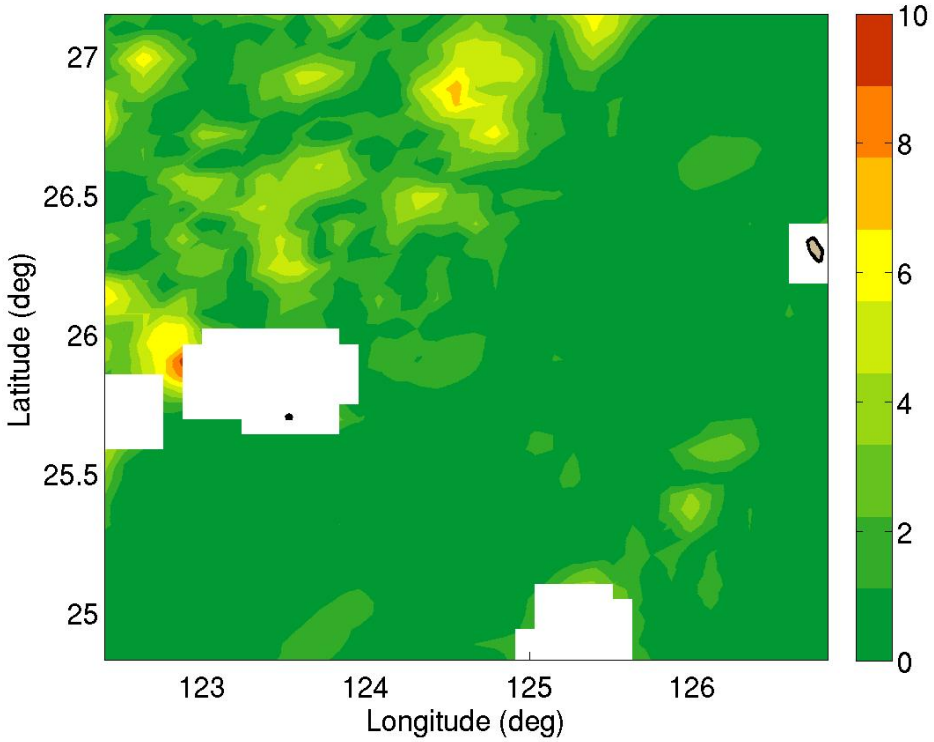

Figure 59. Averaged difference in percent between brute force and critical factors representative environment PAC for 1000 Hz, source at 80 m, receiver at 10 m.

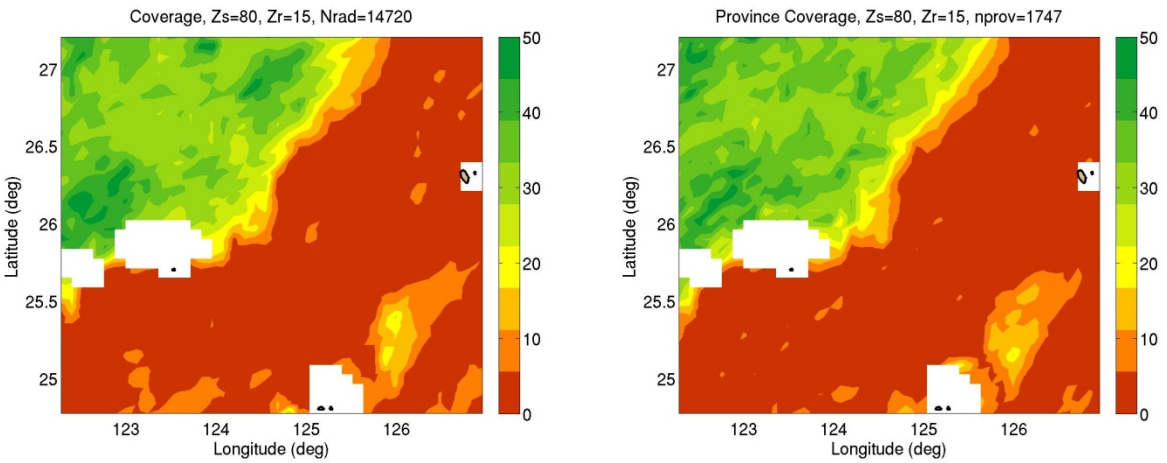

Figure 60. Brute force (left) and critical factors representative environment (right) PAC for 1000 Hz, source at 80 m, receiver at 15 m.

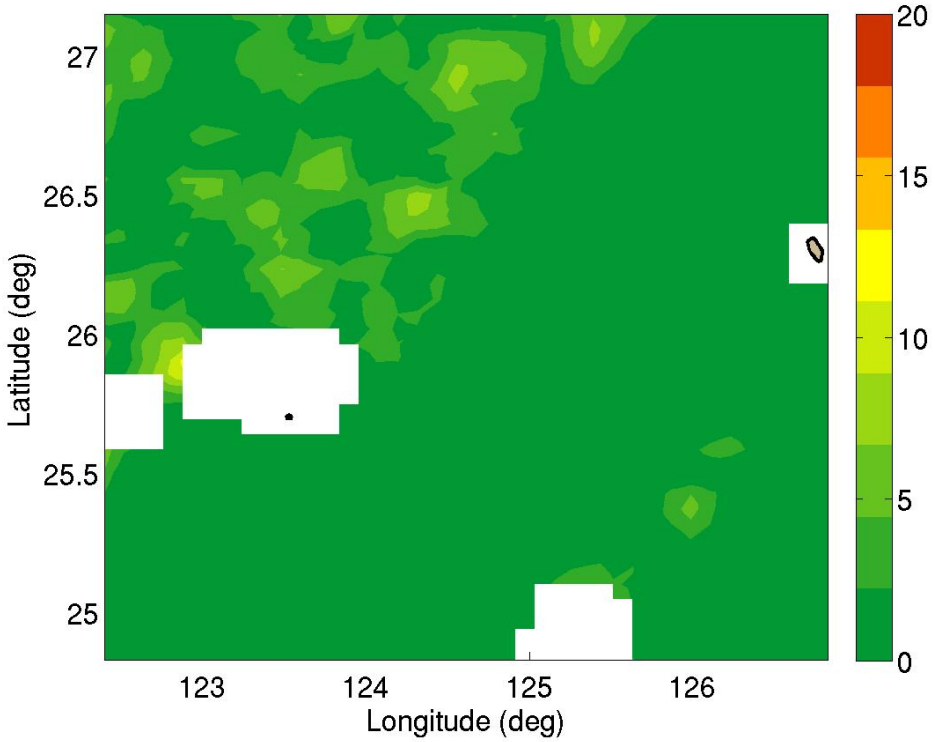

Figure 61. Averaged difference in percent between brute force and critical factors representative environment PAC for 1000 Hz, source at 80 m, receiver at 15 m.

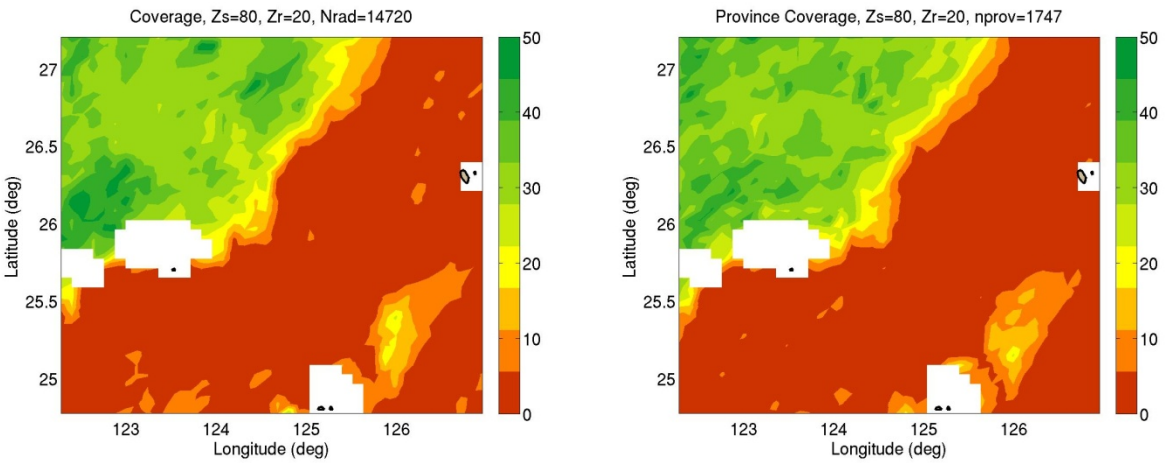

Figure 62. Brute force (left) and critical factors representative environment (right) PAC for 1000 Hz, source at 80 m, receiver at 20 m.

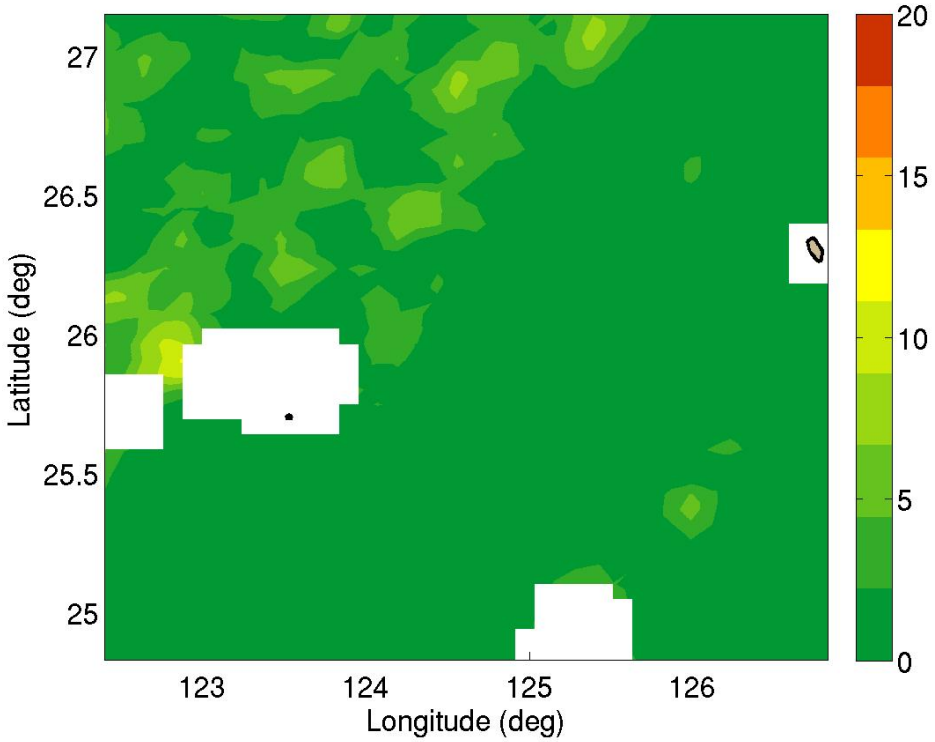

Figure 63. Averaged difference in percent between brute force and critical factors representative environment PAC for 1000 Hz, source at 80 m, receiver at 20 m.

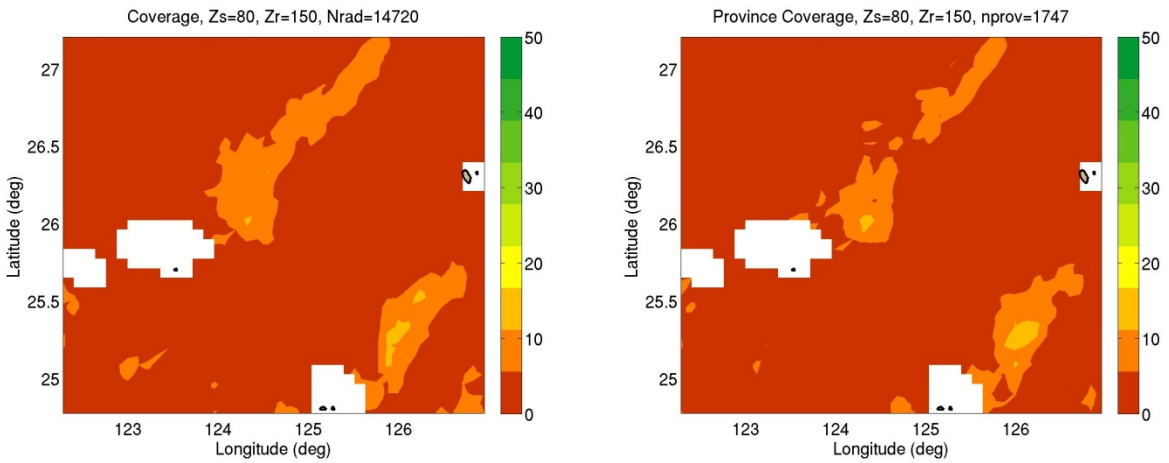

Figure 64. Brute force (left) and critical factors representative environment (right) PAC for 1000 Hz, source at 80 m, receiver at 150 m.

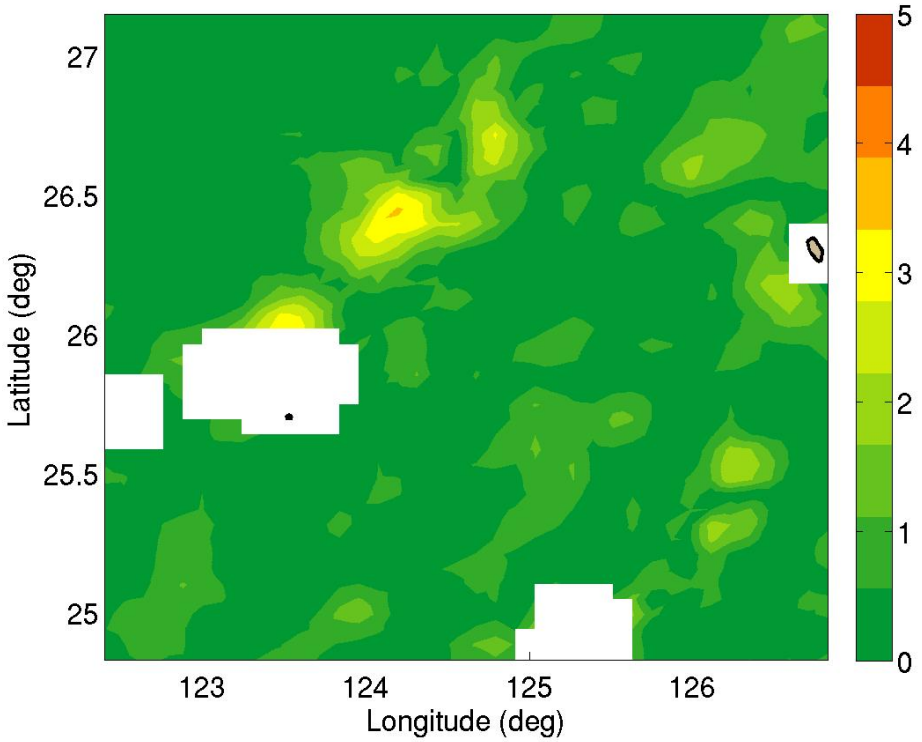

Figure 65. Averaged difference in percent between brute force and critical factors representative environment PAC for 1000 Hz, source at 80 m, receiver at 150 m.

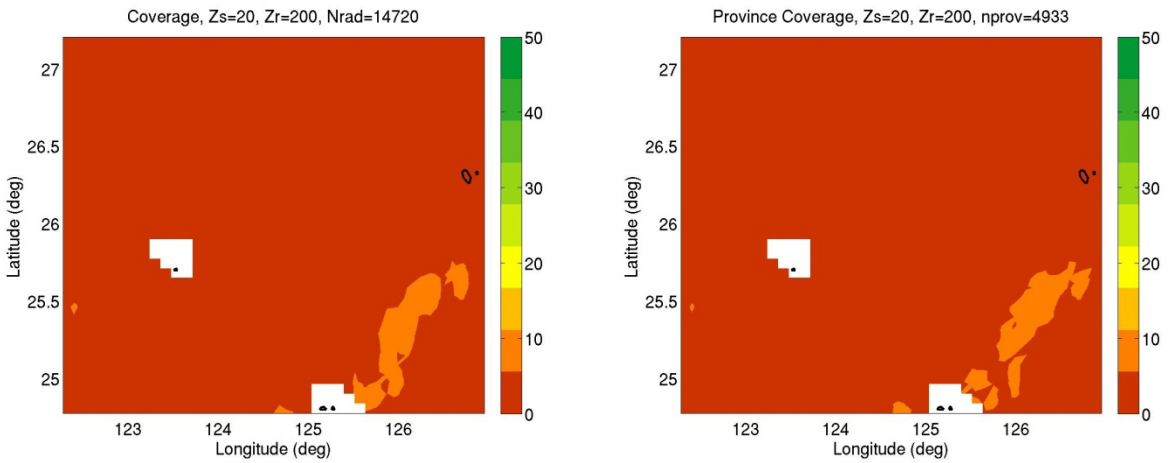

Figure 66. Brute force (left) and critical factors representative environment (right) PAC for 1000 Hz, source at 80 m, receiver at 200 m.

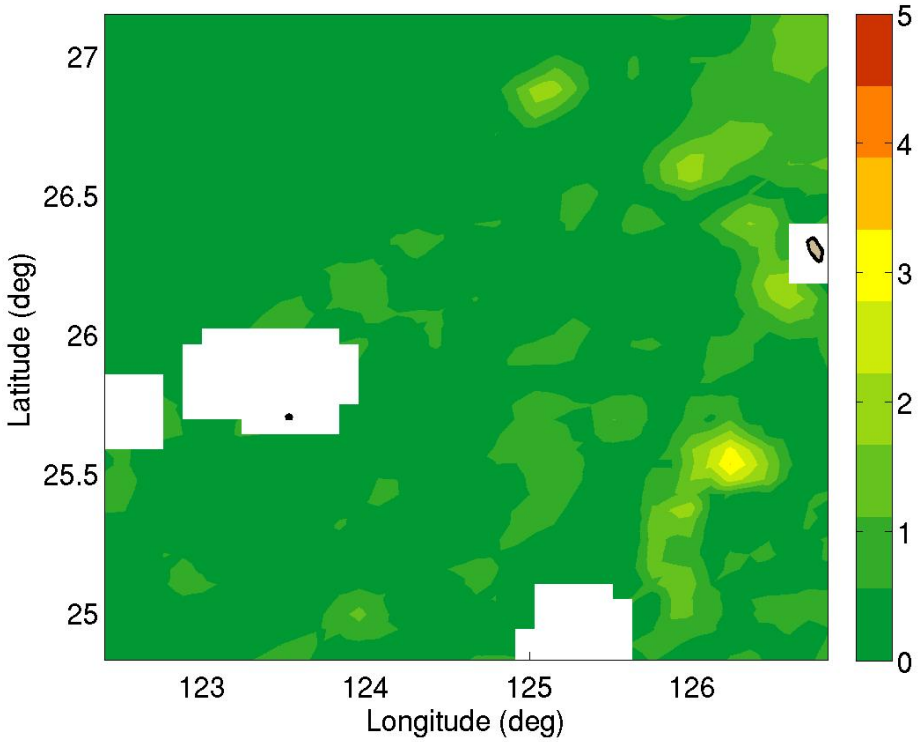

Figure 67. Averaged difference in percent between brute force and critical factors representative environment PAC for 1000 Hz, source at 80 m, receiver at 200 m.

Table 2. Summary of maximum and mean PAC differences for OT AOI at 1000 Hz.

Source Depth (m)	Receiver Depth (m)	Maximum % difference	Mean % difference
20	10	18.36	2.95
	15	18.76	3.00
	20	18.94	2.98
	150	3.48	0.35
	200	2.02	0.22
	250	1.36	0.19
	300	1.49	0.19
	500	1.61	0.18
80	10	9.43	1.10
	15	11.52	1.23
	20	11.46	1.28
	150	3.41	0.49
	200	3.37	0.37
	250	2.48	0.35
	300	2.18	0.36
	500	1.95	0.33

Single point analysis was completed on a point of fairly high difference (~20%) near 125E and 25.5, 270° as indicated by the large black dot in Figure 68, the representative for the selected radial is north and east of the chosen point. The 6 member radials are shown in black. Here the spread in both cost functions is low, however one outlier leads to a high TL spread.

Figure 69 shows the analysis for a point with less difference (< 5%). The selected point is near 124E, 26.5N, 270°. The representative is just south at that point and the 6 members are shown in black. This example shows a fairly large spread in mode cost function which was overcome by the SLD cost function to yield a low TL spread.

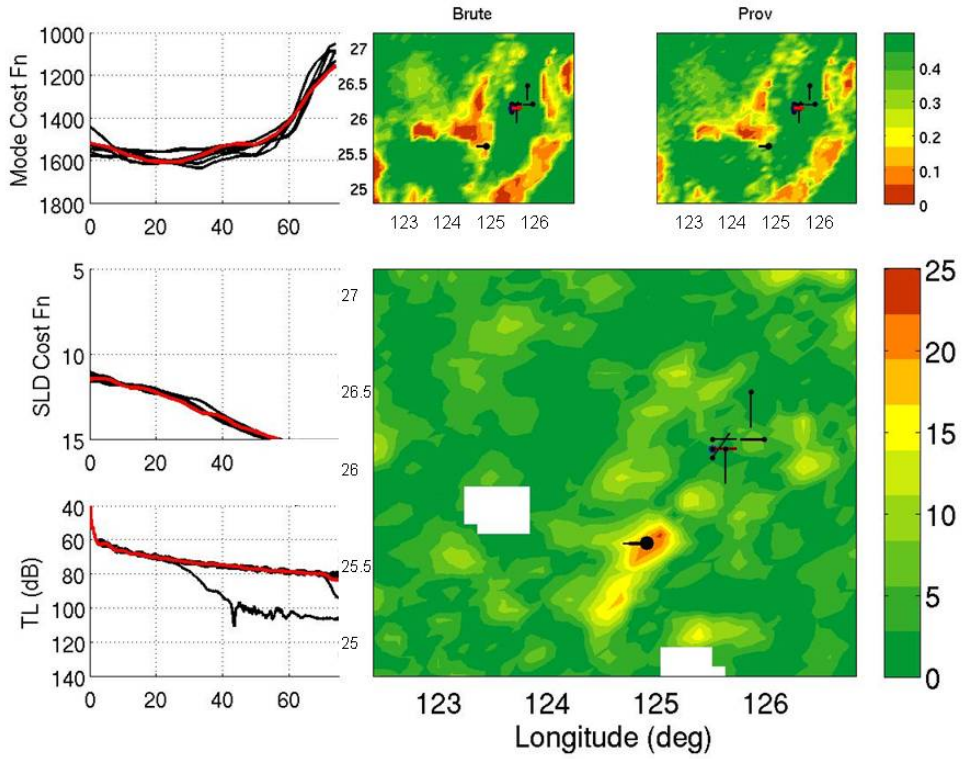

Figure 68. Single point (06) representative analysis for 1000Hz, source at 20 m, receiver at 15 m.

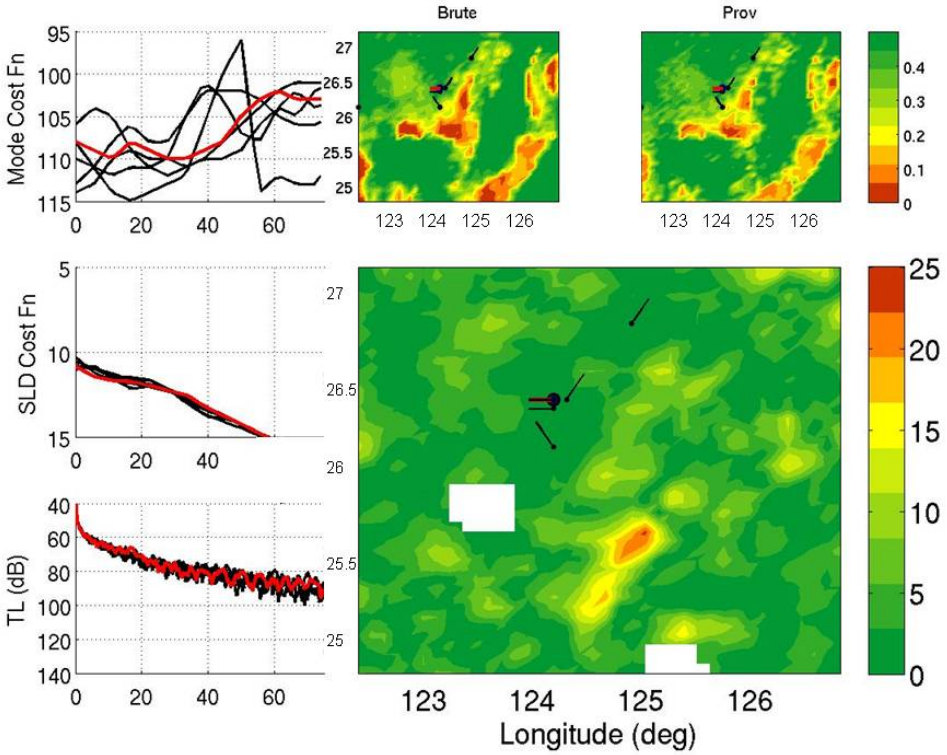

Figure 69. Single point (07) representative analysis for 1000Hz, source at 20 m, receiver at 15 m.

High Frequency

High frequency (3000 Hz) acoustic predictions were generated for two source depths. Again the source depths were chosen so that one is in the sonic layer most of the time and the other is in the layer some of the time. At this frequency, the layer is stronger than for previous, lower frequencies. Again, the number of radials (TL predictions) used to compute coverage for this case (8 radials per grid point) is 14,720, and the number of TL predictions required to generate the provinced coverage is 4,983, resulting in an approximate 3-fold computational savings. By reducing the number of original mode provinces and the number of sub-provinces computed, this computational savings can be increased.

The left plots in Figure 70, Figure 72, Figure 74 and Figure 76 show the PAC computed using the brute force (14,720 TL predictions) method for the shallow source and receivers at 10, 15, 20 and 150 m. Other receivers were computed, but are not shown due to their similarity to the figures presented. The right plots in Figure 70, Figure 72, Figure 74 and Figure 76 show the corresponding PAC estimates using only representatives (4,983 TL predictions) from each province. The boxcar differences for these cases are shown in Figure 71, Figure 73, Figure 75 and Figure 77. Again the differences are primarily less than 10%, with difference that don't exceed 19% only in a small area. Similar results for the deeper source are shown in Figure 78 through Figure 87, with the exception of Figure 86 and Figure 87 in which there is a feature (northern central part of the area) at the 150 m receiver depth that is not captured by the representatives. This feature is shown in the shallow source, 150 m receiver. The location is off a bit, but the deep receiver provincing misses it. Table 3 provides a summary of the maximum and mean differences for the box car difference calculations. The overall predicted difference for this case is around 10% with one exception which is discussed below.

The critical factors representative environments produced very good PAC maps for the Okinawa trough area, resulting in no more than 10% difference.

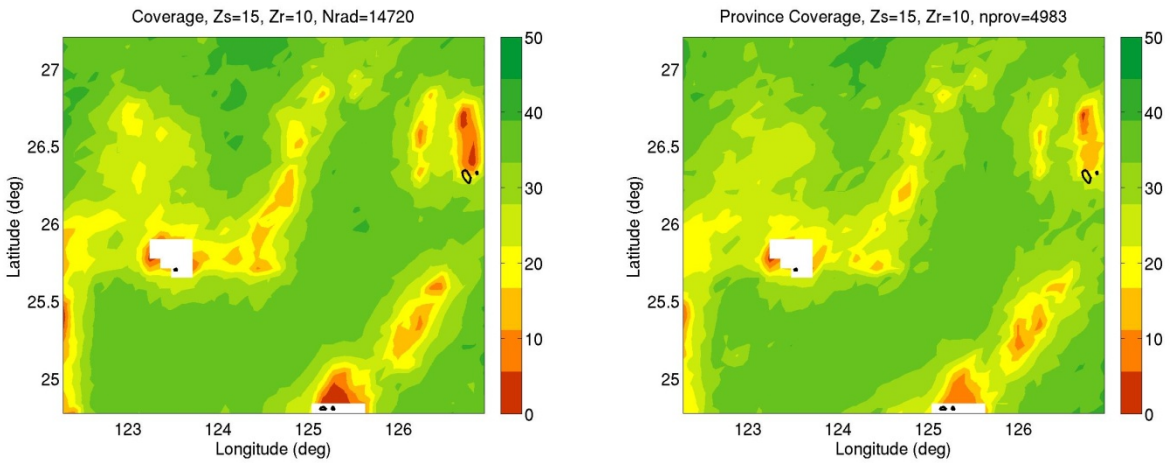

Figure 70. Brute force (left) and critical factors representative environment (right) PAC for 3000 Hz, source at 15 m, receiver at 10 m.

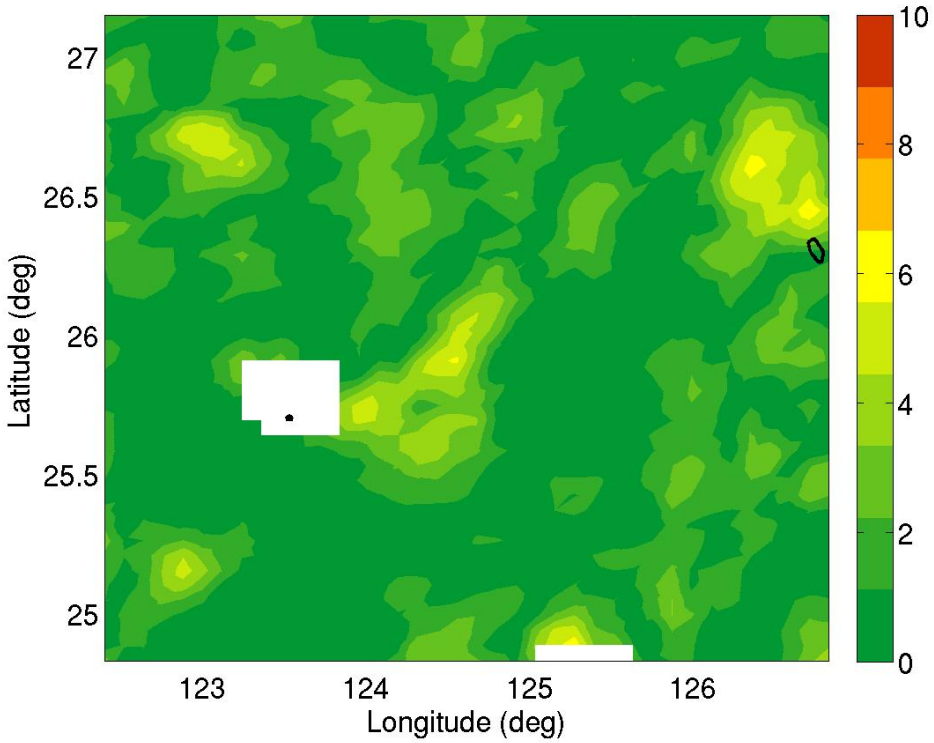

Figure 71. Averaged difference in percent between brute force and critical factors representative environment PAC for 3000 Hz, source at 15 m, receiver at 10 m.

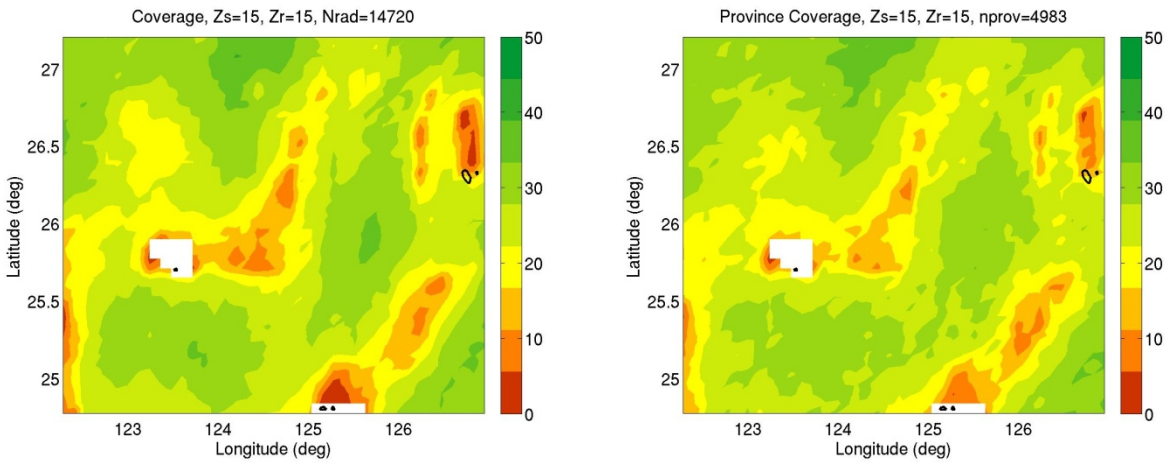

Figure 72. Brute force (left) and critical factors representative environment (right) PAC for 3000 Hz, source at 15 m, receiver at 15 m.

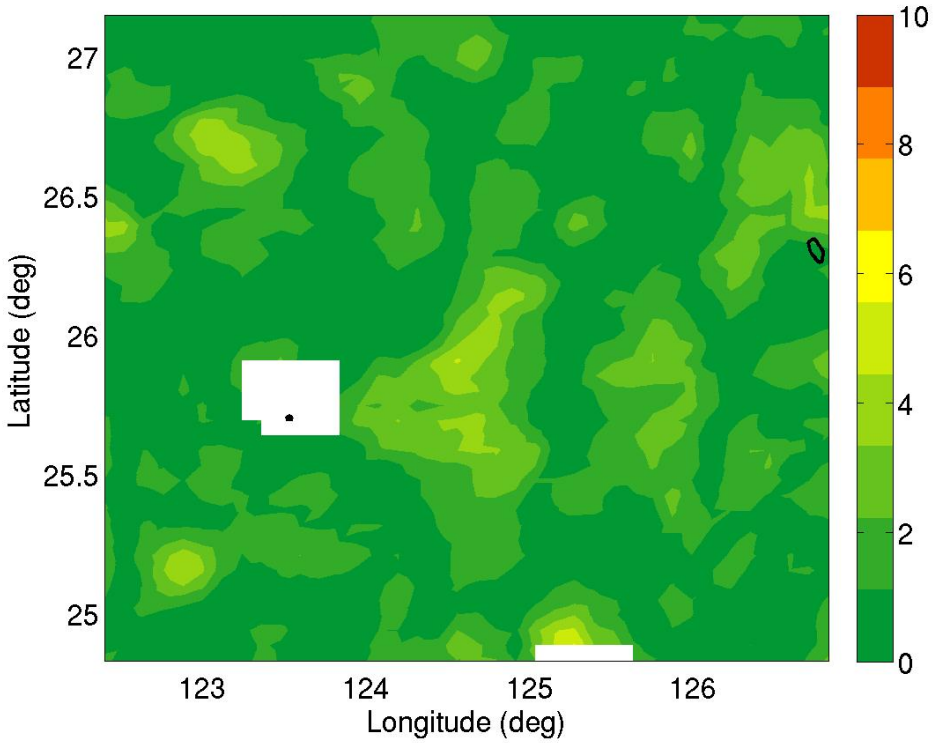

Figure 73. Averaged difference in percent between brute force and critical factors representative environment PAC for 3000 Hz, source at 15 m, receiver at 15 m.

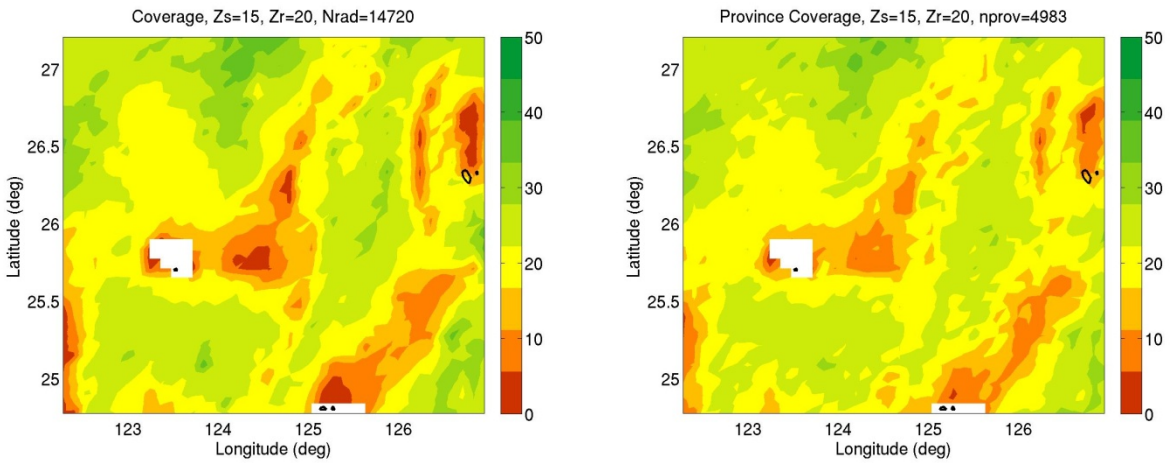

Figure 74. Brute force (left) and critical factors representative environment (right) PAC for 3000 Hz, source at 15 m, receiver at 20 m.

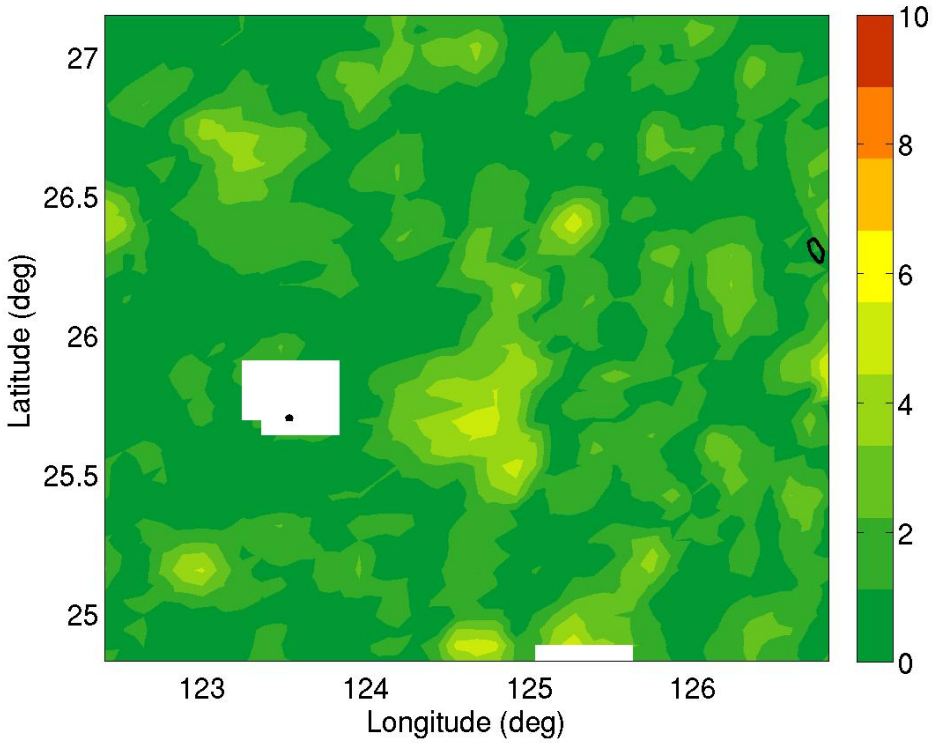

Figure 75. Averaged difference in percent between brute force and critical factors representative environment PAC for 3000 Hz, source at 15 m, receiver at 20 m.

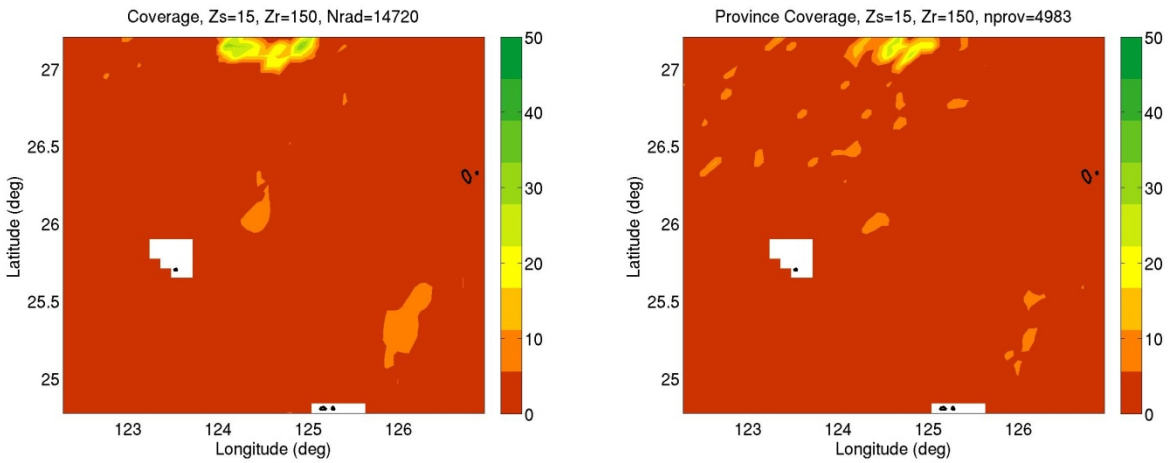

Figure 76. Brute force (left) and critical factors representative environment (right) PAC for 3000 Hz, source at 15 m, receiver at 150 m.

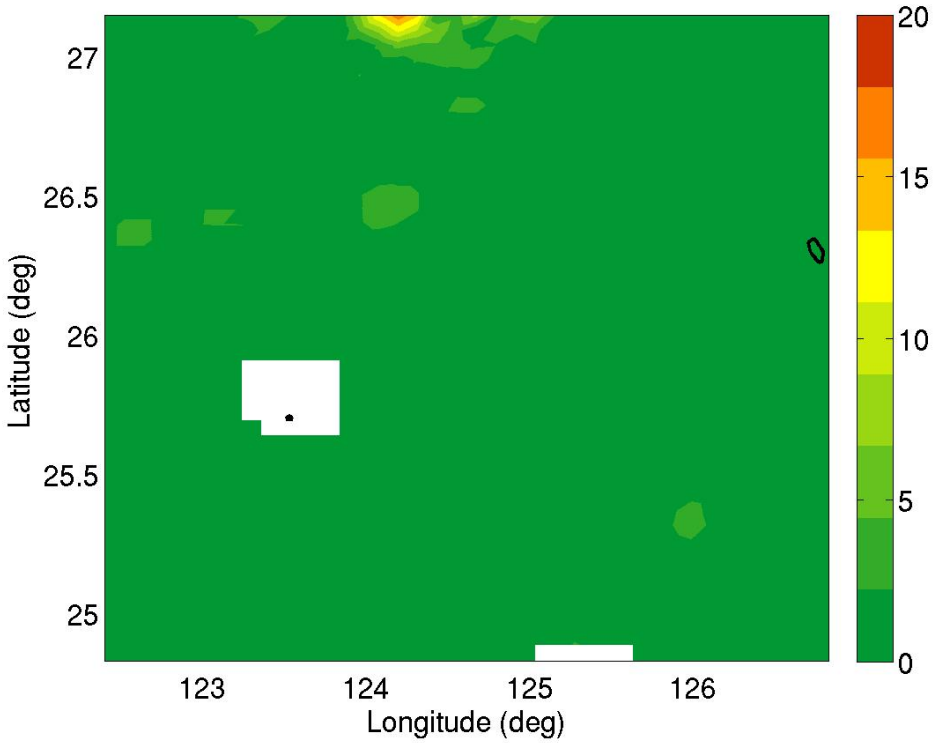

Figure 77. Averaged difference in percent between brute force and critical factors representative environment PAC for 3000 Hz, source at 15 m, receiver at 150 m.

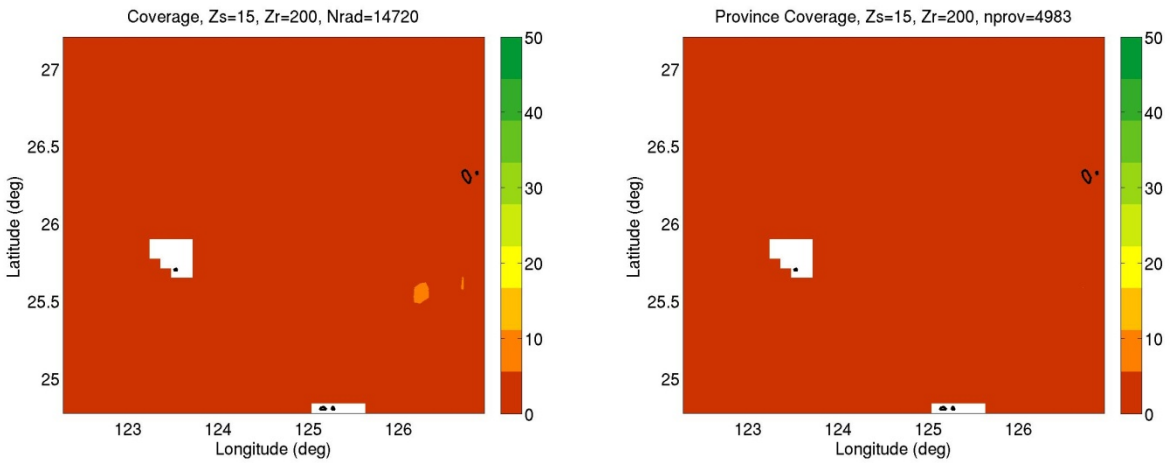

Figure 78. Brute force (left) and critical factors representative environment (right) PAC for 3000 Hz, source at 15 m, receiver at 200 m.

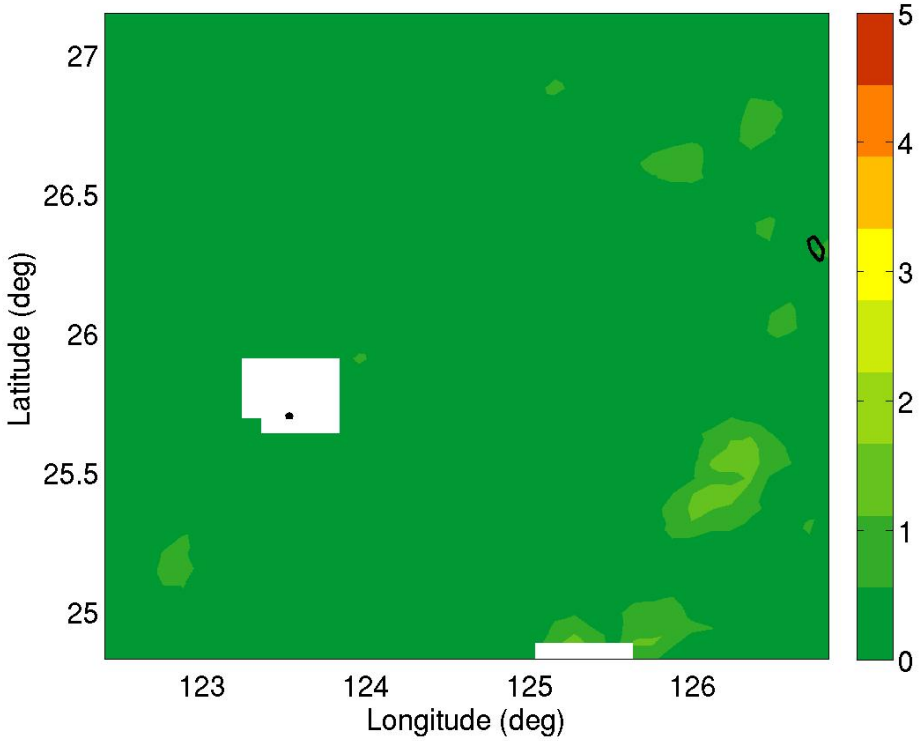

Figure 79. Averaged difference in percent between brute force and critical factors representative environment PAC for 3000 Hz, source at 15 m, receiver at 200 m.

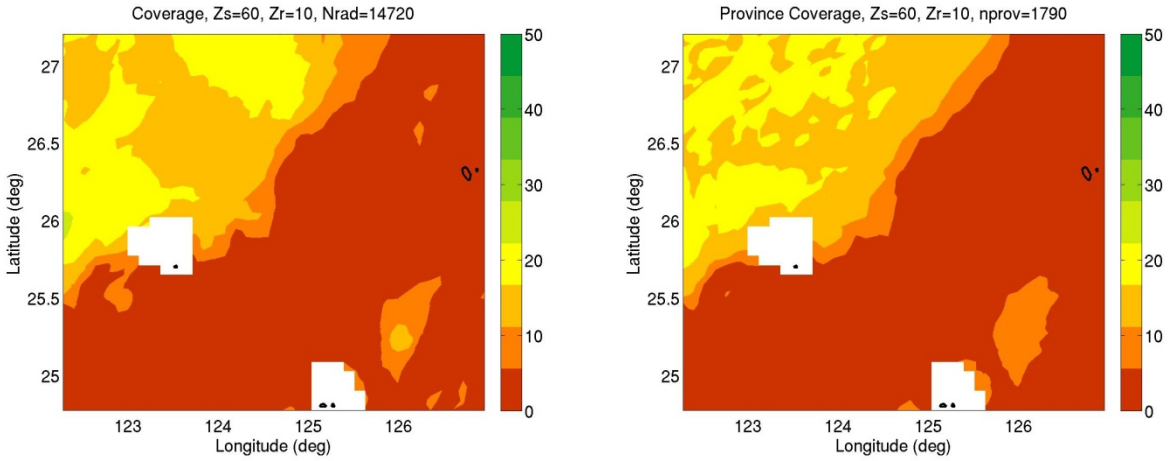

Figure 80. Brute force (left) and critical factors representative environment (right) PAC for 3000 Hz, source at 60 m, receiver at 10 m.

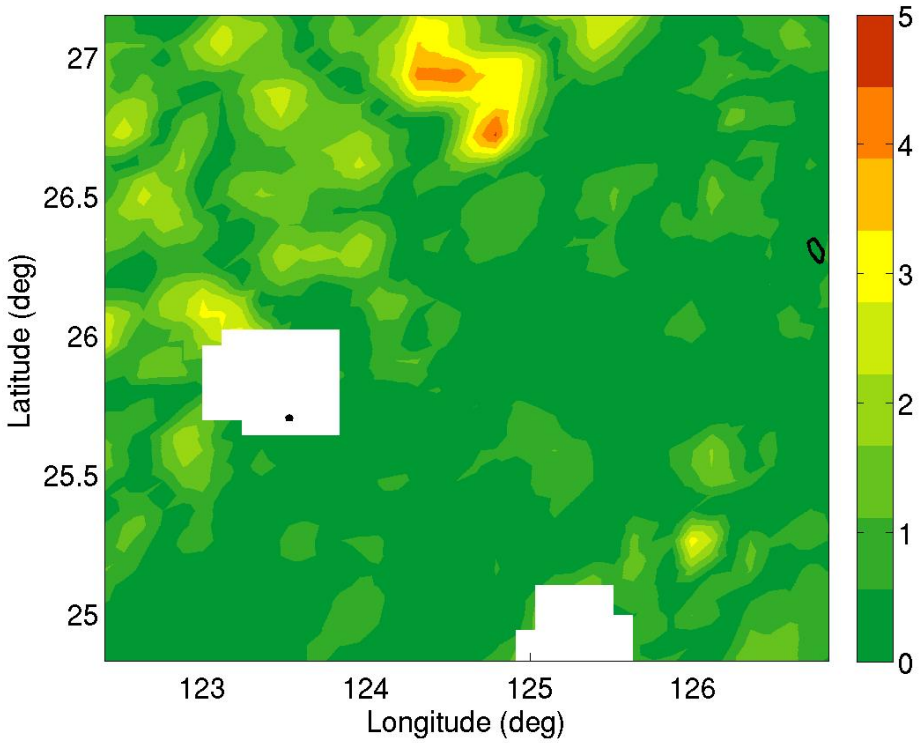

Figure 81. Averaged difference in percent between brute force and critical factors representative environment PAC for 3000 Hz, source at 60 m, receiver at 10 m.

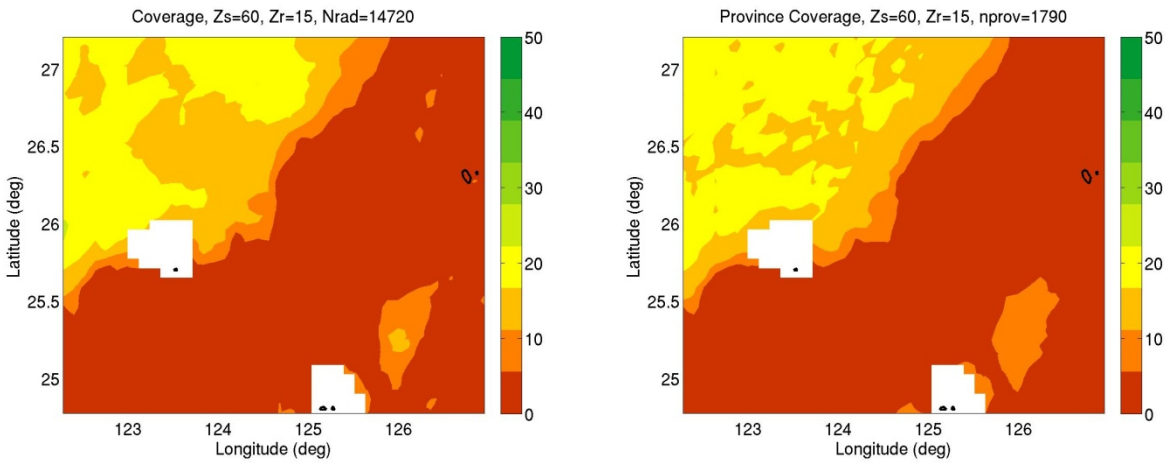

Figure 82. Brute force (left) and critical factors representative environment (right) PAC for 3000 Hz, source at 60 m, receiver at 15 m.

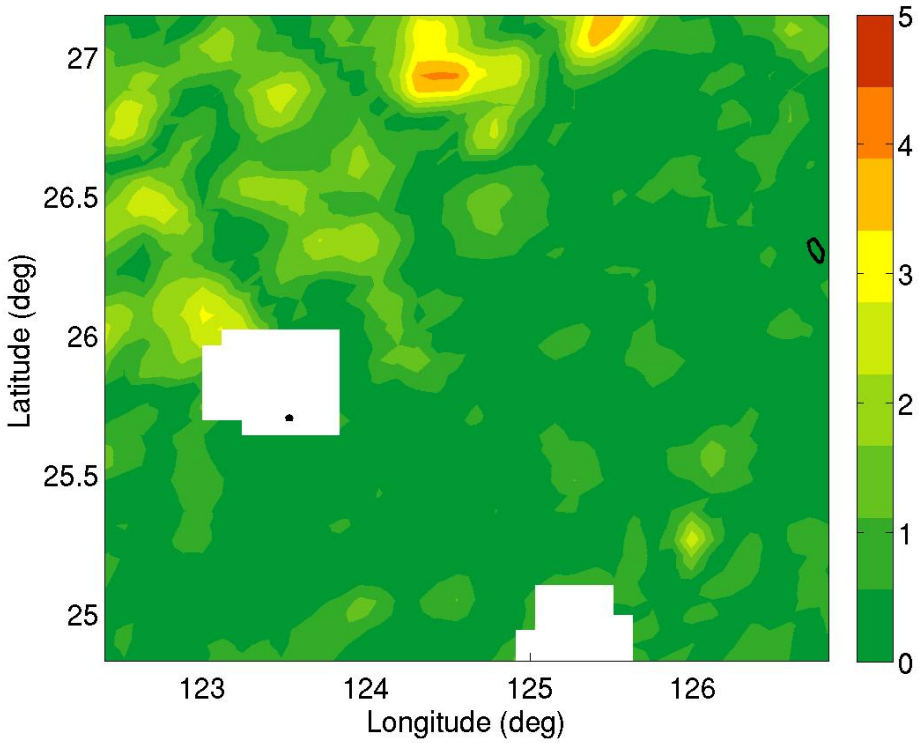

Figure 83. Averaged difference in percent between brute force and critical factors representative environment PAC for 3000 Hz, source at 60 m, receiver at 15 m.

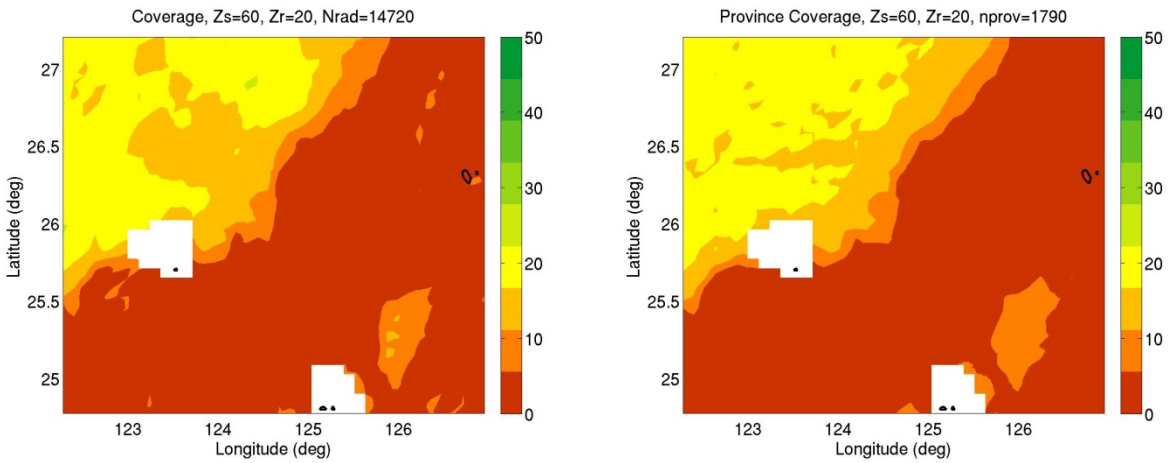

Figure 84. Brute force (left) and critical factors representative environment (right) PAC for 3000 Hz, source at 60 m, receiver at 20 m.

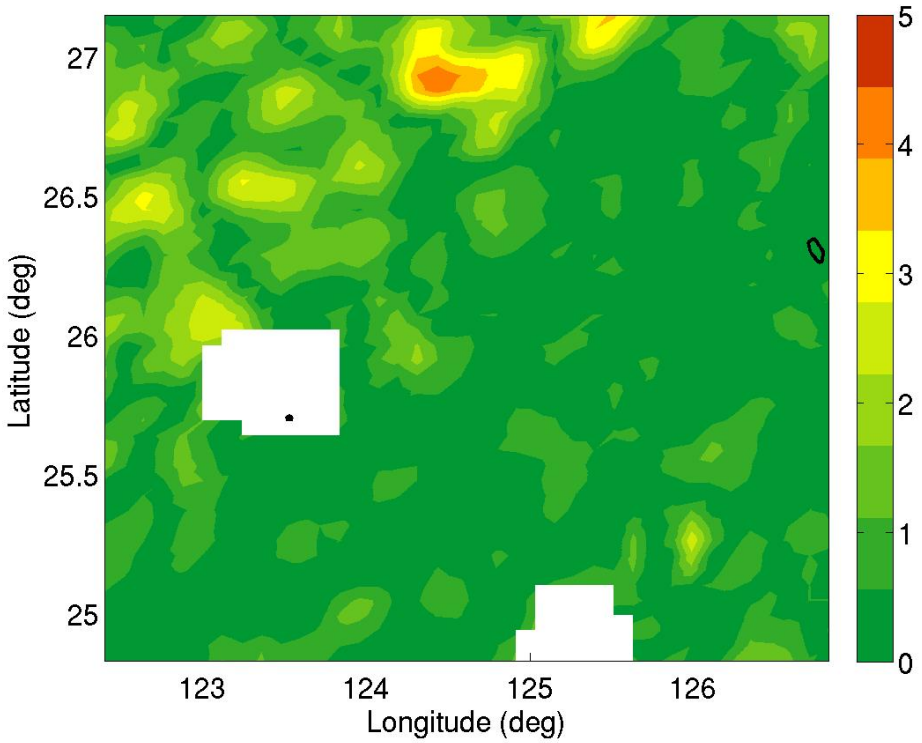

Figure 85. Averaged difference in percent between brute force and critical factors representative environment PAC for 3000 Hz, source at 60 m, receiver at 20 m.

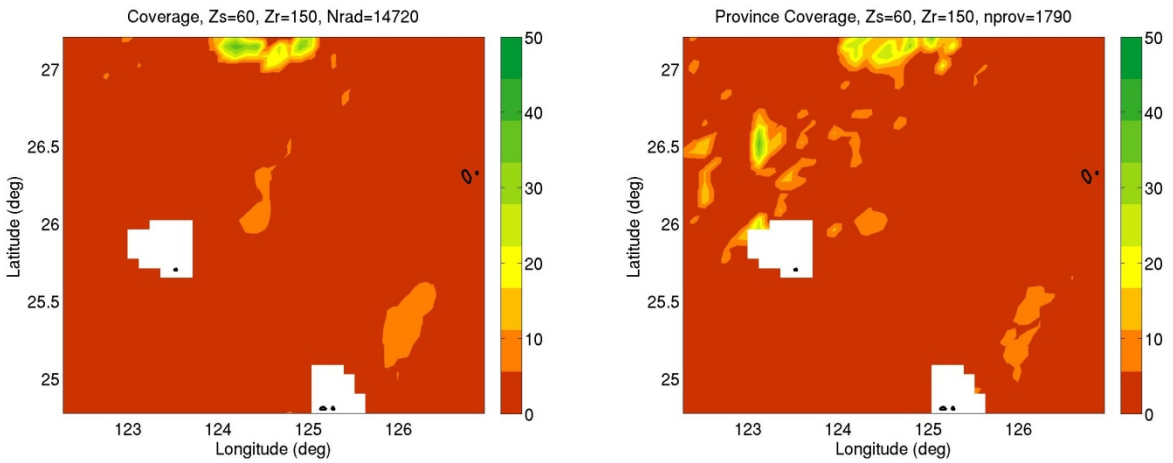

Figure 86. Brute force (left) and critical factors representative environment (right) PAC for 3000 Hz, source at 60 m, receiver at 150 m.

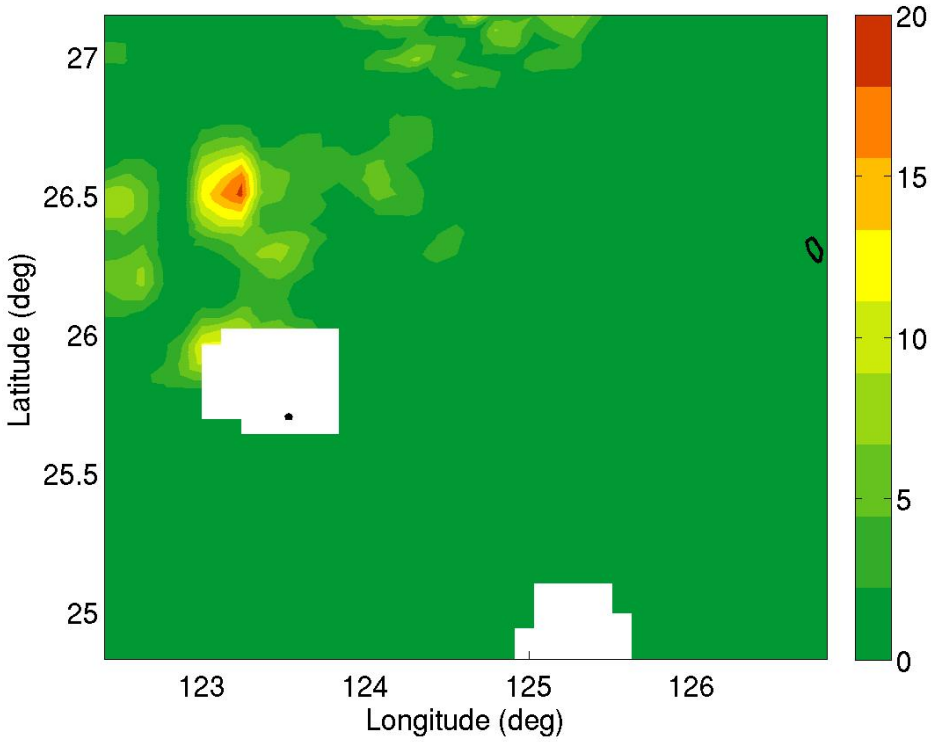

Figure 87. Averaged difference in percent between brute force and critical factors representative environment PAC for 3000 Hz, source at 60 m, receiver at 150 m.

Table 3. Summary of maximum and mean PAC differences for OT AOI at 3000 Hz

Source Depth (m)	Receiver Depth (m)	Maximum % difference	Mean % difference
15	10	6.72	1.30
	15	5.70	1.14
	20	5.66	1.28
	150	17.18	0.48
	200	1.40	0.17
	250	1.16	0.15
	300	1.11	0.14
	500	0.80	0.12
60	10	4.52	0.70
	15	4.04	0.66
	20	4.38	0.68
	150	18.46	0.98
	200	1.68	0.25
	250	1.50	0.25
	300	1.39	0.23
	500	1.26	0.19
150	10	2.36	0.22
	15	2.45	0.23
	20	2.67	0.23
	150	2.37	0.31
	200	2.47	0.29
	250	1.20	0.27
	300	1.21	0.27
	500	1.13	0.22

Hawaii

NCOM oceanographic analysis from an area around the Hawaiian Islands (NOAA, 2010) from January, 2010 was used to generate provinces and acoustic coverage. Bathymetry from DBDBV (NAVO, 2007) for this area is shown in Figure 88, the SLD computed using the NCOM analysis is shown in Figure 89. This area is a typical volcanic island bathymetry regime with primarily deep water and some steeply sloping areas near the islands. There are several sonic layer features throughout the area.

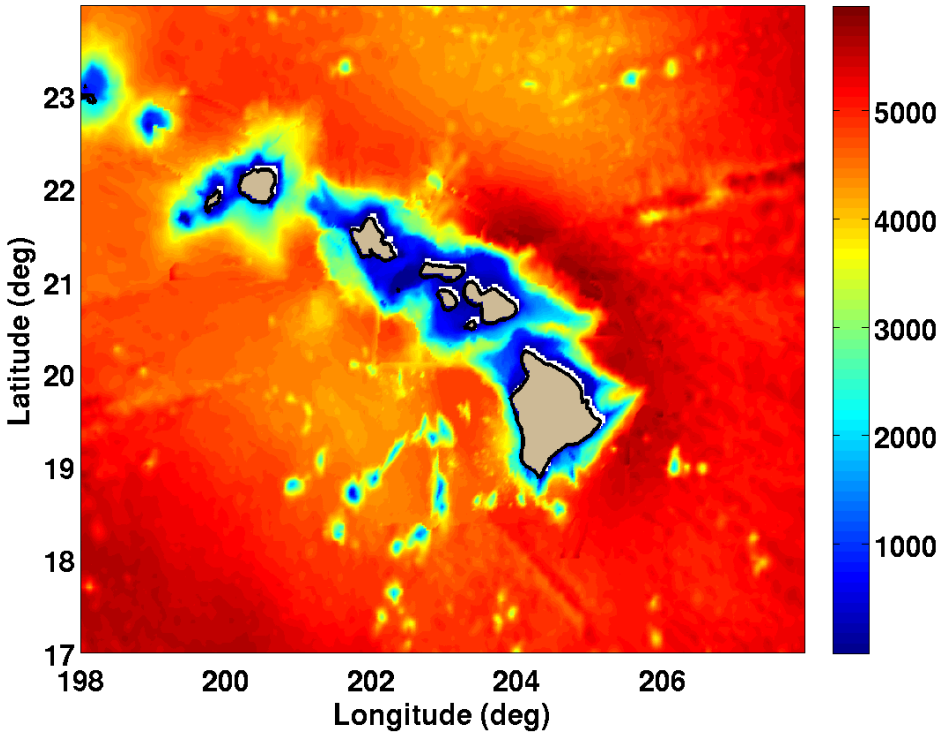

Figure 88. DBDB-V bathymetry in m for the Hawaiian area of interest. The acoustic predictions were computed for the entire box.

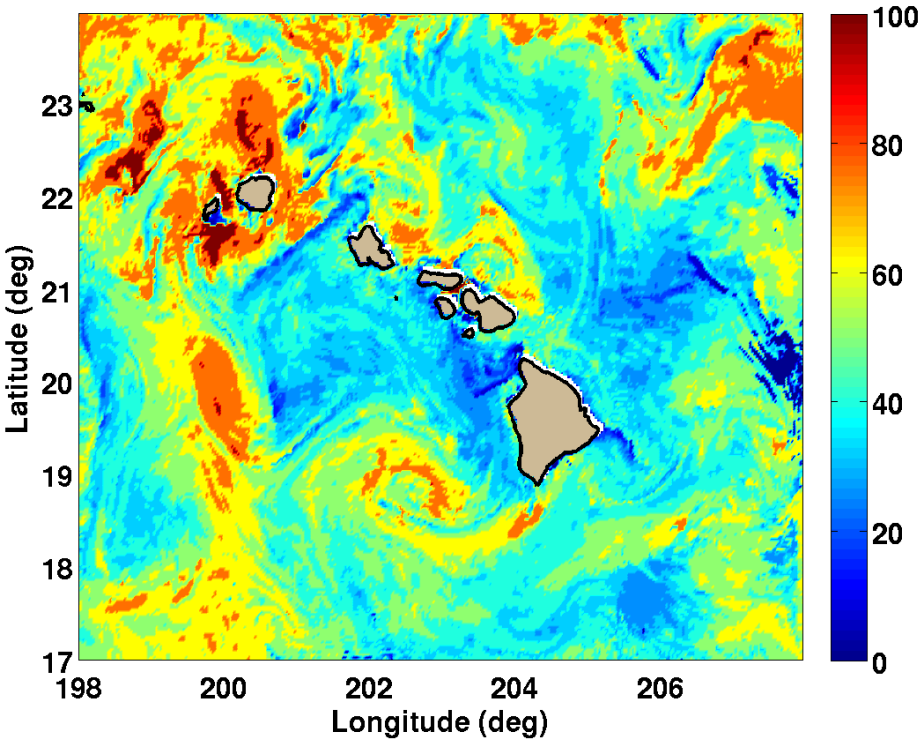

Figure 89. Sonic layer depth in m for Hawaiian area of interest.

Low Frequency

Low frequency, 250 Hz, acoustic predictions were computed using source depths of 15 m and 80 m, so that at least one of the analyses contains sources in the layer. Multiple receiver depths were computed. The number of radials (TL predictions) used to compute the brute force PAC for this case is 13,416, and the number of TL representatives required to generate the provinced PAC is 2,439, resulting in a computational savings of better than 5-fold. Figure 90 shows the mode provinces for the low frequency for this case; again the tendency to province along isobaths is evident.

Figure 91 shows the near surface brute force PAC (left) and the provinced PAC (right) for the 15 m source and the 15 m receiver. The performance for this area is quite low; only 0-10% of the area is covered. The lower percentage coverages don't compare as well as when the predicted performance is better. This is because of the sensitivity of the area metric to long range performance. For example, Figure 92 shows TL predictions for the brute force location near 200E, 23.59N at a bearing of 90 degrees in red. The blue line is the representative TL from

the province that was used to generate the provinced coverage, and the black line is the FOM (83 dB) used to determine coverage. It can be seen that the two curves compare well, and that the TL feature at 120 km accounts for the difference in PAC. This type of difference is typical, particularly at the low TL values. While the features do not seem to compare as well upon examination of Figure 91, the differences are less than 5% as seen in Figure 93. Similar results are shown for the other cases in Figure 94 through Figure 113 for the various source and receiver depth combinations.

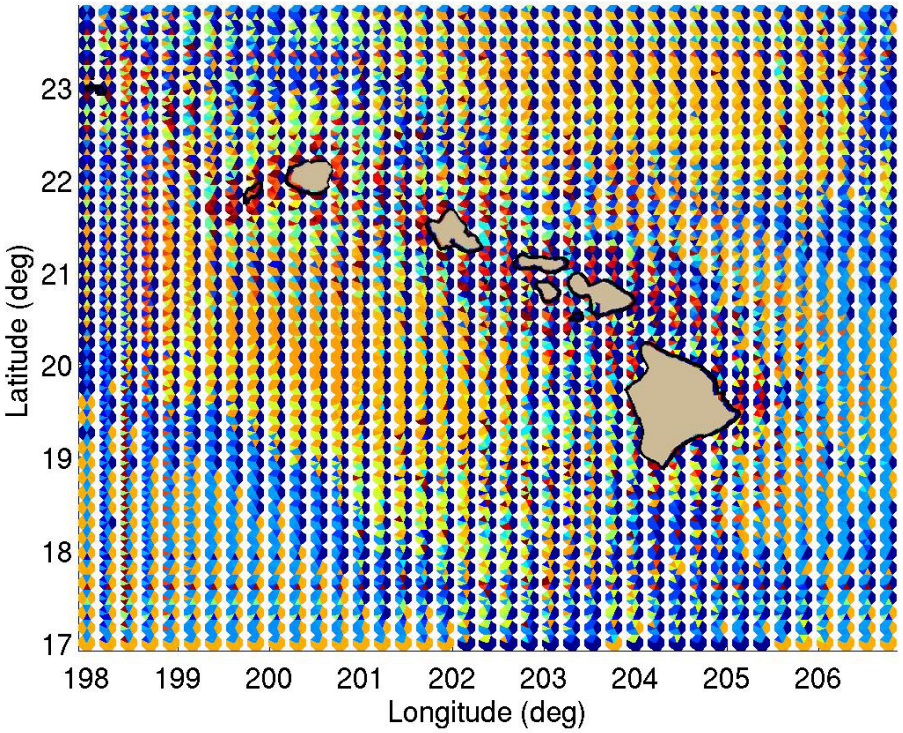

Figure 90. Low frequency mode provinces for the Hawaii area.

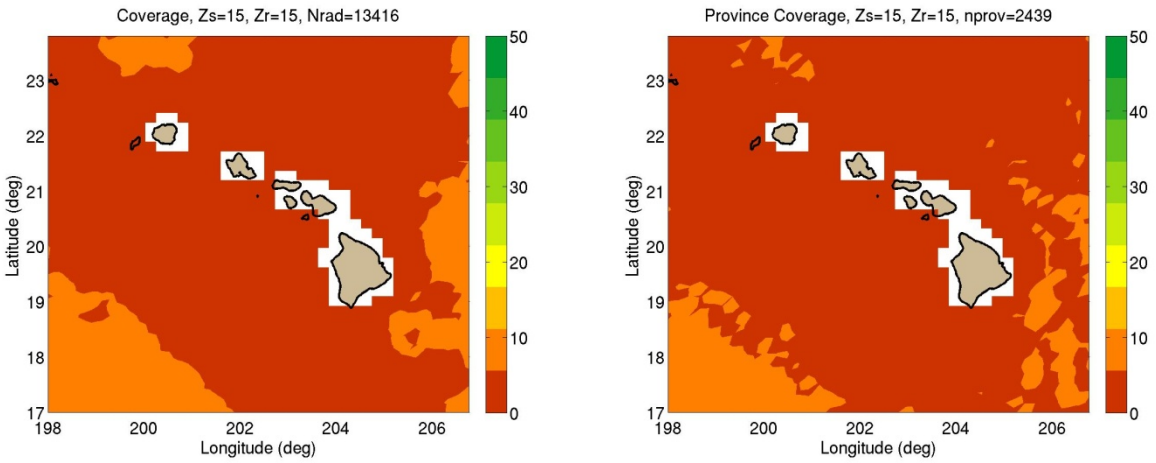

Figure 91. Brute force (left) and critical factors representative environment (right) PAC for 250 Hz, source at 15 m, receiver at 15 m.

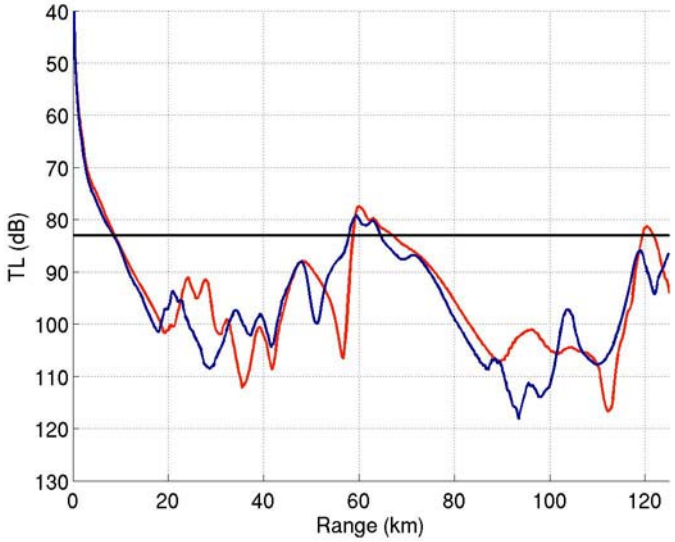

Figure 92. TL for the brute force location near 200E, 23.59N, bearing of 90 degrees, for a source depth of 15 m and receiver depth of 15 m (red), the representative TL from the province (blue) that was used to generate the provinced coverage, and the FOM (black) used to determine coverage.

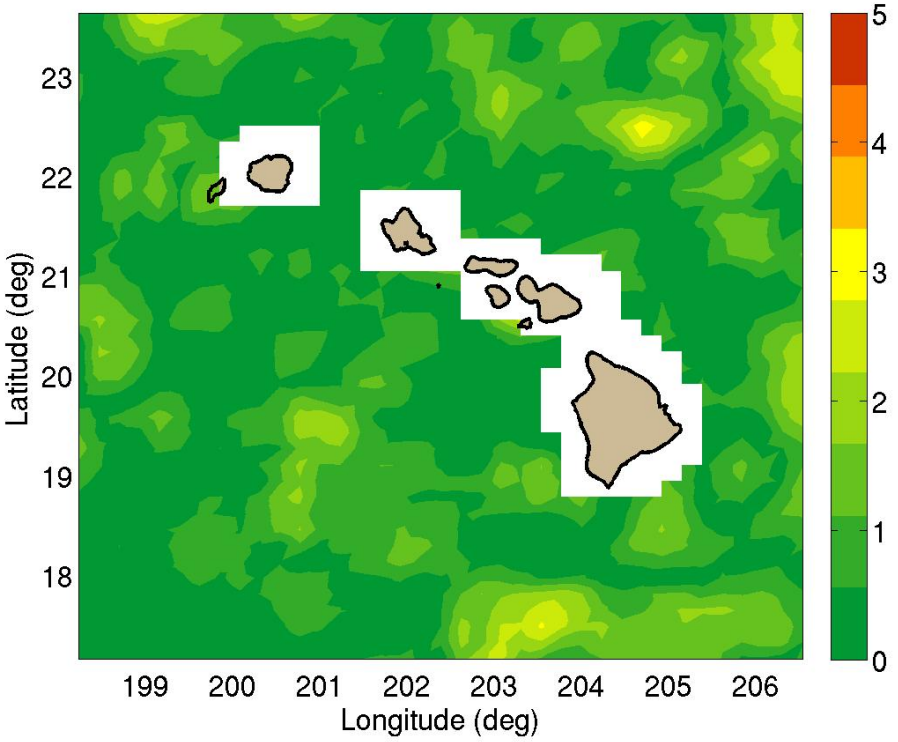

Figure 93. Averaged difference in percent between brute force and critical factors representative environment PAC for 250 Hz, source at 15 m, receiver at 15 m.

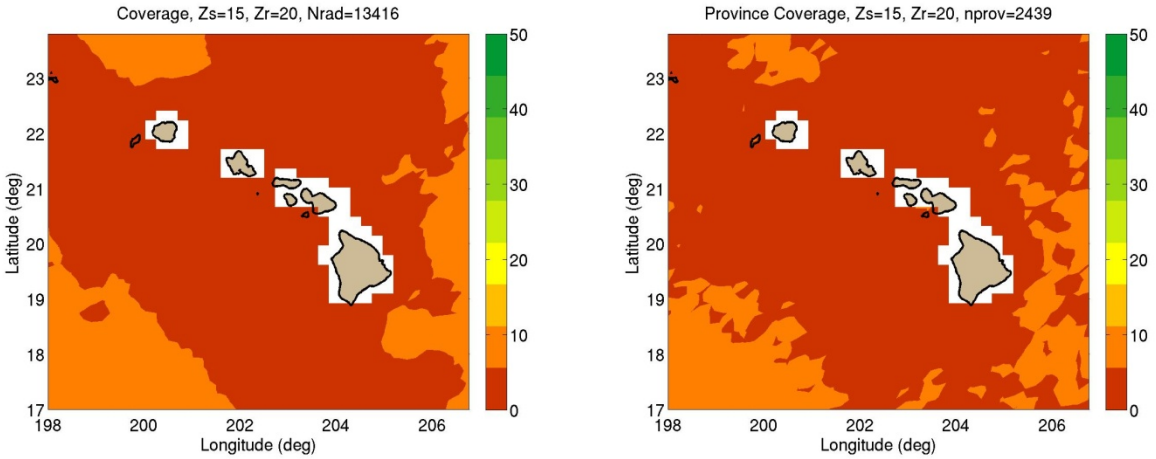

Figure 94. Brute force (left) and critical factors representative environment (right) PAC for 250 Hz, source at 15 m, receiver at 20 m.

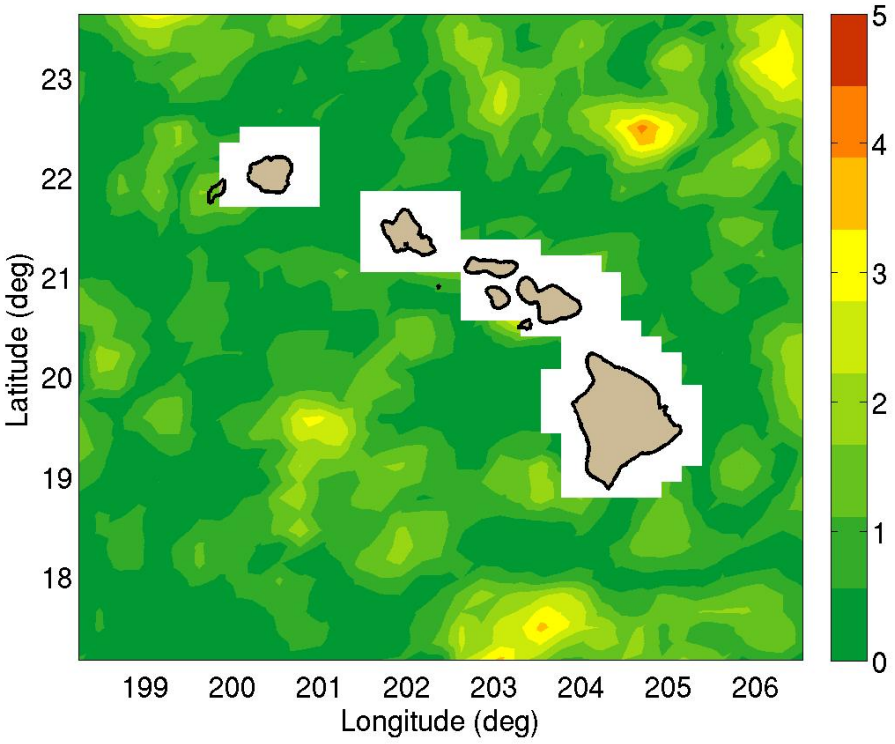

Figure 95. Averaged difference in percent between brute force and critical factors representative environment PAC for 250 Hz, source at 15 m, receiver at 20 m.

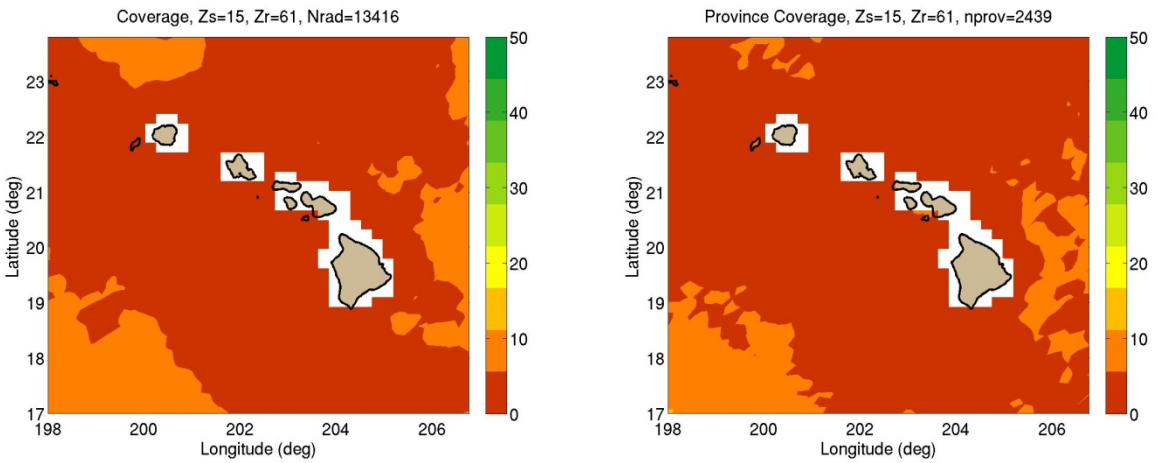

Figure 96. Brute force (left) and critical factors representative environment (right) PAC for 250 Hz, source at 15 m, receiver at 61 m.

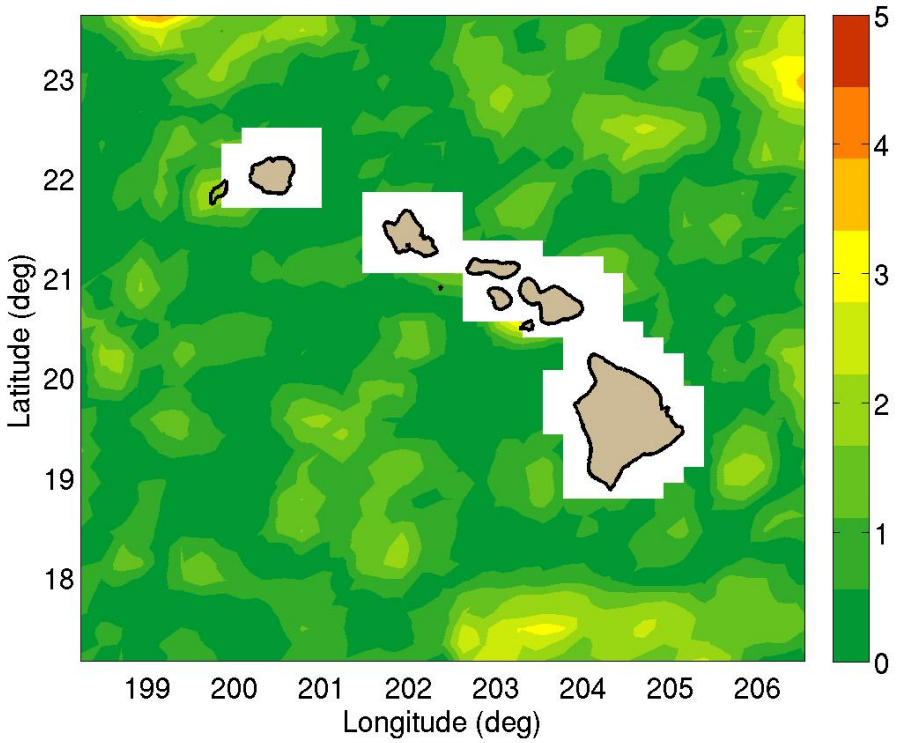

Figure 97. Averaged difference in percent between brute force and critical factors representative environment PAC for 250 Hz, source at 15 m, receiver at 61 m.

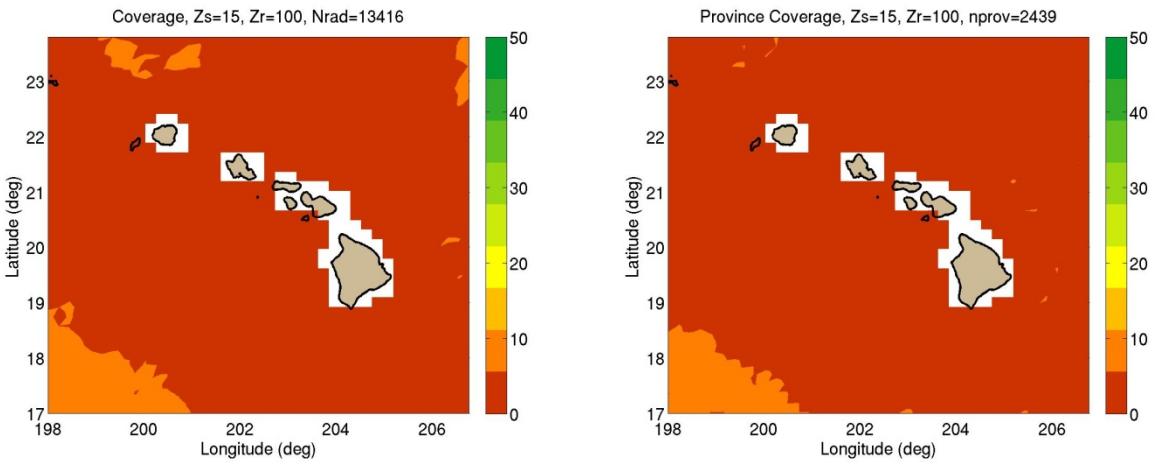

Figure 98. Brute force (left) and critical factors representative environment (right) PAC for 250 Hz, source at 15 m, receiver at 100 m.

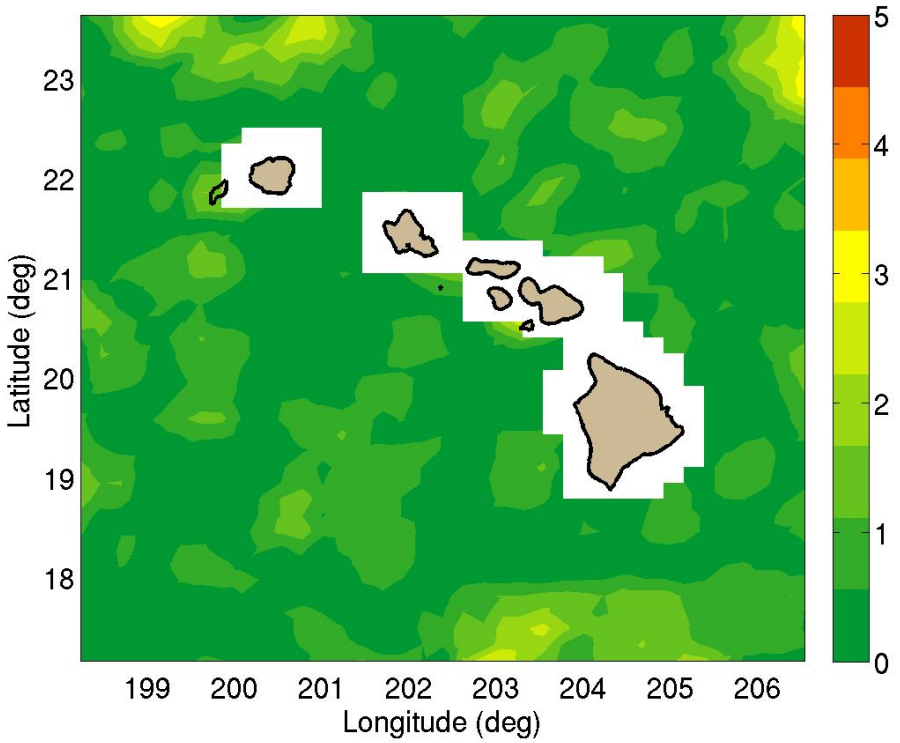

Figure 99. Averaged difference in percent between brute force and critical factors representative environment PAC for 250 Hz, source at 15 m, receiver at 100 m.

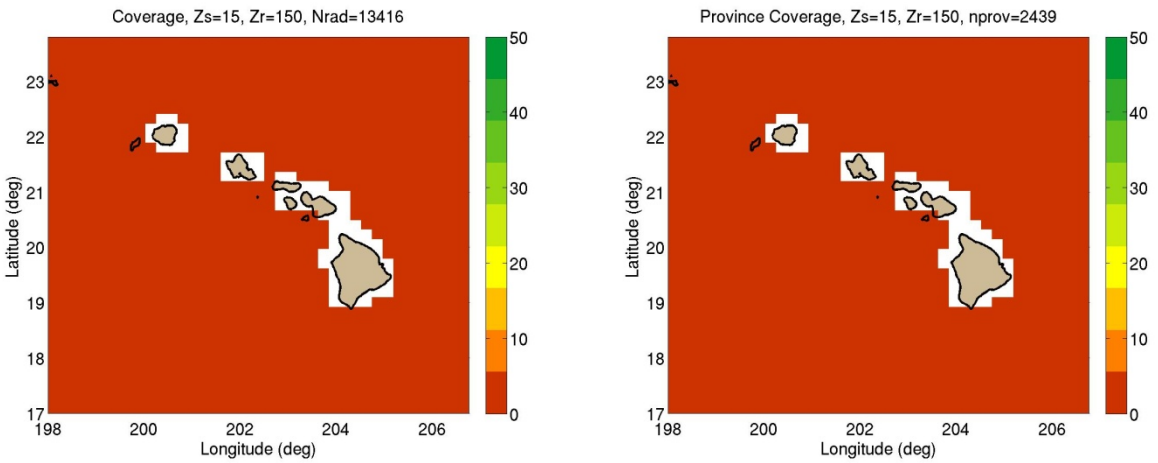

Figure 100. Brute force (left) and critical factors representative environment (right) PAC for 250 Hz, source at 15 m, receiver at 150 m.

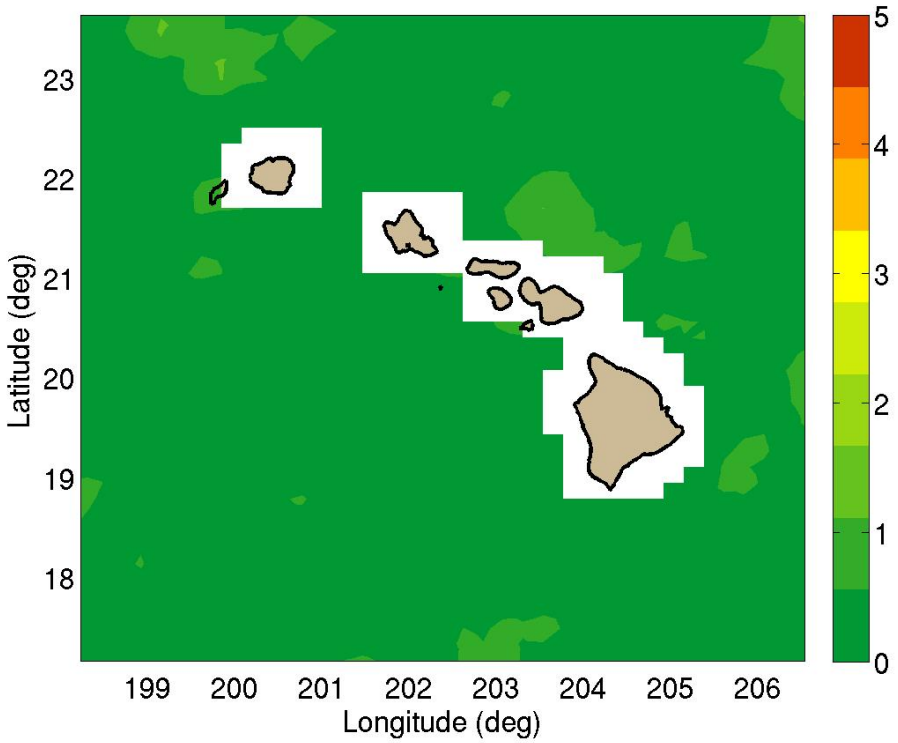

Figure 101. Averaged difference in percent between brute force and critical factors representative environment PAC for 250 Hz, source at 15 m, receiver at 150 m.

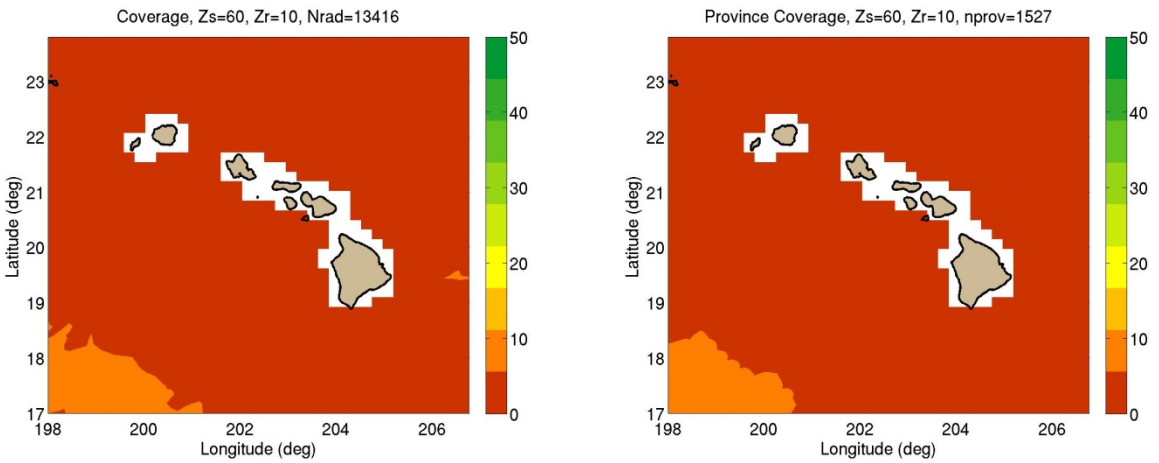

Figure 102. Brute force (left) and critical factors representative environment (right) PAC for 250 Hz, source at 60 m, receiver at 10 m.

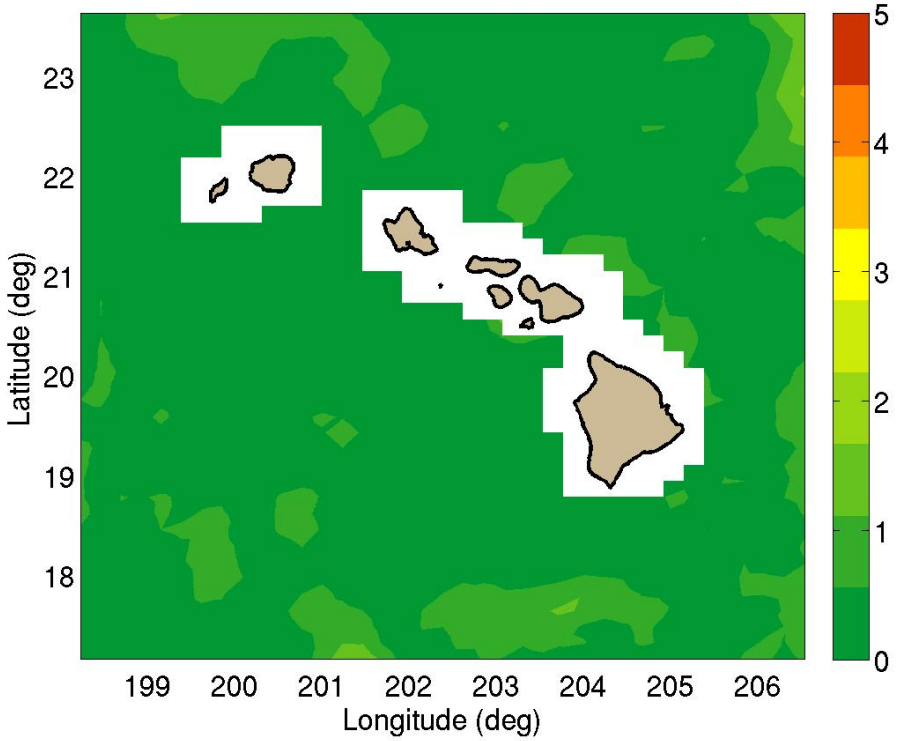

Figure 103. Averaged difference in percent between brute force and critical factors representative environment PAC for 250 Hz, source at 60 m, receiver at 10 m.

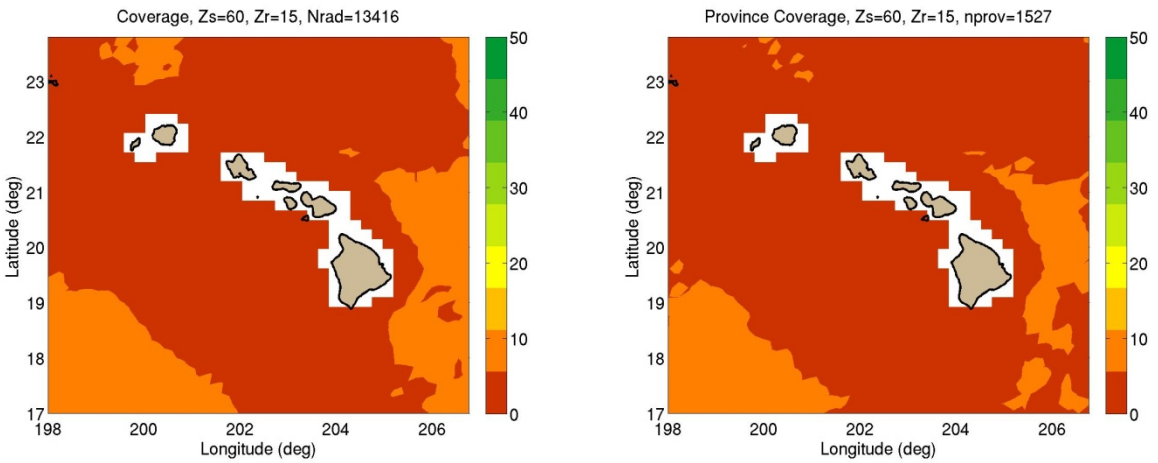

Figure 104. Brute force (left) and critical factors representative environment (right) PAC for 250 Hz, source at 60 m, receiver at 15 m.

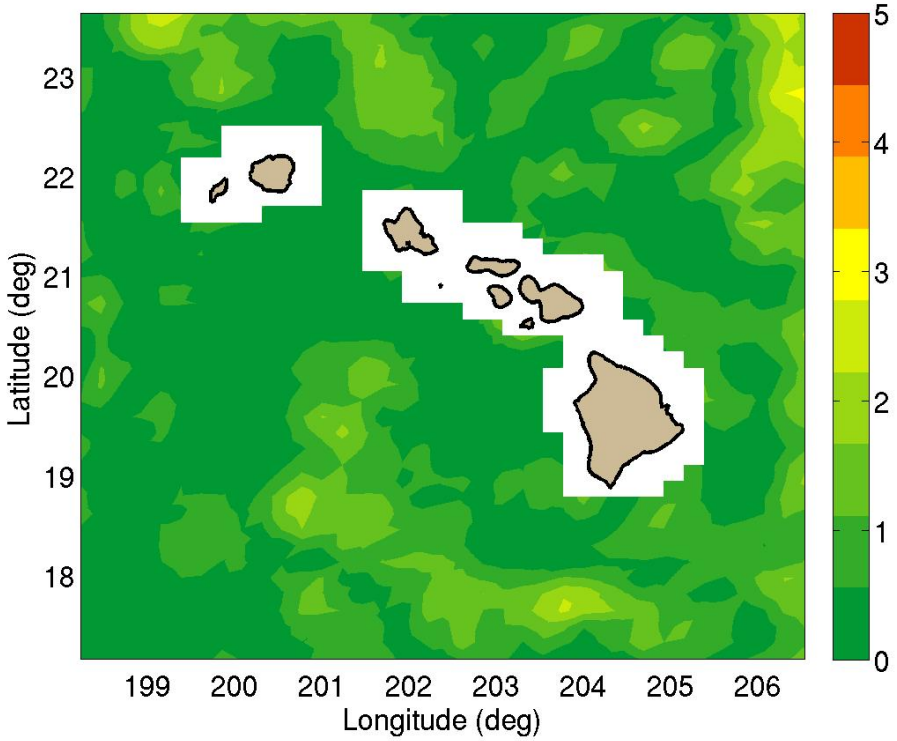

Figure 105. Averaged difference in percent between brute force and critical factors representative environment PAC for 250 Hz, source at 60 m, receiver at 15 m.

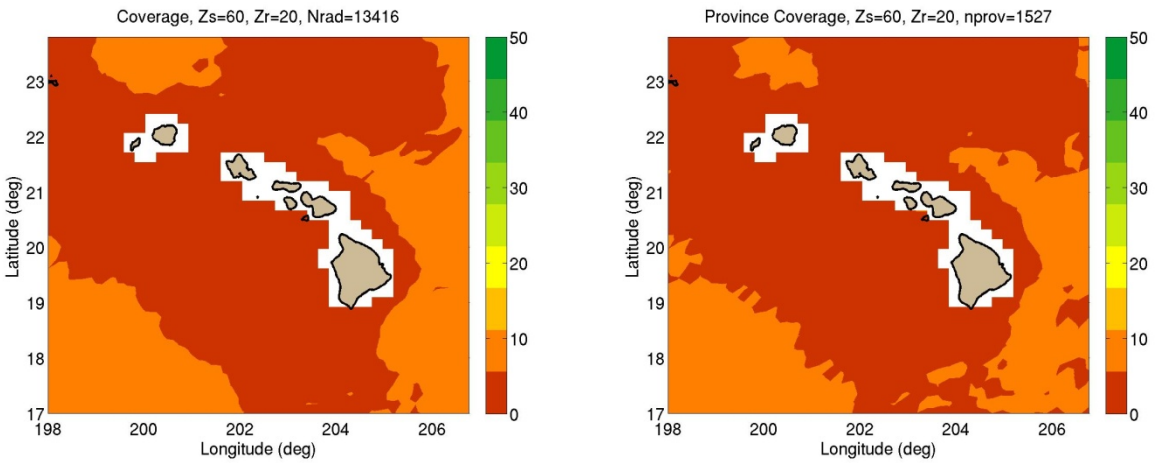

Figure 106. Brute force (left) and critical factors representative environment (right) PAC for 250 Hz, source at 60 m, receiver at 20 m.

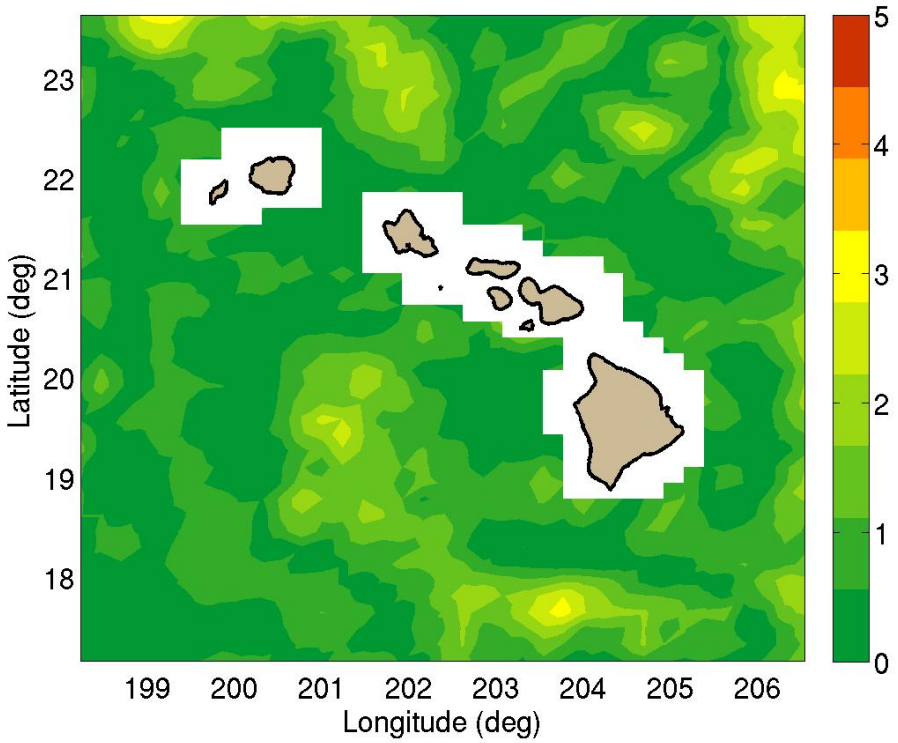

Figure 107. Averaged difference in percent between brute force and critical factors representative environment PAC for 250 Hz, source at 60 m, receiver at 20 m.

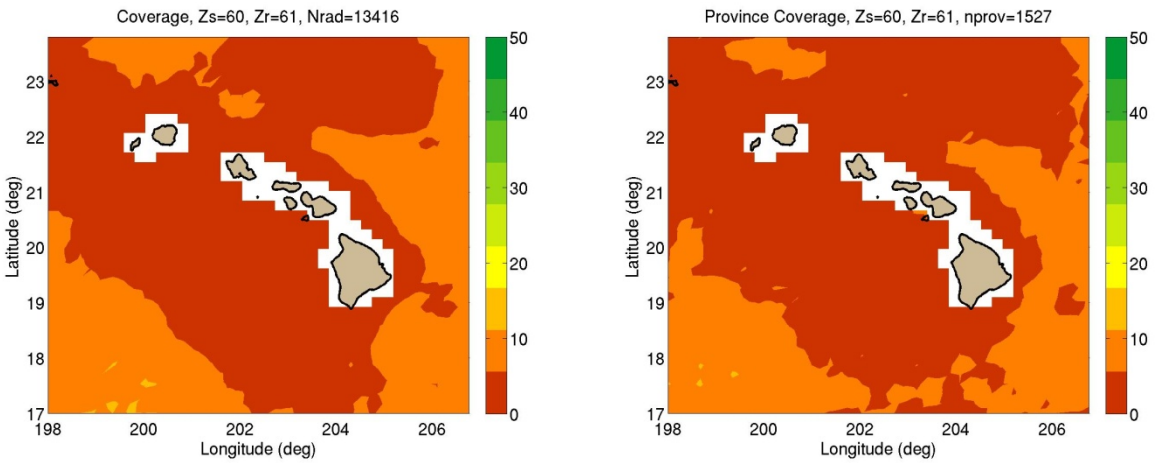

Figure 108. Brute force (left) and critical factors representative environment (right) PAC for 250 Hz, source at 60 m, receiver at 61 m.

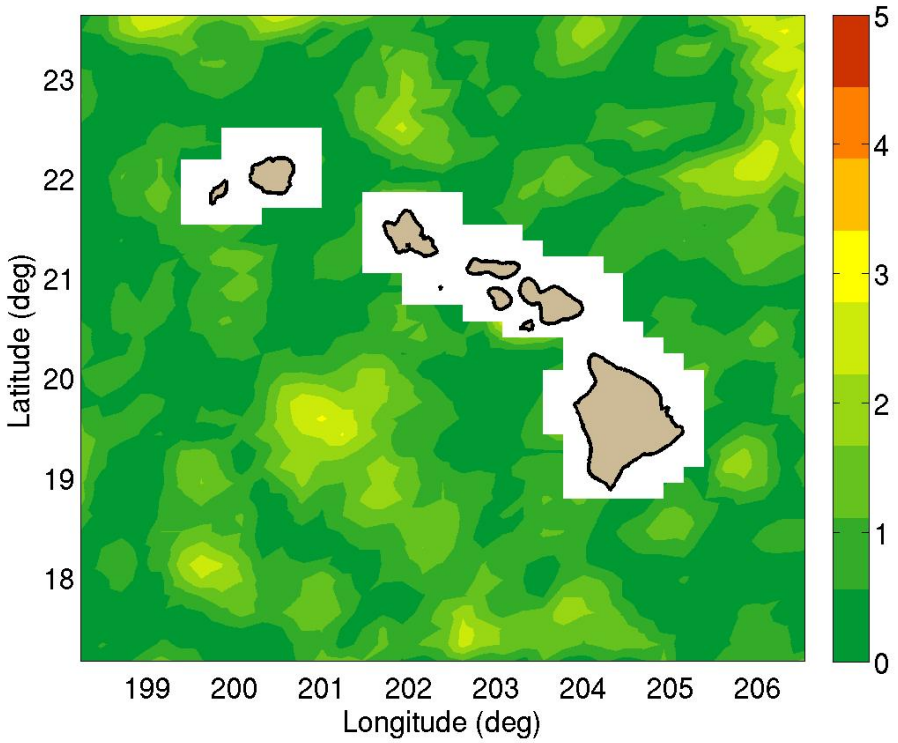

Figure 109. Averaged difference in percent between brute force and critical factors representative environment PAC for 250 Hz, source at 60 m, receiver at 61 m.

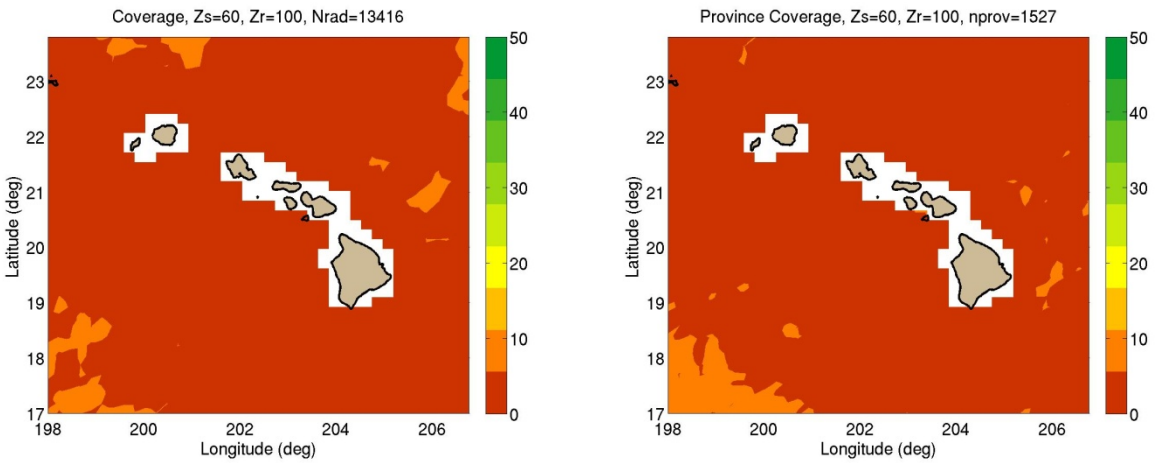

Figure 110. Brute force (left) and critical factors representative environment (right) PAC for 250 Hz, source at 60 m, receiver at 100 m.

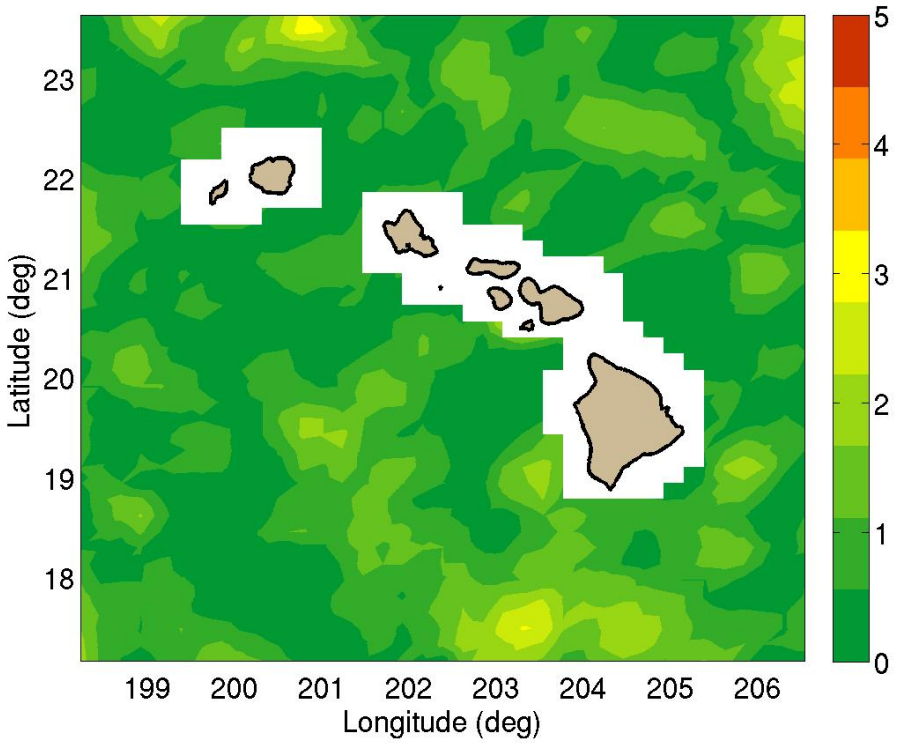

Figure 111. Averaged difference in percent between brute force and critical factors representative environment PAC for 250 Hz, source at 60 m, receiver at 100 m.

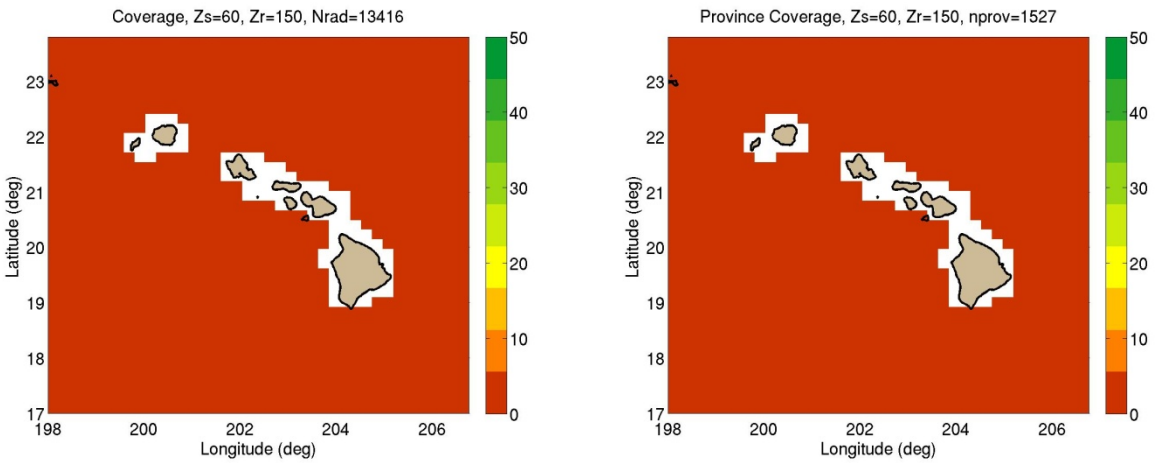

Figure 112. Brute force (left) and critical factors representative environment (right) PAC for 250 Hz, source at 60 m, receiver at 150 m.

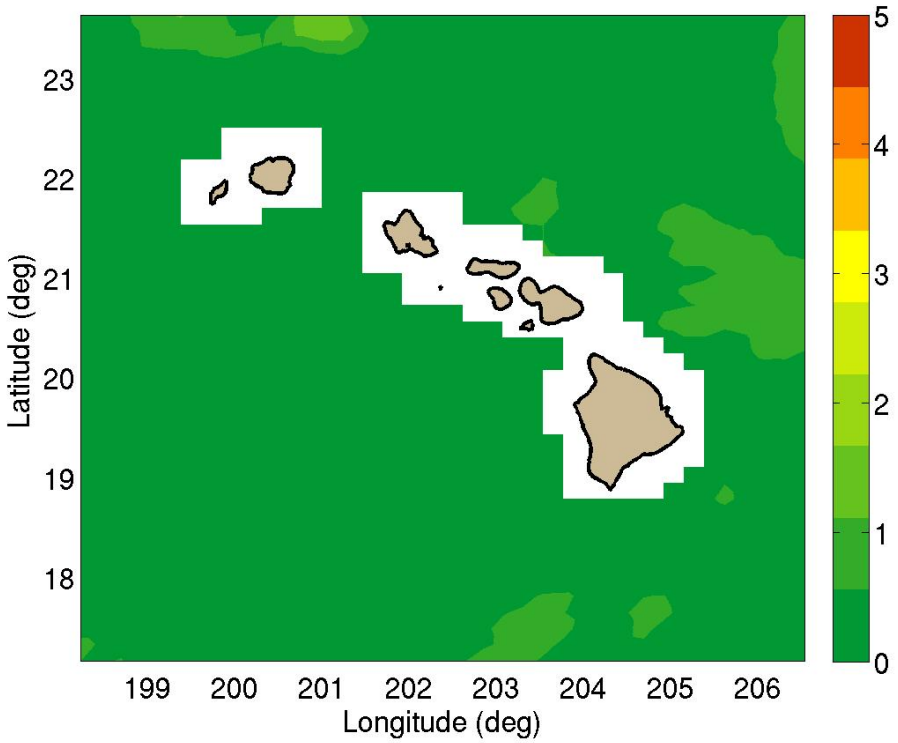

Figure 113. Averaged difference in percent between brute force and critical factors representative environment PAC for 250 Hz, source at 60 m, receiver at 150 m.

Table 4. Summary of differences for the Hawaii AOI at 250 Hz.

Source Depth (m)	Receiver Depth (m)	Maximum % difference	Mean % difference
15	10	2.09	0.43
	15	3.20	0.68
	20	4.16	0.80
	61	4.06	0.77
	100	3.29	0.58
	150	1.22	0.24
	200	0.80	0.11
	250	0.74	0.07
	300	1.15	0.08
	500	1.82	0.06
60	10	1.76	0.33
	15	2.95	0.65
	20	3.06	0.79
	61	3.23	0.77
	100	3.08	0.73
	150	1.63	0.23
	200	0.67	0.08
	250	0.84	0.05
	300	1.04	0.06
	500	0.64	0.05
150	10	1.24	0.08
	15	1.20	0.19
	20	1.56	0.24
	61	1.29	0.17
	100	1.38	0.34
	150	2.47	0.55
	200	1.44	0.32
	250	1.20	0.27
	300	1.31	0.21
	500	0.99	0.05

Mid Frequency

Mid frequency (1,000 Hz), acoustic predictions were computed using source depths of 20 m and 80 m to capture the layer when it exists at that frequency. The number of radials (TL predictions) used to compute coverage for this case is 13,416, and the number of TL predictions required to generate the provinced coverage is 2,628, resulting in a computational savings of approximately 5-fold.

Figure 114 illustrates an advantage of the provincing. The left side of Figure 114 shows the brute force PAC. The red, or poor performance area east of 205°E is an area for which the acoustic model failed to run. The right plot is the PAC generated using the provinces. Note the different color scales. The advantage is that because the provinces are based on the environment, they do not require all the runs to have completed to generate a fairly accurate PAC plot, they use only the representative environments and are therefore less sensitive to a large number of runs being computed.

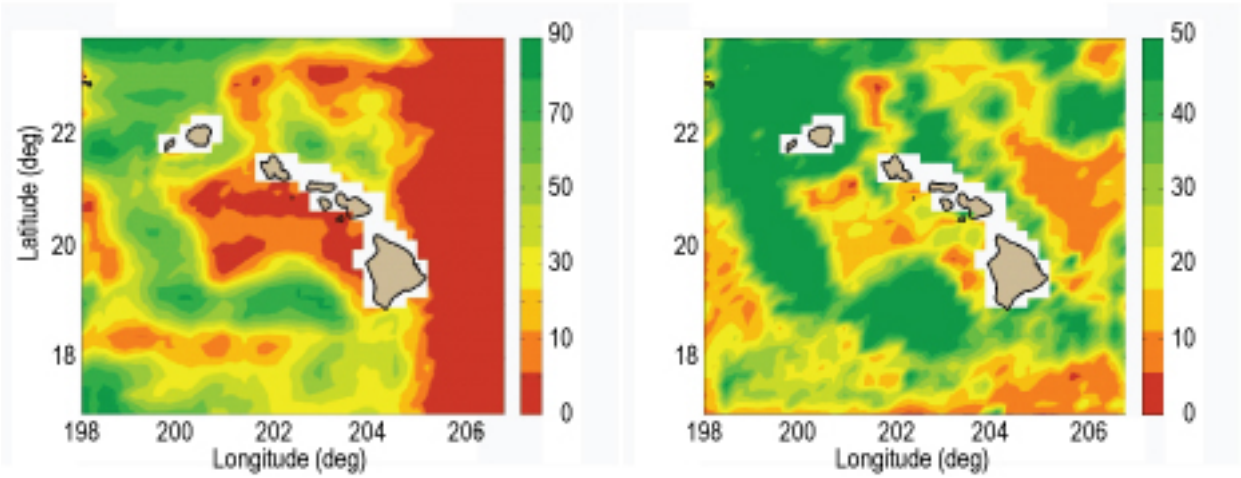

Figure 114. Incomplete brute force (left) and critical factor representative environment (right) PAC for 1000 Hz, source at 20 m, receiver at 15 m.

The left plots in Figure 115, Figure 117 and Figure 119 show the PAC computed using the brute force (13,416 TL predictions) method for the shallow source (20 m) and receivers at 15 m, 61 m and 100 m. Deeper receivers show the same performance as the 100 m receiver so are not shown. The right plots in Figure 115, Figure 117 and Figure 119 show the corresponding PAC estimates using only representatives (2,628 TL predictions) from each province. Figure

118, Figure 120 and Figure 122 show the boxcar differences between the brute force and provinced result. The left plot in Figure 121, Figure 123 and Figure 125 show the brute force PAC for the deeper (80 m) source at the receiver depths of interest, and the right plots show the provinced PAC result. Figure 122, Figure 124 and Figure 126 show the boxcar differences. The overall coverage features compare very well (within 5%) with the exception of the results shown in Figure 115 and Figure 116, which show high differences. Table 5 summarizes the differences over the entire area.

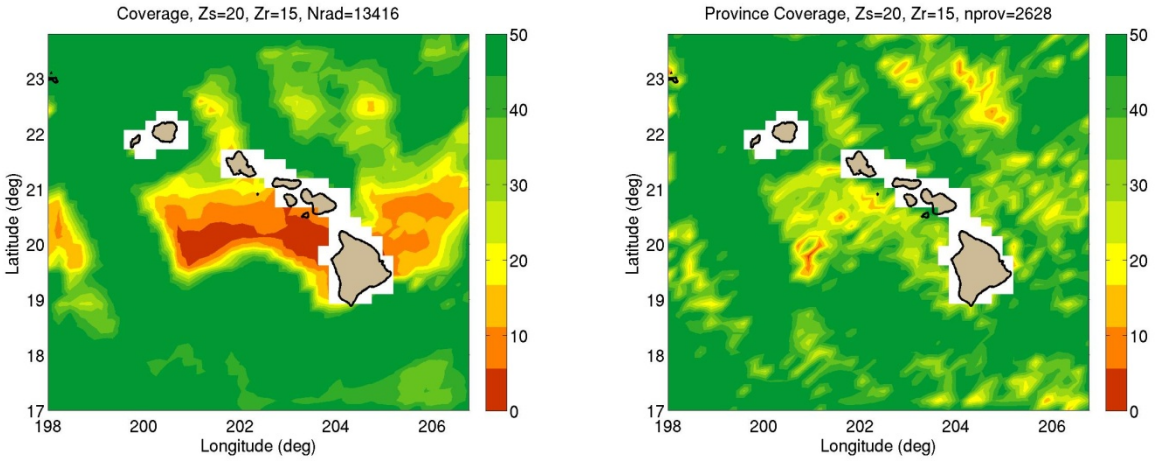

Figure 115. Brute force (left) and critical factors representative environment (right) PAC for 1000 Hz, source at 20 m, receiver at 15 m.

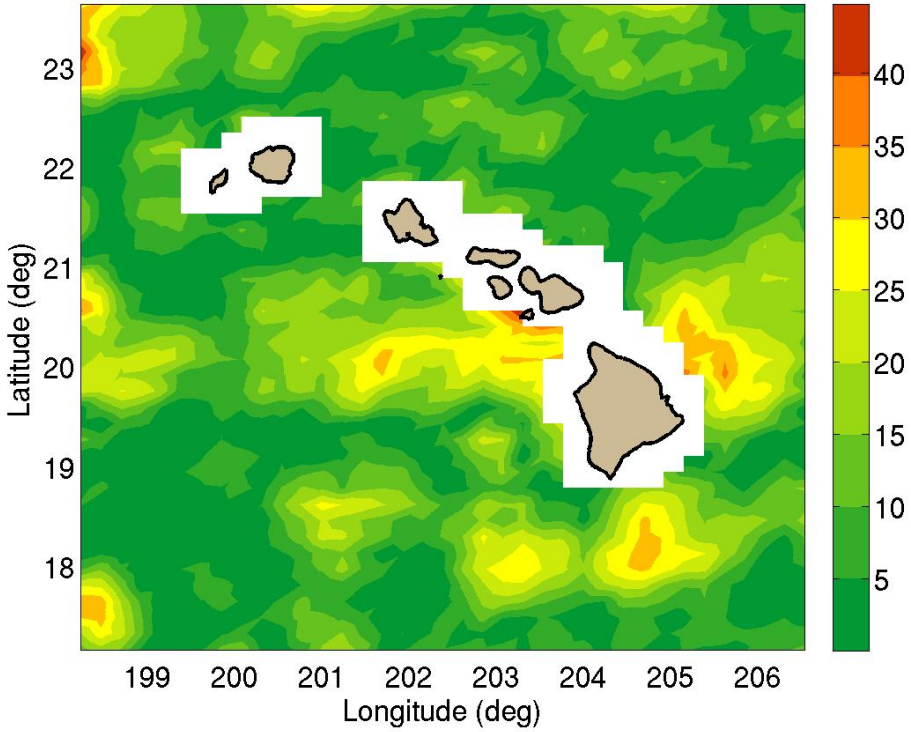

Figure 116. Averaged difference in percent between brute force and critical factors representative environment PAC for 1000 Hz, source at 20 m, receiver at 15 m.

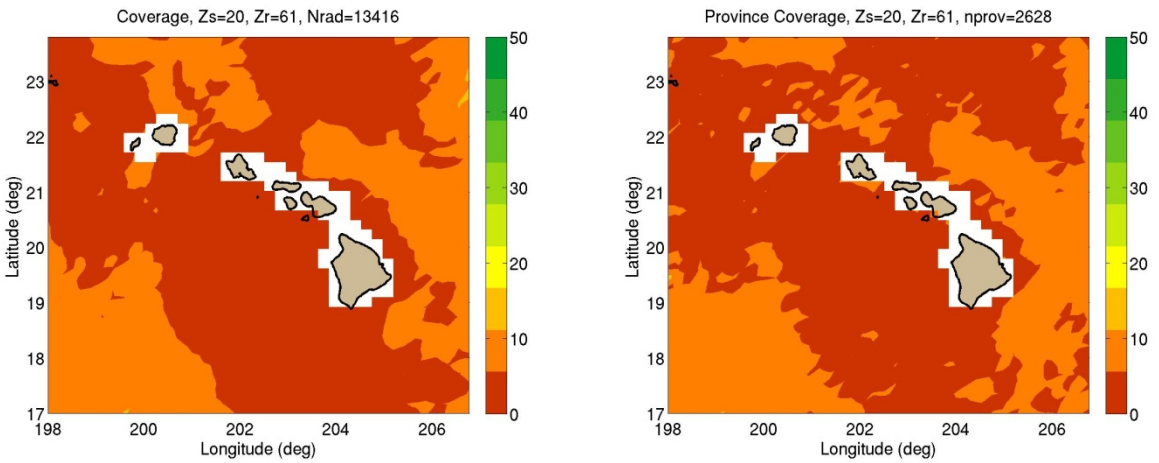

Figure 117. Brute force (left) and critical factors representative environment (right) PAC for 1000 Hz, source at 20 m, receiver at 61 m.

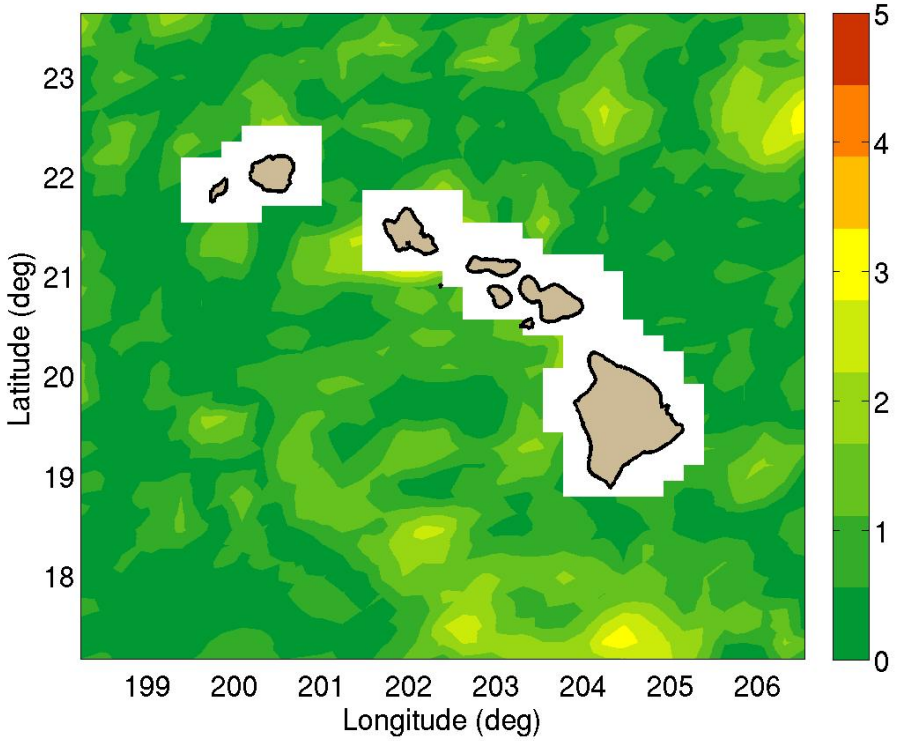

Figure 118. Averaged difference in percent between brute force and critical factors representative environment PAC for 1000 Hz, source at 20 m, receiver at 61 m.

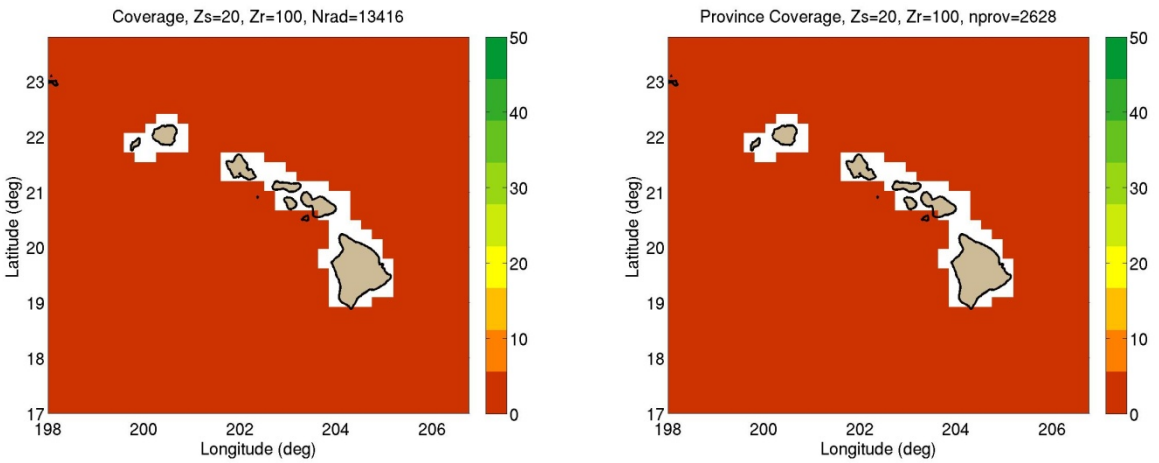

Figure 119. Brute force (left) and critical factors representative environment (right) PAC for 1000 Hz, source at 20 m, receiver at 100 m.

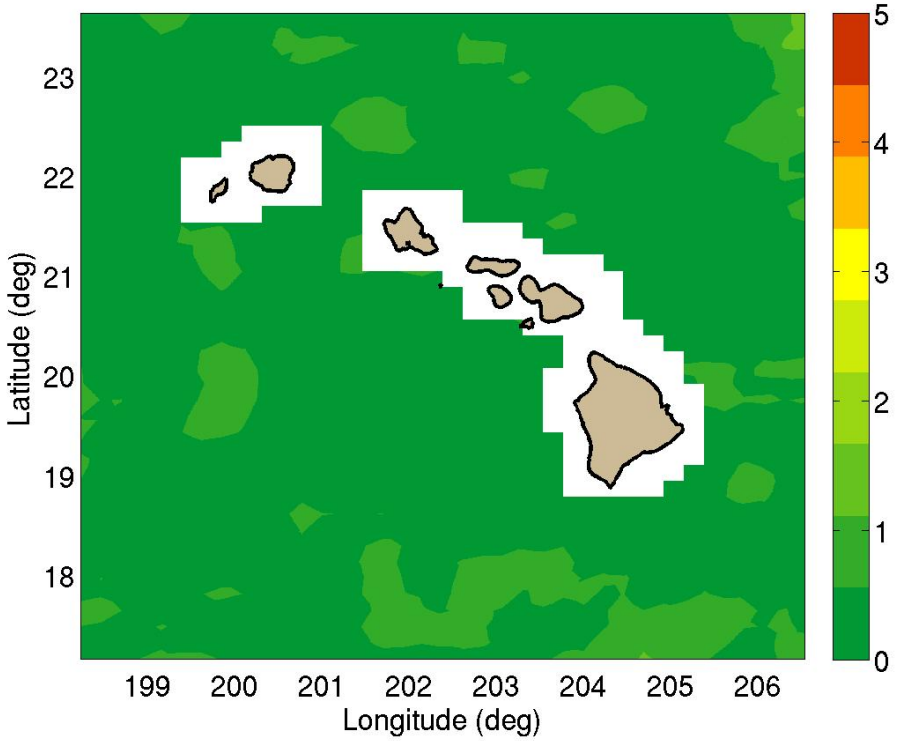

Figure 120. Averaged difference in percent between brute force and critical factors representative environment PAC for 1000 Hz, source at 20 m, receiver at 100 m.

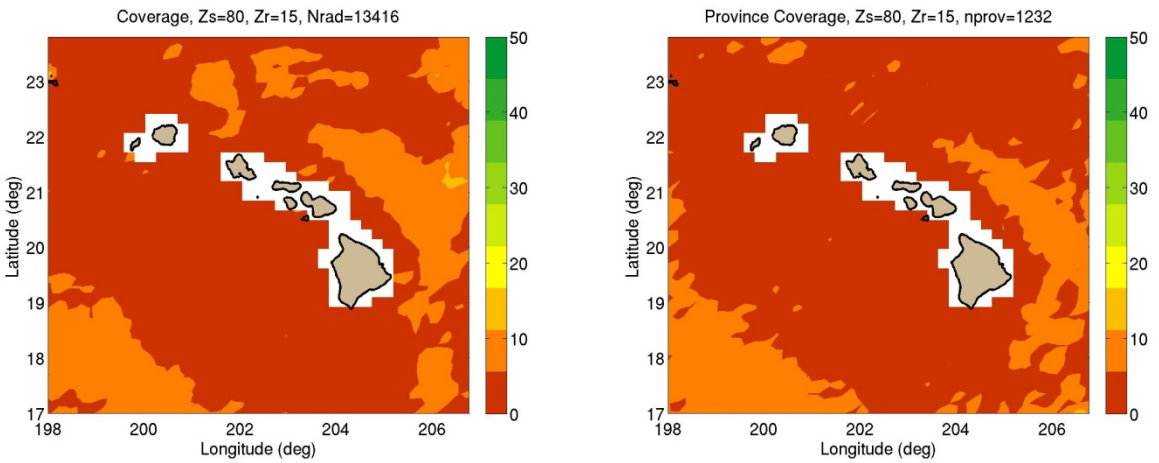

Figure 121. Brute force (left) and critical factors representative environment (right) PAC for 1000 Hz, source at 80 m, receiver at 15 m.

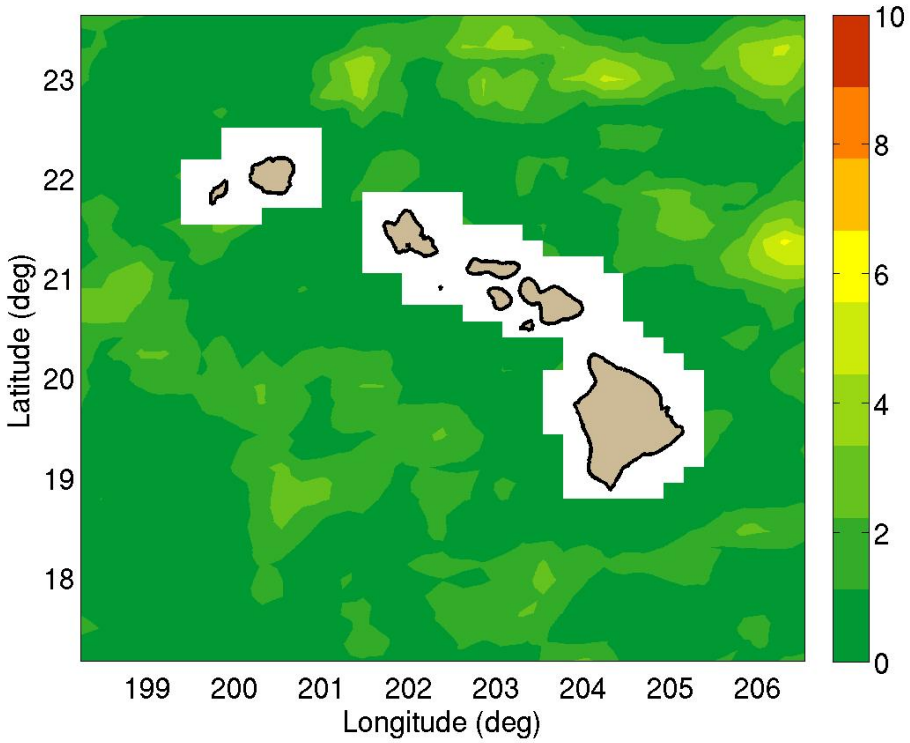

Figure 122. Averaged difference in percent between brute force and critical factors representative environment PAC for 1000 Hz, source at 80 m, receiver at 15 m.

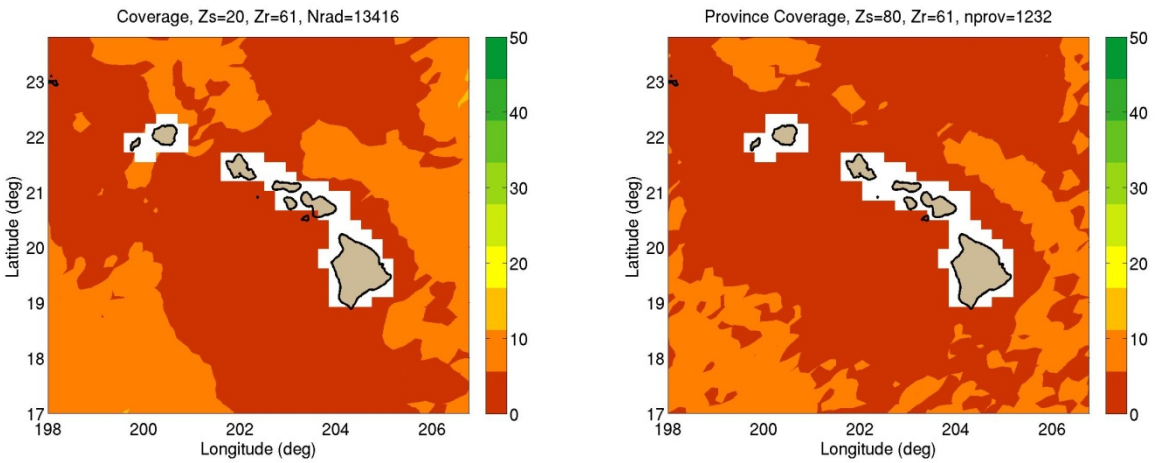

Figure 123. Brute force (left) and critical factors representative environment (right) PAC for 1000 Hz, source at 80 m, receiver at 61 m.

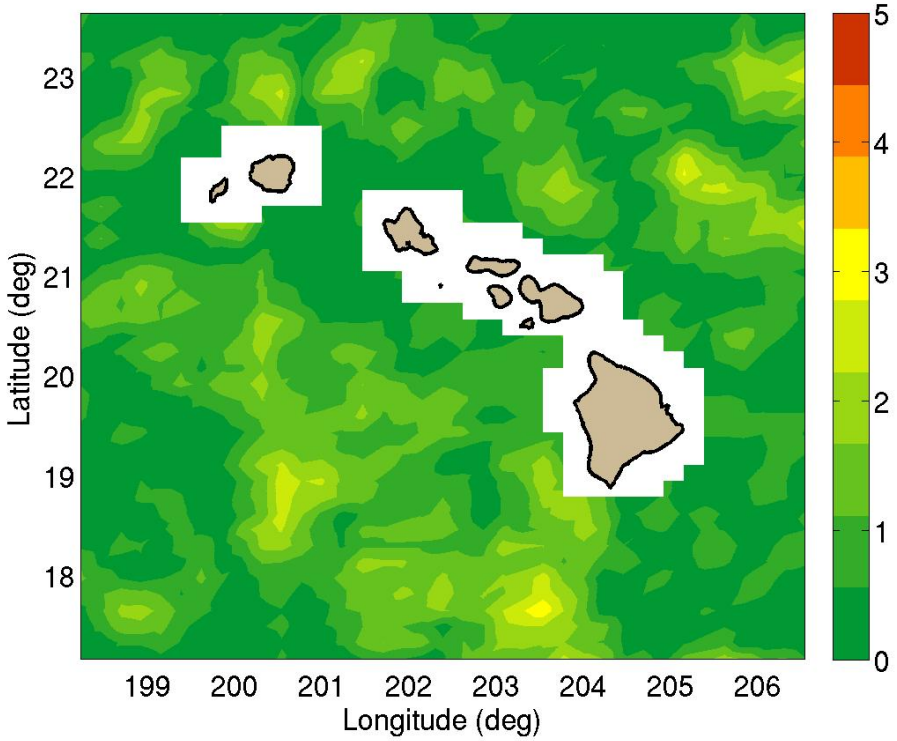

Figure 124. Averaged difference in percent between brute force and critical factors representative environment PAC for 1000 Hz, source at 80 m, receiver at 61 m.

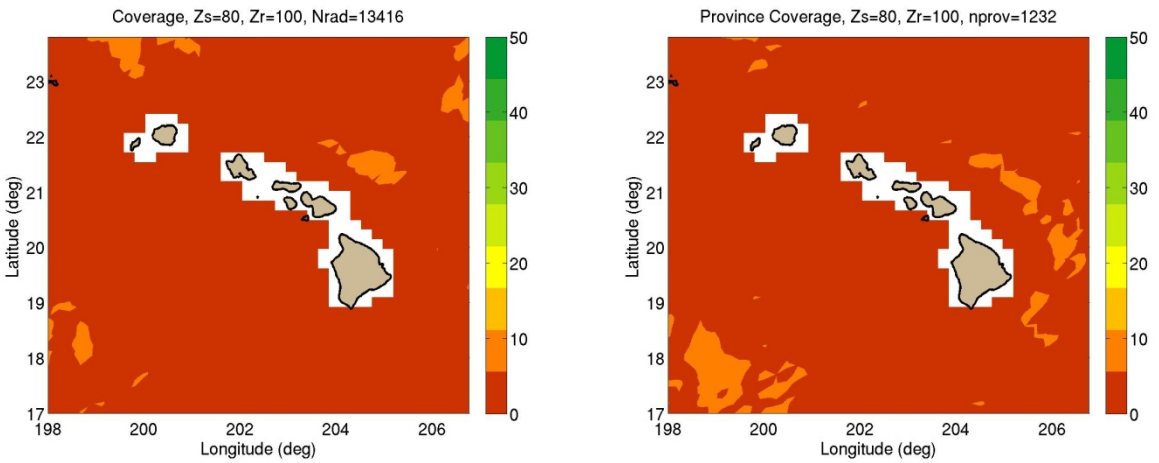

Figure 125. Brute force (left) and critical factors representative environment (right) PAC for 1000 Hz, source at 80 m, receiver at 100 m.

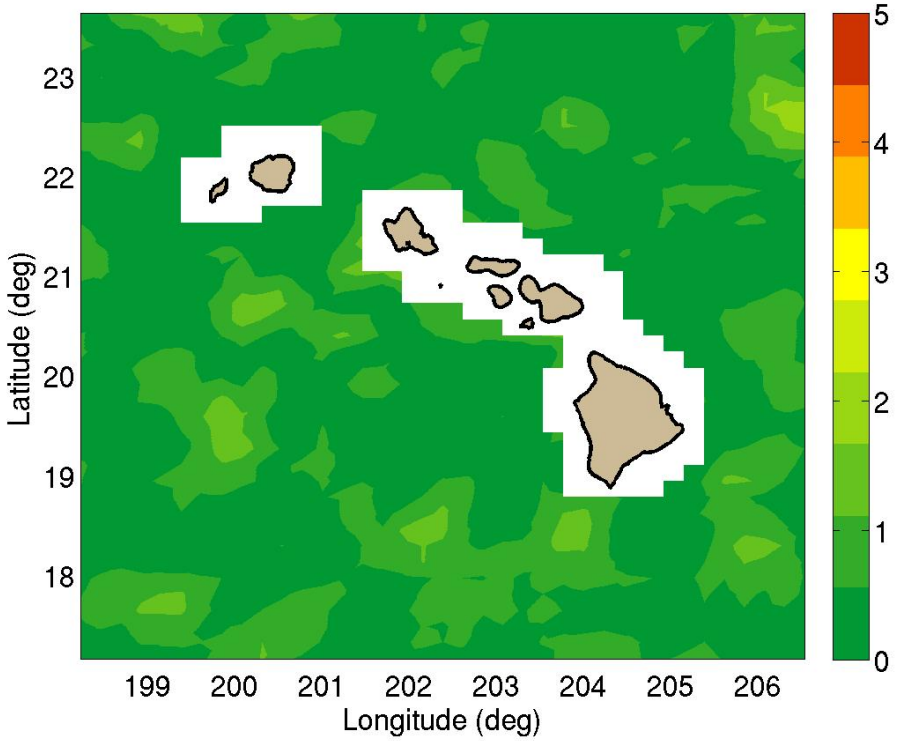

Figure 126. Averaged difference in percent between brute force and critical factors representative environment PAC for 1000 Hz, source at 80 m, receiver at 100 m.

Table 5. Summary of averaged differences.

Source Depth (m)	Receiver Depth (m)	Maximum % difference	Mean % difference
20	15	44.79	10.27
	61	3.29	0.77
	100	1.36	0.31
	150	1.14	0.11
	200	0.88	0.08
	250	0.87	0.07
	300	1.27	0.07
	500	1.81	0.07
80	15	5.82	1.02
	61	3.19	0.77
	100	1.85	0.45
	150	0.73	0.18
	200	0.88	0.10
	250	1.02	0.06
	300	1.46	0.06
	500	1.57	0.07

Southern California

NCOM oceanographic analysis from an area along the coast of California (NOAA, 2010) from January, 2010 was used to generate provinces and acoustic coverage. Bathymetry (m) from DBDB-V (NAVO, 2007) for this area is shown in Figure 127, the SLD computed using the NCOM analysis is shown in Figure 128. This area is a typical continental shelf bathymetry regime with deep water offshore, an intermediate sloping area and shallow water near the coast. The sonic layer is prevalent over the southern portion of the area.

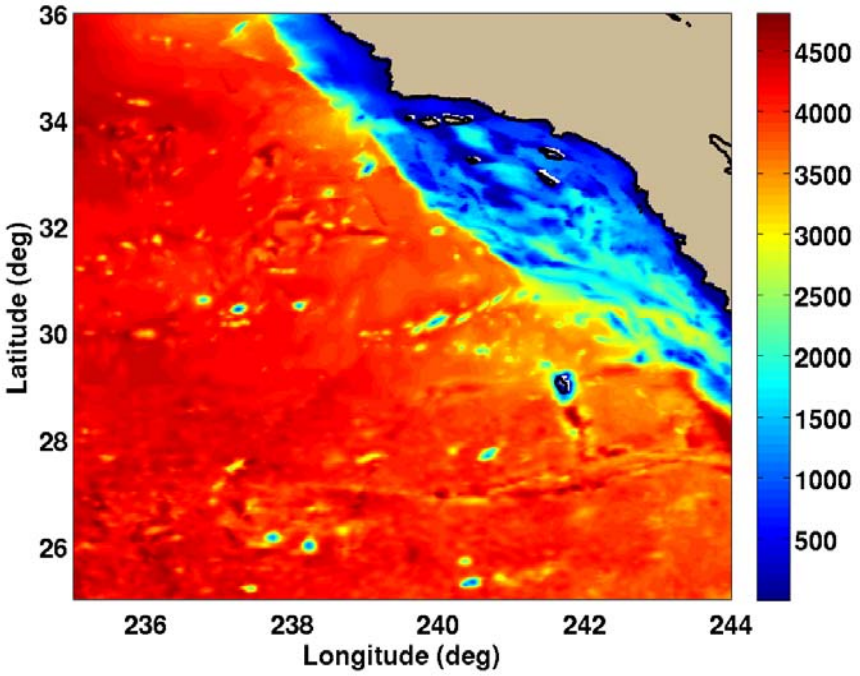

Figure 127. DBDB-V bathymetry in m for the Southern California area of interest.

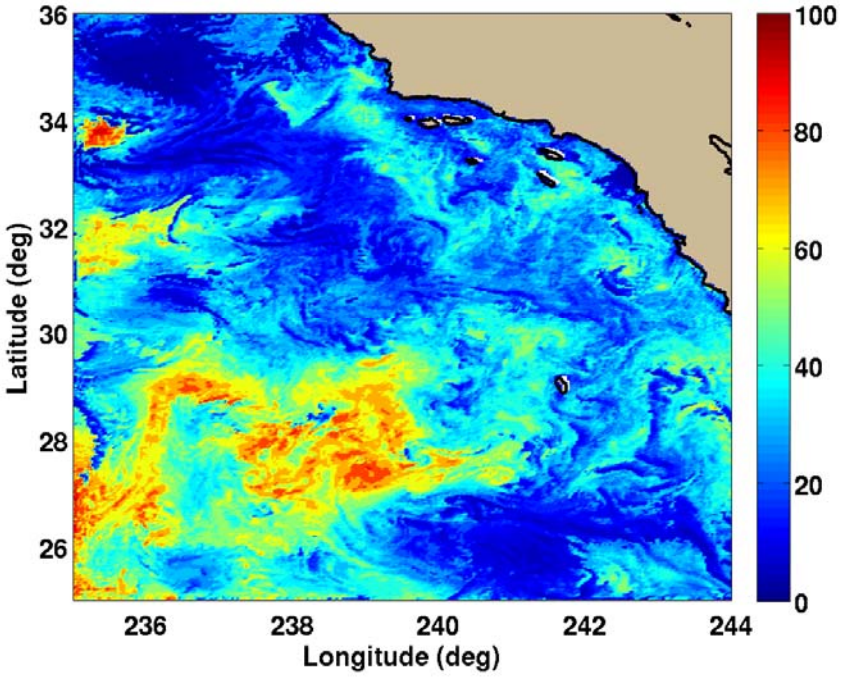

Figure 128. Sonic layer depth in m for Southern California area of interest.

Low Frequency

Low frequency (250 Hz) acoustic predictions at two source depths were computed, 15 m so that if there is a layer, the source will be in it and 60 m, which will be in the layer some of the time. The number of radials (TL predictions) used to compute coverage for this case (8 radials per grid point) is 13,072 and the number of TL predictions required to generate the provinced coverage is 1,363 resulting in a computational savings of approximately 7-fold.

Figure 129 shows the provinced results for this low frequency case. Each province is plotted as a different color. There are not enough colors in the pallet to show all the unique provinces, however, this gives a good view of the provinced results and indicates that the provinces fall along the areas of similar slope, that is they follow isobaths, as expected.

The left plots in Figure 130 and Figure 132 show the PAC computed using the brute force (13,072 TL predictions) method for the shallow source and the various receivers. Other receivers were computed, but are not shown due to their similarity to the figures presented. The right plots in Figure 130 and Figure 132 show the corresponding PAC estimates using only representatives (1,363 TL predictions) from each province. The low performance features seem to not match as well when comparing visually, however, the boxcar averaged differences shown in Figure 131 and Figure 133 show differences no larger than 5%. Table 6 summarizes the overall differences for this case.

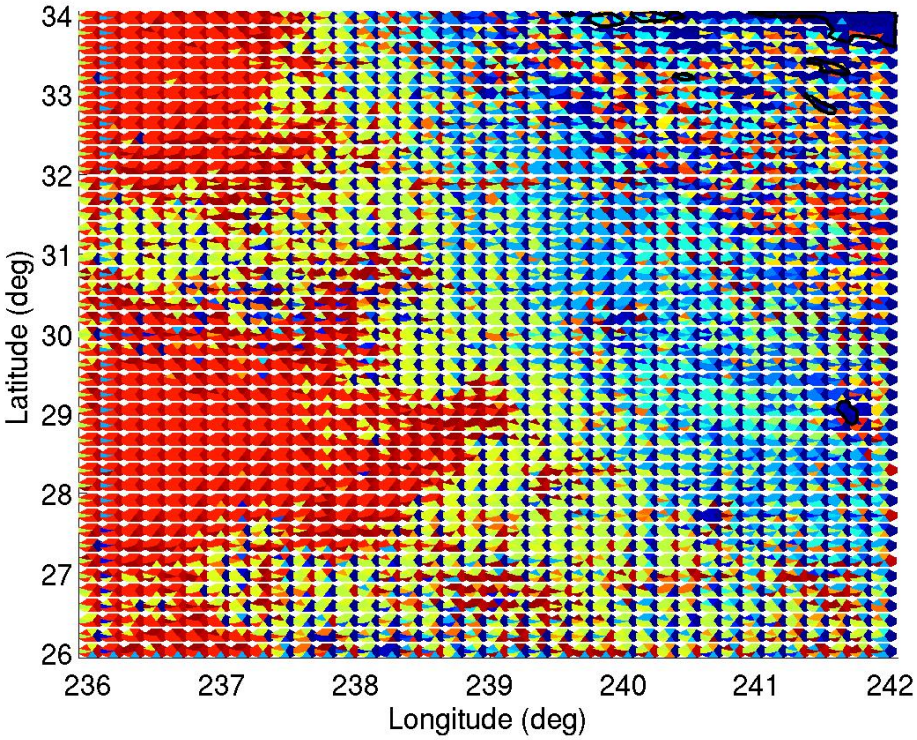

Figure 129. Low frequency mode provinces for the Southern California area.

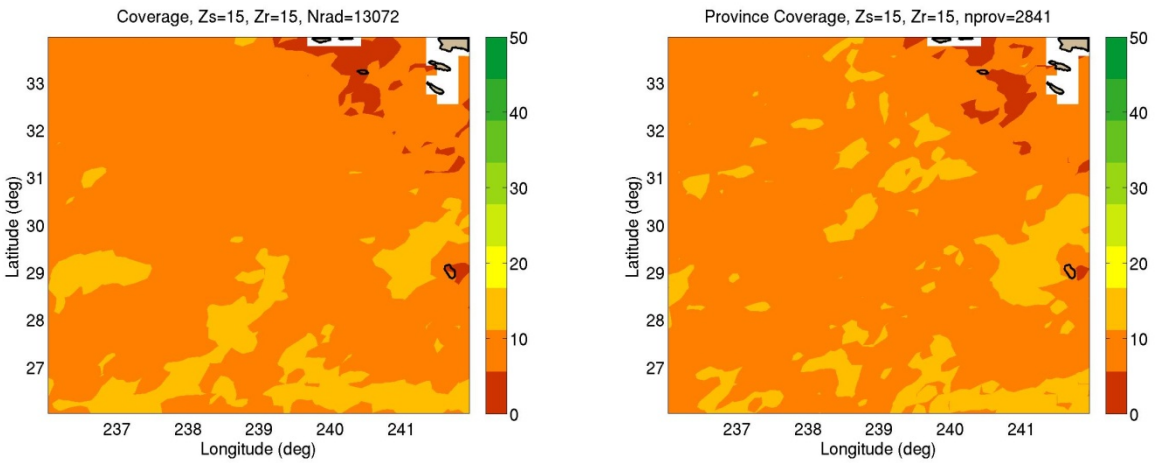

Figure 130. Brute force (left) and critical factors representative environment (right) PAC for 250 Hz, source at 15 m, receiver at 15 m.

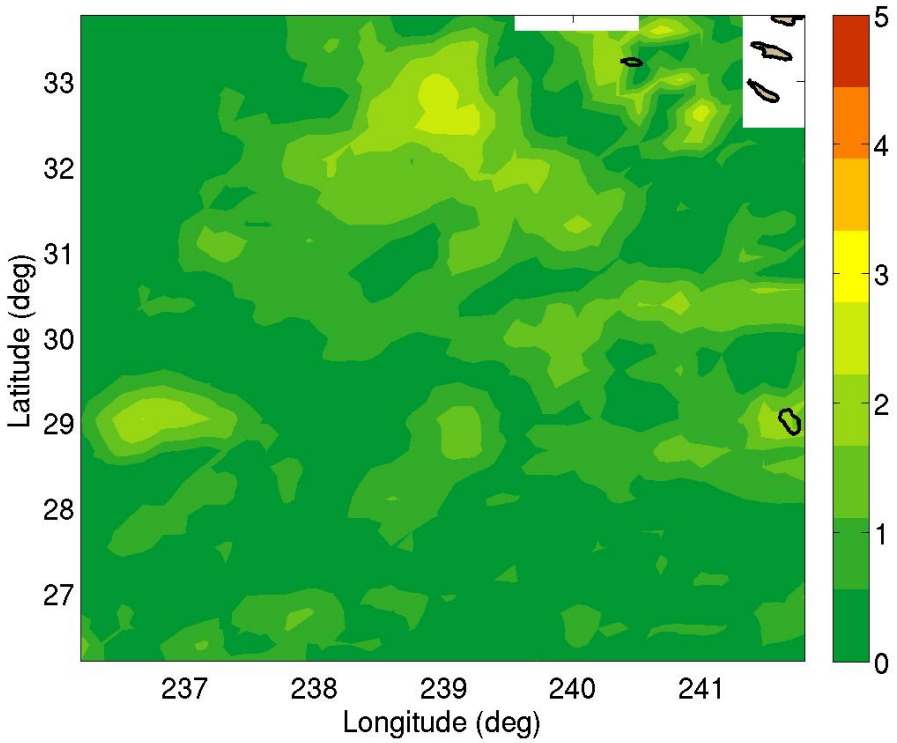

Figure 131. Averaged difference in percent between brute force and critical factors representative environment PAC for 250 Hz, source at 15 m, receiver at 15 m.

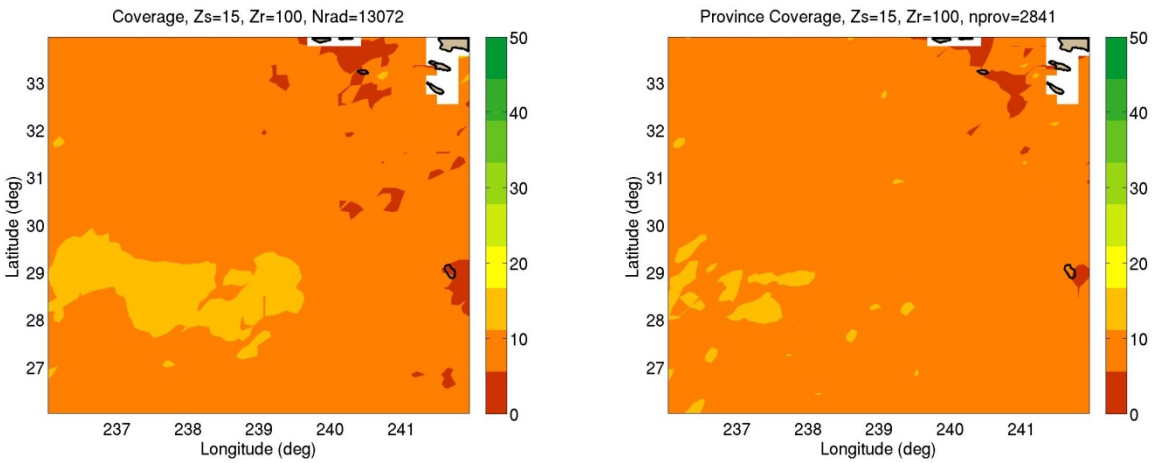

Figure 132. Brute force (left) and critical factors representative environment (right) PAC for 250 Hz, source at 15 m, receiver at 100 m.

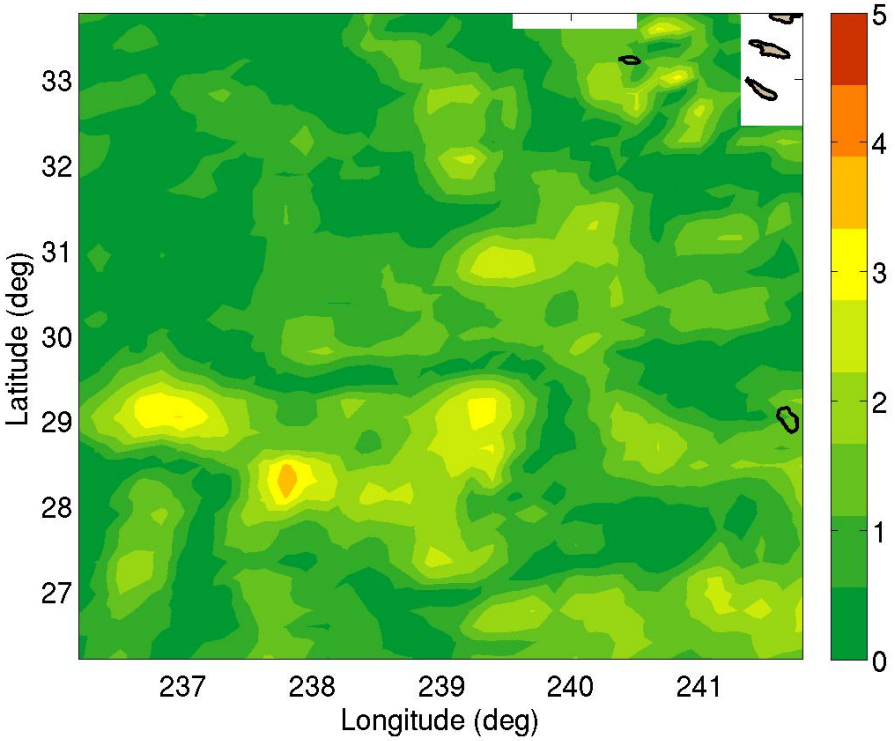

Figure 133. Averaged difference in percent between brute force and critical factors representative environment PAC for 250 Hz, source at 15 m, receiver at 100 m.

Table 6. Summary PAC differences for SOCAL 250 Hz.

Source Depth (m)	Receiver Depth (m)	Maximum % difference	Mean % difference
15	10	3.09	0.73
	15	2.82	0.64
	20	4.85	0.83
	61	8.08	1.47
	100	3.81	0.97
	150	3.44	0.70
	200	2.96	0.55
	250	3.29	0.48
	300	3.16	0.47
	500	2.74	0.48
60	10	3.26	0.85
	15	5.19	1.32
	20	10.60	2.31
	61	28.15	4.26
	100	12.87	2.57
	150	4.52	1.48
	200	3.25	0.79
	250	2.76	0.62
	300	2.50	0.60
	500	2.28	0.53
150	10	7.80	1.50
	15	12.46	2.28
	20	14.16	2.75
	61	16.11	2.04
	100	18.54	2.38
	150	22.14	2.33
	200	18.62	2.53
	250	16.45	2.38
	300	13.26	2.28
	500	7.36	1.93

Uncertainty Band Results for Provinces

In order to estimate the spread of TL over each province, the UBAND algorithm is used as described above. The *rms* differences of the bathymetry and sound speed are computed over each member of the province and input to UBAND, with standard estimates of frequency, source and receiver depth uncertainty, to estimate the TL uncertainty for that province. An example using the Okinawa Trough low frequency case is presented here, but results and conclusions are similar for all the cases studied. Figure 134 shows an example averaged TL (black line) and UBAND (red lines) prediction versus range calculated using the representative environment at 27.1N, 236.4E with a bearing of 270 degrees. The TL versus range for each member of that province is plotted in blue. This shows that the UBAND is predicting the spread over the province very well, particularly at maximum range. Figure 135 shows an example where the TL drops off with range. Here the representative is at 26.4N, 236.9E, 180 degree bearing. In this case, UBAND predicts the spread very well until the performance drops off at a range of approximately 70km. This is likely due to the way the uncertainties are input to the UBAND algorithm (they are not a function of range in this implementation), but for this application, it is an acceptable difference. In the future the inputs can be given to UBAND as a function of range and this performance will improve. There are several known issues with the UBAND algorithm. One is that the relationship between the sound speed *rms* error and the TL spread is empirically derived. In most cases it yields very good results, but not always and this could be the case in this example. Another limitation is that because the algorithm is applied in the range averaging scheme, it does not include error from previous ranges. The example here could also be suffering from this effect. If the errors were to grow with range, UBAND would perhaps do better in obtaining the wide spread at longer ranges. These limitations with UBAND will be addressed in future efforts by Zingarelli *et al*. (2010).

Figure 136 shows an example where the UBAND prediction is offset from the province members. Here the representative is at 26.0N, 237.2E, 315 degree bearing. In this case, UBAND predicts the spread very well but it is offset from the province members, likely because of the choice of the representative. The representative which was chosen using the environmental parameters is a member of the set and indicates the center of the environmental cost functions, but does not always indicate the center of the predicted TL. The overall area wide performance predictions do not suffer significantly from this problem, but the algorithm could be improved

later, when this issue with the selection of the representative can be further examined and addressed.

Figure 137 shows an example TL versus range for UBAND with a representative at 26.0N, 236.55E and 315 degrees bearing, in the OT AOI. For this case, the UBAND is not predicting the spread well because of its limitations. Results similar to those presented in Figure 134 and Figure 135 are most likely, and results similar to those presented in Figure 137 are infrequent, however they do occur. There are many potential causes of these sorts of differences. First, the spread of the province for this case is large. Because the cost function consists of only bathymetry, sediment and sonic layer features, the spread here could be due to some other oceanographic feature that is not captured by this method. This sort of discrepancy will be overcome when the full waveguide ξ function cost function is further developed. It would be beneficial if the UBAND algorithm could predict this spread given the environmental spread, but again, due to the empirical nature of the inclusion of sound speed errors in UBAND, the oceanographic differences may not always be captured appropriately. For the majority of the cases, UBAND is capturing the spread of the provinces using the spread of the environmental inputs very well.

A way this UBAND information can be used is to compute a worst case, using the lower band and a best case, using the upper band. An example using the OT low frequency case for the 15 m source and 20 m receiver is given in Figure 138. This can be compared to the right side of Figure 28, which falls between these two extremes.

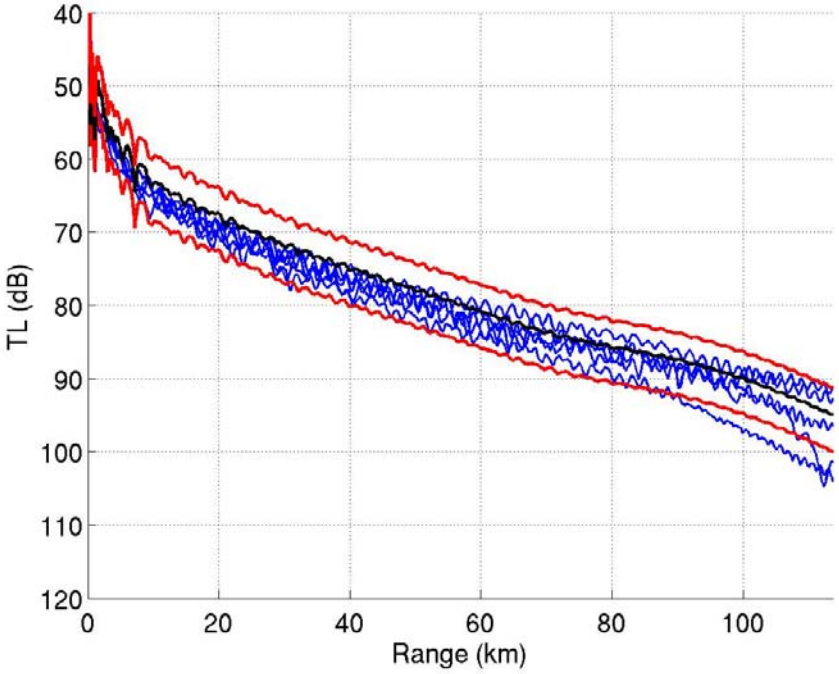

Figure 134. Example of TL versus range of UBAND mean for representative radial at 27.1N, 236.4E , bearing of 270 degrees(black), high and low predictions calculated using the environmental *rms* difference (red) and province members (blue).

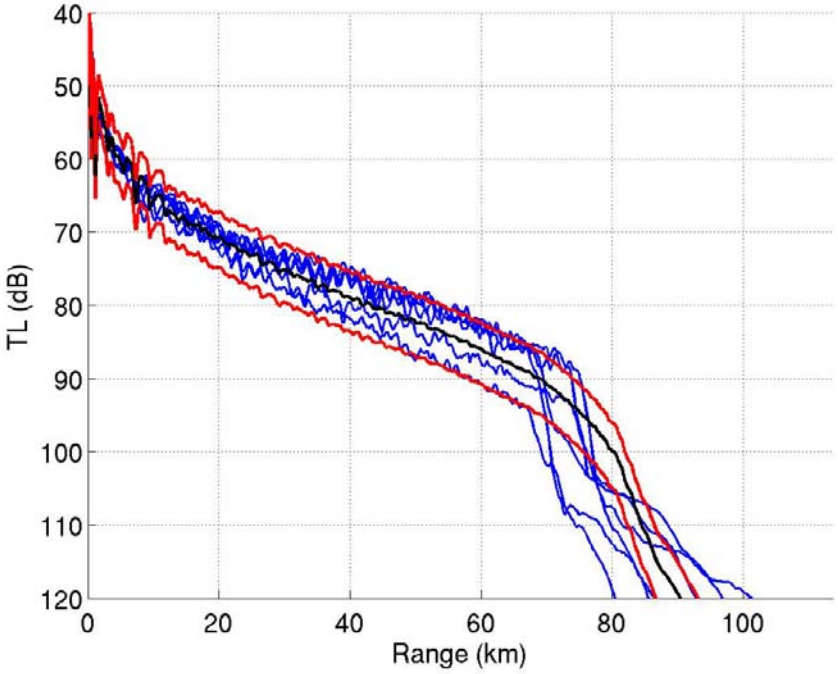

Figure 135. Example of TL versus range of UBAND mean for representative radial at 26.4N, 236.9E, bearing of 180 degrees. (black), high and low predictions calculated using the environmental *rms* difference (red) and province members (blue).

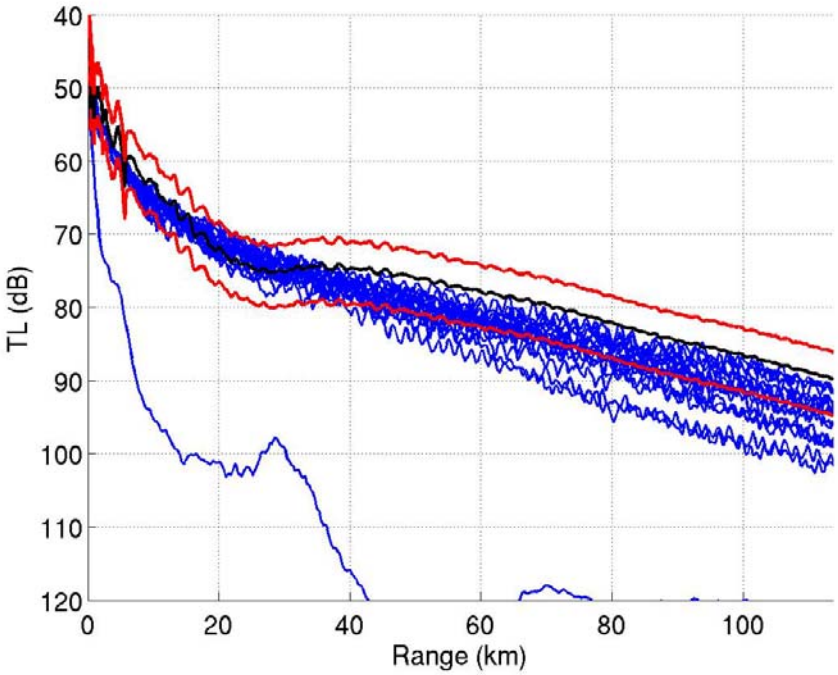

Figure 136. Example of TL versus range of UBAND mean for representative radial at 26.N, 237.2E, bearing of 315 degrees (black), high and low predictions calculated using the environmental *rms* difference (red) and province members (blue).

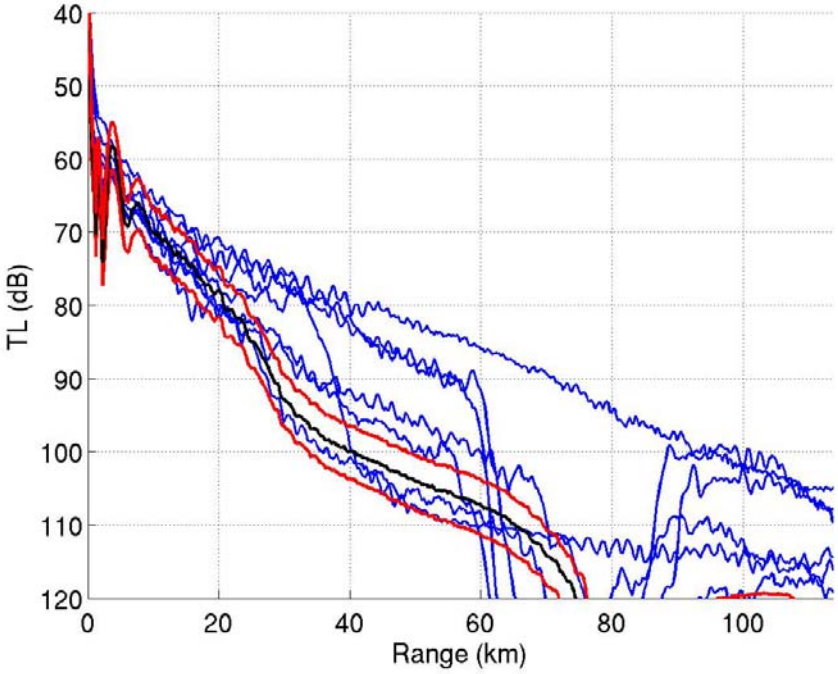

Figure 137. Example of TL versus range of UBAND mean for representative radial at 26.0N, 246.5E, bearing of 315 degrees (black), high and low predictions calculated using the environmental rms difference (red) and province members (blue).

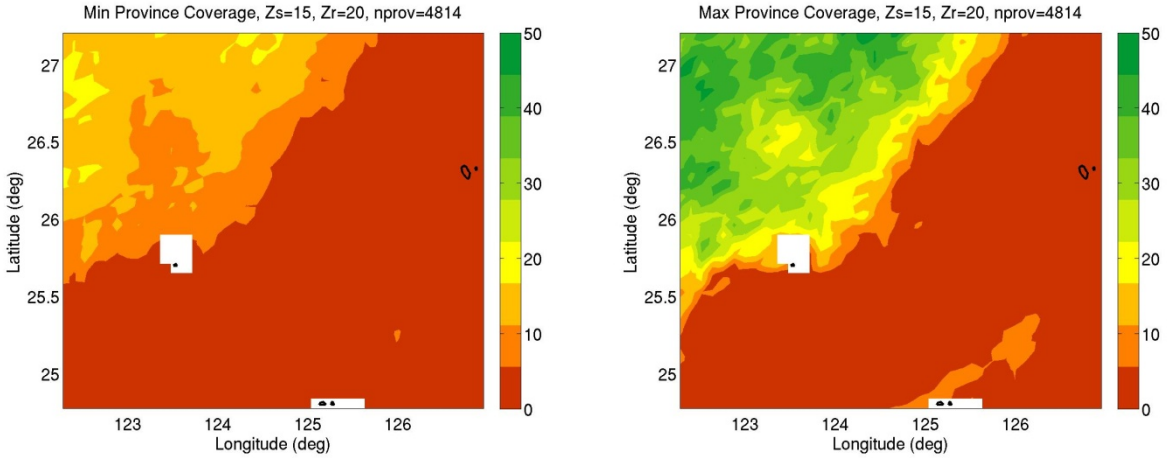

Figure 138. Worst case (left) and best case (right) PAC maps computed using UBAND upper and lower limits in the coverage algorithm. This represents the OT area at 250 Hz, source depth of 15 m and receiver depth of 20 m.

Environmental Parameter (Xi or ξ) Range Independent Provincing

Preliminary results of the range independent provincing using the ξ parameter are presented next. The environmental parameter, ξ, as described in Chapter 2, is used as the environmental cost function to determine similar acoustic environments. Because this sort of provincing analysis will be done on single frequencies over areas where the depth and the sound speed gradients will change, a preliminary analysis is done, examining 3 single layer environments over an absorbing bottom at a single frequency. Each of these environments has the same gradient, but 3 water depths, as shown in the left side of Figure 139. The ξ was computed as described above for each mode and depth, and the sum over the modes for this case at 10 Hz is shown in the right side of Figure 139. It is valid to use the sum over all the modes, in place of the bundling described previously, because these simple cases have very few modes and they are already bundled. The right side of Figure 139 shows that the two shallower ξ functions are closer together, and the theory is that the TL for those two environments is closer. Figure 140 and Figure 141 show the TL versus range and depth for these three cases. Visually, the two shallow cases, the right side of Figure 140 and Figure 141, compare most favorably; this is indicated by the closeness of the ξ parameter in the left side of Figure 139. Quantitatively, in order to determine how the TL's compare, the TL array down to the shallowest common depth (700 m) is input to the k-means code to determine how the TLs compare to each other, that is, the TL is used as the cost function instead of the environmental cost function. The k-means algorithm consistently puts the two shallower environments in one province and the deep environment in a province by itself. This result is consistent with the theory that similar ξ's indicate similar TL.

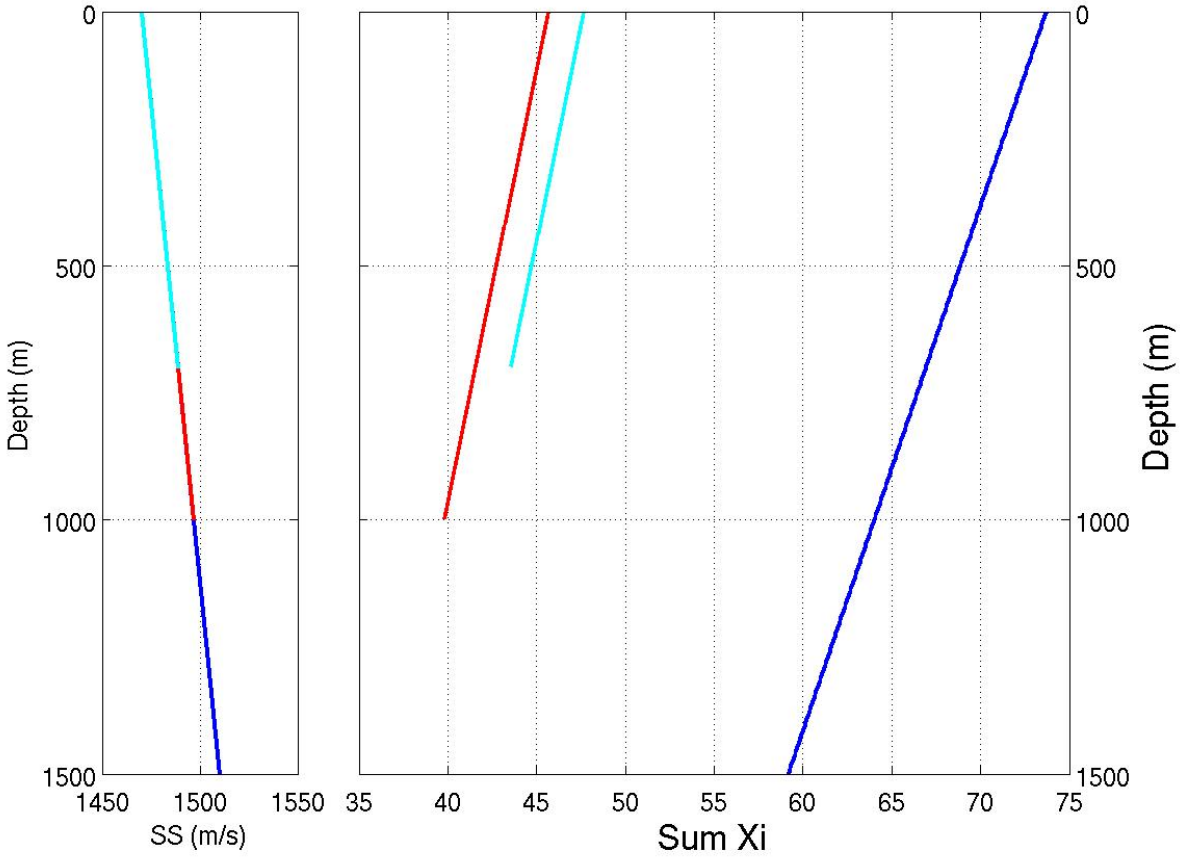

Figure 139. Sound speed versus depth (left) and the sum over the modes of the ξ's with depth (right), for 3 single layer environments.

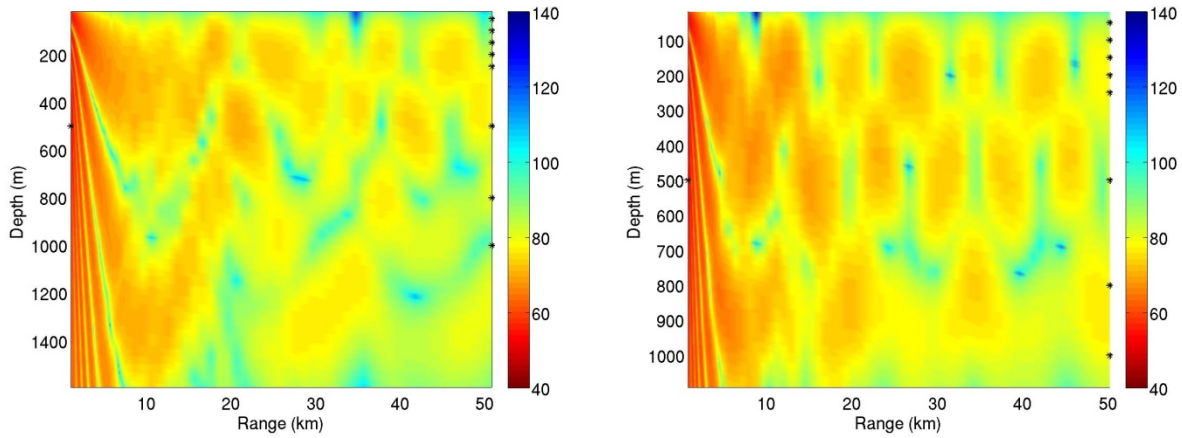

Figure 140. TL versus range and depth for the deep (1500 m) (left) and mid (1000 m) (right) water depths.

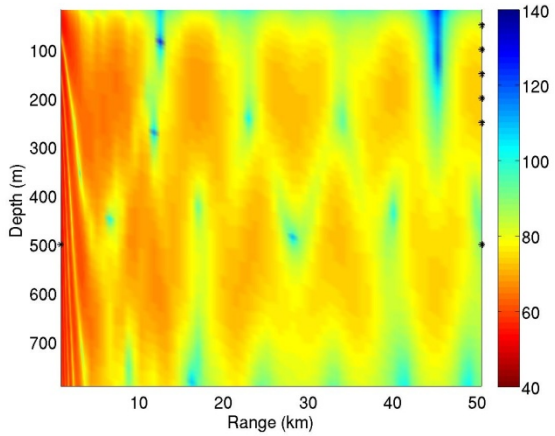

Figure 141. TL versus range and depth for the shallow (700 m) water depth.

The problem is now expanded into slightly more complicated sound speeds for the preliminary testing and proof of concept. Five simple 1-4 linear layer sound speed profiles, with three water depths, 500 m, 1500 m and 2000 m, were generated and are shown in Figure 142. Hard and soft sediments were combined with each profile to generate 10 environments summarized in Table 7. RAM TL predictions were made at 100Hz for sources at 500 m depth to a range of 50km for each run. The TL predictions versus range and depth are shown in Figure 143, Figure 144, Figure 145, Figure 146 and Figure 147.

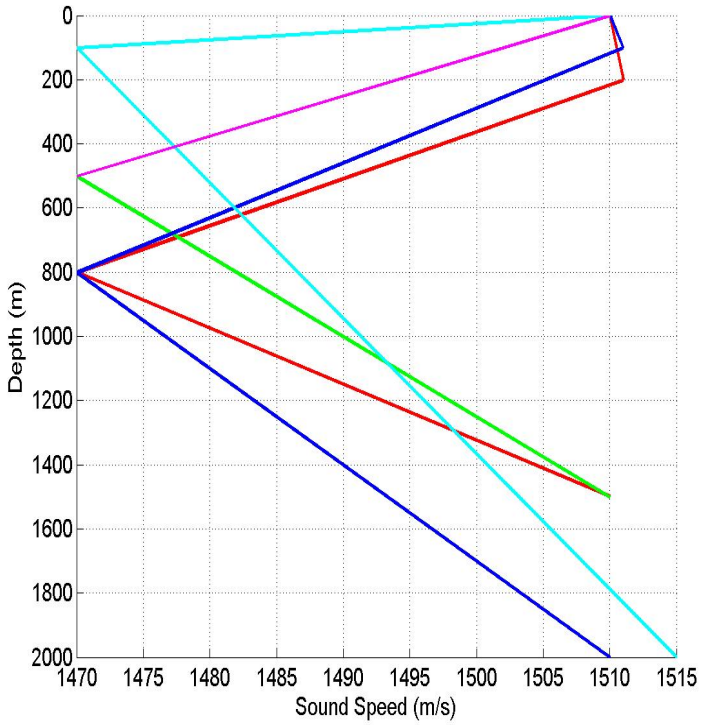

Figure 142. Sound speeds versus depth for the canonical test case.

Table 7. Environmental descriptions for canonical test cases.

Environment	Water Depth	Sound Speed	Sound Speed turn depth	Bottom Type
01 (red)	1500	1510, 1511, 1470, 1510	200, 800	Hard
02 (green)	1500	1510, 1470, 1510	500	Hard
03 (blue)	2000	1510, 1511, 1470, 1510	100, 800	Hard
04 (cyan)	2000	1510, 1470, 1515	100	Hard
05 (magenta)	500	1510, 1470	None	Hard
06 (red)	1500	1510, 1511, 1470, 1510	200, 800	Soft
07 (green)	1500	1510, 1470, 1510	500	Soft
08 (blue)	2000	1510, 1511, 1470, 1510	100, 800	Soft
09 (cyan)	2000	1510, 1470, 1515	100	Soft
10 (magenta)	500	1510, 1470	None	Soft

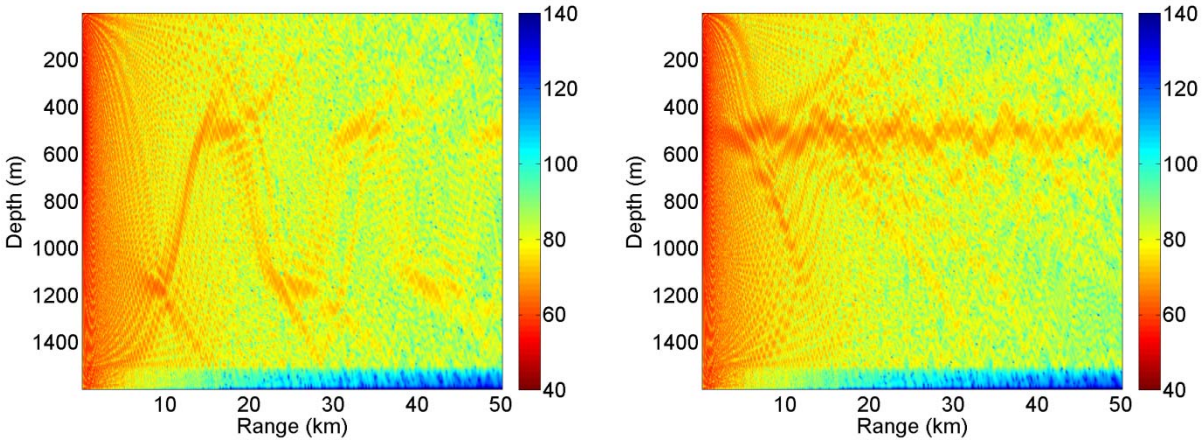

Figure 143. TL (dB) predictions for environments 01 (left) and 02 (right).

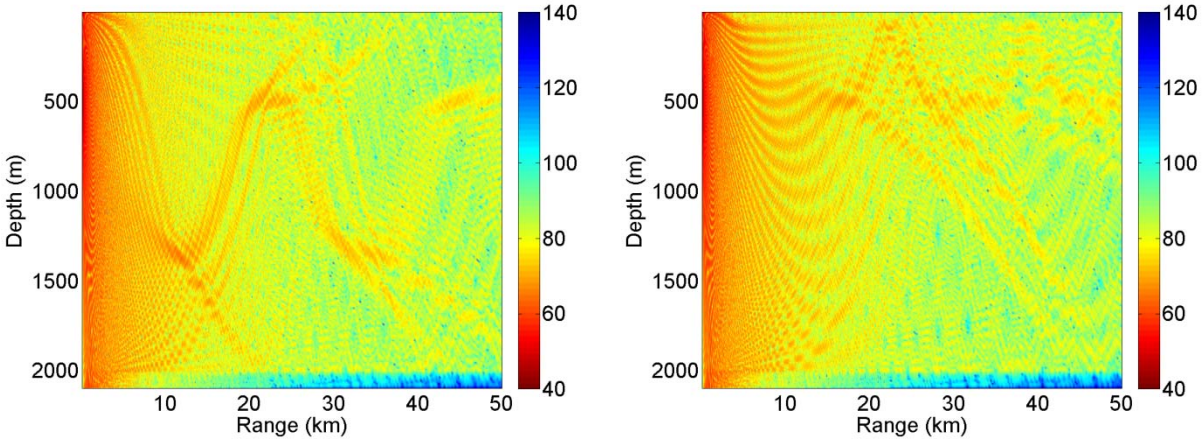

Figure 144. TL (dB) predictions for environments 03 (left) and 04 (right).

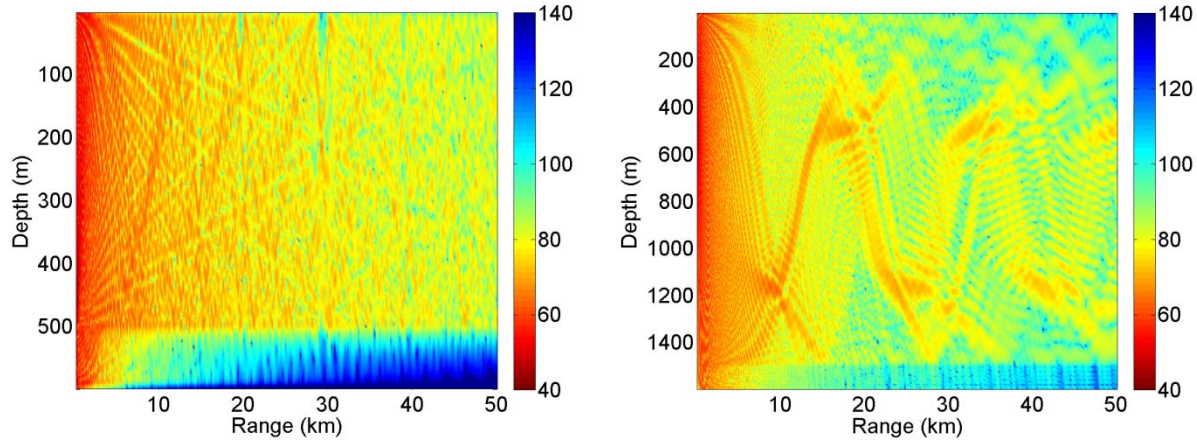

Figure 145. TL (dB) predictions for environments 05 (left) and 06 (right).

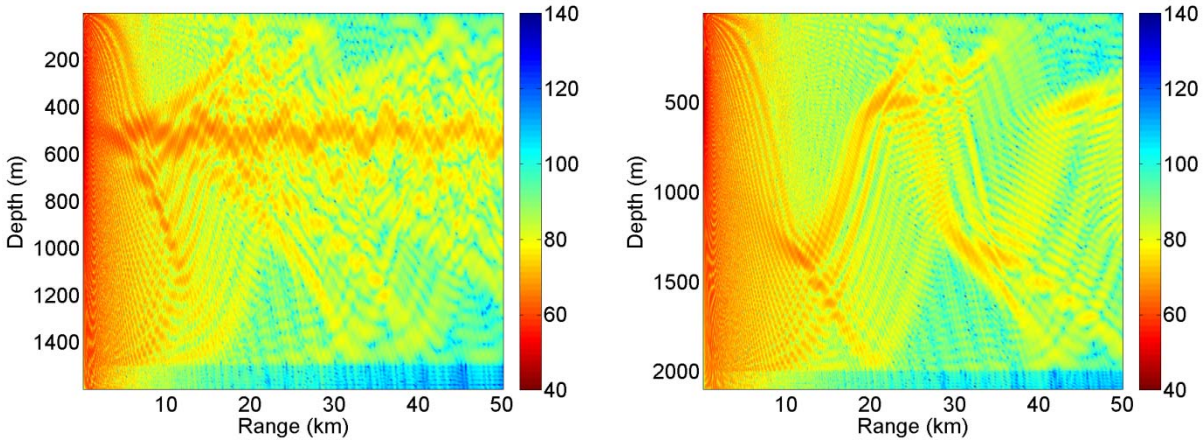

Figure 146. TL (dB) predictions for environments 07 (left) and 08 (right).

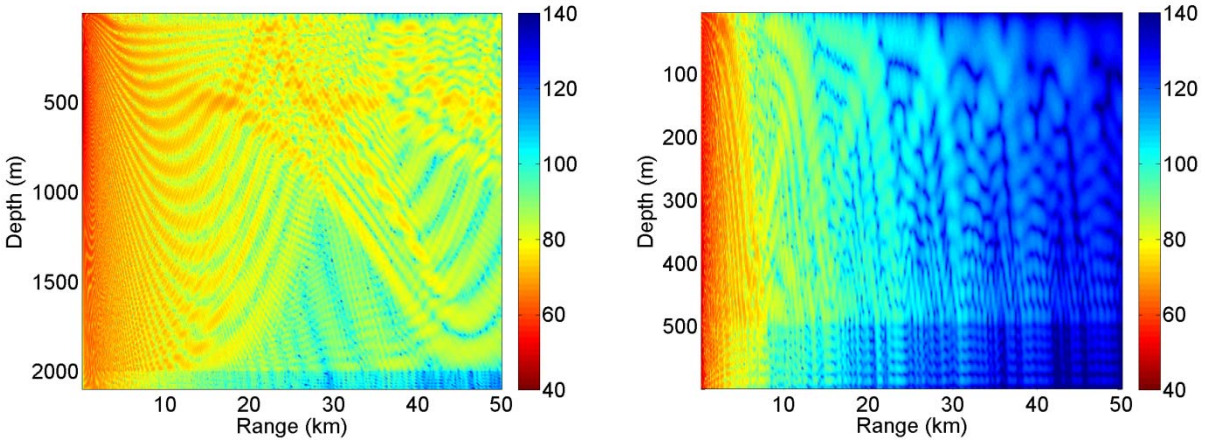

Figure 147. TL (dB) predictions for environments 09 (left) and 10 (right).

The ξ environmental cost functions, computed as described above, are bundled into the 4 mode regimes, and are input to the k-means algorithm to obtain 4 clusters. The k-means algorithm put 4 members into province 1, and 2 members in each of the other 3 provinces. To determine how well the provinces were clustered using ξ, the TL for each member of each province is again examined visually. Figure 148 shows the TL for the members of province 1, environments 01, 03, 06 and 08. These environments are characterized by energy convergence in a sinusoidal pattern centered at around 800 m depth. Figure 149 shows the TL for the members of province 2, environments 05 and 10, the two shallow water provinces, which are characterized by energy trapped near the surface and a release of the energy below the duct at a range of around 20 km. Figure 150 shows the TL for the members of province 3, environments 04 and 09, This province is characterized by energy filling the waveguide and not converging. Figure 151 shows the last province with members 02 and 07 which both contain a sound channel around a depth of approximately 500 m. These results show that the provinces determined using the ξ cost function are quite good at choosing similar TLs. Quantitatively, for comparison, the TL is fed as the cost function into the k-means algorithm and the provinces are assigned consistently as they were when using ξ as the cost function.

These two simple cases show that ξ, can be used to determine similarities in the acoustic performance without having to run the acoustic model. This is a very promising result. The development will continue with improvements to the angle bundling, faster mode computation and extension to range dependence.

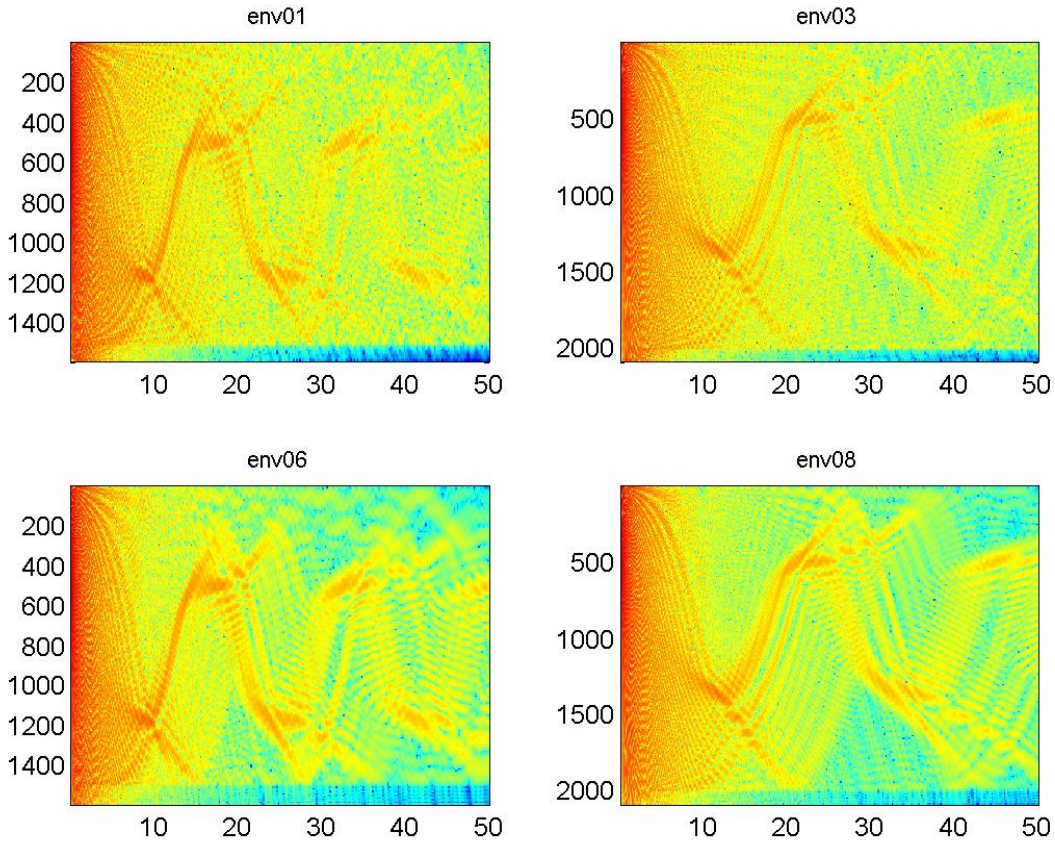

Figure 148. Province 1, environments 01, 03, 06 and 08.

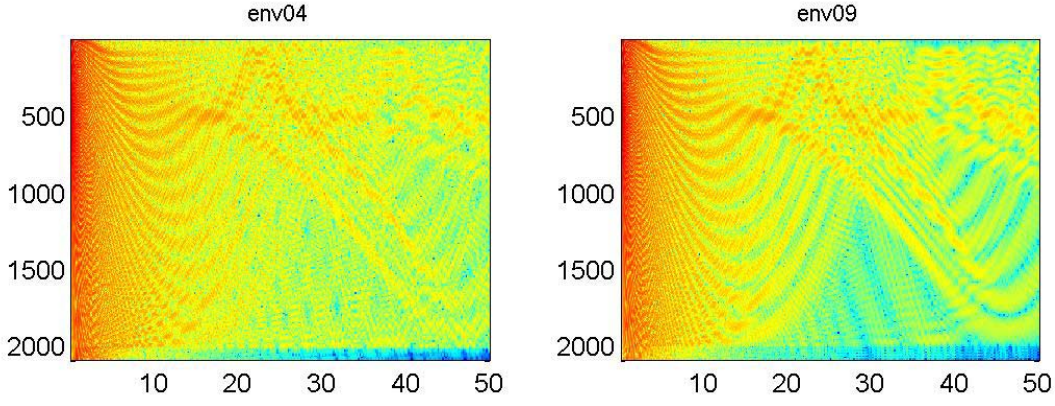

Figure 149. Province 2, environments 05 and 10.

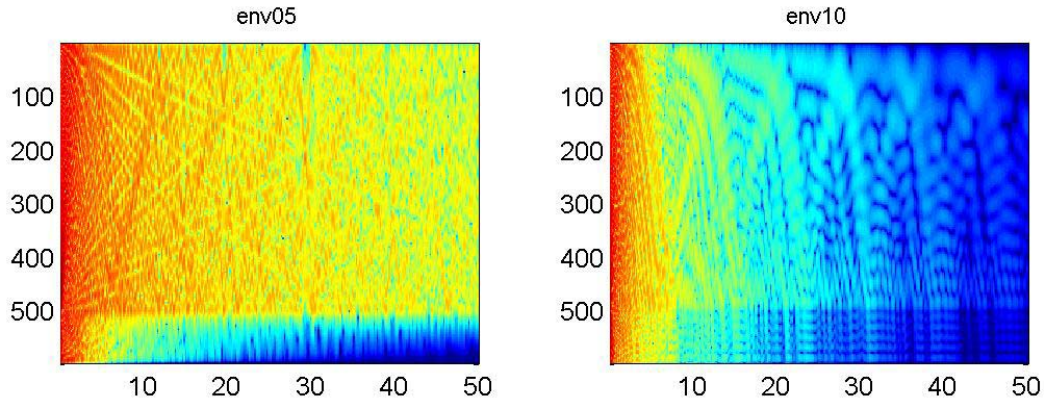

Figure 150. Province 3, environments 04 and 09.

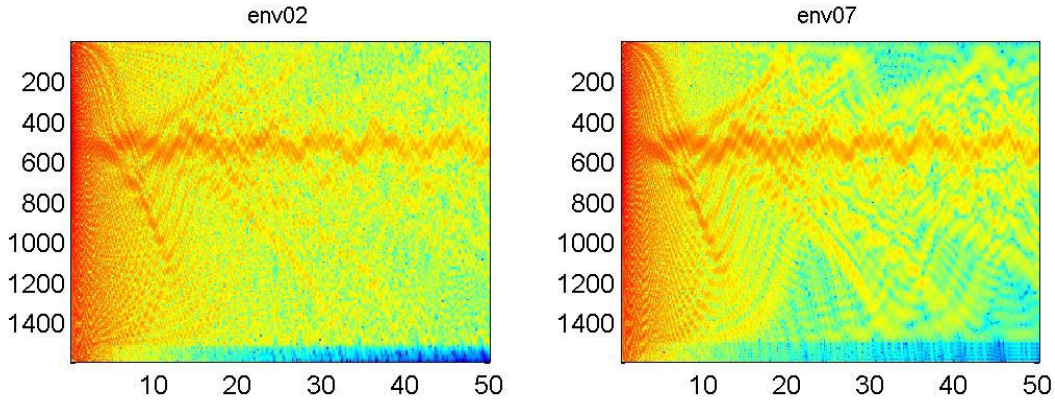

Figure 151. Province 4, environments 02 and 07.

Chapter 4. Applications

Now that the provincing has been proven to be effective, it can be used for various applications. One of the limitations of existing capabilities is the inability to predict all the scenarios of interest in the analysis / experimental time frame. The 4-9 fold improvements in computational time afforded by this provincing allows for more predictions to be made for the analysis.

Additionally, Fabre (2007) has noted that narrowband predictions for fixed point source depths are insufficient to predict real world performance. Integrated signal excess, while time consuming to compute, can now be run due to the computational gains achieved via provincing.

Ocean time series and ocean ensembles are available (Coelho, 2009) but could not be run due to computational limitations. The provincing can be expanded to work over a whole time series, rather than the presented snapshot and can therefore result in even larger speed improvements.

Finally, small area, high resolution analysis is frequently done to assess changes near a sensor or to reconstruct an exercise. The representative environments can be used to speed up this process.

Multiple Scenarios

The ability to characterize additional frequencies is a direct by-product of the run time improvements as more frequencies can be run due to the time savings. Because the source depth is not part of the mode cost function, that step in the critical factors provincing does not have to be recomputed when changing the source depth. If the source depth changes, but does not change its relationship to the duct (it is either in or out) then the reclassification of the duct cost function does not have to be recomputed. For future efforts, the duct loss cost function can be examined and representatives chosen based on how this parameter changes or doesn't change.

Time Series

Each NCOM forecast provides an analysis and forecasts every three hours out to 48, 72 or 96 hours. That gives 17 to 33 3-dimensional ocean fields to analyze. Currently, a single field is chosen nearest the time of interest, however, understanding the fluctuations in time as well as the uncertainty associated with the modeling of ocean dynamics is important to correctly assess

the acoustic performance. To support this current capability, the representative environments are computed for the single time frame of interest. The extension of this capability to the time series is discussed and preliminarily tested.

Once the provinces are obtained for one snapshot in time, radial cost functions from alternate snapshots are compared to the centroids from the original provinces using the same distance function as the k-means. This will determine which province the new radials are members of. The TL is not recomputed for the new radials and the PAC map is generated based on the representatives found using the first snapshot. The only limitation on this is that if there is an ocean feature that is significantly different from any ocean features depicted by the first snapshot, it may not do well in placing the new radial cost function in a province.

Integrated Signal Excess

There are a number of benefits to this provincing capability, primarily derived from the enhanced speed of computation for an area and / or a time series. Ocean ensembles are becoming available to estimate the uncertainty (*e.g.* Rowley *et al*., 2009) but are currently too computationally expensive to generate acoustic predictions for each ensemble member. Fabre (2007) introduced integrated signal excess (ISE) and integrated acoustic coverage (IAC) over time to improve performance predictions by including variations around source and receiver depths and frequencies. Because a scenario may not be known or may be uncertain, multiple source depths, receiver depths and frequencies are run for the area for each grid point and multiple bearings. The SE can then be computed and integrated over the possible scenarios. Figure 152 shows an example (from Fabre, 2007) of single scenario SE and ISE over 5 frequencies and 5 source depths.

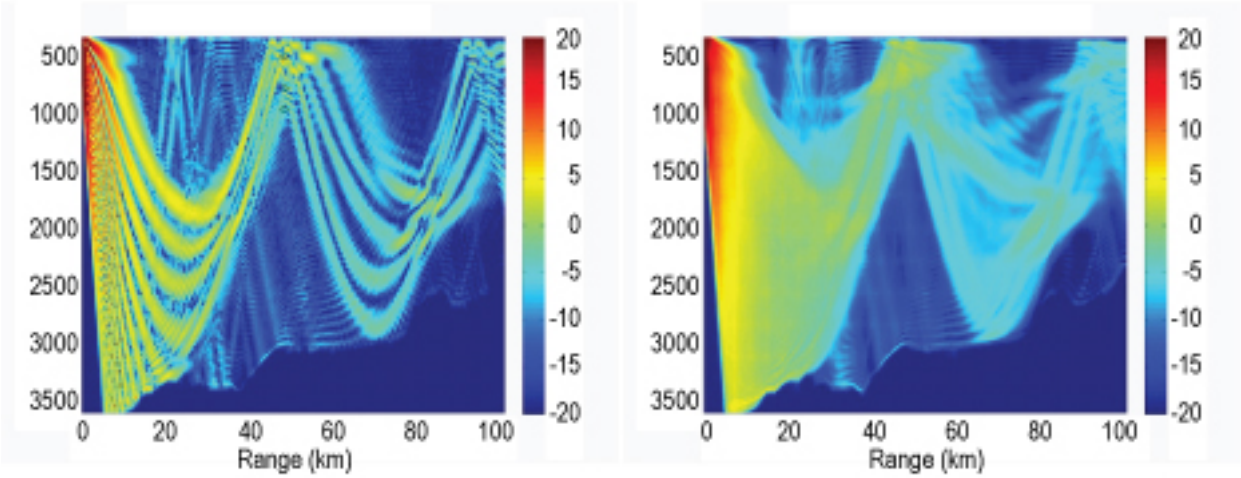

Figure 152. Examples of single frequency and source SE and integrated SE from Fabre (2007).

Figure 153 shows a single depth slice of TL versus range from Figure 152. The green lines are individual SE predictions for 5 source depths and 5 frequencies, the blue line is a single prediction chosen from this set and the red line is the SE integrated over the depths and frequencies. If the blue line were used to estimate a performance prediction, a significantly different value would be obtained than if the ISE were used. This is illustrated in Figure 153 at a single range point where the SE is 4 dB on the chosen scenario, but is 11 dB on the integrated scenario. The integrated answer encapsulates all the cases and therefore gives a more realistic answer, as exact frequencies, source depths, and receiver depths will never be known in a planning scenario. If these values are known, they are never as narrow as the model assumes. For example, a sound source is usually larger in depth extent than a single depth bin in the acoustic model computational grid.

ISE is used to create integrated acoustic coverage (IAC) (*e.g.* Dennis and Fabre, 2007). IAC uses the coverage area algorithm described previously on the ISE (vice SE) to produce a performance metric that captures more of the variability in the acoustic model, thus producing a better estimate of performance. This IAC can be examined over time for planning purposes. Figure 154 shows a very low frequency case for the OT area using 7 frequencies (44, 46, 48,50, 52, 54 and 56 Hz), depicted in the columns and 5 source depths (13.5, 15.0, 17.5, 20.0 and 22.5 m) in the rows and a single receiver depth slice at 10 m. Each thumbnail is longitude versus latitude and the color represents 0 (red) to 50% (green) of the area covered. This emphasizes the previous point that the performance predictions can vary over small variations in frequency and

source depth, neither of which are mathematically narrow in the real world. Here, as the frequency increases, (to the right in the plot), the performance improves, and as the source depth deepens, (down in the plot), the performance improves. Additionally as the receiver depth deepens, the performance improves. The primary feature locations stay the same, however the edges and strengths change, therefore, an IAC, as shown in Figure 155, is useful to capture potential deviations from the current narrow assumption. The overall placement of sensors might yield similar results, however, performance predictions estimated from Figure 155 would be considerably different than those from a single snapshot in Figure 154.

The primary limitation of ISE or IAC is the time it takes to compute. The case shown above takes 35 (=7 frequencies *5 source depths) times longer to run than the single narrow assumption. Application of the representative environments to this method allows this sort of analysis to become more viable.

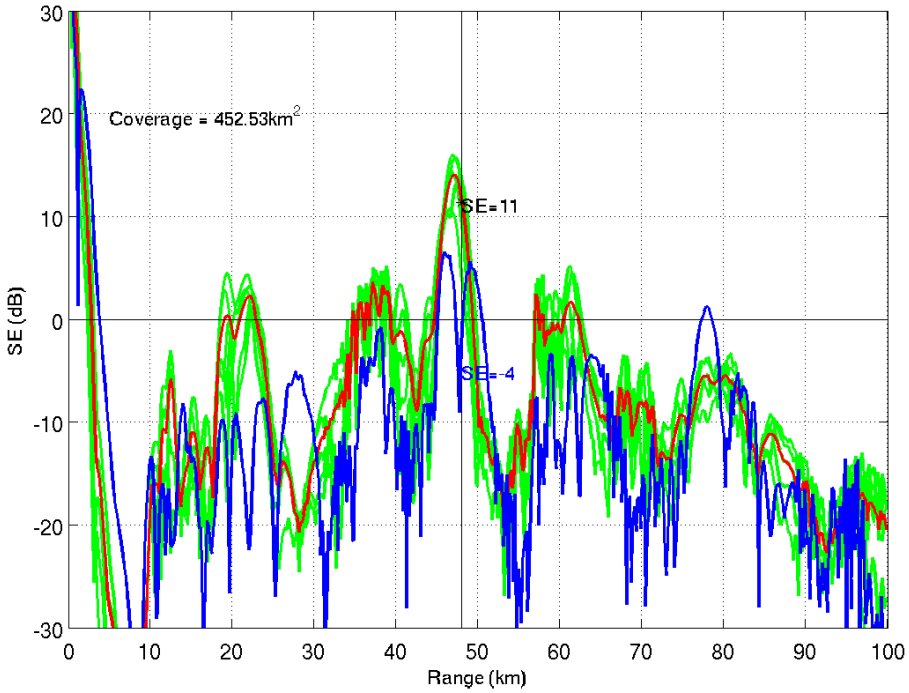

Figure 153. Single depth slice illustrating utility of ISE.

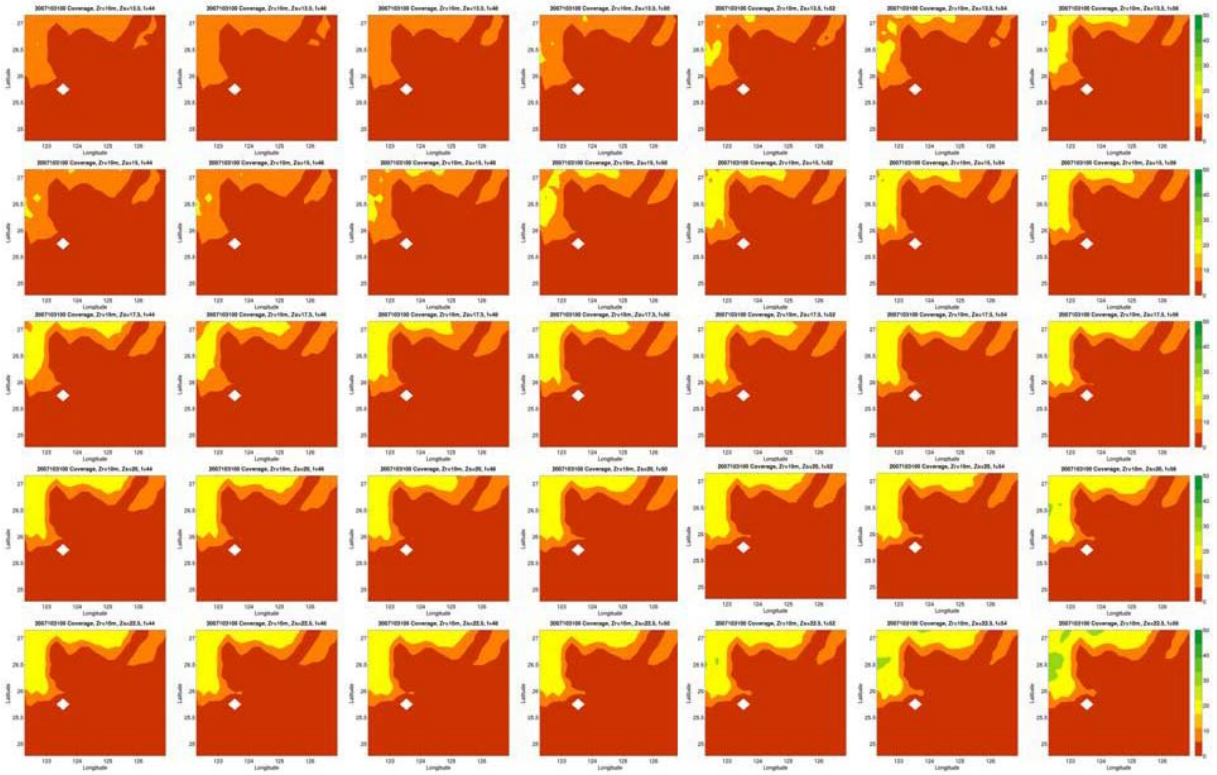

Figure 154. Thumbnails of geographic PAC plots for 7 frequencies (44 to 56 Hz by 2 Hz) in the columns, 5 source depths (13.5 to 22.5 m by 2.5 m) in the row and one receiver depth of 10 m for the OT AOI.

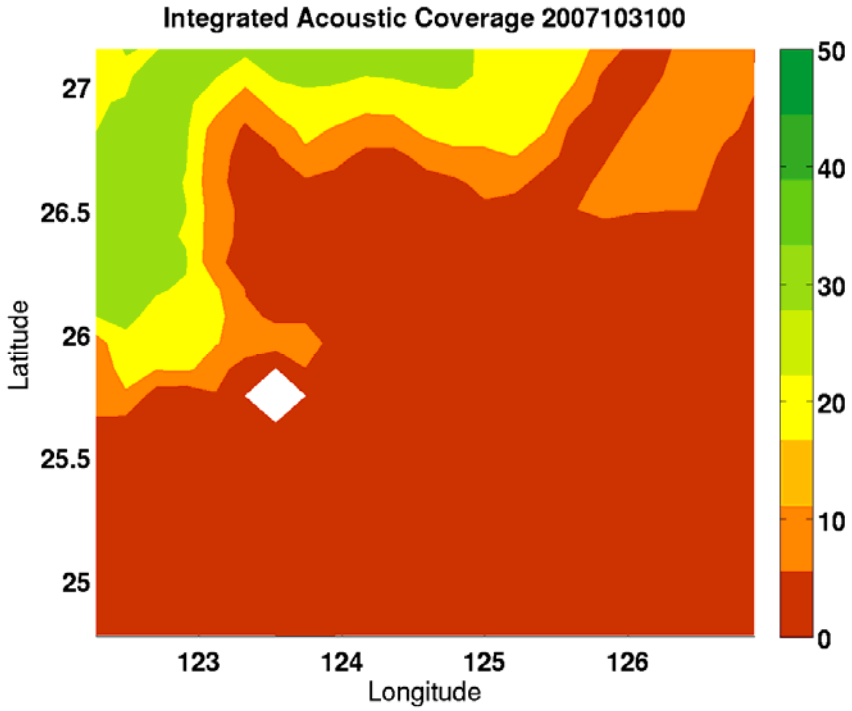

Figure 155. IAC over 7 frequencies, 5 source depths and 3 receiver depths for OT very low frequency case.

High Resolution Radial

As previously noted, acoustic analysis is usually done for a small number of radials, however, when analyzing small scale environmental changes, or variations close to the source or receiver, much finer resolution modeling is required. Figure 156 shows the critical factors mode (or bathymetry-based) province numbers in color, for a 3x3 grid in the OT area at the low frequency, using 180 radials. The environmental symmetry in the different directions is evident and is useful for environmental acoustic analysis. This analysis would require 1,620 acoustic runs for each source, the mode provincing resulted in 49 radials and the sub-provincing resulted in 435 representatives that are required to run for each source. Figure 157 shows typical coverage comparisons for this analysis. These results are very good and the critical factors representative environments analysis does very well for these small area, high resolution cases.

Because this case represents a smaller area of interest, the provincing works very well as indicated by examples of TL versus range at a receiver depth of 20 m which are given for various provinces selected from this case are shown in Figure 158 and Figure 159.

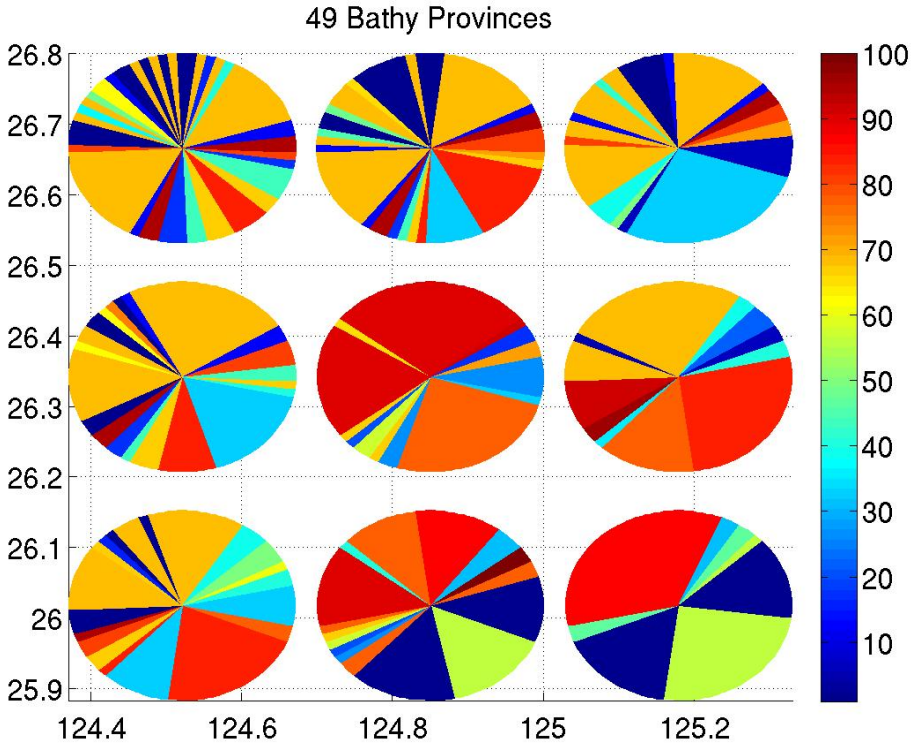

Figure 156. Example high resolution province analysis using small area in OT at 250 Hz with 180 radials.

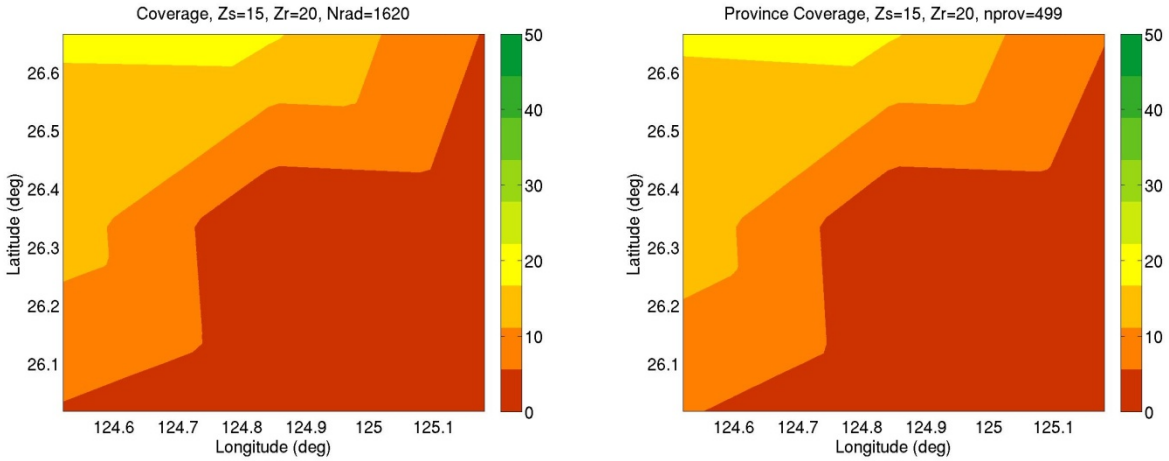

Figure 157. Brute force (left) versus provinced (right) PAC for the high radial resolution case in the OT area at 250 Hz.

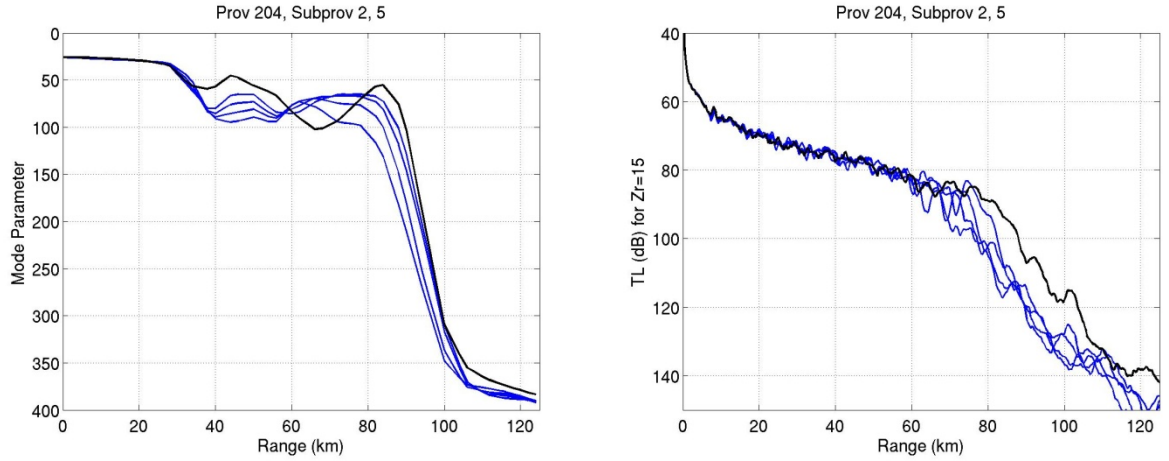

Figure 158 Example downslope province from the high resolution data set. The modes versus range (left) and the TL versus range (right) are in blue for each member, and the black line is the representative that was used to generate the provinced PAC.

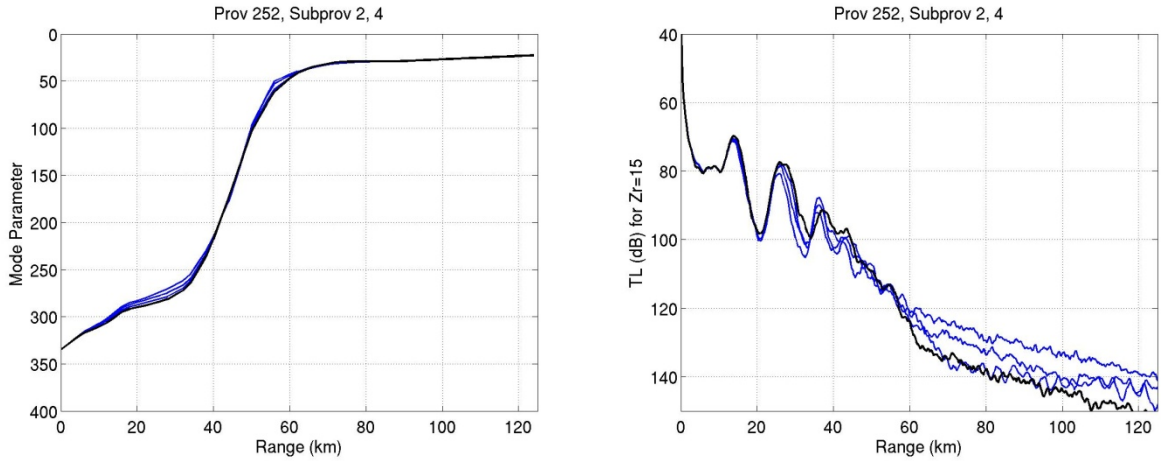

Figure 159. Example upslope province from the high resolution data set. The modes versus range (left) and the TL versus range (right) are in blue for each member, and the black line is the representative that was used to generate the provinced PAC.

Chapter 5. Conclusions

Improvements in ocean modeling and forecasting, uncertainty estimation via ensembles and computational capability have lead to an increased prediction and analysis ability and therefore an increased requirement for acoustic performance estimates over large areas and times. Due to the significant computational requirements of acoustic models, an environmental acoustic provincing methodology has been developed to determine similar acoustic environments for the purpose of reducing the number of computations required to estimate acoustic performance over an area, time, ensemble and multiple scenarios of interest.

The provincing described here begins by examining the environment by considering the features in the ocean that will impact the acoustics. Two viable methods of characterizing the environment have been developed and are presented. These techniques are based on two methods of describing the environment. The first characterizes the environment as a function of range, using features of the waveguide that have a significant impact on the sound traveling through it. This method has limitations if, for example, the waveguide contains a feature that is not accounted for by these features or critical factors. The second, more robust technique uses an acoustic mode-based description of the entire vertical and horizontal extent of the environment and reduces the dimensionality using angular and gradient analysis. This method shows promise, but is not as advanced currently in its development as the critical factors method.

The environmental descriptions are then "clustered" or provinced using the k-means algorithm. Other algorithms can be assessed, but the k-means worked well for the examples presented here. The mathematical clustering algorithm outputs the representatives of each province, known here as the representative environment, and a "map" that lists every source to receiver path in the area and which representative environment (or representative) corresponds to that path. The acoustic model is then run for each representative and substituted for those that it represents to generate a sensor coverage (PAC) or related performance map. In order to capture the variation within the provinces, the UBAND algorithm (Zingarelli, 2008) has been applied to obtain upper and lower bounds on the TL that can be converted to error bars on the performance predictions.

For testing purposes, the maps generated using the provinces are compared to those generated by running every acoustic radial. Results for the critical factors acoustic provincing were computed for four areas of interest at various frequencies, source depths and receiver depths. The percentage of area covered (PAC) by the acoustic sensor estimates were compared to brute force PAC estimates. Run time improvements with less than ~20% PAC difference were shown to be between 4 and 9-fold. Such improvements in computational speed allow for more analyses of acoustic scenarios of interest (frequencies, source depths, etc.) and consideration of more ocean environments, resulting in more information with which to make more informed decisions.

Preliminary results of the mode-based method show promise in the ability to estimate acoustic provinces using a range independent environmental parameter that describes the entire depth extent of the waveguide. Future development of this parameter will focus on faster, more accurate angular analysis, range dependence and clustering of these larger environmental parameter cost functions.

Future work also includes extending the capability of the provincing algorithm to work over multiple time snapshots or ensembles so that the entire set can be estimated with many fewer acoustic runs.

References

Barron, C. N., R. W. Helber, G. A. Jacobs, M. Gunduz, P. Spence, “Acoustic Impact of Short-term Ocean Variability in the Okinawa Trough”, 2009 Marine Technology Society, Biloxi, Mississippi, 26-29 October 2009.

Barron, Charlie N., A. Birol Kara, Paul J. Martin, Robert C. Rhodes, Lucy F. Smedstad, "Formulation, implementation and examination of vertical coordinate choices in the Global Navy Coastal Ocean Model (NCOM)," pp 347-375, *Ocean Modeling* 11 (2006).

Carter, D. J. T., “Echo-sounding correction tables, 3rd edition,” The Hydrographic Dept, Ministry of Defence, Taunton, 1980.

Chen, Michael. "K-means Clustering." Matlab Central. The Mathworks, 01 July 2009. Web. Dec. 2009. <http://www.mathworks.com/matlabcentral/fileexchange/authors/49739>

Chin-Bing, Stanley A. Personal communication, 2008.

Coelho, E.F., Rowley, C., Jacobs, G., “Ocean Data Assimilation Guidance Using Uncertainty Forecasts”, 090611-014, 2009 Marine Technology Society, Biloxi, Mississippi, 26-29 October 2009.

Collins, M. D. “Applications and time-domain solution of higher-order parabolic equations in underwater acoustics,” *J. Acoust. Soc. Am*., **86** (3), pp. 1097-1102, 1989.

Collins, M. D. "A higher-order parabolic equation for wave propagation in an ocean overlying an elastic bottom", *J. Acoust. Soc. Am.* 86, 1459-1464, 1989.

Collins, M.D., R. J. Cederberg, D.B. King, and S.A. Chin-Bing, "Comparison of Algorithms for Solving Parabolic Wave Equations," *J. Acoust. Soc. Am.* **100**, 178-182 (1996)

Dennis, Steven M., "Coverage Metric for Acoustic Receiver Evaluation and Track Generation," 0-933957-38-1, 2009 Marine Technology Society, Biloxi, Mississippi, 26-29 October 2009.

Dennis, Steven M. and J. Paquin Fabre, “Characterization of the range dependence of an ocean environment to reduce acoustic estimation time,” IEEE Proceedings of the Oceans 2007, Vancouver, October 2007.

Fabre, J. Paquin “Integrated signal excess as a metric for environmental acoustic assessment.” *J. Acoust. Soc. Am.* **122** (5) Pt. 2, p. 2942, November 2007.

Fabre, J. Paquin and David H. Fabre, "Examples of Carter Corrected DBDB-V Applied to Acoustic Propagation Modeling," NRL/MR/7182--08-9100, March, 2008.

Fulford, James, "Broad geoacoustic assessment of some regional areas," Naval Research Laboratory Memorandum Report, MR-7055, 1993.

Gough, Mr. Edward, Mrs. Pamela McDowell, Mr. Steven Dennis and Mrs. Josette Fabre, "Performance Surface - A New Approach to ASW Modeling," NDIA Joint Undersea Warfare Technology Conference, <http://www.ndia.org/meetings/9240/Documents/9240_agenda.pdf>, September, 2009.

HDF Group, "HDF5 User's Guide - Release 1.8.4," http://www.hdfgroup.org/HDF5/doc/PSandPDF/HDF5_UG_r184.pdf, November, 2009.

Jensen, Finn B., William A. Kuperman, Michael B. Porter and Henrik Schmidt, **Computational Ocean Acoustics**, Springer-Verlag New York Inc., 2000.

W. A. Kuperman, M. B. Porter, J. S. Perkins and R. B. Evans, ``Rapid computation of acoustic fields in three-dimensional ocean environments," *J. Acoust. Soc. Am.* **89**, 125--133 (1991)

Helber, Robert W., Charlie N. Barron, Michael R. Carnes, and Robert A. Zingarelli “Evaluating the sonic layer depth relative to the mixed layer depth” *J. of Geophys. Rsch*, vol. 113. C07033, 2008 .

Mathworks, "k-means clustering," Mar, 2009, <http://www.mathworks.com/access/helpdesk/help/toolbox/stats/bq_679x-18.html>

Monach, Reynolds and Max Karlovitz, "Adaptive Gridding in Complex Physical Environments to Reduce Uncertainty," Navy SBIR <http://www.dodsbir.com/Awards>, Topic N05-079, N051-079-0726, 2008.

Moore-Head, M. E., W. Jobst, and E. S. Holmes, "Parabolic-equation modeling with angle-dependent surface loss", *J. Acoust. Soc. Am.* **86**, 247-251, 1989.

NAVO (Naval Oceanographic Office), “Data Base Description for Surface Marine Gridded Climatology (SMGC), Version 1.0”, OAML-DBD, DRAFT, March 1996.

NAVO (Naval Oceanographic Office), "Digital Bathymetric Data Base Variable Resolution (DBDB-V) Version 5.2 Level 0," Oceanographic and Atmospheric Master Library (OAML), 24 May 2007.

NGDC, *"ETOPO2v2 Global Gridded 2-minute Database,"* National Geophysical Data Center, National Oceanic and Atmospheric Administration, U.S. Dept. of Commerce, http://www.ngdc.noaa.gov/mgg/global/etopo2.html.

NOAA, "*National Weather Service, Ocean Prediction Service*." Ed. David Feit. NOAA, 12 May 2009. Web. 3 Feb. 2010. <http://www.opc.ncep.noaa.gov/>.

Norton, G. V. and Novarini, J. C., “The effect of sea-surface roughness on shallow water waveguide propagation: A coherent approach,” *J. Acoust. Soc. Am.* 99, 2013-2021, 1996.

Pflug, Lisa A. and Donald R. Delbalzo, "Adaptive predictive-error optimal gridding," *J. Acoust. Soc. Am.* **119,** 3352 (2006)

Pierce, Allan D. Acoustics**: An Introduction to Its Physical Principles and Applications**, Second Printing, Acoustical Society of America, 1991.

Porter, Michael B. “The KRAKEN Normal Mode Program”, SACLANT Undersea Research Center, May, 2001.

Powell, Mark D. , Peter J. Vickery & Timothy A. Reinhold , "Reduced drag coefficient for high wind speeds in tropical cyclones" **Nature** 422, 279-283 (20 March 2003).

Rew, R. K., G. P. Davis, S. Emmerson, H. Davies, and E Harner "NetCDF User's Guide,", <http://www.unidata.ucar.edu/software/netcdf/docs/netcdf.pdf > February 2010.

Rike, Erik R. and Donald R. Delbalzo, " Objective sampling with EAGLE to improve acoustic prediction accuracy," *J. Acoust. Soc. Am.*, **114** 2459 (2003).

Rike, Erik R. and Donald R. Delbalzo , "Sparse acoustic gridding in an azimuthally complex environment," *J. Acoust. Soc. Am.* **112** 2310 (2002).

Rike, Erik R. and Donald R. DelBalzo "An iso-deviant approach for acoustic computations using efficient adaptive gridder for littoral environments" *J. Acoust. Soc. Am.* **117,** 2463 (2005)

Rodriguez, Orlando Camargo, "General description of the BELLHOP ray tracing program," http://oalib.hlsresearch.com/Rays/GeneralDescription.pdf, June, 2008.

Rowley, Clark D. "The NRL relocatable ocean/acoustic ensemble forecast system," *Geophysical Research Abstracts*, Vol. 11, EGU2009-13498, <http://meetingorganizer.copernicus.org/EGU2009/EGU2009-13498.pdf>, 2009.

Rowley, Clark D., Personal Correspondence, 2009.

Smith, George B., "Bounded Elliptical Modes," Naval Research Laboratory Memorandum Report, NRL/MR/7183--07-9062, August 7, 2007.

Spofford, C. W., "The ASTRAL Model Volume I, Technical Description," DTIC AD-A956 124, 1979.

Weinberg, Henry, "CASS Roots", http://ieeexplore.ieee.org/stamp/stamp.jsp?arnumber=00881744, 2000.

Wikipedia contributors, "Sea state," Wikipedia, The Free Encyclopedia, http://en.wikipedia.org/w/index.php?title=Sea_state&oldid=337039749 (accessed November 2010).

Urick, R. J. (1983). **Principles of Underwater Sound** (3rd ed.). New York: McGraw-Hill.

Zingarelli, Robert A. and J. Paquin Fabre, “Operational Acoustic Transmission Loss Uncertainty Characterization,” NRL Review 2009.

Zingarelli, R.A. “A mode-based technique for estimating uncertainty in range-averaged transmission loss results from underwater acoustic calculations,” *J. Acoust. Soc. Am*. 124, EL218-222 (2008).

Zingarelli, R. A. and D. King, " RAM to Navy Standard Parabolic Equation: Transition from Research to Fleet Acoustic Model", < http://www.nrl.navy.mil/research/nrl-review/2003/simulation-computing-modeling/zingarelli/> NRL Review, 2003.

Zingarelli, R. A. Personal communication, 2010.

Appendix - Glossary

absorption - in seawater, absorption is the conversion of sound energy into heat due to chemical processes and is assumed to be negligible by most acoustic models (e.g. Wikipedia, 2010). However, near the surface, the bubbles due to breaking waves increase the absorption near the surface (e.g. Fabre et al., 2009).

acoustic performance metric - an estimate that quantifies how an acoustic system will perform. Typical performance metrics are sensor coverage, probability of detection and detection range.

adiabatic - the adiabatic assumption in acoustic propagation is the assumption that energy does not transfer between modes.

Airy function - a special function that is a solution to the differential equation

$$x'' - bx = 0$$

bandwidth - the width of the frequency band of interest in Hz (Hertz)

bathymetry - the depth of the ocean measured using an acoustic return off the bottom.

BELLHOP ray trace model - "Bellhop is a highly efficient ray tracing program, written in Fortran by Michael Porter as part of the Acoustic Toolbox (available at the website of the Ocean Acoustic Library). Bellhop is designed in order to perform two-dimensional acoustic ray tracing for a given sound speed profile c(z) or a given sound speed c(r; z), in ocean waveguides with at or variable absorbing boundaries. Output options include ray coordinates, travel time, amplitude, eigenrays, acoustic pressure or transmission loss (either coherent, incoherent or semi-coherent)." (Rodriguez, 2008).

boundary condition - constraints put on a problem at the boundaries to make it solvable.

bounded elliptical modes - a method for estimating the acoustic modes. This technique assumes the elliptical dependence of wave number on the mode number to estimate the modal wave numbers given the sound speed and sediment geo-acoustics extremes (Smith, 2007).

boxcar average - an average taken over a number of bins of data, usually in a "box" around the point of interest.

brute force - refers to solving a problem by calculating all possible answers.

bundled modes - grouping acoustic normal modes by examining the propagation angles associated with each mode. In the context of this work, modes are grouped, or bundled by considering surface interacting, volume propagating and bottom interacting modes.

canonical data set - a idealized dataset for which solutions are generally well known.

Carter tables - tables used to convert nominal depth (or bathymetry) to true depth. (Carter, 1980).

centroid - mathematical center of points or vectors.

clustering - grouping data by examining the distances between each data point and classifying closest points into groups.

conformal mapped surface - "The discrete rough surface is assumed to be a piecewise linear surface. The range step of the marching algorithm is chosen to be the grid spacing over which the rough surface is defined, hence at each range step only one segment of the piecewise linear surface is involved. That segment can be thought of as being the upper boundary of a trapezoidal 2-D section of the waveguide. By neglecting the bottom topography the geometry can be simplified even further, mapping one semi-infinite trapezoidal strip onto a rectangular strip. This is a valid approximation because the effect of the surface roughness on depth through the mapping extends only a few meters from the surface. The local angle of inclination of the surface segment is represented through the non-dimensional parameter ν (fraction of π). For all practical applications, the effect of the surface roughness on depth through the conformal mapping is extinguished well before reaching the bottom. Only one segment of the surface is mapped at a time, using a different conformal mapping for each range step. The marching algorithm is implemented in a transformed or *pseudospace*. The field is advanced one range step in pseudospace and then transformed back to physical space. The solution to the original rough surface problem has been advanced one range step in physical space and the previous pseudospace is discarded.

Dozier [9] has shown that each local conformal mapping transforms the elliptic wave equation into another elliptic equation of the same form in the transform space. That is, the wave equation in the physical space (r,z) defined by the trapezoidal strip, is transformed into a flat surface rectangular strip in pseudospace $(\tilde{r},\tilde{z})$. The wave equation in pseudospace has the same form as in physical space, with a modified sound speed profile given by

$$\tilde{c}(\tilde{r},\tilde{z}) = \frac{c\left[r(\tilde{r},\tilde{z}),z(\tilde{r},\tilde{z})\right]}{\left|f'(\tilde{z})\right|}, \quad (1)$$

where $f'(\tilde{z})$ is the magnification factor of the mapping. This factor is either larger or smaller than unity but, in all cases, tends rapidly toward unity as depth increases.

The net result of the conformal mapping technique is then to convert a rough surface scattering problem into a succession of locally flat surface problems, each one with its own modified sound velocity profile. Even if the original sound velocity profile (i.e. in physical space) is isovelocity, in pseudospace where the "ocean surface" is flat, it becomes depth and range dependent (due to the magnification factor). At each range step there is a unique velocity profile in physical space and two velocity profiles in pseudospace, one associated with the left side and the other with the right side of the surface segment. Each profile leads to a different unevenly spaced mesh in physical space. FEPE is marched over the range step in pseudospace making use of the average profile, whereupon the result is transformed back to physical space.

The FEPE-CM technique for handling surface roughness has been thoroughly validated by Norton *et al*. [5] by comparison with a full wave scattering model for the case of periodic surfaces, as well as for single realizations of randomly rough surfaces having a power spectrum characteristic of a sea surface. " Excerpt from Fabre *et al.*, 2009.

convergence - area where energy constructively interferes.

cost function - a mathematical description of something that can be optimized on.

coverage, acoustic or coverage area - (Dennis and Hemsteter, 2007) the area covered by a sensor centered at the grid point. Acoustic coverage, described in Fabre and Dennis (2007), is simply the area for which acoustic TL is below a threshold, or the area over which there is positive or some threshold (FOM) of signal excess.

critical factors - parameters or factors, that have been identified to have a high correlation with the end result, in this case environmental critical factors that are highly correlated with the acoustic response.

decibel - (dB) a logarithmic measure of sound intensity referenced to some reference level.

detection threshold - "the ratio, in decibel units, of the signal power (or mean-squared voltage) in the receiver bandwidth to the noise power (or mean-squared voltage), in a 1-Hz band,

measured at the receiver terminals, required for detection at some pre-assigned level of correctness of the detection decision." from Urick, 1983, p378.

directivity index - "When the signal is a unidirectional plane wave and is therefore perfectly coherent, and when the noise is isotropic, that is when the noise power per unit solid angle is the same in all directions ... the array gain reduces to the quantity called directivity index, which has a long historical use in underwater sound." Urick, 1983.

duct leakage - refers to acoustic energy leaking out of a duct, due to high angle scattering or change of duct characteristics.

eigenvalues - distinct values. In acoustics, the depth dependent normal mode portion of the wave equation has multiple solutions described by eigenvalues, which are the wave numbers for each mode and the eigenvectors, which are the mode amplitude functions versus depth for each mode.

eigenvectors - distinct vectors. See eigenvalues.

ensembles - multiple realizations of a numerically modeled dynamic field that attempt to capture the uncertainty of the model and/or data included.

figure of merit (FOM) - a threshold used to characterize the performance of a system. In underwater acoustics the FOM contains all the terms of the sonar equation except the transmission loss (TL). See also sonar equation.

forecast - a prediction of some future state of a dynamic system.

frequency - number of cycles occurring in a certain time.

Gauss's theorem - or divergence theorem, relates a surface integral to a volume integral:

$$\iint_S A \cdot n \, dS = \iiint_V \nabla \cdot A \, dV$$

where *A* is a vector field,

$$\nabla \cdot A = \frac{\partial A_x}{\partial x} + \frac{\partial A_y}{\partial y} + \frac{\partial A_z}{\partial z}$$

is the divergence of *A*, *n* is the normal to the volume, *V* and *S* is the surface (from Pierce, 1991).

geoacoustic - describing the acoustics of the geology, typically on the sea floor. Seafloor geoacoustic descriptions often contain profiles of sound speed, attenuation, density versus depth in the sediment.

gradient - change in sound speed with change in depth.

harmonic - cycles with time

Helmholtz equation - solution to the wave equation in the frequency domain for a harmonic plane wave

$$\nabla^2 P + k^2 P = 0$$

where k is the wave number:

$$k = \frac{\omega}{c} = \frac{2\pi f}{c}$$

P is the acoustic pressure, f is the source frequency and c is the speed of sound. (Pierce, 1991). See Chapter 1 for derivation.

Hertz - unit of frequency, cycles per second, named after Heinrich Hertz 1857-1894 (http://en.wikipedia.org/wiki/heinrich_hertz).

homogeneous - having the same or similar properties. E.g. if a waveguide is homogeneous, the sound speed is the same throughout.

integrated signal excess (ISE) - the signal available to detect integrated over some quantity, such as frequency, source depth, receiver depth, etc. (Fabre, 2007).

intensity - power per unit area. Acoustic intensity is proportional the acoustic pressure times its complex conjugate. Average acoustic intensity the average power passing through a unit area.

isobath - lines of constant bathymetry or depth, depth contours.

k-means - "*K*-means clustering is a partitioning method. The [Matlab™] function k-means partitions data into *k* mutually exclusive clusters, and returns the index of the cluster to which it has assigned each observation. Unlike hierarchical clustering, *k*-means clustering operates on actual observations (rather than the larger set of dissimilarity measures), and creates a single level of clusters. The distinctions mean that *k*-means clustering is often more suitable than hierarchical clustering for large amounts of data." Mathworks, 2009.

Kraken model - A robust, accurate and efficient underwater acoustic normal mode model. Kraken models 3-D environments and has many options for treating ocean-acoustic problems. Porter, 2001.

leakage coefficient - acoustic energy trapped in a duct is subject to high angle and other effects which allow energy to leak out of the duct. The leakage coefficient is an empirically derived quantity that accounts for energy leaking out of a surface duct or sonic layer. Baker, 1975.

metric - a quantity that allows comparison or evaluation of some process. For example, a common metric used to evaluate acoustic performance is sensor coverage.

Navy Coastal Ocean Model (NCOM) - (*e.g.* Barron *et al*., 2009) is a primitive equation ocean circulation model that uses ocean dynamics and measured data to predict nowcasts and forecasts of the oceanography including temperature, salinity, currents and wind stress. NCOM also uses winds as the surface boundary condition and outputs horizontal and vertical components of wind stress.

noise, noise level (NL) - sound that is not part of the source of interest. The Noise Level (NL) is the level of noise in dB.

nominal depth - the depth of the ocean assuming a constant sound speed through the water column (*e.g.* Fabre and Fabre, 2007).

normal mode - modes of vibration roughly comparable to the modes of a vibrating string. Jensen *et al*. 2000.

nowcast - a numerical prediction for the current time or a time very near the current time.

perturbed field - a field that has been varied from its mean state.

plane wave - a (acoustic) wave for which all acoustic field quantities vary with time and space, but are independent of position along planes normal to the spatial component (Pierce, 1991). An example acoustic plane wave is

$$P(r,t) = P(r)e^{-i\omega t}$$

where P is the acoustic pressure, r is the range from the acoustic source, i is the square root of -1 and ω is the angular frequency ($2\pi f$)

pressure-density relation - "The classical model of a compressible fluid presumes the existence of some definite relation $p=p(\rho)$, between pressure [p] and density [ρ]." Pierce, 1991 - see Pierce for further discussion.

prediction - an estimate of some future state of a system.

provincing - estimating groupings of some field based on their similarity.

proxy - substitute.

quiescent - independent of time and no motion.

Range Dependent Acoustic Model (RAM) - a finite element parabolic equation (PE) model that "is based on a user-selected multiple-term Padé approximation of the PE operator. Because this solution allows range steps much greater than the acoustic wavelength and does

not require fine vertical gridding, RAM is a very fast research model. (Collins *et al*., 1996) Additionally, RAM's grid can be tuned to smoothly trade accuracy and speed as the operational situation requires". (Zingarelli and King, 2003).

refraction - change in direction of a wave due to a change in its speed, http://en.wikipedia.org/wiki/Refraction.

representative environment - an environment (or set of environmental inputs to a model) that can be used in place of (or as a representative for) other similar environments for the purposes of saving time in modeling or for similarity assessment.

ray, ray trace - the path of a wave front in time or space, can be visualized as a line.

receiver, acoustic - hardware consisting generally of hydrophones, that can sense the pressure due to a source of sound.

sea state - general condition of the surface of the ocean. Can be characterized by wave action. http://en.wikipedia.org/wiki/Sea_state

signal excess - the amount of detectable signal remaining once noise and other factors are estimated.

smodes - smoothed modes, see Spofford 1979.

sonar equation - describes the balance of energy, typically in decibels (dB), of an underwater acoustic source of energy. For passive acoustics, the sonar equation, as given by Urick (1983) is

$$SL - TL = NL - DI + DT$$

$$SE = SL - TL - NL + DI - DT$$

$$SE = FOM - TL$$

where SL is source level, TL is transmission loss, NL is noise level, DI is directivity index, DT is detection threshold, SE is signal excess, and FOM is the figure of merit which includes all the terms other than TL into one number.

sonic layer depth - the depth from the ocean surface to a maximum in sound speed in which acoustic energy can be trapped.

source, acoustic - hardware consisting typically of transducers, that sends acoustic energy into a waveguide generally at some duration and frequency band of interest.

Taylor series expansion - representing a function as an infinite sum of terms calculated from the values of its derivatives. http://en.wikipedia.org/wiki/Taylor_series_expansion

$$f(x) = \frac{1}{1!}\frac{\partial f(a)}{\partial x}(x-a) + \frac{1}{2!}\frac{\partial^2 f(a)}{\partial x^2}(x-a)^2 + \frac{1}{3!}\frac{\partial^2 f(a)}{\partial x^3}(x-a)^3 + \cdots$$

true depth - the depth of the ocean accounting for the vertical sound speed in the water column

uncertainty - there are many definitions of uncertainty. (Pang*) reports on the uncertainty defined by ONR: "Uncertainty was defined to be related to the environmental variability that might be knowable and that we might simulate, the environmental variability that might be knowable but that we can not simulate, the environmental variability that is not knowable, and the error inherent in representations and calculations of the environmental field, acoustic field, and target estimation. The following mathematical definition of uncertainty was presented at the workshop in order to initiate and further discussion.

E = estimated value of some quantity (measured, predicted, calculated ..)

A = actual value (unknown truth or unknown nature)

U = E-A

The uncertainty in *E* can be represented by the probability density function (pdf) of U. The pdf need not be normal, have a mean of zero, or uni-modal. "

*http://www.spatial.maine.edu/~worboys/SIE565/papers/pang%20viz%20uncert.pdf

http://www.onr.navy.mil/sci_tech/chief/cuwg/index.html

uncertainty band (UBAND) - an algorithm developed by Zingarelli (2008), based on Harrison and Harrison (1995), who noted that a range average of TL is very similar to a frequency average over the system band width, due to the mathematical similarity of the two techniques using sums over normal modes. Zingarelli (2008) extended that range averaging technique to calculate upper and lower boundaries on a TL prediction by estimating an uncertainty in the number of modes used in the mode sum, based on the uncertainty in the environmental inputs. This technique has been shown (*e.g.* Zingarelli and Fabre, 2009) to be quite accurate for various applications.

wave equation - an equation describing the propagation of waves (*e.g.* sound, light) in a media.

waveguide - a field which guides waves. In underwater acoustics, the waveguide is described as the surface, the ocean and the sediment through which the acoustic energy travels.

wavelength - the length of a wave. Frequency (*f*) and wavelength (λ) are inversely related

$$f = c / \lambda$$

wave number - number of wavelengths in a specified distance. In acoustics, the wavenumber is also the eigenvalue

wind stress - the force of the wind on the sea surface.

ξ parameter - the argument to the Airy function formulation of the wave equation. See Chapter 2 for derivation.

Vita

Ms. Fabre graduated from Slidell High School in 1984. She graduated from Millsaps College in Jackson, MS in 1988 with a Bachelor of Science in Physics. While working as a Scientist at Neptune Sciences Incorporated (1990-2003), she attended UNO part time and completed a Master of Science in Applied Physics in 1996. She received the Bill Good Award in recognition of outstanding research in physics and was a runner up for the Sigma Xi distinguished research award for her Master's research. Ms. Fabre was enrolled intermittently at UNO from 2000 to 2006 while raising her children and continuing to work as a Scientist. Since 2003, she is a Research Physicist for the Naval Research Laboratory Acoustics Division. She will complete her PhD in Engineering and Applied Science, specializing in Acoustics, with the completion of this dissertation in 2010.